Cosmological Singularity Resolution

Classical and Quantum Approaches

DISSERTATION

zur Erlangung des akademischen Grades

DOCTOR RERUM NATURALIUM

(Dr. rer. nat.)

im Fach Physik

Spezialisierung: Theoretische Physik

eingereicht an der

Mathematisch-Naturwissenschaftlichen Fakultät

der Humboldt-Universität zu Berlin

von

Sebastian F. Bramberger

Präsidentin der Humboldt-Universität zu Berlin:

Prof. Dr.-Ing. Dr. Sabine Kunst

Dekan der Mathematisch-Naturwissenschaftlichen Fakultät:

Prof. Dr. Elmar Kulke

Tag der Disputation am 19.12.2019

Gutachter: Prof. Dr. Hermann Nicolai
Prof. Dr. Claus Kiefer
Dr. Olaf Hohm

Abstract

In the face of ever more precise experiments, the standard model of cosmology has proven to be tremendously robust over the past decades. Inflation or ekpyrosis provide a basis for solving some of its remaining conceptual issues - they are a beautiful and natural simplification to our understanding of the universe's early history; yet they leave many questions unanswered and raise new problems. For example, inflationary theories fail to be predictive as long as eternal inflation is not better understood. At the same time, ekpyrotic theories struggle to explain the transition from a contracting to an expanding phase - the so-called bounce. Both of them lack any understanding or description of the origin of everything and contain cosmological singularities. Here, we provide concrete steps towards shedding a light on these mysteries.

The overarching theme that guides most chapters in this thesis is how to deal with cosmological singularities and whether they can be resolved without invoking extraordinary physics. In the first part, we construct classically non-singular bounces in the most general closed, homogeneous but anisotropic space-time. In special cases we find analytic solutions to Einstein's equations which, in addition, describe inhomogeneities and electro-magnetic fields. Looking at the general case, we find bounces numerically and show that they leave the universe in a state well-suited for inflation to commence. In the second part we analyze the effect of introducing quantum mechanics semi-classically to cosmology. Our methods, which are based on Feynman's sum over histories framework, reveal novel and interesting properties of the early universe. We scrutinize both processes responsible for eternal inflation: false vacuum decay and slow-roll inflation. In the first case, we are able to show that instabilities may occur during false vacuum decay independent of the scale at which the decay happens. In the second case, we provide a new framework which can be used to describe quantum effects during an inflationary phase and goes beyond the usual treatment of Quantum Field Theory in curved space-time. We calculate the dominant contributions to transition amplitudes during slow-roll and eternal inflation as well as their properties. Finally, we show that quantum effects are helpful in resolving cosmological singularities. We demonstrate that anisotropies do not hinder the universe's creation from nothing. Furthermore, we construct numerical solutions in which the universe tunnels to a different state before reaching a singularity. With that, we resolve for the first time cosmological singularities without the use of extravagant physics.

Zusammenfassung

Das Standardmodell der Kosmologie stellte sich in den letzten Jahrzehnten, trotz immer genauerer experimenteller Tests, als sehr robust heraus. Darüber hinaus schaffen ekpyrotische und inflationäre Theorien eine Grundlage um viele konzeptuelle Probleme des frühen Universums zu lösen. Dennoch bleiben viele Fragen unbeantwortet. So ist es in inflationären Theorien schwierig präzise Vorhersagen zu treffen so lange die ewige Inflation nicht besser verstanden wird. Auf der anderen Seite haben ekpyrotische Theorien Schwierigkeiten den Übergang zwischen kontrahierenden und expandierenden Phasen - den so-genannten kosmischen Rückprall - zu erklären. Zudem beschreibt keine der beiden Theorien den Ursprung von Allem und beinhalten kosmologische Singularitäten. Hier stellen wir Denkansätze bereit um diese Unklarheiten näher zu beleuchten.

Im ersten Teil der Arbeit konstruieren wir klassische, singularitätenfreie Rückpralle in der generellsten geschlossenen, homogenen aber anisotropischen, Raumzeit. In speziellen Fällen finden wir analytische Lösungen der Einsteingleichungen die zusätzlich sogar Inhomogenitäten und elektromagnetische Felder beschreiben. Im Allgemeinen finden wir rückprallende Lösungen numerisch und zeigen, dass sie das Universum in einen Zustand lassen, der für eine subsequente Inflationsphase gut geeignet ist.

In dem längeren, zweiten Teil beschäftigen wir uns mit den Konsequenzen auf die Kosmologie, die eine konsistente, semiklassische Quantisierung mit sich bringt. Unsere Methoden, die auf Feynmans Summe über Pfade basiert, offenbart neue und interessante Phänomene des frühen Universums. Im Speziellen analysieren wir beide Prozesse, die ewige Inflation verursachen: Der Zerfall des falschen Vakuums und langsam-rollende Inflation. Im ersten Fall zeigen wir, dass Instabilitäten während des Zerfalls auftreten können unabhängig von der Energie des Zerfalls. Im zweiten Fall stellen wir einen neues Konzept vor mit dem Quanteneffekte während der inflationären Phase beschrieben werden können und das über die übliche Beschreibung in der Quantenfeldtheorie in gekrümmter Raumzeit hinausgeht. Wir berechnen die dominanten Beiträge zu Amplituden die typische und ewige inflationäre Prozesse beschreiben sowie deren Eigenschaften. Schlussendlich zeigen wir wie Quanteneffekte für die Auflösung kosmologischer Singularitäten hilfreich sind. Wir zeigen explizit, dass Anisotropien kein Problem für den Ursprung des Universums durch ein Tunneln aus dem Nichts darstellen. Zudem konstruieren wir numerische Lösungen, in denen das Universum vor dem Erreichen einer Singularität in einen anderen Zustand tunnelt. Damit lösen wir zum aller ersten Mal kosmologische Singularitäten ohne den Einsatz von extravaganter Physik auf.

Contents

Publications

The first part of this thesis is on classically bouncing cosmologies and largely based on the following publications and preprints

[1] S.F. Bramberger, and J-L. Lehners, *"Non-Singular Bounces Catalysed by Dark Energy"*, Phys.Rev. D99 (2019) no.12, 123523, arXiv:1901.10198 [1]

[2] A. Anabalon, S.F. Bramberger, and J-L. Lehners, *"Kerr-NUT-de Sitter as an Inhomogeneous Non-Singular Bouncing Cosmology"*, arXiv:1904.07285, submitted to JHEP [2]

The second part of this thesis, focusing on quantum aspects of early universe cosmology is based on

[3] S.F. Bramberger, G. Lavrelashvili, and J.L. Lehners, *"Quantum Tunneling via Complex Time Paths"*, Phys.Rev. D94 (2016) no.6, 064032, arXiv:1605.02751 [3]

[4] S.F. Bramberger, T. Hertog, J.L. Lehners, and Y.Vreys. *"Quantum Transitions Through Cosmological Singularities"*, JCAP 1707 (2017) no.07, arXiv:1701.05399 [4]

[5] S.F. Bramberger, S. Farnsworth, and J.L. Lehners. *"The Wavefunction of Anisotropic Inflationary Universes With No-Boundary Conditions"*, Phys.Rev. D95 (2017) no.8, 083513, arXiv:1701.05753 [5]

[6] S.F. Bramberger, M. Chitishvili, and G. Lavrelashvili, *"Aspects of the negative mode problem in quantum tunneling with gravity"*, arXiv:1906.07033 [6]

[7] S.F. Bramberger, A. Di Tucci, and J.L. Lehners, *"Homogenous Fluctuations during Inflation: a Description in Quantum Cosmology"*, arXiv:1906.05782 [7]

One of the appendices is based on

[8] S.F. Bramberger, A. Coates, J. Magueijo, S. Mukohyama, R. Namba, and Y. Watanabe. *"Solving the flatness problem with an anisotropic instanton in Hořava-Lifshitz gravity"*, Phys.Rev. D97 (2018) no.4, 043512, arXiv:1709.07084 [8]

1 Introduction

The standard model of cosmology has enjoyed tremendous success despite the scrutiny that increasingly precise experiments such as PLANCK [9, 10] and WMAP [11] provide. provide. They show that the universe is almost completely isotropic and homogeneous at its largest scales. Further, we live in a flat, expanding universe that has an approximately scale invariant spectrum of primordial perturbations. While there is no tension between the standard (ΛCDM) model and observational data, a lot of open conceptual questions about the early universe remain unanswered. Most pressingly, why is the universe the way it is? In other words, it is a complete mystery why the universe is so homogeneous, isotropic, and flat. Furthermore, the Big Bang indicates that a cosmological singularity is looming in our past, suggesting the complete failure of our physical theories.

As a result, many extensions which augment the standard model have been proposed. Inflation [12, 13, 14, 15] is a period of accelerated expansion in the early universe, while ekpyrosis [16, 17] is a high pressure contracting phase. Both of them give a satisfying explanation of the special properties our universe has. At the same time, they suffer from theoretical challenges of their own. In inflationary theories, eternal inflation is a threat to the predictability of theory [18]. Ekpyrotic theories on the other hand struggle to give a consistent description of the transition between the contracting phase of the early universe to the expanding phase we are currently in. Even more crucially, they do not provide an explanation for the beginning of the universe and hence have to be augmented by a theory of initial conditions.

In this thesis we make progress towards solutions to these predicaments in three ways. Firstly, we construct exact classically bouncing solutions [1, 2], which effectively avoid the cosmological singularity. We study the theoretical properties of these solutions as well as specific examples to make contact with observations. Secondly, we study proposals of the very beginning of the universe - a domain in which the physics of the very large and the very small come together. Its description is a display of one of the most beautiful ideas in cosmology: the origin of the largest structures in the universe lie in primordial quantum fluctuations. Inflation and ekpyrosis provide concrete mechanisms that can amplify these fluctuations into essentially classical density perturbations, which can then act as seeds for the formation of structure via gravitational collapse. In this formalism, one fixes a classical background and imposes small, quantized fluctuations around it.

However, despite its attractiveness, this approach also displays its potential downfalls: since the fundamental laws governing the universe are quantum mechanical, are we justified in

making the assumption that quantum effects play solely a minor role? It seems likely that such a treatment misses fundamental, quantum, features in our description of the universe. Especially at its origins we expect this, otherwise valid and precise, approximation to break down. Instead, we require a theory that goes a step beyond, which treats background and perturbations on an equal footing.

This is the realm of quantum cosmology [19]. In its most elegant formulation it is an attempt to generalize Feynman's path integral approach to gravity [20]. Within it, the best known theories of initial conditions were formulated: the tunnelling proposal by Vilenkin [21] and the no-boundary proposal by Hartle and Hawking [22]. Based on the Euclidean gravitational path integral, they are motivated by the Wick rotation commonly employed in Quantum Field Theory (QFT). We extend the no-boundary proposal to a more realistic version which includes anisotropies [5]. Interestingly, it is possible to find no-boundary solutions for arbitrarily large anisotropies. However, they do delay the rate at which the universe becomes classical. The no-boundary proposal is very similar in its description to so-called Coleman-De Luccia instantons [23]. The idea behind them is that the universe is initially in an excited state that, even though it is classically stable, is unstable due to quantum effects. Hence the universe may tunnel from its excited state to the lower energy state. While this, quantum mechanical, decay is well understood in field theory, when gravity is included there are a lot of open puzzles. One of them is the so-called negative mode problem [24]: some tunneling solutions develop pathological perturbations. We further the understanding of this problem by showing that it is not related to Planck scale physics but can happen at any scale of the potential [6].

Finally, we turn towards investigating the framework of quantum cosmology itself. The Euclidean approach to quantum gravity has been plagued by pathologies such as the conformal factor problem since its infancy [25]. Instead, we work with a formulation of the path integral that is defined in a fundamentally Lorentzian manner [26]. Picard-Lefschetz theory [27, 28] is a mathematical tool that gives a precise prescription of how to evaluate the resulting, conditionally convergent, integrals by deforming the integration contour in the complex plane. Using this tool provides a firmer mathematical basis for the path integral framework. As an example of its application, we study the fluctuations arising during inflation [7]. Not only did we gain insight into exactly how quantum transitions occur during inflation and when the usual QFT in curved space-time treatment breaks down, but we could establish a framework which allows asking these questions to begin with. Generalizing this to inhomogeneous

fluctuations might allow us to address one of the big enigmas of inflationary theory: eternal inflation [29]. In slow-roll eternal inflation [30], quantum transitions cause an infinite number of universes with a variety of properties to come into existence. Making predictions for observables in this scenario is notoriously hard and forms a basis for critique of any inflationary model and we provide a fresh, more adequate framework to study its implications.

In the appendix we clarify some details and extensions of the calculations in the main body of the text. More importantly however, we also show that inflation and ekpyrosis are not the only models that can resolve the problems of the standard model of cosmology. Employing the renormalizable Horava-Lifshitz theory of gravity [31], we show that the so-called flatness problem in cosmology is solved due to the special symmetry of the theory [8]. Notably, this solution is achieved without assuming extra ingredients like a scalar field. To conclude, we show that this is not specific to the theory but any theory with appropriately modified dispersion relations is able to solve several problems of standard cosmology.

In summary, we lay the foundations for a consistent and powerful description of quantum effects in the early universe through introducing new analytical and numerical tools to the field of quantum cosmology. By applying our methods to various open problems we demonstrate their utility and reveal a promising road map towards solutions of the most pressing questions in early universe cosmology.

2 The Standard Model of Cosmology

2.1 The Lagrangian description of General Relativity

Einstein's theory of General Relativity (GR) describes space, time and its interaction with matter to an outstanding degree of accuracy. The dynamics of the fundamental degrees of freedom in the theory are governed by its field equations

$$R_{\mu\nu} - \frac{1}{2}Rg_{\mu\nu} + \Lambda g_{\mu\nu} = T_{\mu\nu} \tag{2.1}$$

In four dimensions, these are ten partial differential equations corresponding to the ten degrees of freedom in the symmetric metric tensor $g_{\mu\nu}$. $T_{\mu\nu}$ is the stress-energy tensor describing the interaction between space-time and matter. The Ricci tensor and scalar are given by

$$R_{\mu\nu} = \Gamma^{\alpha}_{\mu\nu,\alpha} - \Gamma^{\nu}_{\mu\alpha,\nu} + \Gamma^{\alpha}_{\alpha\beta}\Gamma^{\beta}_{\mu\nu} - \Gamma^{\alpha}_{\beta\nu}\Gamma^{\beta}_{\mu\alpha}, \qquad R = g^{\mu\nu}R_{\mu\nu} \tag{2.2}$$

where

$$\Gamma^{\alpha}_{\mu\nu} = \frac{1}{2}g^{\alpha\beta}\left(g_{\mu\beta,\nu} + g_{\nu\beta,\mu} - g_{\mu\nu,\beta}\right) \tag{2.3}$$

are the usual Christoffel symbols. We have presented only one - albeit the most common - way, of the many ways that GR can be formulated. In the Lagrangian formalism, employing metric variables, Einstein's equations are derived from the Einstein-Hilbert action via the variational principle. If $\mathcal{M}$ is a Lorentzian manifold with metric $g_{\mu\nu}$, then the action is given by

$$S_{EH} + S_{GHY} = \frac{1}{2}\int_{\mathcal{M}} d^4x\sqrt{-g}R - \int_{\delta\mathcal{M}} d^3y\epsilon\sqrt{h}K \tag{2.4}$$

where g is the determinant of the metric. We require the second term, also known as the Gibbons-Hawking-York boundary term, in order to make the variational principle well defined. It depends on the quantities y, and h which are induced by the bulk coordinates x and metric g respectively on the boundary $\delta\mathcal{M}$ of $\mathcal{M}$. ϵ is a constant equal to +1 for a space-like or -1 for a time-like boundary and finally K is the trace of the extrinsic curvature K_{ij} which is given by

$$K_{ij} = \frac{1}{2}\left[\nabla_\mu n_\nu + \nabla_\nu n_\mu\right] e^{\mu}_i e^{\nu}_j \tag{2.5}$$

Here $e^{\mu}_i = \frac{\partial x^\mu}{\partial y^i}$ project from the bulk coordinates to the boundary coordinates and n_μ is the unit normal to the boundary facing outwards. It is useful to express the induced metric in terms of the projectors

$$h_{ij} = e^{\mu}_i e^{\nu}_j g_{\mu\nu} \tag{2.6}$$

In appendix A.1 we derive the GHY boundary term and show that it cancels the spurious boundary term arising from the Einstein-Hilbert action. Note that depending on the conceptual questions one is asking, it is useful to introduce different boundary terms. For example, in the derivation of the GHY term, we assumed the metric's variation on the boundary to be zero. This corresponds specifying the values of the degrees of freedom at the boundary also known as Dirichlet boundary conditions. However, these might not be appropriate in all physical contexts. In certain situations we are interested in specifying the momenta instead. Most generally, we can enforce Robin boundary conditions where we specify a linear combination of position and momenta. The Einstein-Hilbert action with Robin boundary conditions reads [32, 33]

$$S_R = \frac{1}{2}\int_{\mathcal{M}} d^4x\sqrt{-g}R - \xi\int_{\partial\mathcal{M}} d^3y\sqrt{h} \tag{2.7}$$

where ξ is the proportionality factor between the momenta and positions. We derive this form of the boundary term in appendix A.1 and make extensive use of it in section 8.

2.2 The Big Bang model

Cosmology is the study of the universe and its content on the largest scales, typically by inserting a specific metric ansatz with a high degree of symmetry into Einstein's equations. Two measurements have revolutionized the field in the last century: The first observation, made in 1938, through measuring the recession velocities of galaxies, was that the universe is expanding. This led to the famous Hubble law for the recession velocities of galaxies v

$$v = H_0 d \tag{2.8}$$

where H_0 is the Hubble parameter today, measured by the PLANCK satellite [34] to be $H_0 = 67.36 \pm 0.54$ km s^{-1} Mpc^{-1} and d is the distance to the galaxy. This observation naturally led to the notion that the universe was smaller and thus hotter in its past; however, strictly following the universe's evolution into its past will naturally lead to a point where the universe was infinitesimally small, infinitely hot and infinitely dense. As an attempt to demean this proposal it was termed the Hot Big Bang scenario by Fred Hoyle. Today we know that as the universe becomes smaller and smaller, eventually the framework of General Relativity does not hold anymore and ought to be replaced by a more fundamental theory. As such Hot Big Bang cosmology refers to the idea that the universe expanded from a smaller, hotter stage in its infancy to what it is today. The second crucial experiment was performed on the universe's first light which was emitted when the universe was cool enough for atoms

to form. This primordial light has since been stretched by the expansion of the universe and we observe it today in the microwave frequency range. Remarkably, its spectrum is the one of a thermal black body with a temperature of $T = 2.72548 \pm 0.00057K$ and it is extraordinarily isotropic. This has led to the postulate of the so-called Cosmological Principle which asserts that at its largest scales, the universe is homogeneous and isotropic. The most general metric describing such a universe is the Friedmann–Lemaître–Robertson–Walker (FLRW) metric which, in some suitable coordinates, has line element

$$ds^2 = -dt^2 + a(t)^2 \left[\frac{1}{1-kr^2} dr^2 + r^2 \left(d\theta^2 + \sin^2 \theta d\phi^2 \right) \right] \tag{2.9}$$

where k measures the spatial curvature and may take on the values $-1, 0, +1$ corresponding to negatively curved, flat, and positively curved spatial slices respectively. Hence the high degree of symmetry imposed by assuming the cosmological principle allows for only three different kinds of spatial geometries. The function $a(t)$ is usually called the scale factor and determines the overall contraction or expansion of the universe as the physical (or proper) distance between two comoving (i.e. moving with the expansion or contraction of universe) observers.

With the geometry and thus the left hand side of Einstein's equations fixed we ought to now specify the right hand side of the equation amounting to describing the matter content of the theory. It turns out that the macroscopic properties of the matter in the universe are well described by a perfect fluid which has stress-energy tensor

$$T_{\mu\nu} = (\rho + p) u_\mu u_\nu + p g_{\mu\nu} \tag{2.10}$$

where ρ and p are the proper energy density and pressure in the fluid rest frame and u^μ is the four velocity of the fluid. Choosing a frame comoving with the fluid we may set $u^\mu = (1, 0, 0, 0)$ so that the stress energy tensor simplifies to

$$T_{\mu\nu} = \text{diag}(\rho, -p, -p, -p) \tag{2.11}$$

Finally, having specified both sides of the equation, Einstein's field equations reduce to two coupled ordinary differential equations - the Friedmann equations

$$H^2 = \left(\frac{\dot{a}}{a} \right)^2 = \frac{1}{3}\rho - \frac{k}{a^2} \tag{2.12}$$

$$\dot{H} + H^2 = \frac{\ddot{a}}{a} = -\frac{1}{6}(\rho + 3p) \tag{2.13}$$

where the dot signifies a derivative with respect to the physical time t. Combining the two equations yields a third, which relates the pressure and energy density and is sometimes

called the continuity equation

$$\dot{\rho} + 3H(\rho + p) = 0 \tag{2.14}$$

This makes it clear that, in general, in an evolving universe, the energy density is not conserved. It is typical to introduce a parameter w, called the equation of state, which relates the pressure and energy density via $p = w\rho$. In cosmology it is often times more useful to consider the alternative definition $p = \left(\frac{2}{3}\epsilon - 1\right)\rho$ and we will call ϵ the equation of state from now on. Upon plugging this relationship back into Eq. (2.14), we find that the energy density scales as $\rho \propto a^{-2\epsilon}$. Thus we can read off how the energy density of various matter types evolves as the universe becomes larger or smaller, inferring which matter type is dominant at what time. It is instructive to look at some representative examples of the most commonly used ideal fluids:

- The energy density of ordinary baryonic matter (sometimes referred to as dust) and dark matter scales like the inverse of volume of the universe $\rho = a^{-3}$. Hence they have equation of state $\epsilon = \frac{3}{2}$ and thus are pressure-less.

- For radiation and relativistic particles, the energy density scales like $\rho = a^{-4}$ because in addition to the scaling due to the change in the volume of the universe, their wavelength also scales with the universe's size, adding another factor of a. Radiation has equation of state $\epsilon = 2$.

- The simplest model for dark energy is the energy density of the vacuum which is constant over time and unaffected by cosmic evolution. For that reason, this contribution to the total energy density of the universe is also called the cosmological constant. It has equation of state $\epsilon = 0$.

In conjunction with the Friedmann equation we can write the scale factor as a function of the equation of state

$$a(t) \propto \begin{cases} t^{2/3(1+w)} & \text{for } \epsilon \neq 0 \\ e^{Ht} & \text{for } \epsilon = 0 \end{cases} \tag{2.15}$$

Thus the equation of state of the dominant matter type in the universe will determine its overall behaviour.

2.3 The PLANCK measurements

In order to compare with experiments, it is illuminating to study the Friedmann equation in the presence of various energy sources. Then we can write

$$3H^2 = \frac{\rho_{r,c}}{a^4} + \frac{\rho_{m,c}}{a^3} - \frac{3k}{a^2} + \Lambda \tag{2.16}$$

where Λ is the cosmological constant and we chose units such that $a_0 = 1$ is the scale factor today. Then $\rho_{r,c}$ and $\rho_{m,c}$ correspond to the energy densities in radiation and matter today, respectively. It is common to re-write this equation as

$$\left(\frac{H}{H_0}\right)^2 = \frac{\Omega_{r,c}}{a^4} + \frac{\Omega_{m,c}}{a^3} + \frac{\Omega_k}{a^2} + \Omega_\Lambda \tag{2.17}$$

where the canonically defined fractional energy densities are

$$\Omega_r = \frac{\rho_{r,c}}{3H_0^2}, \qquad \Omega_m = \frac{\rho_{m,c}}{3H_0^2}, \qquad \Omega_k = \frac{-k}{H_0^2}, \qquad \Omega_\Lambda = \frac{\Lambda}{3H_0^2} \tag{2.18}$$

These quantities were measured by the 2015 PLANCK satellite [34] to be

$$\Omega_r = (9.14 \pm 0.34)10^{-5} \tag{2.19}$$

$$\Omega_m = 0.308 \pm 0.012 \tag{2.20}$$

$$\Omega_k = -0.005 \pm 0.017 \tag{2.21}$$

$$\Omega_\Lambda = 0.692 \pm 0.012 \tag{2.22}$$

$$H_0 = (67.36 \pm 0.54)\text{km s}^{-1}\text{Mpc}^{-1} \tag{2.23}$$

Hence they found a very flat universe that is currently dominated by dark energy. Importantly, if this is the full matter content of the universe, curvature *never* dominated cosmic evolution. This is because today the contribution of matter to the total energy is bigger than the curvature contribution and the universe is already dominated by dark energy. From here on out all components will get diluted while dark energy remains constant and dominant. Hence we get the picture of the universe starting from a hot, dense initial state after which radiation was the dominant driver of cosmic evolution followed by baryonic matter and ultimately by dark energy as it is today.

2.4 The Cosmic Microwave Background

In 1964, Penszias and Wilson measured radiation that permeates the entire universe. This signal, known as the Cosmic Microwave Background (CMB), was emitted when the, then very hot, universe cooled enough such that protons and electrons combined into hydrogen

atoms. Before, photons would constantly scatter of the electrons but they interact much less with the electrically neutral hydrogen. Hence from then on, photons were streaming freely and the universe went from opaque to transparent. This event, where atoms first formed, is called recombination and happened at about 370,000 years after the Big Bang when the universe reached about 3,000 degrees Kelvin. Measurements of the CMB are currently the best probes of the very early universe. Today, we measure the photons' frequency to be $\nu = 160GHz$ which corresponds to a black body temperature of $T = 2.7K$ on average. The existence of the CMB provides very strong evidence that the universe was once very hot and dense. Not only that but surprisingly, the temperature distribution of the radiation is very isotropic, implying that the early universe was isotropic to large degree. This is a puzzle in standard hot Big Bang cosmology as we will demonstrate in the next section. First, we take a look at the precise, quantitative results the CMB provides.

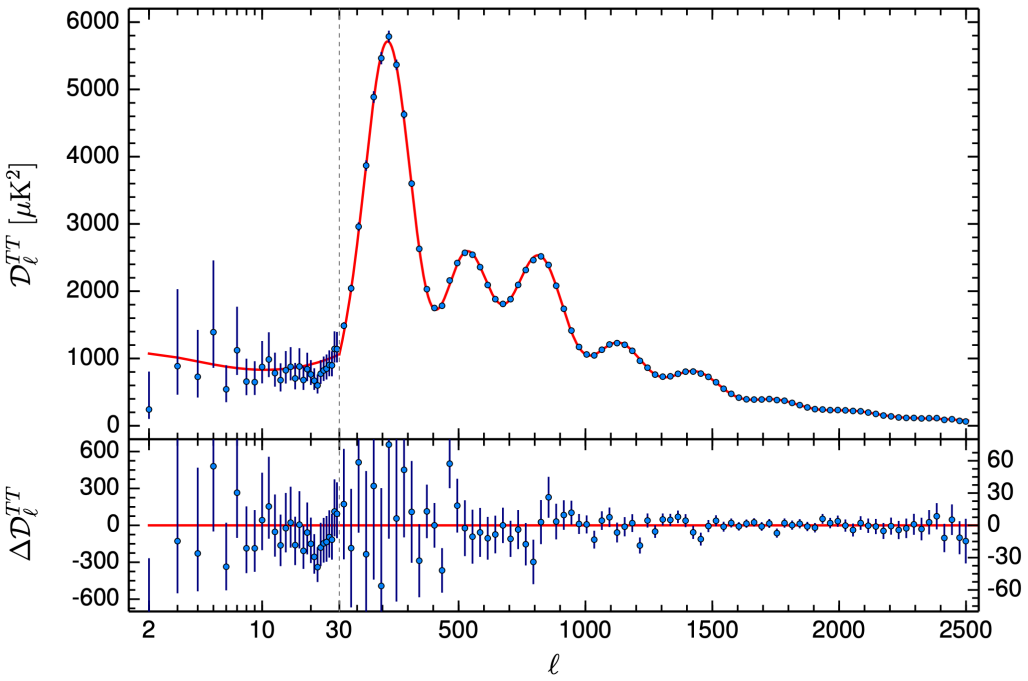

Figure 1: The angular power spectrum of temperature fluctuations as measured by the 2015 PLANCK satellite. Plotted here is the angular power D_l^{TT} as a function of the multipole moment l. Superimposed in red is the best-fit ΛCDM model. The residuals to the fit are plotted in the lower panel and the error bars indicate $\pm 1\sigma$ uncertainties. The figure is taken from [34].

Despite the isotropy of the CMB, there are small temperature fluctuations of order 10^{-5}.

They play a vital role in the structure formation of the universe and can be described by an expansion in spherical harmonics Y_l^m on the sky. In Cartesian coordinates they are polynomials of order l obeying Laplace's equation. l is the multipole moment and thus and integer quantity. In particular, $l = 0$ describes the monopole, $l = 1$ the dipole and so on. m is an integer, running from $-l$ to l and $m = 0$ corresponds to the Legendre polynomials. The temperature fluctuations in the CMB are given by

$$\delta T(n) = T_0 \sum_{l,m} a_{lm} Y_l^m(n) \tag{2.24}$$

where n is the direction in the sky and T_0 is the average temperature and the a_{lm}s are complex coefficients. What is measured in practice (c.f Fig. 1) is the rotationally invariant quantity, constructed out of the factors a_{lm}

$$D_l^{TT} = \frac{l(l+1)}{2\pi} C_l^{TT} \tag{2.25}$$

where

$$C_l^{TT} = \frac{1}{2l+1} \sum_m \langle a_{lm} a_{lm}^* \rangle \tag{2.26}$$

and $\langle ... \rangle$ refers to an ensemble average. Thus, C_l^{TT} represents the angular correlation function of the CMB's temperature fluctuations[1]. Its undulating shape stems from the behaviour of the radiation-matter plasma which was omni-present in the universe before recombination. Since describing this plasma relies on well-understood physics, the angular power spectrum's oscillations can be well explained if one assumes a nearly scale-invariant spectrum of fluctuations before that. One of the main tasks of early universe theories is explaining such a spectrum. Theoretically, the best variable to use in order to describe small departures from a FLRW space-time is the time and spatially dependent, curvature perturbation $\mathcal{R}(t, x)$. It characterizes small perturbations around the mean value of the universe's curvature and therefore is still well-defined when there is no matter or radiation present. In the language of the FLRW metric $\mathcal{R}(t, x)$ implies a small, local and time-dependent change in the scale factor $a(t)$ - the radius of the universe. It is in this way that $\mathcal{R}(t, x)$ and C_l^{TT} are related: A non-zero $\mathcal{R}(t, x)$ implies that in different regions the universe expanded at different rates leading to temperature differences. Explicitly, we write

$$C_l^{TT} = \int \frac{d^3}{(2\pi)^3} P_{\mathcal{R}}(k) T_l^2(k) \tag{2.27}$$

[1]Note that TT refers to the fact that we are dealing with correlations between temperature fluctuations. There are other channels due to the radiation's polarization. These are referred to as E-modes and B-modes.

where $P_{\mathcal{R}}(k)$ is the power spectrum associated with the Fourier transform of the curvature perturbation $\mathcal{R}_k(t)$. It is defined as the two-point correlation function of $\mathcal{R}(t,x)$ in Fourier space

$$\langle \mathcal{R}_k \mathcal{R}_{k'} \rangle = (2\pi)^3 \delta(k+k') P_{\mathcal{R}}(k) \tag{2.28}$$

The transfer function T_l, on the other hand, is a complicated expression with its detailed form usually being computed numerically. Crucially, however, it depends only on *known* physics and hence one can connect theoretical predictions with the observations stemming from the CMB. In order to evaluate the degree to which early universe models predict a scale invariant and deviations thereof, it is useful to define the variance $\Delta^2_{\mathcal{R}}$ and spectral index n_s, associated with the power spectrum of the curvature perturbations, as

$$\Delta^2_{\mathcal{R}} = \frac{k^3}{2\pi^2} P_{\mathcal{R}} \qquad n_s = 1 - \frac{d \ln \Delta^2_{\mathcal{R}}}{d \ln k} \tag{2.29}$$

$n_s = 1$ corresponds to a scale-invariant spectrum. For convenience in calculating one often assumes that the variance takes on the form of a power law

$$\Delta^2_{\mathcal{R}} = \mathcal{A}_{\mathcal{R}} = \left(\frac{k}{\tilde{k}} \right)^{n_s - 1} \tag{2.30}$$

where the Pivot scale $\tilde{k}$ is some reference scale which the PLANCK satellite gives as $\tilde{k} = 0.05 Mpc^{-1}$. With these definitions, the experimentally measured results (with 1σ errors) are [34]:

$$\mathcal{A}_{\mathcal{R}} = (2.139 \pm 0.063) \times 10^{-9} \tag{2.31}$$

$$n_s = 0.9677 \pm 0.0060 \tag{2.32}$$

meaning that the spectrum is, in fact, not entirely scale invariant - even though to a very large degree it is - but slightly red (i.e. there is more power on larger scales). Having established that the standard model of cosmology matches the data very well, we now highlight some puzzles and problems that require further explanation.

2.5 Problems of the Big Bang model

While there are is no observational tension of the ΛCDM model of cosmology with experiments, there remain many mysteries and puzzles of theoretical nature that beg to be addressed.

2.5.1 The singularity problem

When the scale factor a of the flat FLRW model becomes zero, the metric becomes singular. This is a curvature singularity as at the same time coordinate invariants such as the Ricci scalar become infinite. The conditions for when this happens have been generalized to arbitrary metrics by Penrose and Hawking in their famous singularity theorems [35]. They state that as long as all the matter in the universe satisfies certain energy conditions, general relativity predicts a singularity in the past. Qualitatively, this singularity is more troubling than the ones found in black holes as we are separated from those by a horizon. The cosmological one, on the other hand, lies in everyone's past and therefore affects the evolution of everything. Sometimes this extraordinary event is interpreted as the beginning of space and time and the beginning of the universe. However, such an interpretation is not justified as it simply signifies that it lies in a regime where the universe is no longer well described by General Relativity. There are two main approaches to deal with the cosmological singularity. It either gets resolved by a quantum theory of gravity or it is avoided by violating an assumption in the Hawking-Penrose theorems. It is the fundamental goal of this thesis to advance our understanding of the cosmological singularity and will consider complementary solutions that fall in both categories.

2.5.2 The flatness problem

Dividing the Friedmann equation 2.17 by $(H/H_0)^2$ gives

$$1 = \frac{\Omega_{r,c}H_0^2}{a^4H^2} + \frac{\Omega_{m,c}H_0^2}{a^3H^2} + \frac{\Omega_k H_0^2}{a^2H^2} + \frac{\Omega_\Lambda H_0^2}{H^2} \tag{2.33}$$

We have seen before that if an ideal fluid dominates the evolution of the universe we have an explicit expression for the scale factor. Hence the comoving Hubble horizon can be deduced to be

$$(aH)^{-1} \approx \begin{cases} a & \text{radiation domination} \\ \sqrt{a} & \text{matter domination} \end{cases} \tag{2.34}$$

This implies that during matter and radiation domination, the relative energy contribution due to curvature was increasing since a is increasing. Today we measure $\Omega_k = -0.005 \pm 0.017$. Comparing the curvature at the electro-weak scale (at $\approx 1TeV$) to the one at radiation-matter equality (at $\approx 1eV$) implies a growth by a factor of 10^{24}. Depending on where one starts to count, (for example instead of the electro-weak scale one could start at the grand unified

scale) the problem gets even worse. Therefore, it is surprising why this quantity is so small today.

2.5.3 The horizon problem

The comoving particle horizon τ is the maximum distance a light ray can travel between times 0 and t and is defined as

$$\tau = \int_0^\infty \frac{dt'}{a(t')} = \int_0^a \frac{da}{a^2 H} = \int_0^a d\ln a \left(\frac{1}{aH}\right) \tag{2.35}$$

where we expressed it in terms of the comoving Hubble horizon. Just like in the last section for $\epsilon > 1$ the comoving Hubble horizon grows which in turn implies that the comoving particle horizon grows with time. This means that the fraction of the universe which is in causal contact increases with time, presenting a puzzle: At time when the CMB was emitted the universe was already homogenous and isotropic at its largest scales. If the comoving Hubble horizon was increasing beforehand, a large number of causally disconnected regions all had to have the same temperature up to a hundreth of a percent. Note that we could trace the origin of both the flatness and the horizon problem to the growth of the comoving Hubble horizon which suggests a common solution for both problems.

2.5.4 The topological defects puzzle

The symmetries of the standard model are likely to be part of a larger symmetry group in the early universe. These extra symmetries would have been broken in the early universe as it expanded and cooled. However, as they break, they inevitably form topological defects such as magnetic monopoles, domain walls or cosmic strings. So far these defects have not been observed and one might wonder why.

2.5.5 The classicality puzzle

The most fundamental theories to date are General Relativity and Quantum Mechanics. Nevertheless, we do not describe space and time quantum mechanically but classically instead. In the late universe decoherence explains why this assumption is justified. However, it is likely that the creation of space-time was a pre-dominantly quantum effect. As such we ought to include quantum mechanics in our description of the early universe and at the same time strive for a dynamic mechanism which explains the classicality of space-time.

3 Beyond the Standard Model of Cosmology

3.1 Inflation

As illustrated in the last section, both the horizon and the flatness problems arise because the co-moving Hubble radius $1/aH$ grows in an expanding universe, dominated by any of the matter sources discussed above. Hence it is feasible that a prior phase in which the co-moving Hubble radius was shrinking by the same or larger magnitude than the subsequent growth, solves both problems [12, 13, 14, 15] (see Fig. 2)

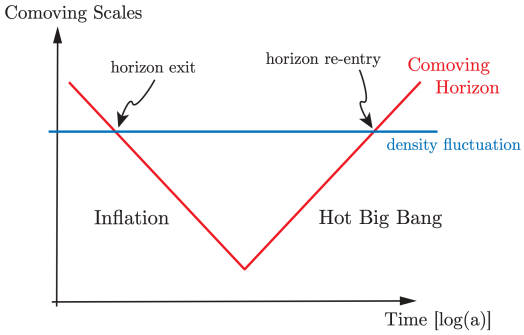

Figure 2: During inflation the co-moving Hubble radius $(aH)^{-1}$ as indicated by the red line. That means that at any given point in time, scales with wavenumber k leave the horizon only to re-enter it again in the subsequent hot big bang evolution. The figure is taken from [15].

If we assume an expanding universe, then a shrinking of the co-moving Hubble radius during that time implies that

$$\frac{d}{dt}\left(\frac{1}{aH}\right) < 0 \quad \rightarrow \quad \frac{d}{dt}\left(\frac{1}{\dot{a}}\right) < 0 \quad \rightarrow \quad \ddot{a} > 0 \tag{3.1}$$

since an expanding universe means that $\dot{a} > 0$. This condition is the essence of inflation. How can we obtain such a phase? The acceleration equation (2.13) tells us that to obtain $\ddot{a} > 0$, we require

$$-2(\rho + 3p) > 0 \tag{3.2}$$

or, written in terms of the equation of state

$$-\frac{1}{3}\rho(\epsilon - 1) < 0 \tag{3.3}$$

Therefore, if we the universe is dominated by matter that has $\epsilon < 1$ (or in more physical terms, sufficiently negative pressure $p < -\frac{1}{3}\rho$), inflation will happen.

Inflation is a period of accelerated expansion, dominated by a sufficiently negative pressure energy component.

In the following sections we will examine more closely how inflation can be modelled in practice?

3.1.1 De Sitter space

In fact, we have already encountered one example of an inflationary matter type: The cosmological constant Λ. When the universe is dominated by a positive cosmological constant, the Einstein equations can be solved for any curvature. The solution is called de Sitter space-time and is given by FLRW metric where the scale factor $a(t)$ takes on the form

$$a(t) = \begin{cases} \frac{1}{H}\sinh(Ht) & \text{for } k = -1 \\ e^{Ht} & \text{for } k = 0 \\ \frac{1}{H}\cosh(Ht) & \text{for } k = 1 \end{cases} \tag{3.4}$$

Locally these metrics describe the same space-time but they correspond to different ways of slicing the 3-dimensional spatial sections. This is possible to the special structure of de Sitter: It is a maximally symmetric space-time (i.e. in four dimensions it has ten killing vectors) just like Minkowski space-time. Globally, however, the structure is different as, for example, only the closed, $k = 1$, slicing covers the whole space-time. The hypberbolic global structure of de Sitter space can be investigated by considering its embedding in flat five-dimensional Minkowski space. As can be seen from Eq. (3.4), the scale factor grows exponentially while the universe is dominated by a cosmological constant and provides the simplest inflationary model.

3.1.2 Slow-roll inflation

More generally, inflation can be modelled by the dynamics of a scalar field evolving in an appropriate potential $V(\phi)$, which is chosen in precisely such a way that inflation can happen. The stress energy tensor for a scalar field which is minimally coupled to gravity is given by

$$T_{\mu\nu} = \phi_{,\mu}\phi_{,\nu} - g_{\mu\nu}\left(\frac{1}{2}\phi^{,\sigma}\phi_{,\sigma} + V(\phi)\right) \tag{3.5}$$

and the field equation of motion is

$$\frac{1}{\sqrt{-g}}\left(\sqrt{-g}\phi^{,\mu}\right)_{,\mu} + V_{,\phi} = 0 \tag{3.6}$$

Then, assuming the FLRW metric for $g_{\mu\nu}$ and a homogeneous field (i.e a field obeying $\phi(x,t) = \phi(t)$), the energy-momentum tensor for it, reduces to the form of a perfect fluid with

$$\rho_\phi = \frac{1}{2}\dot{\phi}^2 + V(\phi) \tag{3.7}$$

$$p_\phi = \frac{1}{2}\dot{\phi}^2 - V(\phi) \tag{3.8}$$

Therefore we find that the equation of state is given by

$$\frac{2}{3}\epsilon - 1 = \frac{\frac{1}{2}\dot{\phi}^2 - V(\phi)}{\frac{1}{2}\dot{\phi}^2 + V(\phi)} \qquad \rightarrow \qquad \epsilon = 3\frac{\dot{\phi}^2}{\dot{\phi}^2 + 2V(\phi)} \tag{3.9}$$

and conclude that if the potential energy $V(\phi)$ is larger than twice the kinetic energy $\frac{1}{2}\dot{\phi}^2$ the universe undergoes inflation. That is, the condition for inflation to happen is that the scalar field's dynamics is potential dominated $V(\phi) > \dot{\phi}^2$. The equations of motion for the scale factor and scalar field as well as the constraint are given by

$$3H^2 = \frac{1}{2}\dot{\phi}^2 + V(\phi) \tag{3.10}$$

$$\dot{H} = -\frac{1}{2}\dot{\phi}^2 \tag{3.11}$$

$$\ddot{\phi} + 3H\dot{\phi} + V_{,\phi} = 0 \tag{3.12}$$

only two of which are linearly independent. Using these equations, we can re-express ϵ in a variety of ways, all of which are useful in different contexts.

$$\epsilon = -\frac{\dot{H}}{H^2} = \frac{1}{2}\frac{\dot{\phi}^2}{H^2} \tag{3.13}$$

An observationally viable scenario of inflation is when the equation of state is very small $\epsilon << 1$ and remains that way over extended period of time $\ddot{\phi} << H\dot{\phi}$. This is the so-called slow-roll regime as the kinetic energy of the scalar field is vastly dominated by the potential energy $\frac{1}{2}\dot{\phi}^2 << V(\phi)$. In that regime the equations of motion can be approximated as

$$3H^2 \approx V(\phi) \tag{3.14}$$

$$\dot{H} = -\frac{1}{2}\dot{\phi}^2 \tag{3.15}$$

$$3H\dot{\phi} \approx -V_{,\phi} \tag{3.16}$$

and $\epsilon \approx \frac{1}{2}\frac{V_{,\phi}^2}{V^2}$ is usually called the (first) slow-roll parameter. Higher order slow-roll parameters may be defined in analogy to

$$\epsilon = -\frac{d\ln H}{d\ln a} \tag{3.17}$$

For example the second slow-roll parameter η is defined as

$$\eta = -\frac{d\ln \epsilon}{d\ln a} \tag{3.18}$$

The fact that the scale factor needs to roll slowly over an extended period of time is then quantified by setting $\eta << 1$. Using this approximation is particularly useful because in that case we can solve the equations of motion by expanding the Hubble rate and scalar field as a Taylor series in time. To first order we obtain

$$a(t) \approx a_0 \exp\left(\sqrt{\frac{V}{3}}t - \frac{\epsilon V}{6}t^2\right) \tag{3.19}$$

$$\phi(t) \approx \phi_0 - \sqrt{\frac{2\epsilon V}{3}}t \tag{3.20}$$

where a_0 and ϕ_0 are integration constants.

3.1.3 The end of inflation?

In order to match the CMB observations, it is necessary that inflation lasts for a certain amount of time. In terms of the number of e-folds defined via

$$N = \ln a|H| \tag{3.21}$$

we require $N \approx 60$. In that case, inflation resolves, the flatness and horizon problem and creates quantum fluctuations consistent with the ones observed on the CMB. Inflation ends when the scalar fields leaves the region where $\epsilon < 1$ and oscillates around a minimum in the potential. That phase is called reheating because during this phase, the scalar field acts like pressure-less matter which decays into the particles found in the standard model and the usual Hot Big Bang commences. It is important to mention here that this is the desired behaviour of the inflation. However, the exact nature of reheating is very ill understood especially since we do not know what particle the inflation is precisely. Conceptually, the idea of reheating was that it ends inflation everywhere in the universe. These hopes were quickly extinguished by the discovery of eternal inflation.

3.1.4 Eternal inflation

An important characteristic of inflation is that once it starts it never ends globally [29, 36]. There are two mechanisms leading to eternal inflation. In one scenario the inflaton is in a metastable state often called the "false vacuum". During inflation parts of the false vacuum decay and create a "pocket" universe [29]. The creation of these pocket universes will go on forever as pieces of the exponentially expanding false vacuum region undergo decay. There even has been effort recently to include semi-classical effects within this picture which confirmed the standard results [37]. We will take a closer look at false vacuum decay in chapter 5.

The second mechanism is called slow-roll eternal inflation [30] which may occur when $\epsilon < 1$. In the usual cosmological perturbation theory, the constraints show that when the slow-roll parameter is very small, $\epsilon \ll 1$, the metric perturbations are negligible compared to the scalar field fluctuations $\delta\phi$ since they are suppressed by factors of $\sqrt{\epsilon}$. This is the basis for the standard intuition that in slow-roll inflation one may think of the background space-time as being constant, with only the scalar field fluctuating.

This picture is reinforced by the fact that at cubic order in interactions, up to a numerical factor of order one, the leading contribution in the Lagrangian is a term of the form $\sqrt{\epsilon}(\dot{\delta\phi})^2\delta\phi$, which is also small in the slow-roll limit. Hence, in the presence of a very flat potential, the system is perturbative. In other words, to a first approximation the system is described by free scalar field fluctuations in a fixed geometry.

In flat gauge the comoving curvature perturbation (we review cosmological perturbation theory briefly in appendix B) is given by $\mathcal{R} = \psi - \frac{H}{\dot{\phi}}\delta\phi = -\frac{H}{\dot{\phi}}\delta\phi \approx -\frac{1}{\sqrt{2\epsilon}}\delta\phi$. A classic calculation shows that inflation amplifies quantum fluctuations and induces a variance of the curvature perturbation which on super-Hubble scales and in the slow-roll limit is given by [38, 39, 40, 41]

$$\Delta^2_{\mathcal{R}} = \frac{H^2}{8\pi^2\epsilon}\,. \tag{3.22}$$

The relation between the curvature perturbation and the scalar field perturbation then implies that the variance of the scalar field is given by

$$\Delta\phi_{qu} \equiv \langle(\delta\phi)^2\rangle^{1/2} = \frac{H}{2\pi}\,. \tag{3.23}$$

This is the typical quantum induced change in the scalar field value during one Hubble time. By comparison, the classical rolling of the scalar field during the same time interval induces

a change

$$\Delta\phi_{cl} \equiv \frac{|\dot{\phi}|}{H} \tag{3.24}$$

Note that the quantum fluctuation dominates over the classical rolling when

$$\Delta\phi_{qu} > \Delta\phi_{cl} \quad \leftrightarrow \quad \frac{H^2}{2\pi|\dot{\phi}|} \approx \frac{H}{\sqrt{8\pi\epsilon}} > 1 \quad \leftrightarrow \quad \Delta^2_{\mathcal{R}} > 1\,, \tag{3.25}$$

i.e. precisely when the variance of the curvature perturbation is larger than one, and when perturbation theory becomes questionable. In this regime, inflation is thought to be eternal, leading to severe paradoxes in its interpretation [18]. There has been significant activity in analyzing eternal inflation, via false vacuum decay [42] or during slow roll inflation, within the framework of stochastic inflation [43, 44, 45]. The stochastic approach also relies on the separation of classical background and quantum fluctuations rendering a similar outcome to the usual calculation unsurprising. In chapter 8 we will set-up a framework that will allow us to go beyond this treatment and quantize both the scale factor and scalar field simultaneously. Thus we provide a set-up to study eternal inflation in a more consistent fashion.

3.2 Ekpyrosis

The crucial insight to arrive at the concept of inflation was the observation that the Hubble horizon had to shrink in the early universe in order to solve the flatness and horizon problems. This immediately led to a phase of accelerated expansion. However, we made the assumption that the universe was expanding by imposing $\dot{a} > 0$. What happens if instead we had a contracting phase? Now the horizon problem is trivially solved since the contracting phase gives ample time for the entire observable universe to have been in causal contact, if it lasts long enough [16, 17]. The arguments for the other puzzles now reverse and other challenges arise. Let's go back to the Friedmann equation but now also include the contributions from anisotropies σ:

$$3H^2 = \Lambda - \frac{3k}{a^2} + \frac{\rho_m}{a^3} + \frac{\rho_r}{a^4} + \frac{\sigma^2}{a^6} + \cdots + \frac{\rho_\phi}{a^{2\epsilon}} \tag{3.26}$$

The reason why σ scales like a^{-6} can be seen by considering a metric more general than FLRW, which allows for anisotropies. The Bianchi I metric is an example of such a metric which reads:

$$ds^2 = -dt^2 + a(t)^2 e^{2\beta_i} dx_i^2 \tag{3.27}$$

where $\sum_i \beta_i = 0$ such that $a(t)$ is the average scale factor while the β_is describe the anisotropies in the three spatial directions. Consequently, the Friedmann equation is augmented by an extra term

$$3H^2 = \Lambda - \frac{3k}{a^2} + \frac{1}{2}\sum_i \dot{\beta}_i^2 \tag{3.28}$$

At the same time, the ij Einstein Equations yield a dynamical equation for the anisotropies

$$\ddot{\beta} + 3H\dot{\beta} = 0 \tag{3.29}$$

It is straightforward to solve this equation yielding $\dot{\beta} \propto \frac{1}{a^3}$. Therefore, the anisotropies as they appear in the Friedmann equation fall off as $\dot{\beta}_i^2 \propto a^{-6}$ which is what we wanted to show. Hence in a contracting universe the anisotropies will eventually dominate over the conventional matter types. Since this would leave us with a highly anisotropic universe, in contradiction with observations, we need a matter type to suppress the energy in the anisotropies - that is one scaling with a higher negative power than a^{-6}. To do that we can therefore introduce a scalar field for which we require $\epsilon > 3$ or equivalently $p > \rho$. This is the defining characteristic for ekpyrosis.

Ekpyrosis is period of contraction, dominated by a high pressure energy component.

3.3 Scaling solutions

Upon adding a scalar field, GR's equations of motion can no longer be solved analytically for any potential and typically some approximations (like the slow-roll conditions)are invoked. However, there does exist a family of potentials for which the equations can be solved. Taking an exponential potential (plotted in Fig. 3)

$$V = V_0 e^{-\sqrt{2\epsilon}\phi} \tag{3.30}$$

gives two different solutions when evaluating the equations of motions depending on the sign of the pre-factor V_0 and the magnitude of ϵ. For positive V_0 and $\epsilon < 3$ we obtain an expanding solution

$$a(t) = a_0 t^{1/\epsilon} \qquad \phi(t) = \frac{1}{\sqrt{2\epsilon}} \ln\left(\frac{V_0\epsilon^2}{3-\epsilon}t^2\right) \tag{3.31}$$

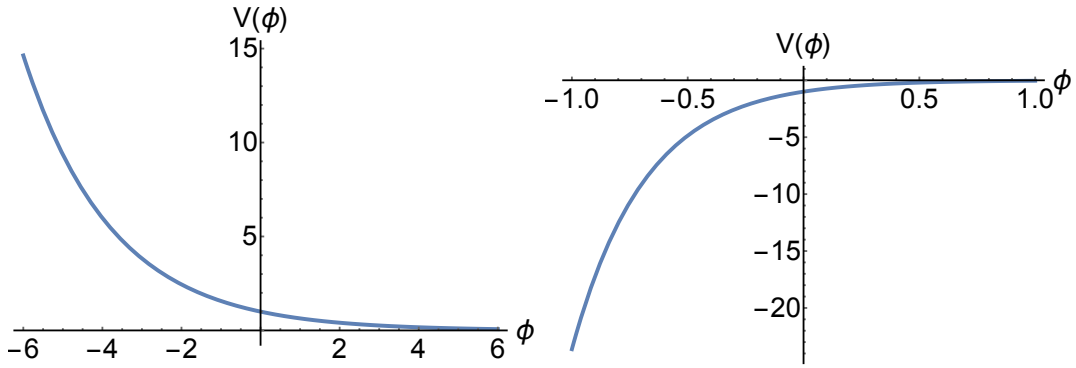

Figure 3: Representative examples of an inflationary exponential potential on the left (with $\epsilon = 1/10$ and $V_0 = 1$) and an ekpyrotic one on the right (with $\epsilon = 5$ and $V_0 = -1$).

where a_0 is an integration constant and $0 < t < \infty$ so that at $t = 0$ we have $a = 0$ corresponding to the big bang. A contracting solution can be found by setting V_0 to be negative and $\epsilon > 3$. In that case we have

$$a(t) = a_0(-t)^{1/\epsilon} \qquad \phi(t) = \frac{1}{\sqrt{2\epsilon}} \ln\left(\frac{V_0\epsilon^2}{3-\epsilon}t^2\right) \tag{3.32}$$

and the time coordinate now runs from $-\infty < t < 0$ such that at $t = 0$ a big crunch occurs where the scale factor shrinks to zero value. While these models allow us to compute salient features of inflation and ekpyrosis they cannot be a realistic description of the universe as these phases cannot end and reheating followed by the hot big bang evolution of the universe does not occur.

3.4 Problems of inflation and ekpyrosis

3.4.1 Inflation

While inflationary theory has become widely popular soon after its inception, there still remain a host of unresolved problems with the paradigm [18]. This has been worsened in recent years due to the observational constraints from experiments probing the early universe. The original idea of inflation was to have a mechanism that transforms a generic universe into the very special one we observe today: That is to say the mechanism should be able to convert an anisotropic, inhomogenous universe into an isotropic and homogenous one. As we saw however, in order for inflation to happen, the potential energy of the scalar field must dominate over its kinetic energy. Large gradients in the scalar field following from the inhomogeneity of the universe, for example, quickly lead to the universe's recollapse. It has been argued in the past that all the various components of the total energy density of the

universe should all be roughly of order one in Planck units

$$\frac{1}{2}\dot{\phi}^2 \propto V(\phi) \propto \nabla\phi \propto O(1) \tag{3.33}$$

which would allow for the potential term to quickly dominate and inflation to commence. However, due to the improved bounds on the scalar-tensor ratio r, the energy scale of inflation has to be at least three orders of magnitude below the Planck scale in order for inflation to explain the features in the CMB. Thus to get inflation started a region of roughly a billion Hubble radii needed to be homogeneous and isotropic *already*.

As a result of the PLANCK measurements it was found that power law potentials such as polynomial or exponential potentials are disfavoured and instead so-called plateau potentials like Higgs inflation or Starobinsky inflation are preferred. It turns out, however, that within the paradigm of inflation itself, inflation in a power law potential is exponentially more likely than inflation in a plateau region of the potential [46].

The final and most troubling issue with inflation is its tendency to create infinitely many universes: a behaviour called eternal inflation. Quantum mechanics is responsible for enabling the scalar field to tunnel either up the inflationary potential (so-called slow roll eternal inflation) or between different local minima (so-called false vacuum eternal inflation). The consequence is that inflation never ends globally as there are always regions in the universe where it still persists. Together with this type of multiverse comes a host of problems. First of all there, so far, does not exist a sensible measure that allows one to prescribe probabilities to different outcomes. Hence it has been said that *"anything that can happen, will happen"*, which calls into question the predictability of the theory or if it is scientific theory at all. Another unresolved issue is the "youngness paradox", which postulates that we are exponentially more likely to live in a younger universe than we do.

In the past, a primary focus of cosmologists working on inflation has been to match observations by building increasingly complex models. However, the above, fundamental, problems remain to be solved and must be addressed to have a satisfactory theory of the early universe.

3.4.2 Ekpyrosis

In order to explain the observed spectrum of perturbations, an ekpyrotic phase with a single scalar field is not sufficient since the comoving curvature perturbations are not amplified.

Instead a second one is required which introduces extra complexity and fine-tuning into the model. Furthermore, they typically predict large non-Gaussianities which have not been observed. However, the biggest challenge for any contracting model of the universe is how it transitioned to the current phase of expansion. For that to be possible the evolution of the universe's size had to have a local minimum: the bounce. A realization of a healthy bouncing cosmology is challenging and even though significant progress has been made in the last two decades, the current models typically either invoke exotic matter [47, 48] or exotic extensions of General Relativity, none of which have been observed.

3.5 Beyond FLRW: symmetries in cosmology

As we have seen, the principles of homogeneity and isotropy of the universe as a whole, are strongly ingrained in the study of cosmology. Instead of simply postulating these features, mechanisms that dynamically drive the universe towards anisotropy and homogeneity, like inflation or ekpyrosis, are an attractive alternative. In order to study how anisotropies and inhomogeneities behave it is necessary to include them in the theoretical model which we use to describe the universe and thus go beyond the FLRW metric. More generally, it is useful to classify cosmological models according to their symmetries. For this section we will follow the review of Ellis and van Elst [49] and consider continuous symmetries only.

3.5.1 Rotations and Translations

A symmetry is a transformation of the metric along some curve such that the metric remains unchanged. Such curves are generated by so-called Killing vectors ξ_i which are found by enforcing Killing's equation

$$\nabla_i \xi_j + \nabla_j \xi_i = 0 \tag{3.34}$$

where ∇ is the covariant derivative related to the metric. The set of all Killing vectors forms a Lie Algebra with basis elements $\{\xi_a\}_{a=1,2,\ldots,r}$ where r denotes the dimension of Lie Algebra. Since any Killing vector can be written as a sum of the basis elements with constant coefficients, the commutator of two Killing vectors gives another Killing vector

$$[\xi_a, \xi_b] = C^c_{ab} \xi_c \tag{3.35}$$

Considering the properties of the metric tensor, the dimension of the Lie Algebra is given by $r \leq \frac{1}{2} n(n+1)$ where n is the dimension of space-time. Continuous symmetries form a group and are generated by the Lie Algebra of Killing vectors. It is further useful to separate the

symmetries into translations and rotations. The isometry group is transitive on a surface S (of any dimension) if it can move any point in S into any other point in S. The largest surface through each point on which the group is transitive is the called the orbit whose dimension s is bounded by the dimension of space-time $s \leq n$. Rotations, on the other hand, are described by the isotropy group. At each point, the group of isometries that leave that point fixed is generated by all the Killing vectors that vanish at that point. The dimension q of the isotropy group is given by $q \leq \frac{1}{2}n(n-1)$. Of course we have $r = q + s \leq \frac{1}{2}n(n+1)$.

3.5.2 All Cosmological Models

In a cosmological setting we take the space-time dimension n to be 4 which means that the possible values for the dimension of the orbit are $s = 0, 1, 2, 3, 4$. If we assume perfect fluid models with $\rho + p \neq 0$ then the isotropy group can take values $q = 0, 1, 3$. A value of 2 is not possible because the four-velocity of the perfect fluid is invariant implying that the isotropy group at each point has to be a subgroup of the rotations which act orthogonally to the four-velocity. Therefore, it must be a subgroup of $O(3)$ which, however, does not have a two-dimensional subgroup. In simple terms, s specifies the number of coordinates that the metric is independent of while q is a measure of the anisotropy. In particular $q = 3$ corresponds to a completely isotropic metric. $q = 0$ means that it is anisotropic and $q = 1$ means that the kinematical quantities are rotationally symmetric about a preferred spatial direction. This, reduced rotational symmetry is also known as local rotational symmetry (LRS). Table (3.5.2) lists all possibilities and the names by which these models are usually referred to.

Notice that our universe is, in general, not homogenous and isotropic and hence is described by the $s = 0$ and $q = 0$ case. As we have seen earlier, the FLRW metric is a good approximation to our current universe on large scales. Tracing the evolution of the universe back to very early times however, anisotropies become of importance. When we include them in the models used in this thesis we will, for the most part, consider the metrics from the, still large, class of Bianchi models, which we will further classify next.

3.5.3 The Bianchi Classification

A very simple way of classifying all metrics that have $s = 3$, $q = 0$ or in other words metrics that are spatially homogeneous but completely anisotropic, is by using an orthonormal tetrad [50]. The formalism is based on the fact that we are dealing with a spatially homogeneous metric and hence we can choose one basis vector to be the one orthonormal to the surfaces

	q = 0 anisotropic	q = 1 LRS	q = 3 isotropic
s = 0 inhomogeneous	Szekeres-Szafron Swiss-cheese models	-	-
s = 1 inhomogeneous	General metric indep. of one coordinate	-	-
s = 2 inhomogeneous	General metric indep. of two coordinates	Lemaitre-Tolman- Bondi family	-
s = 3 spatially homog.	Bianchi models	Kantowski-Sachs Axial Bianchi models	FLRW
s = 4 space-time homog.	Osvath/Kerr	Gödel metric	Einstein's static universe

Table 1: A list of all possible cosmological models, categorized by their translational and rotational symmetries.

of homogeneity. The tetrad basis further chosen in such a way that it is invariant under the group of isometries. In that case the basis elements obey the commutation relation

$$[e_a, e_b] = \gamma^c_{ab}(t)\xi_c \tag{3.36}$$

where the γ^c_{ab} are equivalent to the structure constants of the Lie Algebra that generate the isometries C^c_{ab} and the latin indices run from 0 to 4. It can be shown that γ^c_{ab} can be decomposed as $\gamma^c_{ab} = n_{ab}a^c$. Finally, invoking the fact that the tetrad basis needs to satisfy the Jacobi identity we obtain

$$n_{ab}a^b = 0 \tag{3.37}$$

Without loss of generalization, one can choose [50] the tetrad basis to diagonalise $n_{ab} = (n_1, n_2, n_3)$ and set $a^c = (a, 0, 0)$ reducing the Jacobi identity to

$$n_1 a = 0 \tag{3.38}$$

Hence we have to classes of Bianchi models. The ones (sometimes referred to as class A) which have $a = 0$ (and n_1 can be chosen freely) and the ones (class B) that have $n_1 = 0$ (and a can be chosen freely). Table (3.5.3) lists all possible combinations of a, n_1, n_2, n_3 which obey the Jacobi identity.

Type	a	n_1	n_2	n_3
I	0	0	0	0
II	0	+ve	0	0
VI_0	0	+ve	-ve	0
VII_0	0	+ve	+ve	0
VIII	0	+ve	+ve	-ve
IX	0	+ve	+ve	+ve
V	+ve	0	0	0
IV	+ve	0	0	+ve
VI_h	+ve	0	+ve	-ve
VII_h	+ve	0	+ve	+ve

Table 2: A list of all possible Bianchi models. Type III is absent because it is a subclass of type VI_h. The parameter h is given by $h = a^2/n_2n_3$. It is important to note the special role of types I,V, and IX since they include the flat, open and closed FLRW models as subcases respectively.

Having written down all possible structure constants, we can obtain the metric by writing

$$ds^2 = g_{\mu\nu}\omega^\mu\omega^\nu \tag{3.39}$$

where the ωs provide a basis of one-forms. It can be shown that their exterior derivative is related to the structure constants via

$$d\omega^\mu = -\frac{1}{2}C^\mu_{\alpha\beta}\omega^\alpha \tag{3.40}$$

We will be particularly interested in the Bianchi IX case which we will turn to next.

3.5.4 Bianchi IX

Physically, one can think of the spatial part of this metric as an evolving three-sphere with two different squashing parameters, so that it represents an anisotropic generalisation of a closed Robertson-Walker spacetime. An alternative point of view is that Bianchi IX represents a fully non-linear completion of a gravitational wave, again in a closed cosmology. More quantitatively, the Bianchi IX metric takes the form [51, 52],

$$ds^2_{IX} = -N^2(t)dt^2 + \sum_m \left(\frac{l_m(t)}{2}\right)^2 \sigma^2_m\,, \tag{3.41}$$

where $\sigma_1 = \sin\psi d\theta - \cos\psi \sin\theta d\varphi$, $\sigma_2 = \cos\psi d\theta + \sin\psi \sin\theta d\varphi$, and $\sigma_3 = -(d\psi + \cos\theta d\varphi)$ are differential forms on the three sphere such that $0 \leq \psi \leq 4\pi$, $0 \leq \theta \leq \pi$, and $0 \leq \phi \leq 2\pi$. For our purposes, it is most useful to consider General Relativity coupled to a scalar field ϕ moving in a potential $V(\phi)$,

$$S = \int d^4x\sqrt{-g}\left(\frac{R}{2} - \frac{1}{2}g^{\mu\nu}\partial_\mu\phi\,\partial_\nu\phi - V(\phi)\right), \tag{3.42}$$

where we are using natural units $8\pi G = c = \hbar = 1$. It is particularly useful to re-write the three scale factors as (we will employ the original definition of Misner [52] – note that some authors re-scale the βs by a factor of 2),

$$l_1(t) = a(t)\exp\left(\frac{1}{2}\left(\beta_+(t) + \sqrt{3}\beta_-(t)\right)\right) \tag{3.43}$$

$$l_2(t) = a(t)\exp\left(\frac{1}{2}\left(\beta_+(t) - \sqrt{3}\beta_-(t)\right)\right) \tag{3.44}$$

$$l_3(t) = a(t)\exp\left(-\beta_+(t)\right) \tag{3.45}$$

which makes it obvious that a will yield information about volume change while the βs quantify shape change. When $\beta_- = \beta_+ = 0$ one recovers the isotropic case. The Lorentzian action in these coordinates becomes

$$S = 2\pi^2\int dtNa\left[\frac{1}{N^2}\left(-3\dot{a}^2 + a^2\left(\frac{1}{2}\dot{\phi}^2 + \frac{3}{4}\dot{\beta}_+^2 + \frac{3}{4}\dot{\beta}_-^2\right)\right) - \left(a^2V(\phi) + U(\beta_+,\beta_-)\right)\right], \tag{3.46}$$

where

$$U(\beta_+,\beta_-) = -2\left(e^{2\beta_+} + e^{-\beta_+ - \sqrt{3}\beta_-} + e^{-\beta_+ + \sqrt{3}\beta_-}\right) + \left(e^{-4\beta_+} + e^{2\beta_+ - 2\sqrt{3}\beta_-} + e^{2\beta_+ + 2\sqrt{3}\beta_-}\right). \tag{3.47}$$

Varying with respect to the lapse N we obtain the Friedman constraint equation

$$3\dot{a}^2 = a^2\left(\frac{1}{2}\dot{\phi}^2 + \frac{3}{4}\dot{\beta}_+^2 + \frac{3}{4}\dot{\beta}_-^2\right) + N^2\left(a^2V(\phi) + U(\beta_+,\beta_-)\right), \tag{3.48}$$

while the equations of motion for a, β_+, β_- are given by

$$\frac{\ddot{a}}{a} + \frac{1}{2}\frac{\dot{a}^2}{a^2} - \frac{2}{aN}\dot{a}\dot{N} + \frac{3}{8}\left(\dot{\beta}_+^2 + \dot{\beta}_-^2\right) - \frac{N^2}{6a^2}U(\beta_+,\beta_-) + \frac{1}{2}\left(\frac{1}{2}\dot{\phi}^2 - N^2V(\phi)\right) = 0, \tag{3.49}$$

$$\ddot{\beta}_+ + 3\frac{\dot{a}}{a}\dot{\beta}_+ - \frac{\dot{N}}{N}\dot{\beta}_+ + \frac{2}{3}\frac{N^2}{a^2}U_{,\beta_+} = 0, \tag{3.50}$$

$$\ddot{\beta}_- + 3\frac{\dot{a}}{a}\dot{\beta}_- - \frac{\dot{N}}{N}\dot{\beta}_- + \frac{2}{3}\frac{N^2}{a^2}U_{,\beta_-} = 0. \tag{3.51}$$

Finally we have the equation for the scalar field,

$$\ddot{\phi} + 3\frac{\dot{a}}{a}\dot{\phi} - \frac{\dot{N}}{N}\dot{\phi} + N^2V_{,\phi} = 0. \tag{3.52}$$

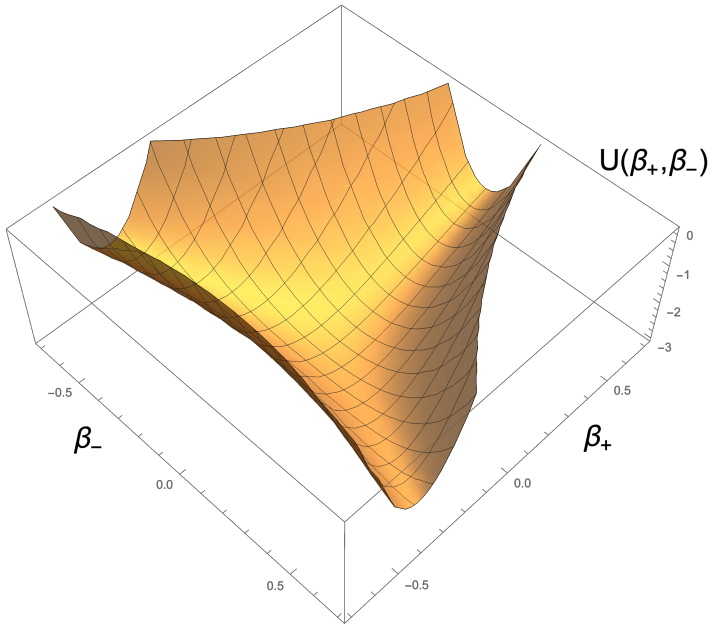

Figure 4: The anisotropy potential $U(\beta_+, \beta_-)$. The minimum is at $U(0,0) = -3$. Around the minimum the potential has an approximate circular symmetry, while at larger values of the anisotropy parameters it has the symmetries of an equilateral triangle. The potential asymptotes to zero from below in the "corner" directions.

One can simplify the equation for a by plugging in the Friedman constraint (4.48) into it. Then we get

$$\frac{\ddot{a}}{a} + \frac{1}{2}\left(\dot{\beta}_+^2 + \dot{\beta}_-^2\right) + \frac{1}{3}\left(\dot{\phi}^2 - N^2 V(\phi)\right) = 0\,. \tag{3.53}$$

Similarly, once we have a solution to the equations of motion, we can simplify the calculation of the value of the on-shell action by plugging in the Friedman equation 3.48,

$$S_{on-shell} = -4\pi^2 \int dt N a \left[U(\beta_+, \beta_-) + a^2 V(\phi)\right]\,. \tag{3.54}$$

In the numerical calculations, it turns out to be computationally favourable if one eliminates the $U(\beta_+, \beta_-)$ potential from the action. In that case the action becomes

$$S_{on-shell} = 6\pi^2 \int dt \frac{a^3}{N}\left(-2\dot{a}^2 + \frac{1}{2}(\dot{\beta}_+^2 + \dot{\beta}_-^2) + \frac{1}{3}\dot{\phi}^2\right)\,. \tag{3.55}$$

The potential for the anisotropy parameters $\beta_\pm$ is shown in Fig. 4. For small βs it is given approximately by

$$U(\beta_+, \beta_-) \approx -3 + 6\left(\beta_+^2 + \beta_-^2\right), \tag{3.56}$$

and hence near the origin it has a circular symmetry. For larger anisotropies, the potential becomes exponentially steep and has the symmetry of an equilateral triangle, with one axis of symmetry being the $\beta_- = 0$ line [52]. This forms the basis for describing the dynamics close to a cosmological singularity as that of a ball on this (or a closely related) effective triangular billiard table [53] (with different boundary conditions, this system has also been quantised [54, 55]). Here we will however not need the billiards description.

3.6 Beyond General Relativity

General Relativity is the simplest theory of gravity we know of that perfectly fits all experiments that have been performed so far. It has been tested and verified for a wide range of parameters, putting it on extremely firm ground. Nevertheless, the existence of singularities in the theory and the fact that it is not renormalizable indicate that it is interesting to consider alternative theories of gravity. These must, of course, reproduce the predictions of General Relativity in the regimes for which it has been already tested. Nevertheless there are a host of interesting alternatives such as e.g massive gravity [56], tensor theories such as f(R) gravity [57] and scalar-tensor theories such as Brans-Dicke theory [58]. Some of them can help tremendously with the early universe puzzles described above. It is our attitude in this thesis to focus on pure General Relativity only with one exception. Horava-Lifshitz gravity [31, 59] is an alternative theory of gravity that does not have Lorentz symmetry has its fundamental symmetry but is fully renormalizable. At low energies it recovers General Relativity but the behaviour at high energies is different due to the inclusion of higher curvature terms. In the appendix we describe the theory in detail and show that the flatness and horizon problem are solved automatically, without the need for inflation or ekpyrosis. The theory also provides a natural dark matter candidate and provides a near scale invariant spectrum of primordial perturbations. In the appendix we further show that the horizon and flatness problem can be solved in any modified gravity theory that has an appropriately modified dispersion relation.

4 Classically Bouncing Cosmologies

In the last section we have seen that the main challenge for ekpyrotic models or any kind of cyclic model is transitioning from contraction to expansion. One of the main hurdles that must be overcome in any model of the universe that contains such a bounce is a set of theorems known as the Hawking-Penrose singularity theorems [35]. They show on rather general grounds and in particular, in the presence of matter that satisfies the null energy

condition, that the current expansion of the universe must have been proceeded by a curvature singularity. In the simplest example of flat FLRW cosmology this can be seen directly from the Friedman equations:

$$\dot{H} = -\frac{1}{2}(\rho + p) \tag{4.1}$$

Having a bounce corresponds to taking $H(t_b) = 0$ while simultaneously ensuring that $\ddot{a}(t_b) > 0$ so that expansion follows from the universe reaching its smallest size at t_b. Immediately we see that these conditions require a violation of the null-energy condition (NEC) $\rho + p > 0$. There is, however, a caveat to the singularity theorems when one considers the combination of a positive cosmological constant and positive spatial curvature. [60]. The most well-known example is pure de Sitter space in closed coordinates. The metric is then given by [2]

$$ds^2 = -dt^2 + \ell \cosh\left(\frac{t}{\ell}\right)^2 d\Omega_3^2\,, \tag{4.2}$$

and it solves Einstein's equations in the presence of a cosmological constant $\Lambda = 3\ell^{-2}$,

$$R_{\mu\nu} = \frac{3}{\ell^2} g_{\mu\nu}\ . \tag{4.3}$$

Other approaches rely either on exotic matter - that is to say matter that has not been observed in our universe though theoretically possible - or exotic theories where gravity is no longer described by general relativity. Much studied in recent times have been exotic matter models that allow for violations of the null energy condition while being carefully constructed to avoid a myriad of potential pathologies, such as ghosts, gradient instabilities and causality violations, see e.g. [61, 62, 63, 64, 65, 66]. However, there exists a simple manner in which the singularity theorems may also be avoided, namely by having a spatially closed universe and matter violating only the strong energy condition [60]. This is in no way exotic, as dark energy is known to have a pressure that is equal to minus its energy density to better than 10 percent accuracy [67], in clear violation of the strong energy condition. The above example thus crucially relies on the existence of cosmological constant or dark energy. Moreover, although the spatial sections of our current universe are measured to be nearly flat, this is not inconsistent with the early universe having had a significant positive spatial curvature, as long as there is a mechanism that can dissipate the curvature at later times. Another alternative could be that the universe reaches very high energies during the bouncing phase

[2]Indeed, in the case of pure de Sitter space-time the bounce is an artifact of the coordinates. The de Sitter space-time is completely homogenous and isotropic. Namely, all the points on the manifold can be reached by means of a isometry. Hence, the location of the bounce is coordinate dependent.

so that we no longer trust general relativity and quantum effects become important. One then expects quantum gravitational effects to become of preeminent importance, offering a way to describe the emergence of space-time out of a quantum state (possibilities that have been put forward include for instance string gas cosmology [68] or the no-boundary state [69]). Within this chapter, which is based in its entirety on [2, 1] we will explore classically non-singular bouncing cosmologies within the framework of general relativity. In particular we will construct analytic, classically bouncing solutions that are not only inhomogenous but also anistropic and may include electro-magnetic fields. It turns out that they may be interpreted as the interior of black holes [2]. In the more general Bianchi IX setting, we analyze the space-time numerically in the presence of a cosmological constant and a scalar field. In the end we are able to put bounds on the degree of anisotropies allowed in order to obtain a bounce. Furthermore we show that a bouncing phase provides suitable initial conditions for inflation [1].

4.1 Anisotropic bounces

Having introduced the Bianchi IX metric in detail in section (3.5.4) we will now investigate whether we can construct cosmological bounces in this metric and investigate their properties. A useful way to re-write the metric is

$$ds^2 = -\frac{dt^2}{N(t)} + g(t)\sigma_1^2 + h(t)\sigma_2^2 + f(t)\sigma_3^2 \ , \tag{4.4}$$

where the differential forms are given exactly as before in equation (3.41). If we enhance the symmetry of the space-time by setting $h(t) = g(t)$, there is an exact analytic cosmology satisfying the Einstein equations with $N(t) = \frac{\sigma^2}{4\ell^4} f(t)$ and

$$f(t) = \frac{4\ell^2}{\sigma^2} \frac{t^4 + (6-\sigma)t^2 + \mu t + \sigma - 3}{t^2 + 1} \ , \tag{4.5}$$

$$g(t) = \frac{\ell^2}{\sigma}(t^2 + 1) \ . \tag{4.6}$$

The function $f(t)$ never vanishes provided

$$12 > \sigma > 3 \ , \qquad |\mu| < \frac{2}{3\sqrt{3}}(12-\sigma)\sqrt{\sigma - 3} \ , \tag{4.7}$$

and with these inequalities satisfied the solution describes a non-singular bounce. The parameter μ may be interpreted as the time asymmetry of the metric, which asymptotically approaches de Sitter space as $t \to \pm\infty$. This bouncing space-time, with two scale factors being equal, belongs to the class of metrics known as biaxial Bianchi IX. It was obtained in [70] by analytic continuation from a wormhole solution in asymptotic Anti-de Sitter space. Let us extend this solution to more general cases.

4.1.1 Adding an electromagnetic field

In order to include an electromagnetic field we may add a gauge vector of the form

$$A = q(t)\sigma_3 \, , \tag{4.8}$$

bearing in mind the symmetries of the metric. Then we need to solve the familiar Einstein-Maxwell system of equations

$$R_{\mu\nu} - \frac{1}{2}g_{\mu\nu}R + \Lambda g_{\mu\nu} = T_{\mu\nu} \, , \tag{4.9}$$

$$\nabla^\mu F_{\mu\nu} = 0 \, , \tag{4.10}$$

where

$$T_{\mu\nu} = F_{\mu\sigma}F^{\sigma}_{\nu} - \frac{1}{4}g_{\mu\nu}F_{\rho\sigma}F^{\rho\sigma} \, , \tag{4.11}$$

and

$$F_{\mu\nu} = \partial_\mu A_\nu - \partial_\nu A_\mu \tag{4.12}$$

is the anti-symmetric field-strength corresponding to A. Maxwell's equations for this gauge vector and metric ansatz reduce to a single equation,

$$\ddot{q} + \frac{\dot{g}}{g}\dot{q} + 4\frac{\ell^4}{\sigma^2}\frac{q}{g^2} = 0\,, \tag{4.13}$$

which admits the solution

$$q(t) = 2\sqrt{2}\left(\frac{q_1 t}{t^2+1} + \frac{q_2}{t^2+1} - \frac{q_2}{2}\right)\,, \tag{4.14}$$

with two integration constants q_1, q_2. The Einstein equations are solved provided

$$g(t) = \frac{\ell^2}{\sigma}(t^2+1) \tag{4.15}$$

$$f(t) = 4\frac{\ell^2}{\sigma^2}\frac{t^4 + (6-\sigma)t^2 + \mu t + \sigma - 3}{t^2+1} - 4\frac{q_1^2+q_2^2}{t^2+1}\,. \tag{4.16}$$

To eliminate the magnetic monopoles at large t is necessary to set $q_2 = 0$ – we will get back to this case later in the paper. Note that there are new constraints on the allowed parameters now, if we want to avoid reaching a singularity near $t = 0$. The absence of a curvature singularity now implies the inequalities

$$\mid \mu \mid < \frac{\sqrt{2}}{3\sqrt{3}}\frac{6\sigma\left(\sqrt{1-X}+4\right) - \sigma^2\left(1+X+\sqrt{1-X}\right) - 72}{\sqrt{\sigma\left(1+\sqrt{1-X}\right)-6}}. \tag{4.17}$$

and $\sigma_+ > \sigma > \sigma_-$ with

$$\sigma_\pm = 3\frac{4(1\pm 3)\sqrt{1-X}}{1+X+\sqrt{1-X}}, \qquad X = \frac{12(q_1^2+q_2^2)}{\ell^2} < 1\,, \tag{4.18}$$

where the bound of σ can be found by demanding that the numerator of the bound on μ never vanishes. An interesting feature of this solution is that the gauge field is non-trivial even though there is no singularity in the metric nor in the gauge field, i.e. there is no source. In fact it is the geometry alone that supports the electromagnetic field lines, and we will explore this aspect in more detail below when discussing the inhomogeneous solution. Here we simply note that the gauge potential grows in the approach to the bounce, and decays again as the universe expands, allowing electromagnetic fields to pass through the bounce.

4.2 Inhomogeneous and anisotropic bounces

Extending from the metric considered thus far, the cosmological solution can be generalised as follows,

$$\begin{aligned} ds^2 = &\ell^2\left(t^2+(\alpha y+1)^2\right)\left(-\frac{dt^2}{\Delta(t)}+\frac{dy^2}{G(y)}\right)+\frac{4\ell^2}{\sigma^2}\frac{\Delta(t)+\alpha^2 G(y)}{t^2+(\alpha y+1)^2}d\psi^2 \\ &+\frac{4\ell^2}{\sigma^2}\frac{y\left(\alpha y+2\right)\Delta(t)-\alpha\left(t^2+1\right)G(y)}{t^2+(\alpha y+1)^2}d\psi d\phi \\ &+\frac{\ell^2}{\sigma^2}\frac{\left(t^2+1\right)^2 G(y)+y^2\left(\alpha y+2\right)^2\Delta(t)}{t^2+(\alpha y+1)^2}d\phi^2\,, \end{aligned} \tag{4.19}$$

where

$$\Delta(t) = t^4+(6+\alpha^2-\sigma)t^2+\mu t+(\sigma-3)\left(1-\alpha^2\right)\,, \tag{4.20}$$

$$G(y) = \left(1-y^2\right)\left(\alpha^2 y^2+4\alpha y+\sigma\right)\,. \tag{4.21}$$

The homogeneous solutions of the previous section are recovered when $\alpha = 0$. The range of the new coordinate is $\cos(\theta) = y \in [-1,1]$. The condition $\alpha^2 < 1$ is necessary for regularity of the metric. Indeed, the would be singularity is at $t = 0$ and $y = -\frac{1}{\alpha}$, however this region can never be reached as long as $\alpha^2 < 1$. Once again we have bounds on the anisotropy parameters we are allowed to take. The effect of α on these is essentially a reduction of the parameter space to obtain non-singular solutions. We shall give the bounds on μ and σ below when discussing the charged solution. The uncharged case can be retrieved by setting the charge to zero.

This solution is a new type of everywhere regular bouncing cosmology when the range of the parameters is such that $\Delta(t)$ never vanishes. When $\Delta(t)$ has zeroes there exist black hole and cosmological horizons and the solution is Kerr-Taub-NUT-de Sitter with the standard pathological interpretation of the NUT parameter. We will comment more on this correspondence below. But when the parameters are chosen such that $\Delta(t)$ remains positive throughout, these solutions describe pathology-free non-singular bounce cosmologies. The parameter α determines the amount of inhomogeneity in the y direction.

4.2.1 Adding an electromagnetic field

We may once again add an electromagnetic field. The metric retains the same form as in (4.19), though the function Δ gets augmented by a term,

$$\Delta(t) = t^4+(6+\alpha^2-\sigma)t^2+\mu t+(\sigma-3)\left(1-\alpha^2\right)-\sigma^2\ell^{-2}\left(q_1^2+q_2^2\right)\,. \tag{4.22}$$

Regularity requires again that $\alpha^2 < 1$. $\Delta(t)$ must remain positive throughout if we want a singularity-free metric. This condition translates into the following requirement for μ

$$| \mu | < -\frac{1}{3\sqrt{6}} \frac{(12(12 - 4\sigma - \sigma\sqrt{1-\tilde{X}}) + 2\sigma^2(1 + \tilde{X} + \sqrt{1-\tilde{X}}) + \alpha^2(\alpha^2 - 23\sigma + \sigma\sqrt{1-\tilde{X}} + 84))}{\sqrt{-6 - \alpha^2 + \sigma(1 + \sqrt{1-\tilde{X}})}}, \tag{4.23}$$

while σ must reside in the range

$$\sigma_+ > \sigma > \sigma_- , \tag{4.24}$$

with

$$\sigma_\pm = \frac{3}{4} \frac{16 + 4(1-\tilde{X})^{1/2} \pm \Xi^{1/2}}{1 + (1-\tilde{X})^{1/2} + \tilde{X}} - \frac{1}{4} \frac{(1-\tilde{X})^{1/2} - 23}{1 + (1-\tilde{X})^{1/2} + \tilde{X}} \alpha^2 , \tag{4.25}$$

$$\Xi = 144(1-\tilde{X}) + 168\alpha^2 - 24\alpha^2(1-\tilde{X})^{1/2} - 72\alpha^2\tilde{X} + 58\alpha^4 - 6\alpha^4(1-\tilde{X})^{1/2} - \alpha^4\tilde{X} , \tag{4.26}$$

and $\tilde{X}$ must satisfy

$$1 \geq \tilde{X} = \frac{12(q_1^2 + q_2^2)}{\ell^2} - \frac{\alpha^2(48 + \alpha^2 - 14\sigma)}{\sigma^2} , \tag{4.27}$$

where the last condition yields a bound on the charge. The vector potential is generalised to

$$A = \frac{2\sqrt{2}}{(t^2 + (\alpha y + 1)^2)} \left(\left[\frac{q_2}{2} \left(1 + y^2\alpha^2 - t^2\right) - q_1 t \right] d\psi - \frac{y}{2} \left[q_2 \left(t^2 - 1 - y\alpha\right) + q_1 t \left(2 + \alpha y\right) \right] d\phi \right) , \tag{4.28}$$

where q_1 and q_2 are again the integration constants describing the electromagnetic field.

In order to interpret the gauge potential as giving rise to electric and magnetic fields, we should first shift the description to a local tangent frame. For this we need the vielbeine, which for the metric (4.19) are given by

$$e_t^{\bar{0}} = \frac{\ell}{\Delta(t)^{1/2}} \left(t^2 + (\alpha y + 1)^2\right)^{1/2} \qquad e_y^{\bar{1}} = \frac{\ell}{G(y)^{1/2}} \left(t^2 + (\alpha y + 1)^2\right)^{1/2} \tag{4.29}$$

$$e_\phi^{\bar{2}} = \frac{\ell}{\sigma} y(\alpha y + 2) \left(\frac{\Delta(t)}{t^2 + (\alpha y + 1)^2} \right)^{1/2} \qquad e_\psi^{\bar{2}} = 2\frac{\ell}{\sigma} \left(\frac{\Delta(t)}{t^2 + (\alpha y + 1)^2} \right)^{1/2} \tag{4.30}$$

$$e_\phi^{\bar{3}} = \frac{\ell}{\sigma}(t^2 + 1) \left(\frac{G(y)}{t^2 + (\alpha y + 1)^2} \right)^{1/2} \qquad e_\psi^{\bar{3}} = -2\alpha\frac{\ell}{\sigma} \left(\frac{G(y)}{t^2 + (\alpha y + 1)^2} \right)^{1/2} \tag{4.31}$$

and all other components are zero. Now we can define the electric and magnetic fields as they would be measured by a local free-falling observer,

$$E_{\bar{a}} = F^{\bar{0}}{}_{\bar{a}} , \qquad B_{\bar{a}} = \frac{1}{2} \epsilon_{\bar{a}bc} F^{bc} . \tag{4.32}$$

Curiously in local coordinates both the electric and the magnetic fields only point in a single spatial direction,

$$E_{\bar{2}} = -\frac{\sqrt{2}\sigma\left(q_1\left(t^2-(\alpha y+1)^2\right)-2q_2 t(\alpha y+1)\right)}{\ell^2\left(t^2+(\alpha y+1)^2\right)^2}\,, \tag{4.33}$$

$$B_{\bar{2}} = \frac{\sqrt{2}\sigma\left(q_2\left(t^2-(\alpha y+1)^2\right)+2q_1 t(\alpha y+1)\right)}{\ell^2\left(t^2+(\alpha y+1)^2\right)^2}\,, \tag{4.34}$$

and all other terms are zero. The Maxwell equations are nevertheless satisfied because the geometry provides the additional terms required. Thus the geometry supports the electric and magnetic fields, which exist without the presence of a source. The general structure of the E and B fields is that they grow in the approach of the bounce, and decay again afterwards. The integration constant q_1 corresponds to a time-symmetric electric field and an odd magnetic field (vanishing at $t = 0$), while for q_2 this correspondence is reversed. An example is shown in Fig. 5.

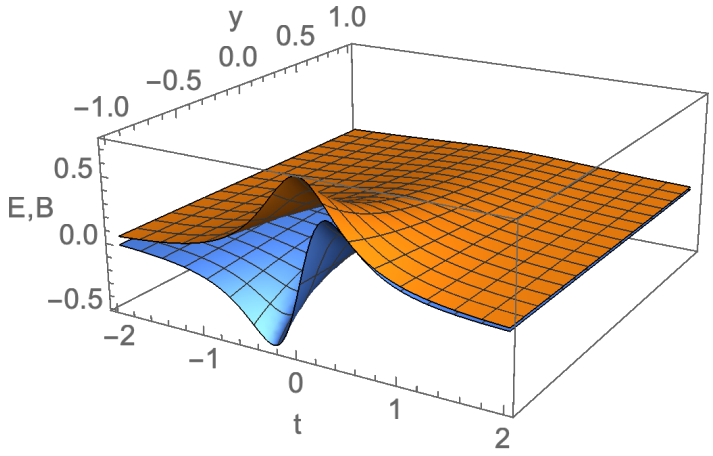

Figure 5: The local electric (in orange) and magnetic (in blue) fields for $\sigma = 4, \alpha = 1/2$, $\ell^2 = 3$, $q_1 = -1/10$ and $q_2 = 0$. For $\alpha > 0$, the growth of the fields in the approach of the bounce is largest near $y = -1$.

4.3 A black hole - bounce correspondence

In order to appreciate how cosmological and black hole metrics sometimes happen to be related to each other, it is instructive to start with the example of the familiar Schwarzschild black hole metric with mass M [71],

$$ds^2 = -\left(1-\frac{2M}{r}\right)dt^2 + \frac{dr^2}{\left(1-\frac{2M}{r}\right)} + r^2 d\Omega_2^2\,. \tag{4.35}$$

Outside the horizon, $r \geq 2M$, the spacetime is static with the curvature depending solely on the distance to the horizon. But in the interior of the black hole, $r < 2M$, the coefficients of

dt^2 and dr^2 switch sign, so that these coordinates exchange their roles – t becomes a space direction, and r a time direction. Near $r = 0$, the metric can be approximated as

$$ds^2 \approx +\frac{2M}{r}dt^2 - \frac{r}{2M}dr^2 + r^2 d\Omega_2^2 \,. \tag{4.36}$$

Now we can redefine $r \equiv T^{2/3}$ and call $t \equiv R$, with the consequence that up to some trivial re-scalings the metric becomes

$$ds^2 \approx -dT^2 + T^{-2/3}dR^2 + T^{4/3}d\Omega_2^2 \,. \tag{4.37}$$

This shows that in the black hole interior the metric is of Kantowski-Sachs type [72], i.e. it has the topology $\mathbb{R}^2 \times S^2$. Near the centre of the Schwarzschild black hole, at $T = 0$, the metric is of approximate Kasner form with exponents $(-\frac{1}{3}, \frac{2}{3}, \frac{2}{3})$. In other words, the interior of the Schwarzschild black hole is a time-dependent contracting universe ending in a big crunch singularity at $T = 0$. From the point of view of classical general relativity, this interior solution is not particularly useful (although one may speculate what the fate of the crunch may end up being in quantum gravity). But for more general black hole metrics, the interior region can be considerably more interesting.

We will be particularly interested in the Kerr-Newman-NUT-deSitter solution in Boyer-Lindquist coordinates [73],

$$\begin{aligned} ds^2 = &-\frac{Q}{\rho^2}\left[dt - \left(a\sin^2\theta + 4n\sin^2\frac{1}{2}\theta\right)d\phi\right]^2 + \frac{P}{\rho^2}\sin^2\theta\left[adt - \left(r^2 + (a+n)^2\right)d\phi\right]^2 \\ &+ \frac{\rho^2}{Q}dr^2 + \frac{\rho^2}{P}d\theta^2 \end{aligned} \tag{4.38}$$

with

$$\rho^2 = r^2 + (n + a\cos\theta)^2 \,, \tag{4.39}$$

$$P = 1 + \frac{4}{3}\Lambda an\cos\theta + \frac{1}{3}\Lambda a^2\cos^2\theta \,, \tag{4.40}$$

$$Q = (a^2 - n^2 + e^2 + g^2) - 2mr + r^2 - \Lambda\left[(a^2 - n^2)n^2 + (\frac{1}{3}a^2 + 2n^2)r^2 + \frac{1}{3}r^4\right] \,, \tag{4.41}$$

where m is the mass, e and g are the electric and magnetic charges, n is the NUT parameter, a is the spin and Λ is the cosmological constant. Horizons are located at zeroes of Q. Meanwhile the corresponding vector potential is given by

$$A = \frac{2\sqrt{6}}{\sqrt{\kappa\Lambda}}\frac{1}{\rho^2 n^2}\left(d\psi\left[gn(n + a\cos\theta) - enr\right] + \frac{\cos\theta}{2}d\phi\left[g\left(n^2r^2 - 1 - a\cos\theta\right) + e\left(2n + a\cos\theta\right)\right]\right) \tag{4.42}$$

From here we make the following coordinate transformations and redefinitions

$$r = t\sqrt{\frac{\ell^2}{\sigma}}\,, \qquad \cos\theta = y\,, \qquad t = \psi\,, \tag{4.43}$$

$$a = \alpha\sqrt{\frac{\ell^2}{\sigma}}, \qquad n = \sqrt{\frac{\ell^2}{\sigma}}, \qquad m = \frac{1}{2}\mu\ell\sigma^{-3/2}, \qquad \Lambda = \frac{3}{\ell^2}, \qquad e = \frac{\ell}{\sigma}q_1, \qquad g = \frac{\ell}{\sigma}q_2\,, \tag{4.44}$$

which precisely recover the inhomogeneous/anisotropic non-singular bounce solution (4.19) we have used above. Horizons would be located at zeroes of Q, but we have chosen parameters and coordinate ranges such that for the bouncing solution $Q < 0$ everywhere. This means that one should think of the bouncing cosmology as the smooth joining of the region outside the cosmological horizon with the region inside the event horizon of the Kerr-NUT-de Sitter black hole. The fact that the cosmological constant is positive is in fact crucial for this to be possible, as can be seen from Eq. (4.41). Note also that a curvature singularity is reached at $\rho = 0$. But from Eq. (4.39) we can see that if the NUT parameter n is larger than the rotation a, then ρ can never be zero. In our notation this translates into the requirement $\alpha^2 < 1$, so that we can see that a sufficiently large NUT charge is required to change the big bang into a non-singular bounce. In the stationary region of the black hole, the NUT charge is considered pathological, as it leads to the appearance of closed timelike curves, but in the interior region it takes on the new role of preventing a singularity. When the cosmological constant is positive this interior region can be extended to a geodesically complete spacetime representing the bouncing cosmologies we discuss here.

Note also that the switch between spacelike and timelike directions means that the mixed time-space component of the metric morphs into a mixed spatial component only, and, together with the definite sign of all metric coefficients, this is the reason why no closed timelike curves can appear in the interior region. Related to this is the fact that a no longer characterises the rotation/angular momentum of the black hole, and in fact comes to parameterise the spatial inhomogeneity α of the bounce. Finally, we note that the mass m of the black hole ends up simply parameterising the time asymmetry μ of the bouncing solution. Thus there is a complete re-shuffle of the physical significances of the various parameters, the most important one being that the NUT charge n looses its stigma. In the cosmological setting the NUT parameter is controlled by σ, which measures the amount of anisotropy that the metric has at large times. When $\sigma = 4$ the anisotropic cosmology evolves towards the closed FLRW metric with a round sphere.

4.4 Examples

In order to highlight the non-trivial features of the non-singular bounce solutions that we have described so far, it is useful to present a few representative examples. These examples may also point to several directions of research that will be worthwhile exploring in more detail in the future. We will characterise the solutions by looking at the size of the spatial hypersurfaces at fixed times, and at the contributions of the various forms of gravitational and matter energy densities that determine the contraction/expansion history of the solutions.

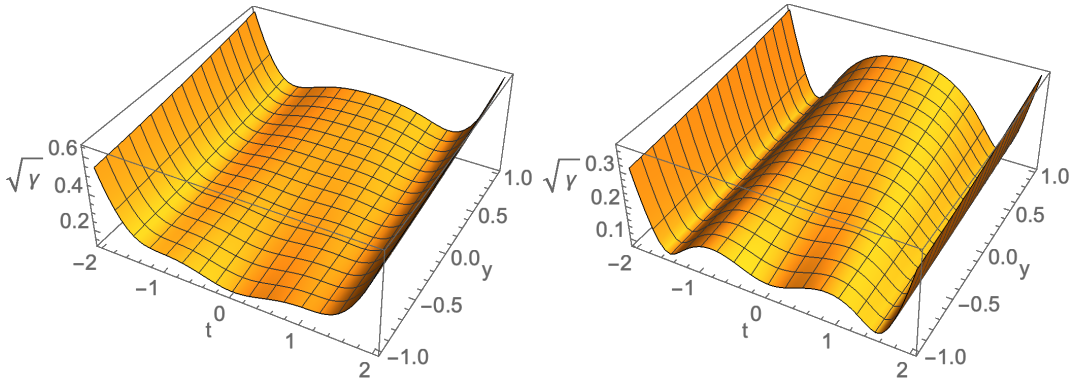

Figure 6: Plots of the average local scale factor (cubed) as a function of y and t. The solutions can be significantly inhomogeneous: for instance there can be one bounce near $y = -1$ and two bounces near $y = +1$ (left panel, with $\alpha = 1/2, \sigma = 10, q_1 = q_2 = 0$) or two bounces on one side and three on the other (right panel, with $\alpha = 1/2, \sigma = 11, q_1 = q_2 = 0$). All our plots have $\ell^2 = 3, \mu = 3$.

The solutions that we are describing are both anisotropic and inhomogeneous. Nevertheless, we can define a local scale factor $A(t, y)$ which averages over the anisotropies, but shows the inhomogeneity and the dependence on time, by making use of the determinant of the metric γ_{ij} on constant t slices (the integral of which would yield the volume),

$$A(t,y)^3 \equiv \sqrt{\gamma} = \frac{2\ell^3}{\sigma^2}\left[(t^2 + (\alpha y + 1)^2)\Delta(t)\right]^{1/2} . \tag{4.45}$$

This allows us to highlight an interesting feature of the bounces: there are solutions for which the inhomogeneity is so large that the number of bounces a local observer experiences depends on the location in y, see Fig. 6. As the figure shows, there exist solutions where one region of the universe bounces once, while far away regions bounce twice. Likewise, there are solutions containing two or three bounces depending on location. Three bounces is however the maximum possible number, since the equation $\dot{A} = 0$ contains five real roots at most, corresponding to three bounces separated by two occurrences of re-collapse. Asymptotically

however, as $t \to \pm\infty$, the metric becomes independent of α and the inhomogeneity is diluted – hence it is only near the bounce(s) that the inhomogeneity is really pronounced.

Another useful way to characterise the inhomogeneity as well as other features of the solutions is to look at the contributions of the different forms of stress energy: gravitational, vacuum and of electromagnetic type. For this, it is convenient to decompose the metric (4.19) into a $3+1$ split [74],

$$g_{00} = -N(t,y)^2\,, \qquad g_{0i} = 0\,, \qquad g_{ij} = \gamma_{ij}\,, \tag{4.46}$$

where we note that for our metric the shift is equal to zero (here we use Roman letters for spatial indices and Greek ones for spacetime indices). The three dimensional hypersurfaces have extrinsic curvature K_{ij} arising from their embedding into the four-dimensional spacetime,

$$K_{ij} = -\frac{1}{2N}\partial_t \gamma_{ij}\,. \tag{4.47}$$

Then the time-time component of the Einstein equations, usually referred to as the Friedman equation in a cosmological context, reads

$$\frac{1}{2}\left(K^2 - K_{ij}K^{ij} + {}^{(3)}R\right) = T^0{}_0 = \frac{3}{\ell^2} + \frac{\sigma^2}{\ell^4}\frac{\left(q_1^2+q_2^2\right)}{\left[t^2+(\alpha y+1)^2\right]^2}\,. \tag{4.48}$$

On the right hand side of Eq. (4.48) we have contributions both from the cosmological constant and from the stress-energy of the electromagnetic field. The left hand side, given in terms of the extrinsic curvature and the three-curvature, reads more explicitly

$$K^2 - K_{ij}K^{ij} = \frac{2t\left(\dot{\Delta}\left(t^2+(\alpha y+1)^2\right) - t\Delta - \alpha^2 tG\right)}{\ell^2\left(t^2+(\alpha y+1)^2\right)^3}\,, \tag{4.49}$$

$${}^{(3)}R = -\frac{2(\alpha y+1)^2(\Delta+\alpha^2 G) + \left(t^2+(\alpha y+1)^2\right)\left(G''\left(t^2+(\alpha y+1)^2\right) - 2\alpha(\alpha y+1)G'\right)}{\ell^2\left(t^2+(\alpha y+1)^2\right)^3}\,. \tag{4.50}$$

In a FLRW context the extrinsic curvature term (4.49) would simply have been $3H^2$ (where H denotes the Hubble rate), while the spatial curvature term would have been $\frac{3k}{a^2}$ for spatial slices that are closed ($k=1$), flat ($k=0$) or open ($k=-1$). In such a FLRW context a positive curvature term is needed in order to obtain a non-singular bounce. Meanwhile, in the present inhomogeneous context, all these terms, apart from the cosmological constant term, can have a strong spatial and temporal dependence.

As a first example, consider Fig. 7. This provides an example of a highly inhomogeneous solution, with $\alpha = 9/10$. We are plotting various contributions to the Friedman equation: in blue, the stress-energy from the electromagnetic field, in orange that of the cosmological

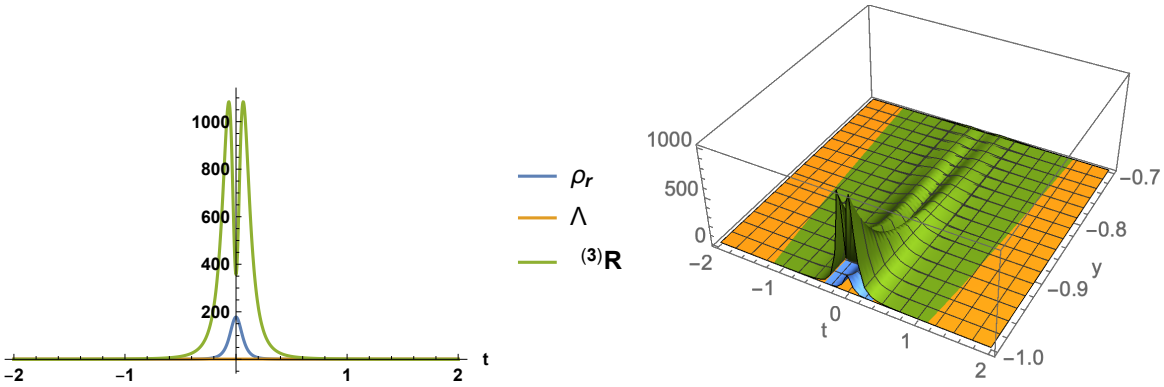

Figure 7: An example with large spatial curvature. In blue is shown the energy density of the electromagnetic field, in orange that of the cosmological constant (equal to $\Lambda = 1$), while the green curve/surface shows the 3-curvature. The parameter values are $\sigma = 8, \alpha = 9/10, q_1 = 1/20, q_2 = 0$. Left panel: $y = -1$. Right panel: $-1 \leq y \leq -0.7$.

constant (set to $\Lambda = 1$ here) and in green we are showing ${}^{(3)}R$. Both the electromagnetic energy density and the 3-curvature are growing towards the bounce, and then decaying again. Near $y = -1$ the growth is by far the strongest, and in this region the 3-curvature can become a full three orders of magnitude larger in magnitude than the cosmological constant. The right panel shows that this growth is far less pronounced at larger y.

This solution is also interesting in the context of inflation. An unresolved open problem of all inflationary models is how to explain the initial conditions that are required for inflation to begin [3]. But it remains an open issue in and of itself to understand in general what the range of allowable initial conditions is (for recent work see e.g. [75]). An intuitive expectation would be to require a Hubble sized region to be roughly homogeneous and isotropic, with inflationary potential energy dominating over the kinetic energy. Recently, numerical studies have largely confirmed these expectations, but have also indicated that a larger inhomogeneity may in fact be tolerable (while still assuming the inflaton kinetic energy to be very small) [76, 77]. Our explicit analytic bounce solutions are interesting in this regard, as they all link to a phase of accelerated/inflationary expansion, albeit one induced by a cosmological constant, where the issues with kinetic energy do not arise. Our solutions demonstrate that the inhomogeneity can indeed be surprisingly large, while still allowing accelerated expansion to take place afterwards. Nevertheless, one should note that in the present case the regions of large curvature are surrounded by regions of small curvature at larger y, so that it may

[3] Quantum cosmology may offer a setting where this question can be addressed. We provide an overview of quantum cosmology in chapter 6 and detail our recent progress in chapters 7 and 8.

also be the case that these low curvature regions are pulling the large curvature regions along into the ensuing phase of accelerated expansion. It would certainly be interesting to study these questions numerically for initial conditions that are obtained as deformations of the exact solutions presented here, to verify the robustness of the comments above.

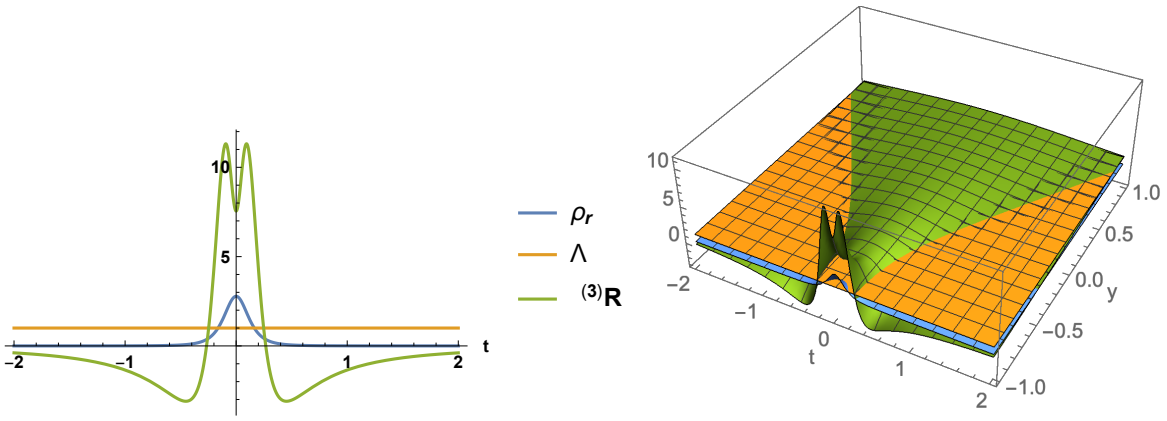

Figure 8: An example where the spatial curvature changes sign in some regions, just before and after the bounce, which occurs at $t = 0$. In blue is shown the energy density of the electromagnetic field, in orange that of the cosmological constant (equal to $\Lambda = 1$), while the green curve/surface shows the 3-curvature. The parameter values are $\sigma = 4, \alpha = 4/5, q_1 = 1/20, q_2 = 0$. Left panel: $y = -1$. Right panel: $-1 \leq y \leq +1$.

Another example of interest is presented in Fig. 8. Here a different, though equally surprising effect takes place. As discussed in the introduction, it is the combination of vacuum energy and positive 3-curvature that allows the singularity theorems to be evaded. Thus we know that at the bounce the 3-curvature is necessarily positive. However, for a significant range of parameters, the 3-curvature switches sign and becomes negative right before/after the bounce, again in the region of the largest inhomogeneity, near $y = -1$. This is interesting again in the context of "initial" conditions, in particular regarding the flatness problem [78]. From the fact that current observations provide a stringent upper bound on the homogeneous spatial curvature today, we can infer that at the onset of the hot big bang phase the relative importance of the 3-curvature must have been extremely tiny. Considering that non-singular bounces (without exotic matter that can violate the null energy condition) require a significant positive spatial curvature then seems to be in direct conflict with observations, unless there exists a mechanism that dilutes this curvature after the bounce. Of course, inflation could potentially provide such a mechanism [13]. But here we see that the case against pure curvature-induced bounces is perhaps less watertight than assumed so far: the fact that the

3-curvature can change sign right after the bounce also implies that it will vanish or nearly vanish in some regions. It would be a strong use of the anthropic principle to simply postulate that we might live in such a region, and we do not want to pursue this line of reasoning here. However, we simply wish to point out that it might be interesting to investigate this question further, and to see under what conditions the dynamics might cause large regions of the universe to become flat or nearly flat in the aftermath of a non-singular bounce.

4.5 Bounces in the presence of a cosmological constant

In the previous section we found exact solutions to the reduced Bianchi IX metric by setting two of the scale factors equal right away. As we have seen in section 3.5.4, the most general homogenous, closed metric, however, contains all three scale factors. In that case, analytic solutions cannot be found and the system has to be studied numerically. To begin, we simplify the discussion by considering constant positive vacuum energy density $\Lambda > 0$, as the only matter type in the universe. That means we can make full use of all equations in section (3.5.4) by simply setting $V(\phi) = \text{constant} = \Lambda$ and choosing $N = 1$. These choices imply that the scalar field will not evolve and hence sit a at certain value of the potential forever, mimicking a cosmological constant.

4.5.1 Time symmetric bounces

The requirements for a non-singular bounce are straightforward to derive: the equations of motion must allow for the scale factor of the universe to turn around (i.e. they must allow for $\dot{a} = 0$) and they must allow for this moment to represent a minimum size, $\ddot{a} > 0$. At the bounce ($a \equiv a_b, H = 0$), the Friedman equation (4.48) reads

$$-\frac{1}{a_b^2}U(\beta_+, \beta_-) = \frac{3}{4}\left(\dot{\beta}_+^2 + \dot{\beta}_-^2\right) + \Lambda \quad |_{bounce} \ . \tag{4.51}$$

Since the right hand side is positive definite, we see that the anisotropy potential must be negative at the bounce, $U < 0$, which implies that at the bounce, the anisotropy parameters $\beta_\pm$ must reside in the approximately triangular region shown in Fig. 4.The bounce radius a_b is then given by

$$a_b = \sqrt{\frac{-U}{\Lambda + \frac{3}{4}(\dot{\beta}_+^2 + \dot{\beta}_-^2)}} \, . \tag{4.52}$$

Negative U is a necessary condition for a bounce, but it is not sufficient: the acceleration equation (3.53) shows that in order to obtain $\ddot{a} > 0$, we must have

$$\frac{3}{2}(\dot{\beta}_+^2 + \dot{\beta}_-^2) < \Lambda \quad |_{bounce} \ . \tag{4.53}$$

Thus we must have suitably small velocities for the anisotropies at the time of the bounce. In other words, for $\dot{\beta}_{\pm} \mid_{bounce} = 0$ we obtain the largest possible set of anisotropy values leading to a bounce. Roughly speaking, the conditions for a successful bounce are that at the bounce the kinetic energy associated with the anisotropies is smaller than the vacuum energy, which in turn must be smaller in magnitude than the (negative) potential energy due to spatial curvature. Note that it is indeed the combination of spatial curvature (leading to $U < 0$) and vacuum energy, as exemplified in Eq. (4.53), that allows for non-singular bounces to occur.

With the exception of a special sub-class of solutions presented in subsection 4.5.3 and for which an analytic expression exists, we must find the bouncing solutions numerically. We will start with the best possible case, where we demand that the time derivatives of the anisotropy parameters are set to zero at the moment of the bounce, $\dot{\beta}_+(t_b) = \dot{\beta}_-(t_b) = 0$ at $\dot{a}(t_b) = 0$. Without loss of generality we will choose the origin of the time coordinate to be at the bounce, $t_b = 0$. Since the derivatives are all zero at the bounce, these solutions will be symmetric in time, i.e. the contraction phase leading up to the bounce will be the time reverse of the ensuing expanding phase. Our numerical results for this case are presented in Figs. 9 – 12. In all these plots we have chosen $\Lambda = 3 \times 10^{-4}$, so that the Hubble radius is given by $1/H = \sqrt{3/\Lambda} = 100$ in Planck units, i.e. we made the assumption that the vacuum energy was large in the early universe. The solutions presented here however exist for any chosen value of Λ and can be obtained using suitable re-scalings of the coordinates.

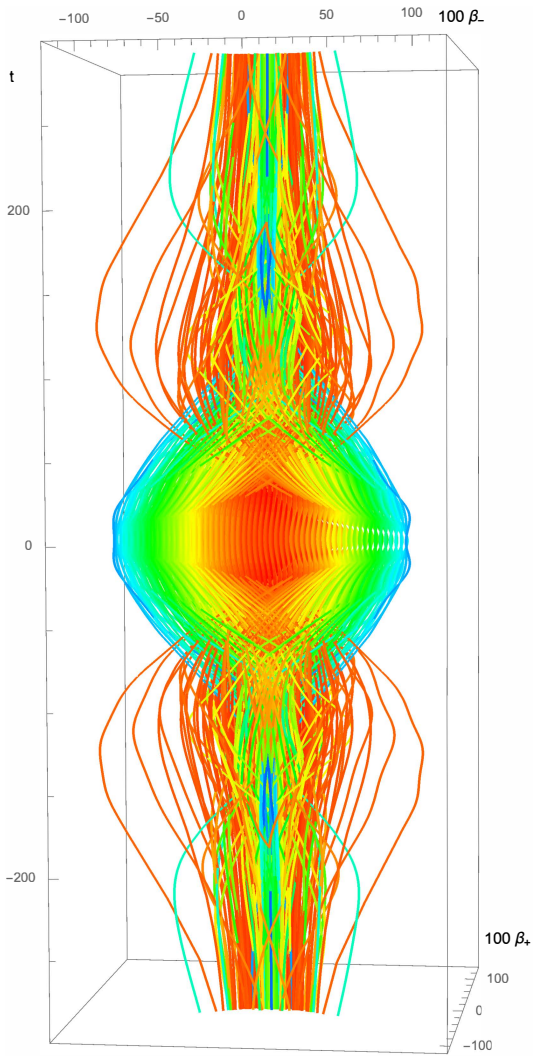

Figure 9: This plot shows the evolution of the anisotropies $\beta_\pm$ as a function of time. Time is height in the graph, the plotted ranges are $-7/10 < \beta_+ < 11/10, -9/10 < \beta_- < 9/10$ and $-300 < t < 300$, for $\Lambda = 3 \cdot 10^{-4}$ so that the Hubble radius is $1/H = 100$ Planck lengths. The bounce occurs in the middle, with zero derivatives $\dot{a} = \dot{\beta}_+ = \dot{\beta}_- = 0$ at $t = 0$. There is a general focussing towards smaller values of the anisotropies away from the bounce. The coloured curves show the evolution of the anisotropies near the bounce for solutions that evolve to a large universe asymptotically. The colour changes as a function of the distance from the isotropic (pure de Sitter) solution located at the centre of the plot, see also the next figures and the text for more details.

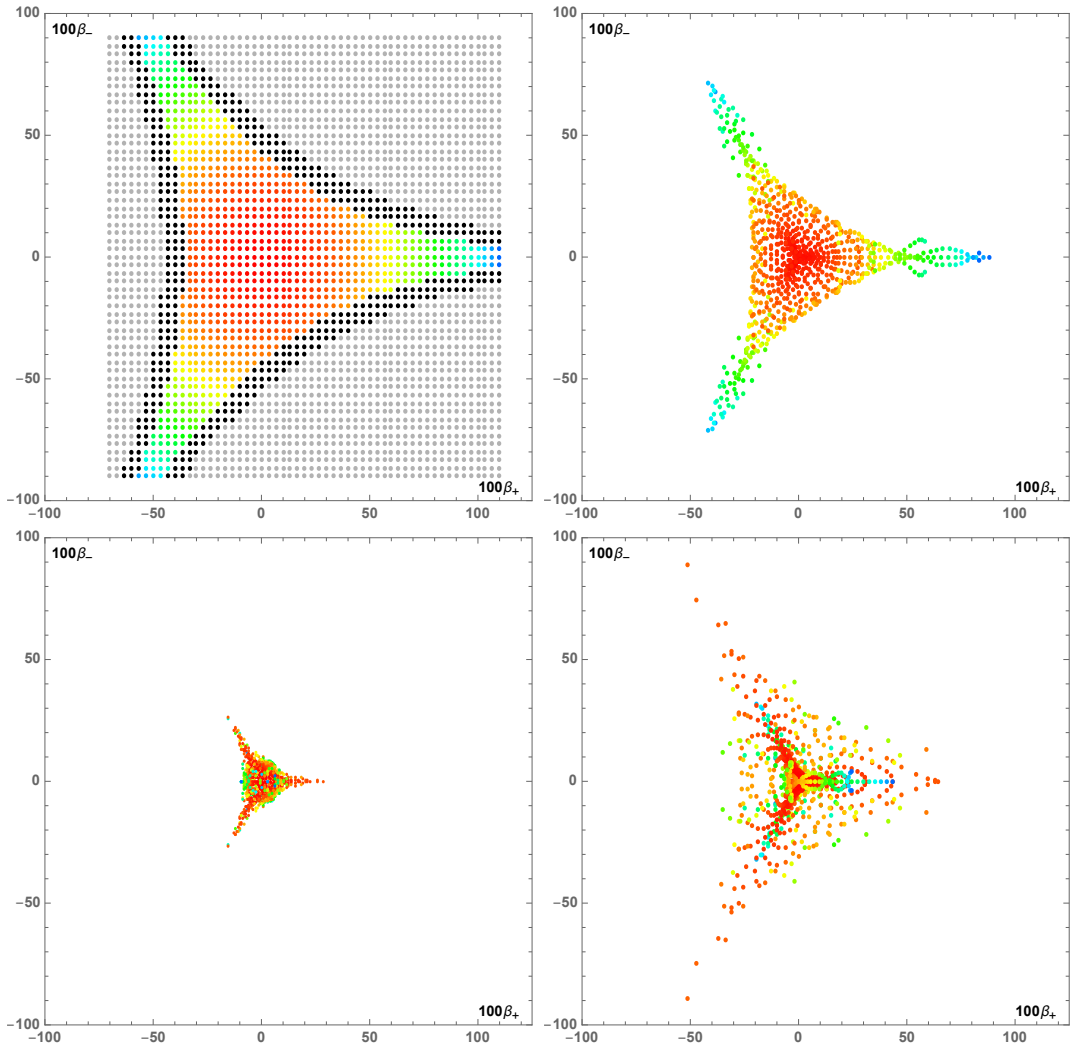

Figure 10: Time slices through the previous figure: clockwise from top left at $t = 0, 50, 100, 500$. The anisotropy parameters are re-scaled by a factor of 100. Gray dots in the $t = 0$ slice indicate values where the potential U is positive (cf. Fig. 4), and where no bounce can occur. Black dots mark the anisotropy values for which the bounce is followed by a rapid re-collapse. As one can see, the rapid re-collapse region surrounds the conditions for a bounce in all anisotropy directions. Overall, the triangular shape of the anisotropy potential is easily recognisable, and the later time slices show how various solutions reflect off the potential walls, while overall there is a general focussing effect towards smaller anisotropy values away from the bounce.

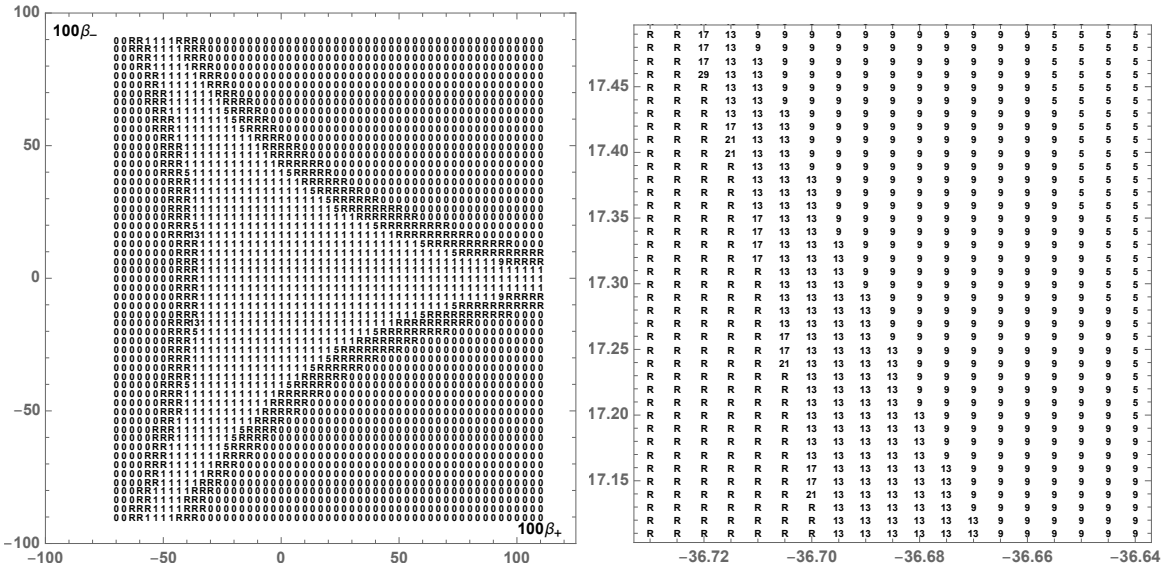

Figure 11: These graphs indicate the number of extrema of the scale factor $a(t)$, as a function of the anisotropy values at $t = 0$. A value of 1 corresponds to a single bounce, while 5 for instance implies three bounces separated by two local maxima of a. An R marks a bouncing solution that rapidly re-collapses to a singularity, while 0 means that no bounce is possible at all. The plot on the right is a zoom-in near the edge of the region of re-collapse.

Fig. 9 shows the evolution of the anisotropy parameters as a function of time. Each trajectory represents a bouncing solution, with the colour determined by the distance $\beta_+^2 + \beta_-^2$ in anisotropy space (at $t = 0$) from the isotropic de Sitter solution for which $\beta_\pm = 0$. Time slices through these solutions are presented in Fig. 10 at times $t = 0, 50, 100, 500$, where we should keep in mind that the characteristic time scale implied by the vacuum energy is 100 Planck times for our choice of Λ. Each coloured trajectory describes a successful bouncing solution, in the sense that at large early/late times these solutions contract/expand exponentially.

They may, however, contain short time intervals of re-collapse, followed by another bounce. This is illustrated in Fig. 11 where the number of extrema of the scale factor is shown. A value of 1 implies a standard non-singular bounce solution for which the scale factor has a typical "U" shape as a function of time. By contrast, a value of 3, for instance, implies that there are two bounces separated by a local maximum of the scale factor, i.e. the scale factor has a profile that resembles the letter "W". We deem a solution to be an unsuccessful bounce if shortly before/after the bounce the scale factor re-collapses to zero size, leading to a curvature singularity. Such re-collapsing solutions are marked with the

letter R in Fig. 11. As we derived above, the anisotropy potential must be negative in order for a bounce to occur. When this is not the case, i.e. when no bounce can occur at all, not even a temporary one followed by re-collapse, we assigned the entry 0 in Fig. 11. From this graph we can see that the region where bounces occur is separated from the region where they cannot occur by re-collapsing solutions that simply shift the singularity in time, without eliminating it. The edge of the re-collapsing region is formed by what might very well be the most interesting bouncing solutions from a mathematical viewpoint: here there exist solutions with increasing numbers of intermediate bounces, and intricate evolutions of the anisotropy parameters. An example with 13 extrema of the scale factor, i.e. 7 bounces and 6 local maxima of a, is shown in Fig. 12. The plot of the evolution of the anisotropies shows that this solution repeatedly reflects off the walls of the anisotropy potential $U(\beta_+, \beta_-)$, reminiscent of the BKL/mixmaster behaviour of singular crunches. The evolution here reveals a substantial sensitivity to initial conditions, although it is not chaotic in the BKL sense, in that there are only a finite number of such reflections before a non-singular bounce occurs. Nevertheless, as one approaches the edge of the re-collapse region in ever smaller intervals, there seems to be no limit to the number of bounces, as illustrated by the right panel in Fig. 11. The latter graph for instance includes a solution with 15 bounces separated by 14 local maxima of the scale factor. It would be interesting, though computationally intense, to find the shape of the curves delineating the borders between solution regions with different numbers of bounces. This question must, however, be left for future work [4].

Overall, there is a significant focussing of the anisotropies towards smaller values as one goes away from the bounce. Also, in all successful bounce solutions, the anisotropies rapidly reach approximately constant values at early and late times, with all of the interesting evolution confined to the time period of the bounce. For the case of zero (or very small) velocities at the bounce, we can also understand the focussing effect analytically. This is because the equations of motion (3.50), (3.51) for the anisotropies simplify near the bounce to give

$$\ddot{\beta}_\pm \approx -\frac{2}{3a_b^2} U_{,\beta_\pm} \,. \tag{4.54}$$

Since the effective potential U rises from the origin in all directions of increasing anisotropy, the above equation implies that the anisotropy will be reduced as we go away from the bounce.

[4] Analyses of the chaotic nature of isotropic solutions (in the presence of a massive scalar field) have already been performed in [79, 80, 81].

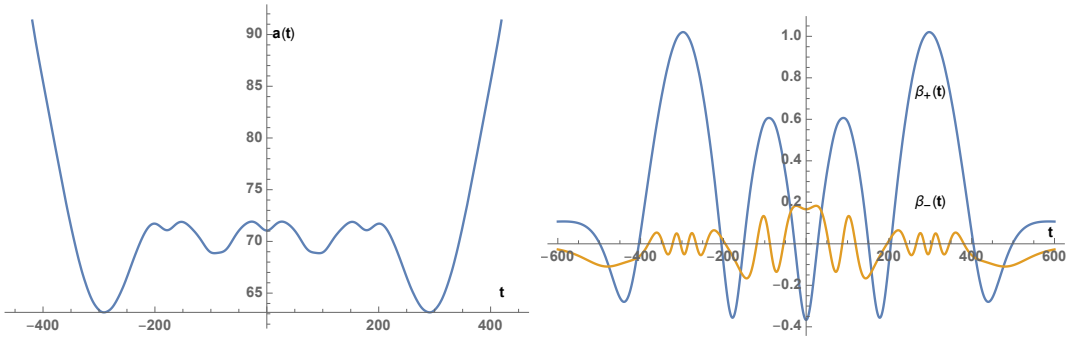

Figure 12: These two graphs show the evolution of the scale factor and the anisotropy parameters for the time symmetric solution with $\beta_+ = -11/30, \beta_- = 1/6$ at the bounce. For this solution there are a total of 7 bounces occurring in succession, while the anisotropy parameters undergo elaborate reflections off the walls of the anisotropy potential. Multi-bounce solutions such as this one occur near the edges of the allowed parameter space, as evidenced in Fig. 11.

4.5.2 Time asymmetric bounces

We can now extend these results by allowing for non-zero time derivatives of the anisotropy parameters at the bounce. The allowed range is indicated by the bound in Eq. (4.53), which can be read to say that the "kinetic energy" in the anisotropy must be smaller than half of the energy density of vacuum energy. Numerically, we find that, increasing this kinetic energy, the results of the previous section are modified very little until one gets close to the upper bound. The left panel in Fig. 13 for instance shows the results for the case where we take $\dot{\beta}_+(0) = \dot{\beta}_-(0) = 1/200$, implying that $\frac{3}{2}(\dot{\beta}_+^2 + \dot{\beta}_-^2) = \frac{1}{4}\Lambda$ at $t = 0$. Even for these values which are just a factor of $1/4$ away from the upper bound, the main effects are a slight time asymmetry in the solutions and a modest reduction of the available anisotropy space leading to bounces. The left panel in Fig. 14 illustrates this.

Interestingly, one may increase the velocities of the β parameters at $t = 0$ even slightly beyond the bound of Eq. (4.53), and still obtain non-trivial results – see the right panels in Figs. 13 and 14, where we took $\dot{\beta}_+(0) = \dot{\beta}_-(0) = 1/80$, implying that $\frac{3}{2}(\dot{\beta}_+^2 + \dot{\beta}_-^2) = \frac{25}{16}\Lambda$ at $t = 0$. Simple bounces have now disappeared (in agreement with the derived bound), but multi-bounce solutions may still exist, since the anisotropy parameters may evolve to smaller velocities away from $t = 0$ and lead to bounces there. An example of such a solution with 3 extrema of the scale factor, translating into two bounces separated by one local maximum of $a(t)$, is plotted in Fig. 15. Overall, the parameter space leading to bounce solutions

is drastically reduced when the kinetic energy in the anisotropy is this large. From these considerations it seems clear that non-singular bounces of the type discussed here can only have played a role in the early universe if the vacuum energy was very large., and if the growth of anisotropies during a prior contracting phase was suitably mitigated. We will discuss this aspect in more detail in section 4.7.

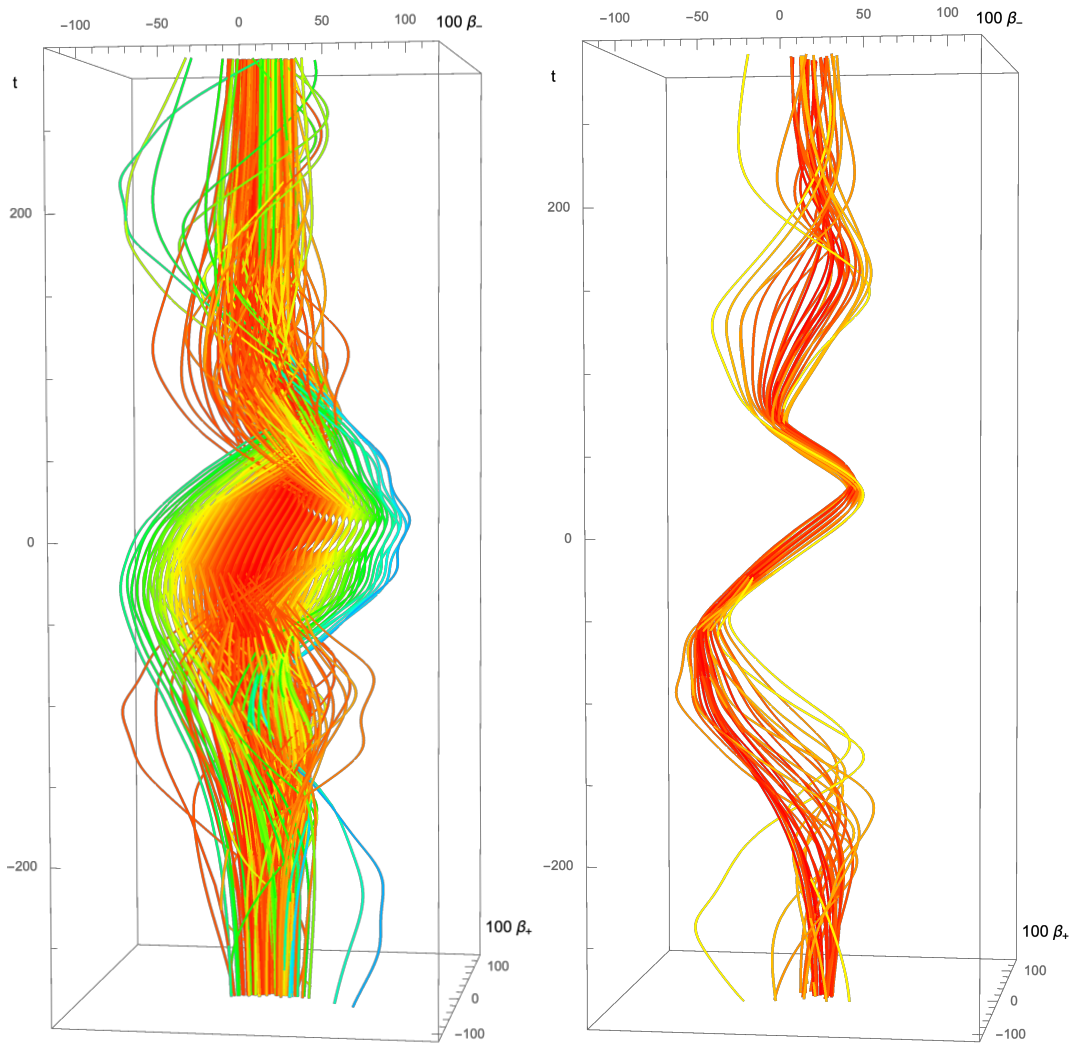

Figure 13: This plot shows the evolution of the anisotropies $\beta_\pm$ as a function of time. Time is height in the graph, the plotted ranges are $-7/10 < \beta_+ < 11/10, -9/10 < \beta_- < 9/10$ at the bounce, and $-300 < t < 300$, for $\Lambda = 3 \cdot 10^{-4}$ so that the Hubble radius is $1/H = 100$ Planck lengths. Initial conditions are imposed at $t = 0$, where $\dot{a} = 0$ and $\dot{\beta}_+ = \dot{\beta}_- = 1/200$ (left graph) and $\dot{\beta}_+ = \dot{\beta}_- = 1/80$ (right graph).

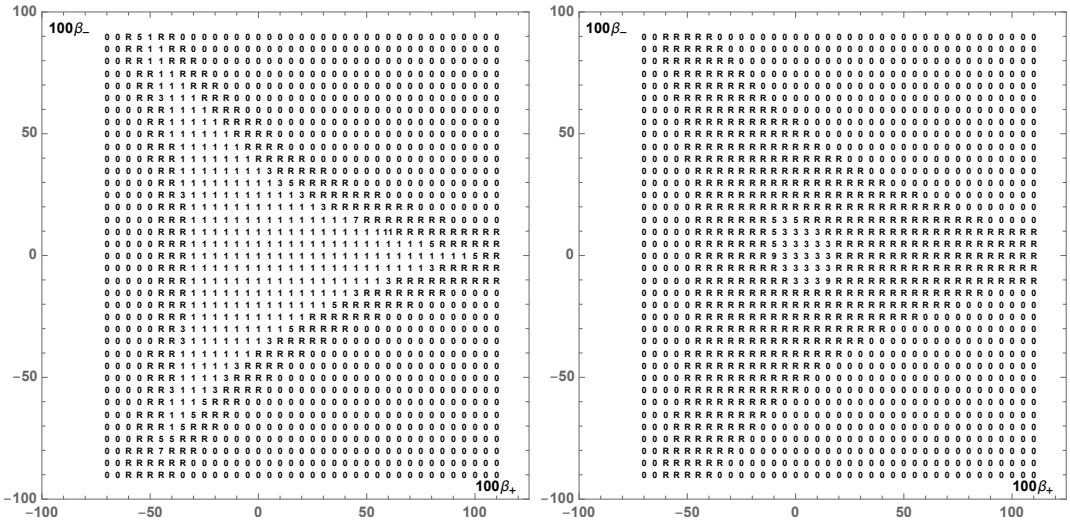

Figure 14: The number of extrema of the scale factor $a(t)$ for the solutions plotted in Fig. 13.

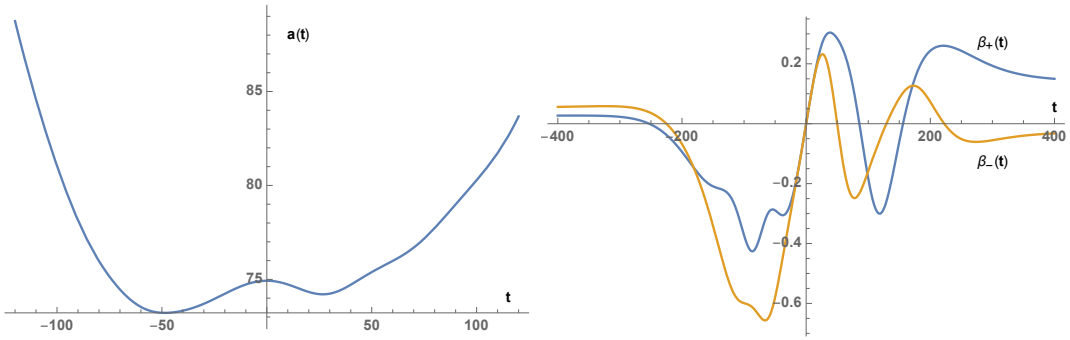

Figure 15: These graphs show the evolutions of the scale factor and of the anisotropy parameters as a function of time, for the solution with $\beta_+(0) = \beta_-(0) = 0$, but with large velocities $\dot{\beta}_+(0) = \dot{\beta}_-(0) = 1/80$. Although the kinetic energy at $t = 0$ is larger than the value that could lead to a bounce, away from $t = 0$ two bounces nevertheless occur since the energy in the anisotropies is slightly reduced there.

4.5.3 Axial Bianchi IX: Comparing to the exact solution

Our discussions so far were based on numerical solutions to the equations of motion, for various boundary conditions. In fact it seems difficult to imagine that a general analytic solution can be found for full Bianchi IX non-singular bounces. However, there exists a special subset of solutions for which the exact solution of the previous section is recovered. We will present it here, again, but this time not in terms of the variables we used before but in terms of the Misner variables, as it confirms our numerical results in the relevant parameter region, and provides useful insights into the general structure of this subset of solutions.

One may consistently truncate the equations of motion (4.48) - (3.51) to a simpler system with just one deformation parameter, along any of the three axes of symmetry of the full Bianchi IX metric. The simplest choice is the axis defined by $\beta_- = 0$, and along this axis β_- will then not be sourced by non-zero β_+. Thus, the anisotropy space is reduced from 2 to just 1 dimension, and sometimes this is called the axial Bianchi IX case. With the choice $\beta_- = 0$, the effective anisotropy potential simplifies to the form

$$U(\beta_+, \beta_- = 0) = -4e^{-\beta_+} + e^{-4\beta_+} \,. \tag{4.55}$$

This potential is shown in the left panel of Fig. 16. It contains a local minimum at negative values of the potential, and asymptotes zero from below as $\beta_+ \to \infty$. The bounce criterium that U must be negative to allow for a non-singular bounce thus suggests that it might be possible to find bounce solutions for arbitrarily large values of β_+ as long as $\beta_- = 0$, and we will see that this expectation is borne out.

Recall that previously we took the line element

$$ds^2 = -\frac{4l^4}{\sigma^2 f(\tau)} d\tau^2 + g(\tau)(\sigma_1^2 + \sigma_2^2) + f(\tau)\sigma_3^2 \,, \tag{4.56}$$

such that the action is given by

$$S = Vol_3 \int d\tau \left[\frac{1}{8l^2\sigma} \left[16l^4 - 2\sigma^2 f_{,\tau} g_{,\tau} - \frac{f}{g} \left(4l^4 + \sigma^2 g_{,\tau}^2 \right) \right] - \frac{2l^2}{\sigma} g\Lambda \right] . \tag{4.57}$$

Hence the solution

$$g(\tau) = \frac{l^2}{\sigma} \left(\tau^2 + 1 \right) \,, \tag{4.58}$$

$$f(\tau) = \frac{4l^2}{\sigma^2} \frac{\tau^4 + (6-\sigma)\tau^2 + \mu\tau + \sigma - 3}{\tau^2 + 1} \,, \tag{4.59}$$

satisfies the equations of motion obtained from varying the action with respect to the fields

$$g g_{,\tau\tau} - \frac{1}{2} g_{,\tau}^2 - 2\frac{l^4}{\sigma^2} = 0 \,, \tag{4.60}$$

$$f_{,\tau\tau} + \frac{g_{,\tau}}{g} f_{,\tau} + \frac{4l^4}{\sigma^2} \frac{f}{g^2} - \frac{8l^4}{\sigma^2} \Lambda = 0 \,. \tag{4.61}$$

Having the metric be non-singular everywhere puts further conditions on the free parameters σ and μ,

$$3 < \sigma < 12\,, \qquad |\mu| < \frac{2}{9}\sqrt{3}\sqrt{\sigma - 3}(12 - \sigma)\,. \tag{4.62}$$

To better illustrate the physical meaning of the variables, we translate them into the scale factor a and anisotropy β_+. By comparing the metrics we find that

$$a = \left(fg^2\right)^{1/6}\,, \qquad \beta_+ = \frac{1}{3}\ln\frac{g}{f}\,. \tag{4.63}$$

The isotropic (de Sitter) limit is restored in the case $\mu = 0$ and $\sigma = 4$. The parameters are related to the anisotropy and its derivative at $\tau = 0$; in fact we have

$$\beta_+(0) = \frac{1}{3}\ln\frac{\sigma}{4(\sigma - 3)}\,, \tag{4.64}$$

$$\frac{d\beta_+}{d\tau}(0) = -\frac{1}{3(\sigma - 3)}\mu\,, \tag{4.65}$$

while asymptotically we have

$$\beta_+(\pm\infty) = \frac{1}{3}\ln\frac{\sigma}{4} + \mathcal{O}(\tau^{-2})\,, \tag{4.66}$$

$$\frac{d\beta_+}{d\tau}(\pm\infty) = 0 + \mathcal{O}(\tau^{-3})\,. \tag{4.67}$$

Eq. (4.65) shows that μ determines the velocity of the anisotropy at the bounce, and as a consequence also the amount of time asymmetry of the solution. Meanwhile Eq. (4.64) implies that non-singular bounces can occur for all values of $\beta_+ > \frac{1}{3}\ln\left(\frac{1}{3}\right) \approx -0.366$ at the bounce. In particular, the anisotropy can be arbitrarily large in the positive β_+ direction, as expected from the shape of the potential. However, there is a lower limit at $\frac{1}{3}\ln\left(\frac{1}{3}\right)$, which is not at the point where the potential turns positive, but rather a little into the negative potential region. This is illustrated in the left panel of Fig. 16. This limiting value also agrees with our numerical results, cf. the location of the re-collapse region on the $\beta_- = 0$ axis in Fig. 11. Asymptotically, Eqs. (4.66) and (4.67) imply that the anisotropy parameter tends to a constant value, and this value is forced to be in the rather small range $\frac{1}{3}\ln\left(\frac{3}{4}\right) < \beta_+(\infty) < \frac{1}{3}\ln 3$. This range reflects the focussing effect towards small values of the anisotropy that we already discussed in subsection 4.5.1.

The exact solution permits us to understand a few additional features analytically. From Eq. (4.63) we can see that a^6 is a 6th order polynomial in time, implying that it can have 5 extrema at most. Explicitly, we have

$$a^6 = \frac{4l^6}{\sigma^4}\left[\tau^6 + (7 - \sigma)\tau^4 + \mu\tau^3 + 3\tau^2 + \mu\tau + \sigma - 3\right]\,. \tag{4.68}$$

For time symmetric solutions, with $\mu = 0$, the extrema are then given by the real solutions to the equation

$$\tau \left(\tau^4 + \left(\frac{14}{3} - \frac{2\sigma}{3} \right) \tau^2 + 1 \right) = 0 \,. \tag{4.69}$$

This straightforwardly implies that time symmetric axial Bianchi IX bounces have a single minimum of the scale factor for $3 < \sigma < 10$, a minimum and two inflection points for $\sigma = 10$ and 3 bounces separated by 2 local maxima for $10 < \sigma < 12$. We cannot have more than 3 bounces for these solutions, a feature that can be understood intuitively in the sense that the vanishing of β_- implies that the potential only contains a wall in the negative β_+ direction, and multiple BKL-type reflections off the potential walls cannot occur. A similar calculation shows that the extrema of β_+ occur (again in the time symmetric $\mu = 0$ case) when

$$\tau = 0, \quad \text{and when} \quad \tau^2 = \frac{3\sigma - 12}{\sigma - 4} \,. \tag{4.70}$$

Thus, except for the de Sitter solution at $\sigma = 4$, the anisotropy always has 3 extrema, a fact that is also nicely seen in the right panel of Fig. 16.

In the appendix we show that the closely related Kantowski-Sachs metric, in which the spatial sections contain a two-sphere rather than a three-sphere, also admit non-singular bounce solutions that are easily describable by an analytic solution, and that have related properties.

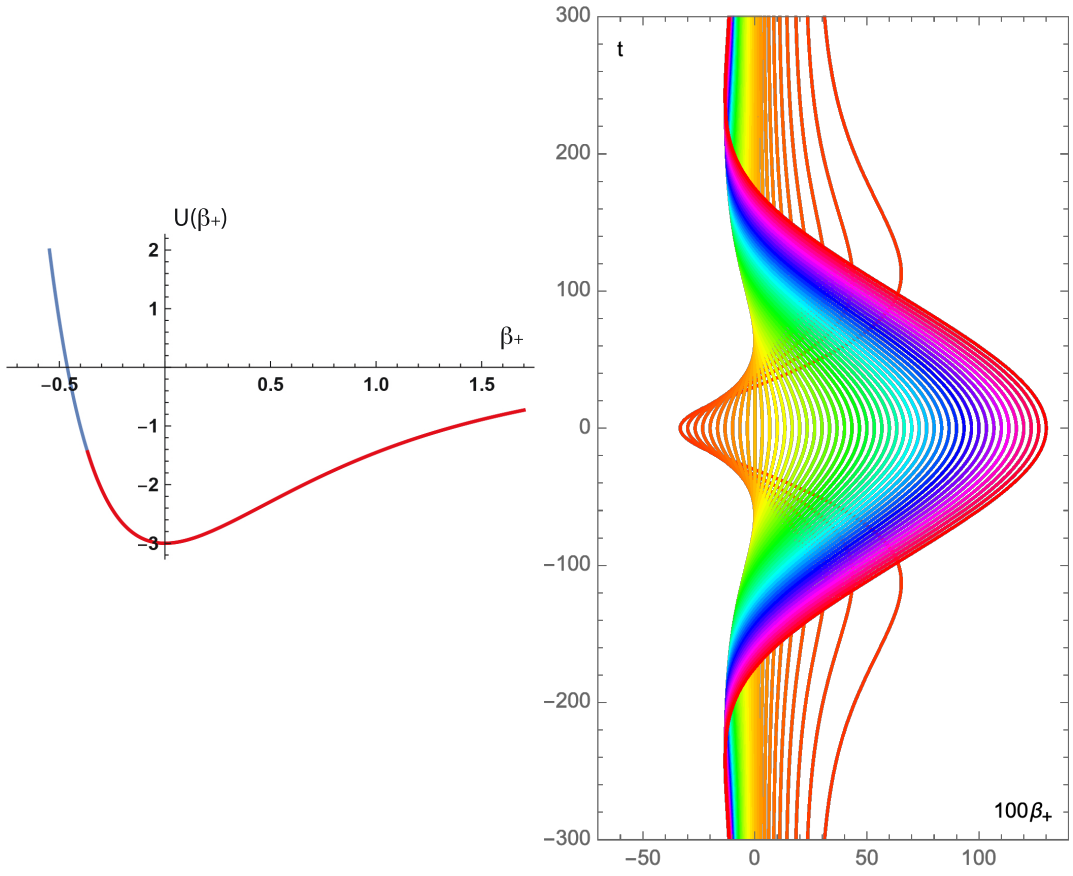

Figure 16: The left plot depicts the anisotropy potential $U(\beta_+, \beta_- = 0)$ along one of the axes of symmetry, here chosen to be the axis $\beta_- = 0$. The range over which non-singular bounces can occur is marked in red. Bounces occur for arbitrarily large positive anisotropies in this direction, and the solutions are strongly focussed towards zero away from the bounce. There is a minimum value $\beta_+ = \frac{1}{3}\ln(\frac{1}{3}) \approx -0.366$ below which the solutions rapidly re-collapse. Below $\beta_+ = \frac{1}{3}\ln(\frac{1}{4}) \approx -0.462$ the anisotropy potential is positive an no bounce can occur at all.

4.6 Bounces in the presence of a scalar field

Up to now we modelled dark energy via a cosmological constant. However, we may also consider the possibility that dark energy evolves over time, a situation which can be described by using a scalar field ϕ in a potential $V(\phi)$. Then the equations of motion are augmented to include contributions from the (minimally coupled) scalar, to become Eq. (3.49) while the Friedman equation is given by Eq. (3.48). This setting is familiar from inflation and quintessence models of dark energy. There are some similarities here, as one of the conditions for obtaining a bounce is that the strong energy condition must be violated, just like for accelerated expansion. The scalar field equation of state is given by the ratio of pressure to energy density, which in the cosmological context can be expressed as

$$w = \frac{\frac{1}{2}\dot{\phi}^2 - V(\phi)}{\frac{1}{2}\dot{\phi}^2 + V(\phi)}\,. \tag{4.71}$$

A violation of the strong energy condition corresponds to $w < -\frac{1}{3}$. In inflation and quintessence models, this condition is realised by the field slowly rolling down the potential, so that the kinetic energy is sufficiently small compared to the potential energy, more precisely such that $\frac{1}{2}\dot{\phi}^2 < \frac{1}{2}V(\phi)$ (in the absence of anisotropies, the acceleration equation (3.53) then immediately implies $\ddot{a} > 0$). This regime where the scalar slowly rolls down the potential is required for such a phase to last for an extended period of time, and for this reason the potential must not only be sufficiently flat in one location, rather it must be so over an extended field range. For non-singular bounces, one could consider a similar scenario where the scalar field rolls down while the universe bounces. This works less well than for inflation/quintessence however, as the scalar field kinetic energy is blue-shifted during contraction, and thus the standard Hubble friction term in the equation of motion (3.52) becomes an anti-friction term. There is however an alternative manner in which a scalar potential can usefully lead to a bounce, and this is to consider the situation in which the scalar field runs *up* the potential during the contracting phase. It can do so again because of the blue-shifting. Moreover, one can then imagine the situation where the scalar slows down as it rolls up, comes to rest at (or around) the time of the bounce, and subsequently rolls down again during the expansion phase. A great advantage of this scenario is that once the scalar comes to rest, the equation of state is precisely that of a cosmological constant, $w = -1$. And for a bounce, which occurs over a relatively short time scale, this is enough. One does not need an extended period of strong energy violation. This implies that bounces can occur even in potentials that are rather steep (in fact, one can momentarily achieve $w = -1$ in any potential), and that one would not con-

sider for inflationary model building. That said, we should now look at the combination of all the conditions required for a bounce, and then compare to numerical examples.

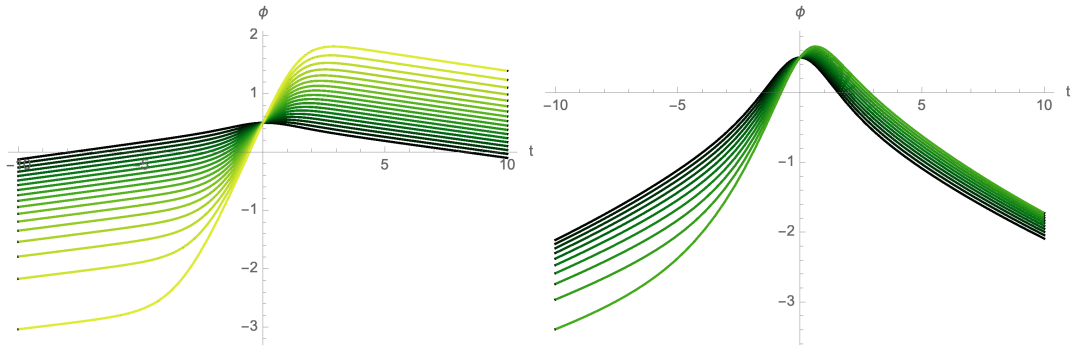

Figure 17: These two plots show the evolution of the scalar field as a function of time, for solutions that bounce at $t = 0$ at a specified value of $a = 10, \phi = 1/2$, for a range of values of $\dot{\phi}$ at the bounce. The left panel is for a potential $V = e^{\phi/10}$, showing solutions with $\dot{\phi}(t = 0)$ up to values of 0.90 while the right panel is for $V = e^{\phi/2}$, showing solutions with $\dot{\phi}(t = 0)$ up to values of 0.48. Lighter curves correspond to larger velocities at the bounce.

The minimal value of the scale factor at the bounce can again be found from the Friedman equation (3.48), and is given by

$$a_b = \sqrt{\frac{-U}{V(\phi) + \frac{1}{2}\dot{\phi}^2 + \frac{3}{4}(\dot{\beta}_+^2 + \dot{\beta}_-^2)}}\,. \tag{4.72}$$

The conditions to obtain a bounce are now given by

$$U(\beta_+, \beta_-) < 0 \quad |_{bounce}\,, \tag{4.73}$$

$$\frac{3}{2}(\dot{\beta}_+^2 + \dot{\beta}_-^2) + \dot{\phi}^2 < V(\phi) \quad |_{bounce}\ . \tag{4.74}$$

We may again study a few numerical examples, this time for potentials of exponential form $V(\phi) = v_0 e^{c\phi}$. We will also limit ourselves to cases with small anisotropies (in all the examples below we set $\beta_\pm = 1/100, \dot{\beta}_\pm = 0$ as an initial condition), since the inclusion of anisotropies is very similar to the discussions of the preceding sections.

Fig. 17 shows the time evolution of the scalar field for a rather flat (left panel) and for a steeper potential (right panel). The initial conditions have been set at the bounce, which occurs at $t = 0$, for a range of values of the scalar field derivative. Thus the solutions that are plotted are automatically selected on the basis that a non-singular bounce occurs. As the scalar field derivative increases, the field runs further up the potential after the bounce, before eventually turning around and rolling back down. In potentials such as these, an inflationary phase would then follow.

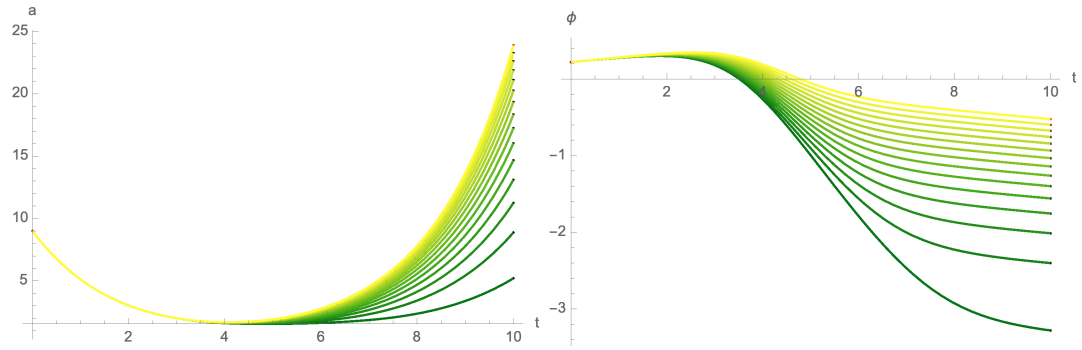

Figure 18: The evolution of the scale factor and the scalar field for a range of initial velocities leading to non-singular bounce solutions. The potential is taken to be $\phi = e^{phi/10}$ here. The initial values for the scale factor and scalar field are $a_i = 9, \phi_i = 23/50$, and the range of initial velocities leading to non-singular bounces is found to be $0.058 \lessapprox \dot{\phi} \lessapprox 0.064$, represented by the curves ranging from black to yellow respectively.

We may also set the initial conditions at an earlier time, in the contracting phase preceding a bounce (or a crunch). This is shown for two different potentials in Figs. 18 (with $V = e^{\phi/10}$) and 19 (with $V = e^{\phi/100}$). The solutions that are plotted are those that lead to non-singular bounces. For the steeper potential in Fig. 18, we find that only solutions that first run up the potential lead to a bounce. In all these solutions the scalar field turns around at or shortly after the bounce, and rolls back down the potential. For the largest initial scalar field velocity, the field runs up the furthest, leading to the largest amount of expansion after the bounce. For a flatter potential, as shown in Fig. 19, non-singular bounces may occur both when the scalar field runs up the potential, or down. Of course, eventually the field always rolls down the potential, and all these non-singular bounces are followed by phases of inflationary expansion. The largest amount of expansion right after the bounce occurs for the case where the scalar field velocity is practically zero at the bounce. For larger velocities, the bounce occurs somewhat later, so that there is less time for expansion. And for smaller initial velocities, the scalar rolls down the potential earlier, so that the bounce occurs while the field is already rolling down, implying a smaller expansion rate right after the bounce. In all cases, the range of initial velocities that lead to a non-singular bounce is small. This is mainly due to the blue-shifting of the scalar kinetic energy during the contraction phase, where one must ensure that the bound in Eq. (4.74) does not get violated. We will discuss the initial conditions in more detail in the next section.

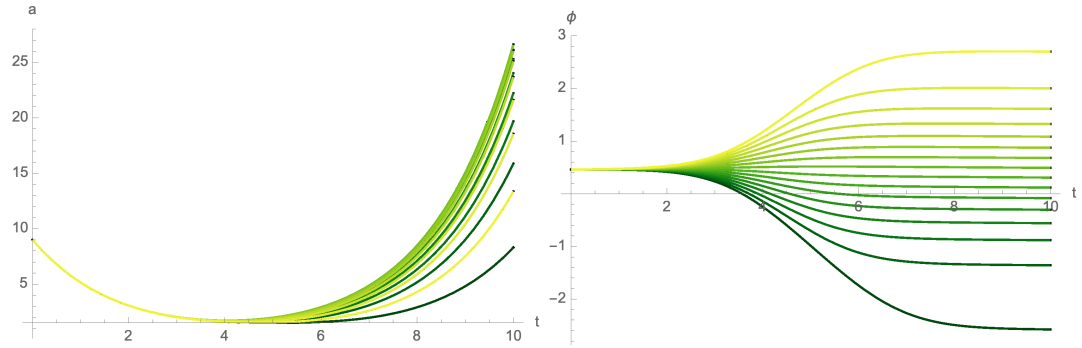

Figure 19: Same as Fig. 18, but for the potential $V = e^{\phi/100}$. The initial values for the scale factor and scalar field are $a_i = 9, \phi_i = 23/50$, and the range of initial velocities leading to non-singular bounces is found to be $0.0024 \lessapprox \dot{\phi} \lessapprox 0.095$, represented by the curves ranging from black to yellow respectively.

4.7 Discussion

Exact solutions of general relativity, in the presence of well-understood matter sources, have played a leading role not only in understanding the structure of relativity itself, but also in understanding its physical consequences for the universe. The most obvious examples that come to mind are the Schwarzschild solution describing the simplest black holes, and the Friedman-Lemaître-Robertson-Walker solutions describing the evolution of the universe on the largest scales. In the present chapter, based on [2] we have morphed a generalised exact black hole solution, namely the Kerr-NUT-de Sitter solution, into a cosmological solution, by focussing on the matching of the interior region of the black hole to the asymptotic region by eliminating the event horizon. This solution, which exists in the presence of a cosmological constant and (optionally) an electromagnetic field, is distinguished by being both anisotropic and inhomogeneous while describing a non-singular bouncing universe.

Could this solution describe the interior of actual black holes? And could such a non-singular bounce lead into a new expanding universe on the "other" side of the black hole, as has been suggested in some scenarios of cosmic evolution [82]? Unfortunately this seems unlikely, as the black holes in question are known to lead to closed timelike curves outside of their horizon due to the presence of the NUT charge, implying that this class of black holes is unlikely to be physically realistic. However, on the inside of these black holes, the various parameters describing the solution take on entirely different meanings, and it is precisely the NUT parameter that pushes the would-be big bang singularity out into an unphysical coordinate range, thus rendering the solution everywhere regular. Meanwhile, the rotation parameter of the black hole ends up describing the inhomogeneity of the bouncing universe solution. The end result is that the bouncing solution is entirely non-pathological.

Could the bouncing solution describe our universe? This remains too early to tell. We do however foresee a number of applications of this solution: for instance, as an exact inhomogeneous solution, it may well have applications in terms of understanding the averaging problem in cosmology better [83]. And since the bounce is followed by a period of accelerated expansion, these solutions may be useful in understanding the initial conditions required for phases of accelerated expansion, i.e. for inflation. Indeed, the issue of how much inhomogeneity is tolerable while still allowing for inflation to get started remains incompletely understood. Most of the recent work in this direction has focussed on numerical techniques, but exact solutions certainly have a role to play in this context, not only to check the accuracy of numerical codes, but also to understand and perhaps uncover qualitatively new effects.

From the purely classical point of view the existence of these solutions is quite satisfactory. Indeed, given a classical field theory it is necessary to find solutions that represent the physics one is trying to describe. Therefore, any singularity of the field should be ruled out in the description of the origin of the universe. The existence of a singularity implies that the solution is not a good model of the region of interest. Indeed, it is likely that the final understanding of the origin of the universe shall require a quantum theory of gravity. However, it is natural to expect perturbation theory around a state where observables are infinite to be ill-defined. Hence, if one expects the existence of a regime where the putative theory yields quantum "corrections" it is necessary to have at hand configurations where the gravitational field is bounded.

It remains an open question then how such non-singular bounces might fit into a more complete cosmological model [17]. However, the mere fact that they can occur in the presence of known matter sources already motivates their study. Somewhere, sometime, the conditions may have been (or will be) just right for them to actually take place. But, perhaps most intriguingly, they display some features that seem worth further exploration: they support electromagnetic fields simply due to their intricate geometry, and these fields grow in the approach to the bounce. It would be interesting to see if there can be any connection with the magnetic fields that are speculated to have been present already in the early universe. Also, the fact that the 3-curvature can vary widely from place to place, and even switch sign in some regions, offers new avenues of inquiry. The usual objections to non-singular curvature-induced bounces, namely that they require highly homogeneous initial conditions, and that the required spatial curvature is eventually at odds with current bounds on the curvature, though not evaded are at the very least relativised by the existence of these solutions. After all, in an inhomogeneous universe not all regions are the same, and some neighbourhoods may be much more interesting than others.

We have analysed non-singular bouncing universe solutions in the simplest possible setting: general relativity in the presence of a cosmological constant, or in the presence of a scalar field with a potential. Here bounces occur due to established physics only (dark energy is observationally established, as is the existence of a scalar particle, the Higgs), and without violations of the null energy condition. From this point of view, these bounces are considerably less speculative than bounces based on theories with specifically tuned higher-derivative kinetic terms, such as Galileon bounces [61, 62, 64][5]. We have demonstrated that

[5]Galileon models can be extended to supergravity theories [63, 84], but it remains unclear whether they can arise in a truly fundamental framework, such as string theory [85, 86]. Moreover, it is not clear if these

the bounces are robust under the inclusion of small anisotropies at the bounce, by studying bounce solutions within the Bianchi IX metric. Near the edge of the parameter space allowing for bounces, we have found solutions with multiple bounces, and accompanying turn-arounds of the anisotropy functions resulting from their non-linear dynamics. These multi-bounce solutions provide the link between non-singular single bounce solutions and chaotic BKL/mixmaster crunches that occur for "most" initial conditions.

This brings us to the issue of initial conditions: even though the theory in which the bounces occur is very simple, the solutions themselves are very special [87][6]. A bounce occurs only if the energy density in homogeneous curvature, and that in dark energy, are larger at the time of the bounce than the kinetic energy coming from the time evolution of the anisotropies and of the scalar field. However, the kinetic energy in the scalar grows much faster during a contracting phase (neglecting the potential, it is proportional to $1/a^6$) than the homogeneous curvature ($\propto 1/a^2$) or the approximately constant dark energy density. Thus it remains an open problem as to what kind of dynamics during the contracting phase could lead to such non-singular bounces. An ekpyrotic phase cannot achieve this, as it suppresses curvature and leads to a fast-rolling scalar [16, 17]. We must leave this as an open question for the future. Let us just mention one mitigating thought: if the dark energy resides at a very high scale in the early universe, say very close to the Planck scale, then the range of allowed kinetic energies compatible with a bounce are rather large. In such a case, one would in fact only trust the theory (considered as an effective theory) for kinetic energies below the Planck scale, and thus the self-consistency of the assumptions would render the bounces more prevalent in the space of available solutions.

If, in light of the preceding discussion, we simply assume that the conditions required for a non-singular bounce have been established, then the bounce would quite naturally lead into an inflationary phase afterwards. The bounce would imply that it is rather natural to find the scalar field high up on the potential (since it would have rolled up during the contracting phase), and the universe would have small anisotropies and be dominated by vacuum energy. Furthermore, the inflationary phase would subsequently dilute the spatial curvature required for the bounce. In this sense, a non-singular bounce can provide a viable prelude to inflation (see also [88, 89] for works in that direction). Of course, the question

theories are consistent at the quantum level, as they typically contain classes of unhealthy solutions in addition to the desired solutions.

[6]Exactly how special depends on having a probability measure, an issue that is far from resolved in cosmology.

of initial conditions for inflation is then not solved, but shifted to the question of initial conditions for the bounce. One could then hope that this new viewpoint might lead to new ideas on how to address this open issue. For instance, could the bounce act as a kind of filter, thereby automatically selecting for universes with suitable "initial" conditions, similar in spirit to the scenario proposed for the "phoenix" universe [90, 91, 92]?

There has been a renewed interest recently in cosmological models arising from string theory, due to proposed consistency requirements for string theoretic solutions [93, 94, 95]. These "swampland" criteria have put a lot of pressure on existing cosmological models, both of inflationary [96, 97] and ekpyrotic [98] type, as they suggest in particular that the scalar field range $\Delta\phi$ must remain smaller than order one in Planck units in a consistent effective description, while any positive potential must remain sufficiently steep throughout ($|V'|/V$ larger than some order one number in Planck units). In the present context it is interesting to point out that non-singular bounces can easily fulfill these criteria: given that the scalar field can run up the potential and come back down afterwards, the range of field values that is traversed can naturally remain small. Moreover, it is not necessary that the scalar field potential be flat: as the scalar comes to rest on the potential, it momentarily acts like a cosmological constant, regardless of the steepness of the potential, and, as we have seen, this can be sufficient to induce a cosmological bounce.

Apart from the open questions listed so far, there are two further avenues for future research that seem particularly promising: the first is related to the question as to what happens when the anisotropy becomes larger than the allowed bound at the bounce, i.e. what happens when the anisotropy potential $U(\beta_+, \beta_-)$ becomes positive? Here, no classical non-singular bounce solutions remain, but perhaps there exist quantum transitions between a contracting and an expanding phase of the universe. This is the domain of quantum cosmology which we will turn to in chapter 6.

5 Quantum Tunnelling

Moving on from the entirely classical discussion of the previous section, we turn our attention towards extending our description to include quantum effects. Particularly in the early universe, we expect them to dominate and no longer be captured by the usual, perturbative, treatment in which small fluctuations are imposed on top of a classical background. Instead we seek to describe the entire space-time as a fundamentally quantum object, at least on a semi-classical level employing Feynman's sum over histories framework. To start with, we will review and extend the path integral formalism in easy setups and then apply the numerical and analytical tools we developed to cosmology in the upcoming sections. In particular our focus will lie on describing quantum tunnelling. When a particle encounters a barrier, its subsequent path depends crucially on the ratio of its kinetic energy to the potential energy of the barrier. If it is larger than one the particle can overcome the barrier and proceed in its original direction. On the other hand, if it is smaller than one, it will be reflected off of it. In classical physics this picture provides a complete description of all the particle's possible behaviours. The story changed crucially with the advent of quantum mechanics in which the particle is now described by a state living in a Hilbert space or equivalently a wavefunction. Crucially, the wavefunction localized on one side of the barrier will, in general, have non-zero support on the other side of the barrier, allowing for a certain probability to observe the particle there. Note that this is the case even if the particle's kinetic energy is smaller than the barrier's potential energy. Numerically, quantum tunnelling can be well and accurately described by evaluating Schrodinger's equation on a lattice. Our focus, however, will lie on Feynman's sum over histories approach to quantum mechanics [20] since it can be extended to quantum field theory and gravity.

5.1 The Simplest Case: 1D Quantum Mechanics

To begin, let us consider a particle travelling in a universe consisting of only one spatial and one temporal dimension. We are interested in describing the position of the particle as a function of time $x(t)$. In Feynman's approach, the amplitude to transition from an initial position and time $(x_i = x(t_i), t_i)$ to a final position and time (x_f, t_f) is given by a sum over all paths obeying the appropriate boundary conditions which are weighted by their classical action S

$$\langle x_f, t_f | x_i, t_f \rangle = \mathcal{N} \int_{x_i, t_i}^{x_f, t_f} D[x(t)] e^{\frac{i}{\hbar} S}. \tag{5.1}$$

$\mathcal{N}$ is a normalization factor and S is given by

$$S = \int L(\dot{x}(t), x(t))dt \tag{5.2}$$

In other words, the action is the time integral of the classical Lagrangian evaluated along the path in question. We choose L such that it describes a particle of unit mass travelling in a potential $V(x)$ which may be specified at a later stage

$$S = \int \left(\frac{1}{2}\dot{x}^2 - V(x)\right) \mathrm{d}t \tag{5.3}$$

Coleman [99] illustrated wonderfully how to describe tunneling in Feynman's formalism. After a Wick rotation to Euclidean time the transition amplitude reads

$$\langle x_f, t_f | x_i, t_f \rangle = \mathcal{N} \int_{x_i, t_i}^{x_f, t_f} D[x(t)] e^{-\frac{S_E}{\hbar}} \tag{5.4}$$

where the Euclidean action is given by

$$S_E = \int \left(\frac{1}{2}\left(x, \tau\right)^2 + V(x)\right) \mathrm{d}\tau \tag{5.5}$$

The measure can now be made more precise: If $\bar{x}$ is any function obeying the boundary conditions then a general function obeying the boundary conditions can be written as

$$x(t) = \bar{x}(t) + \sum_n c_n \delta x_n(t) \tag{5.6}$$

where the x_ns form a complete set of orthonormal functions that vanish at the boundary. Then the measure is defined by

$$D[x(t)] = \prod_n (2\hbar\pi)^{-1/2} \mathrm{d}c_n \tag{5.7}$$

The dominant field configuration contributing to the Euclidean-time path integral goes by the name of bounce or instanton, depending on the boundary conditions (bounces [100] are used in the description of the decay of a metastable vacuum with $x(t_i) = x(t_f) = x_{min}$, while instantons, which correspond to "half-bounces", describe either the splitting of energy levels for potentials with degenerate minima, or tunneling across a potential barrier [101]). These solutions are finite action solutions of the Wick-rotated Euclidean equations of motion.

The standard description goes as follows: imagine a particle with insufficient kinetic energy to overcome a potential barrier. A good approximation is then to treat the particle classically as it runs up the potential barrier until it comes to a momentary stop on the slope of the potential when all its kinetic energy has been converted to potential energy. Here the

possibilities bifurcate: the particle can either roll back down classically, or one can use the Euclidean time instanton solution to describe the tunneling of the particle to the other side of the barrier. The probability for this tunneling event to happen will be determined to leading order by the action of the instanton solution. The particle then emerges on the other side of the potential barrier with zero velocity, whence it can roll down the other side of the barrier classically. Thus the overall classical evolution in Lorentzian time is interrupted at an instant where the Euclidean time "instanton" solution is inserted.

As has often been discussed, this method works well but it is conceptually not very clear: how do we know that we can just put in the instanton solution between classical solutions? This procedure after all seems rather *ad hoc*. In the rest of this chapter, based on [3], we will attempt to answer that question by deriving a *continuous* and generalized formulation of classical-to-quantum-to-classical transitions. Our approach will allow one to identify the relevant solutions for such transitions, and will largely constitute both a justification and an extension of the instanton method. Conceptually our approach is clearer and more intuitive. Moreover, as we will argue, our methods will be useful in more complicated situations, in particular when gravity is included, when singularities are present and when Euclidean time instanton solutions might not exist.

5.2 Tunneling via complex time paths

Instead of employing only solutions of the equations of motion in either Lorentzian/real time or in Euclidean/imaginary time, we will consider solutions in terms of general complexified time. As discussed by many authors (in particular Bender et al. [102, 103, 104, 105], Dunne et al. [106, 107] and Turok [108]) complex solutions of the classical field equations capture salient features of quantum mechanics. Moreover, as shown by Cherman and Ünsal [109], and by Turok [108], deformations of Euclidean time instanton solutions to a "rotated" time coordinate that approaches Lorentzian time seem to offer a sort of real time description of tunneling. In the present work we unify and extend these approaches. We arrive at the following picture – see Fig. 20.

Purely classical evolution corresponds to evolution along a line parallel to the real time axis, with all field values (and derivatives) taking real values. These are the green lines in Fig. 20. It is important to realize that, if the fields take real values, it is not necessary for the evolution to be represented exactly on the real time axis, rather any line parallel to it will do equally fine since the differential $\mathrm{d}t$ is also real on that line, and hence the momenta

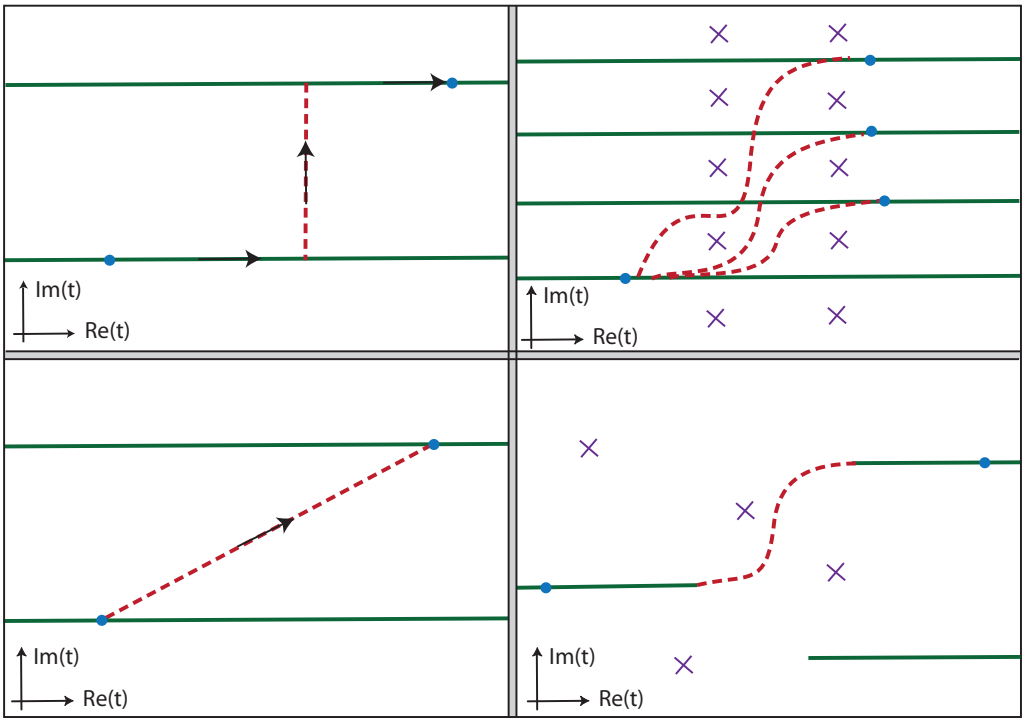

Figure 20: An overview of old and new approaches to describing classical to quantum and back to classical transitions. Green lines denote classical histories, while dashed red lines indicate Euclidean respectively fully complex tunneling paths. Blue dots show the location of initial and final conditions, while purple crosses indicate the location of singularities. For a full description of this figure see the main text.

will also be real. The *upper left* panel then illustrates the picture suggested by standard instanton methods: from a classical solution one can tunnel via a Euclidean time instanton solution (indicated by a dashed red line) to a different classical history. The idea here is that in the classically forbidden region, the leading approximation to the transition amplitude 5.4 is given by a saddle point of the Wick-rotated ($\tau = -it$) Euclidean action

$$S_E = -iS = \int \mathrm{d}\tau \left(\frac{1}{2}(x_{,\tau})^2 + V(x) \right) , \tag{5.8}$$

that is to say by a classical solution of the Euclidean equations of motion with finite action $S_{E,instanton}$. Moreover, to leading approximation the probability for this tunneling to take place is given by the factor $e^{-2S_{E,instanton}}$. We can picture this sequence of events in the complexified time plane, as shown in the figure: two classical histories in real time are joined by a Euclidean solution mediating the tunneling. The fact that the transition is classically forbidden is reflected in a shift along the Euclidean time axis. As soon as one has this picture in mind, it becomes clear that the path taken in the complex time plane may also

be deformed, as long as it does not pass any singularities of the solutions of the *complexified* classical equations of motion. This brings us to the *lower left* panel, which illustrates the approach of Cherman-Ünsal [109] where the tunneling path is rotated so as to be aligned more and more with the classical histories it is meant to join. In [109] only the tunneling part is considered, and rotations arbitrarily close to the real line are advocated, but as our graph indicates, the boundary conditions will limit to what extent such a rotation is feasible. The *upper right* panel illustrates the point of view advocated here: a classical history can tunnel to various other classical histories via various paths in the complex time plane. These paths are equivalent as long as their deformations do not encircle singularities (marked by purple crosses) and of course as long as they respect the specified initial and final conditions (in the figure we show three paths with different final conditions). What is not shown here is that paths that differ in how they circle singularities can take the evolution onto a different sheet of the solution function, and on this new sheet both the singularities and the loci of classical histories may differ from other sheets. We will discuss this in more detail in section 5.3 and present an example illustrating these concepts. The *lower right* panel shows a situation in which our method will be of clear advantage over existing ones: there exist classical histories which cannot be joined via purely Euclidean time instanton solutions. Moreover a variety of singularities are present. In this case our method will nevertheless allow one to determine which complex time paths can mediate a quantum transition between different classical histories.

The crucial question we have not discussed yet is which paths actually contribute to tunneling and which do not. The standard instanton method employs a single path, but how do we know that this is the dominant/relevant path? Evidently, by Cauchy's theorem we can deform a path in the complex time plane as long as it does not cross any singularities. Such deformed paths are entirely equivalent to the original one, and should not be counted multiple times. However, in general singularities will be present, and then there exist inequivalent paths that encircle the singularities in various ways. Should we then sum over all possible (inequivalent) complex paths between fixed initial and final conditions? As we will now argue, the answer to this question is "no". Not all such paths are relevant for tunneling, and we will now identify a criterion for identifying the relevant path(s).

The crucial notion here is to look at *fluctuations* around all possible interpolating paths. For purely Euclidean instantons this analysis was first performed by Callan and Coleman in [110]. Consider again the saddle point approximation. Around the saddle point, where the

solution to the Euclidean equation of motion is denoted by x_{cc}, to quadratic order the action can be approximated by

$$S_E[x, x_{,\tau}] = S_E[x_{cc}] + \frac{1}{2}\int_{x_i,\delta x(\tau_i)=0}^{x_f,\delta x(\tau_f)=0} \mathrm{d}\tau \left((\delta x_{,\tau})^2 + V''(x_{cc})(\delta x)^2\right) + \cdots , \tag{5.9}$$

where $V'' = V_{,xx}$, and where the term linear in δx vanishes precisely because we expand around an extremum. Given the boundary conditions on δx (vanishing at the endpoints), we can expand any fluctuation into a complete set of eigenfunctions of the fluctuation operator,

$$\delta x = \sum_n c_n \delta x_n \,, \tag{5.10}$$

where $\int \mathrm{d}\tau\, \delta x_n\, \delta x_m = \delta_{nm}$, and obeying the eigenvalue equation

$$\left[-\frac{\mathrm{d}^2}{\mathrm{d}\tau^2} + V''(x_{cc})\right] \delta x_n = \omega_n \delta x_n \,, \tag{5.11}$$

where the ω_n are the (real) eigenvalues. The integral above then turns into simple Gaussian integrals, which can be performed to yield the approximation[7]

$$\langle x_f, t_f \mid x_i, t_i\rangle = \mathcal{N}\int_{x_i,t_i}^{x_f,t_f} D[x(t)]\, e^{iS} \sim e^{-S_E(x_{cc})}\frac{1}{\sqrt{\Pi_n \omega_n}} \,. \tag{5.12}$$

The Gaussian integrals result in a prefactor that involves the square root of the product of eigenvalues of the fluctuation operator. If all eigenvalues are positive, then any fluctuation around the saddle point solution will increase the action, resulting in a lower probability. In this case we have found the dominant path. On the other hand, if some of the eigenvalues are negative, then there exist fluctuations that can lower the Euclidean action. Such solutions are thus not actual extrema and must be discarded[8]. (For a related discussion see [111].) How do we know whether negative modes exist? After all, it might be difficult to find the associated eigenfunctions numerically. Here the nodal theorem helps (see e.g. [112] and references therein): we can solve the perturbation equation (5.11) for the zero eigenvalue $\omega = 0$, with the boundary conditions $\delta x(\tau_i) = 0$, $\delta x_{,\tau}(\tau_i) = \pm 1$ (since this is not necessarily an eigenfunction we do not care about normalizability and can in principle choose $\delta x_{,\tau}$ to take any non-zero value). The number of nodes of the corresponding solution, which we refer to as the *perturbation function*, will tell us the number of negative modes[9]. In this way we

[7] When zero modes are present, they must be treated separately. A proper inclusion of the zero modes results in an additional prefactor which is irrelevant for our discussion [110].

[8] A Euclidean solution which describes the *decay* of a metastable vacuum, i.e. a bounce, has exactly one negative mode, which justifies the decay picture. Here we are interested in tunneling solutions, i.e. instantons, which should have at most zero modes in their spectrum of linear perturbations.

[9] Think about the energy eigenfunctions in a potential well: with each increasing eigenvalue an additional node is present. Hence if the solution with zero eigenvalue has n nodes, there must exist n eigenfunctions with lower, i.e. negative, eigenvalues.

can determine whether we have found the relevant tunneling solution without having to find the eigenfunctions and eigenvalues of (5.11) explicitly.

Now we want to adapt this argument to the case where the paths under consideration are complex. In fact, we will retain the Euclidean formulation, but where one should now consider both the Euclidean time coordinate and the fields to be complexified (it may appear baroque to rotate to Euclidean time before complexifying, but this avoids the use of slightly awkward factors of i – we will discuss how to get back to Lorentzian time below). By analytically continuing, the eigenfunctions will become complex but the eigenvalues ω_n remain real as these are simply constants. The problem is that the nodes in the analytically continued perturbation functions will in general disappear, and thus it looks like we might lose our simple criterion for determining which paths are relevant and which are not. However, we can find a resolution of this issue by thinking about the nodes in a little more detail: if a node is present in the Euclidean zero-eigenvalue perturbation function δx_0 at τ_0 then because of the boundary conditions we can expand the perturbation function between τ_i and τ_0 using purely sin functions,

$$\delta x_0 = \sum_k c_k \sin\left(\frac{k\pi}{(\tau_0 - \tau_i)}(\tau - \tau_i)\right) , \tag{5.13}$$

where $k \in \mathbb{N}$ runs over integer values. Now imagine that we deform the solution path by shifting it along the Lorentzian time direction by a constant amount $\Delta\tau = i\Delta t$, where $\Delta t \in \mathbb{R}$. Then along the Lorentzian time direction starting from the node at τ_0 we have

$$\sin(k\pi + i\Delta t) = \sin(k\pi)\cos(i\Delta t) + \cos(k\pi)\sin(i\Delta t) = \mp\sin(i\Delta t) = \mp i\sinh(\Delta t) . \tag{5.14}$$

From a node, and along the Lorentzian time direction, the change in the perturbation function will therefore be purely imaginary! This implies that if we look at the real part of the zero-eigenvalue perturbation function it will still contain a node. Thus we can essentially retain the same criterion for deciding whether solutions are relevant or not as in the pure Euclidean case, with the proviso that we must look only at the real part of the perturbation function. There is one possible caveat: could the complex perturbation function accidentally develop a zero in its real part, i.e. a zero not related to an actual node? This certainly seems conceivable, but in practice it is easy to avoid any ambiguity: the above arguments imply that if one solves for the zero-eigenvalue perturbation function over an extended region in the complex time plane, then there will be an entire line of zeros associated with an actual node. Such a line of zeros is thus the unmistakeable signature of solutions that must be discarded. Furthermore, the freedom to deform the contour in the complex time plane implies that one

can always deform the solution path such that it crosses such a line of zeros and then comes back. Our criterion may therefore be stated more carefully as follows: *if the real part of the zero eigenvalue perturbation function unavoidably crosses a line of zeros, this signals the presence of a negative mode and the solution must be discarded. If the real part of the zero eigenvalue perturbation function does not cross any such line of zeros, the solution is relevant to tunneling.*

We may now go back to Lorentzian time and reformulate this calculation in terms of complexified real time t. The zero-eigenvalue perturbation function ψ must then satisfy the following equation of motion and boundary conditions

$$\left[\frac{\mathrm{d}^2}{\mathrm{d}t^2} + V''(x_{cc})\right]\psi = 0, \qquad \psi(t_i) = 0, \quad \dot{\psi}(t_i) = \pm i\,. \tag{5.15}$$

Since we have also transformed the boundary conditions in accordance with the change of time coordinate, our criterion above remains unchanged and we must look for lines of nodes of $Re(\psi)$, as we will do in section 5.3. The presence of such a line of zeros will imply that a particular solution must be discarded, while a solution without any such nodes in its perturbation function will be relevant to tunneling.

A couple of additional comments: the existence of solutions with more and more negative modes is reminiscent of gravitational oscillating bounces [113, 114, 115], which also seem to represent excited states not relevant to the description of vacuum decay. The existence of such oscillating instantons is usually explained by arguments about Hubble friction and anti-friction, while here we will see that qualitatively similar solutions can exist even in the absence of gravity. Further works discussing the importance of negative modes in quantum tunneling include [116, 24, 117, 118, 119, 120, 121, 122, 123].

5.3 Examples

The discussion so far might have seemed rather generic and abstract. We will now illustrate the ideas discussed above with concrete examples. The core of our approach is the solution of the background and perturbation equations over an extended region of the complex time plane, and the visualization of the results by means of relief plots. Let us briefly describe how exactly this is done. First we note that the Lorentzian action (5.3) can be written in a reparametrization invariant way

$$S = \int n\,\mathrm{d}\lambda \left(\frac{1}{2n^2}(x_{,\lambda})^2 - V(x)\right), \tag{5.16}$$

where $n(\lambda)$ is the (complex) "lapse function" and λ is a parameter. Choosing a particular form for $n(\lambda)$ then allows one to follow a specified path in the complex time plane. For instance, $n(\lambda) = 1$ corresponds to evolving along the Lorentzian time direction, while $n(\lambda) = i$ corresponds to the Euclidean direction – more general choices of $n(\lambda)$ will allow evolution along any desired curve in the complex time plane.

We solve the equations of motion, starting from purely classical boundary conditions. The solution along the Lorentzian time axis then gives the classical solution, with real (conserved) energy, which in the case of a barrier potential means the solution that rolls up the potential until all kinetic energy is converted to potential energy; subsequently the particle simply rolls back down the potential. From this reference solution we branch out in both perpendicular directions, integrating the equation of motion as we go along while periodically sampling the values thus obtained. By repeating this procedure, and shifting the integration path by a small amount every time, we obtain the solution over a dense grid of points in the complex time plane. If no singularities are present, this prescription already gives us the full solution over the required time domain (with a resolution limited by the accuracy of the numerical computation). If singularities are present, then the reference path can be deformed repeatedly so as to encircle the singularities in various ways (where now branch cuts automatically appear "behind" the singularities after branching out from the reference path), until all possible paths are explored. A detailed example of this latter situation will be presented in section 5.3.3. The same procedure can then also be repeated for the perturbed equation of motion, imposing the boundary conditions specified in (5.15). We then employ relief plots to visually represent the real and imaginary parts of the background and perturbation solutions. The three examples below will illustrate this procedure.

5.3.1 Inverted harmonic oscillator

As a first example consider a particle moving in an inverted harmonic oscillator potential (see Fig. 21)

$$V(x) = -\frac{1}{2}\Omega^2 x^2 + V_0\,, \tag{5.17}$$

where Ω, V_0 are constants.

This potential is unbounded from below, but one might imagine that it gets deformed so as to develop a minimum at large field values – in any case, we are just interested in energy differences here. The potential has the advantage that analytic solutions to both the background equation of motion ($\ddot{x} = \Omega^2 x$) and perturbation equation ($\ddot{\psi} = \Omega^2 \psi$) can be

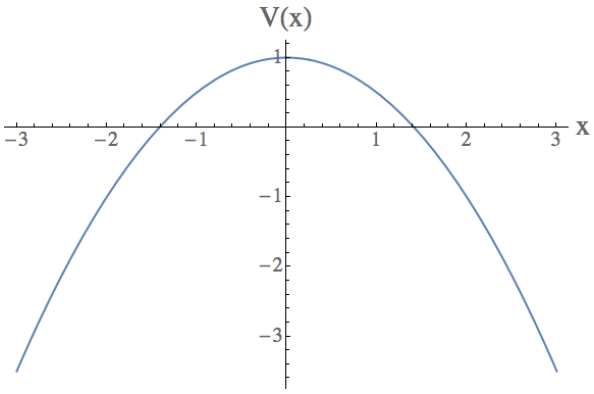

Figure 21: Plot of an inverted harmonic oscillator potential, $V(x) = 1 - \frac{1}{2}x^2$.

found easily. They are both given by

$$x(t), \psi(t) = c_1 e^{\Omega t} + c_2 e^{-\Omega t}, \qquad t \in \mathbb{C}, \tag{5.18}$$

where c_1, c_2 are complex integration constants to be determined. The solution is exponential when t is purely real and periodic when t is imaginary. If we choose the origin of time $t = 0$ to correspond to the moment just before tunneling, then the background solution is

$$x(t) = c \cosh \Omega t, \qquad t \in \mathbb{C} \tag{5.19}$$

where the constant c is the particle's location at the classical turnaround at $t = 0$.

Even though for this particular case analytic solutions are available, this will of course in general not be the case. For this reason we will in general solve the equations of motion numerically over an extended region of the complex time plane. Here we do this in Fig. 22 (where we have taken $c = -3/2$), so that we can directly compare our numerical methods with the analytic results. As explained above, the figures are obtained by solving the equations of motion over a dense grid of points in the complex time plane, and then representing the results with relief plots. Then, by taking a look at $\log |\mathrm{Im(x)}|$ one can immediately identify where the solutions are purely real: note that $\log |\mathrm{Im(x)}|$ blows up to large negative values for small imaginary values of x and thus the locations where x has a tiny or zero imaginary part will be represented by very dark colors. In this way the regions of classicality become obvious by inspection. There are infinitely many lines parallel to the real time axis along which the solution is real and classical. Tunneling then corresponds to considering complex time paths that join different such (horizontal) classical solutions by traversing regions of non-classicality. One path is singled out in the graph, namely the Euclidean instanton solution, which is the vertical dark line in Fig. 22, center panel. This solution stands out since the field values are

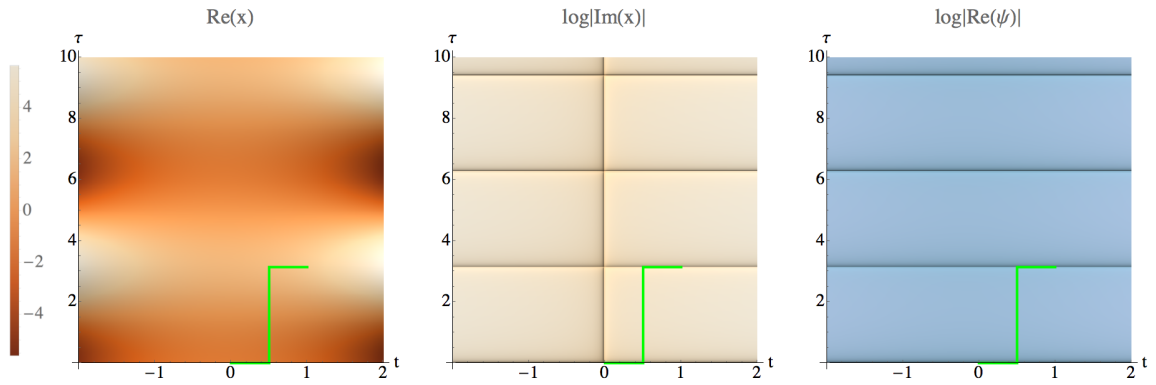

Figure 22: Relief plots of the background (left and center panels) and perturbation (right panel) solutions in the inverted harmonic oscillator potential. Darker colors represents smaller (more negative) values while brighter colors represents larger (more positive) values. Therefore in the center and right images the black lines show the regions where Im(x) and Re(ψ) are zero, indicating the regions of classicality along with the Euclidean instanton solutions (center panel), and the locations of nodes (right panel) respectively. The green line indicates a particular path which is further inspected in figure 23.

purely real along it. However, in our approach this path is now not any more fundamental than other paths through the complex time plane. An example of a possible tunneling path is drawn in Fig. 22, with the evolution of the field and action along this path shown in Fig. 23.[10] After tunneling, the solution is given by

$$x(t) = c\cosh\left(i\pi + \Omega t\right) = -c\cosh\Omega t, \qquad t \in \mathbb{C} \tag{5.20}$$

and it is classical again, as it should.

We have also plotted (the real part of) the perturbation function, which satisfies (5.15) and in the present case is given by

$$\psi(t) = \frac{i}{\Omega}\sinh\Omega t, \qquad t \in \mathbb{C}\,. \tag{5.21}$$

The right panel in Fig. 22 shows the zeros of the real part of the perturbation function. As expected, these nodes are distributed along continuous lines. Paths that join two adjacent lines of classicality can avoid crossing any node, and hence these paths are the relevant ones for tunneling. By contrast, a tunneling path joining two lines of classicality that are separated

[10]Note that we only need to consider tunneling paths in one direction along the Euclidean time direction, namely the direction corresponding to the correct Wick rotation. In practice this direction can be identified by the fact that quantum tunneling is suppressed compared to classical evolution, i.e. that the imaginary part of the action is positive.

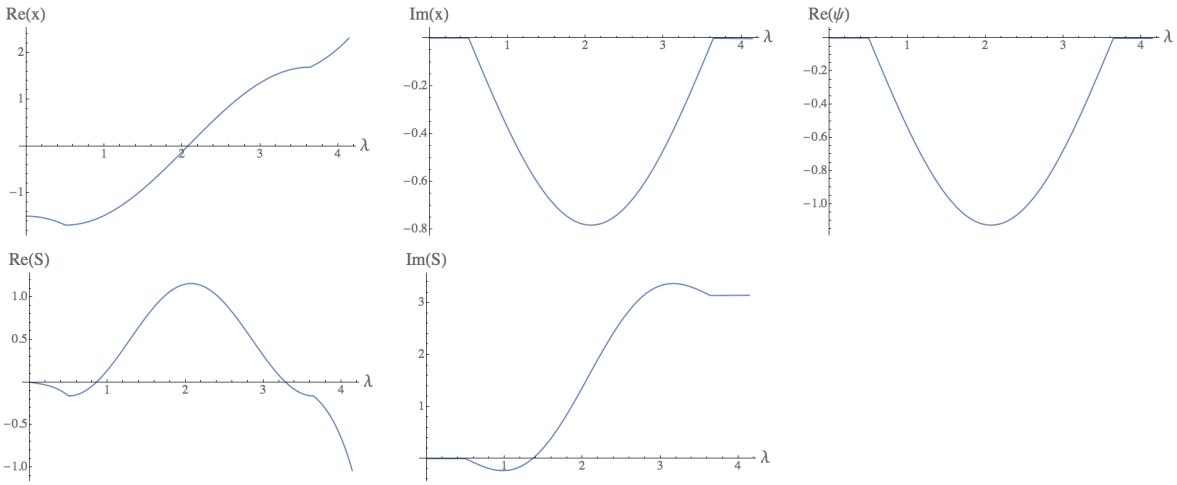

Figure 23: Field values and action for the tunneling path drawn by the green line in Fig. 22. Note that this is an actual tunneling path, with $Re(x)$ interpolating between two different sides of the potential and $Im(x)$ returning to zero after tunneling. The imaginary part of the action reaches a constant after tunneling, and this value will (to leading order) determine the probability for this tunneling event to take place. As required, the real part of the perturbation function ψ does not present any nodes.

by additional lines of classicality in between will contain nodes, and hence must be discarded. This simple example thus illustrates the main concepts advocated in the previous section.

5.3.2 Inverted Higgs potential

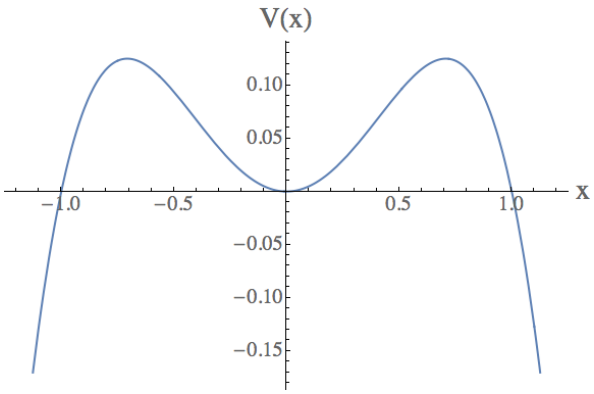

Figure 24: Plot of the inverted Higgs potential $V(x) = \frac{1}{2}x^2 - \frac{1}{2}x^4$.

Next, consider a particle moving in an inverted Higgs potential,

$$V(x) = \frac{1}{2}x^2 - \frac{1}{2}x^4\,, \tag{5.22}$$

which has also been studied by Turok [108]. The potential is shown in Fig. 24. The general solution is [108]

$$x(t) = -\frac{1}{\sqrt{1+m}}\frac{1}{sn(t/\sqrt{1+m}|m)}, \qquad t \in \mathbb{C}\,, \tag{5.23}$$

where sn denotes the doubly periodic Jacobi sn function, and the order m of the function determines the energy of the solution, $2E = m/(1+m)^2$. A particularly simple limit is obtained by setting the energy to zero, $m = 0$, in which case the solution is

$$x(t) = -\frac{1}{\sin t}, \qquad t \in \mathbb{C}\,, \tag{5.24}$$

where for this solution the particle is at negative infinity at $t = 0$ and reaches the turn-around/tunneling location $x = -1$ at $t = \frac{\pi}{2}$. The perturbation function, satisfying the required boundary conditions at $t = \frac{\pi}{2}$, is given by

$$\psi(t) = i\,\frac{\cos(t)}{\sin^2(t)}, \qquad t \in \mathbb{C}\,. \tag{5.25}$$

Plots of the background solution and the real part of the perturbation function are shown in Fig. 25, for the case of a small positive energy. In all plots the double periodicity is immediately apparent. The dark spots in the left panel show the regions where the particle rolls to large field values. The center panel indicates the lines of classicality. Once again we have an infinite number of such lines parallel to the real time axis (there is also a vertical line in the middle along which the field is real – this is the Euclidean instanton solution). Possible tunneling paths then join two such horizontal lines. As the right panel shows, joining two adjacent lines will not result in having nodes in the perturbation function, and such paths thus contribute to tunneling. Lines of classicality that are further separated in the Euclidean time direction are also separated by lines of nodes, and hence the corresponding tunneling solutions must be discarded. For illustration, an example of such an irrelevant solution is given in Fig. 26.

For completeness we should discuss the vertical line of nodes in the right panel of Fig. 25. This line is located at the position in real time where the particle reaches the potential minimum at $x = 0$ (and it is a direct consequence of the cos expansion of the background solution that one can perform around that point). It thus divides the evolution into regions left or right from the local minimum of the potential, and in this manner divides it into regions with the possibility to tunnel across either the left or right barrier. If we imagine having a particle on the left of the local minimum (i.e. at $x < 0$) but say we want to evaluate the transition amplitude to emerge on the far side of the right potential barrier, then we may follow the classical evolution from $x < 0$ to $x > 0$ first, and then tunnel across the right

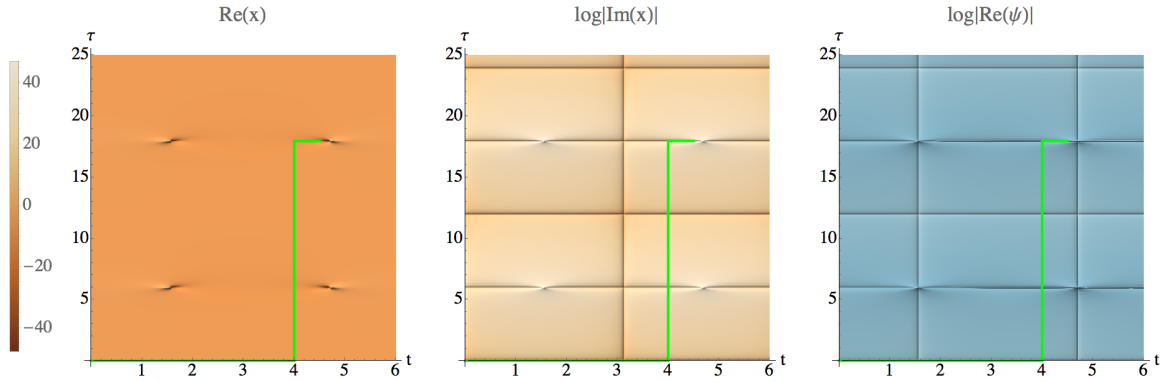

Figure 25: A figure analogous to Fig. 22, but for the inverted Higgs potential. The plots are obtained with the initial condition that the particle is released at $x = 10^{-2}$ with zero velocity.

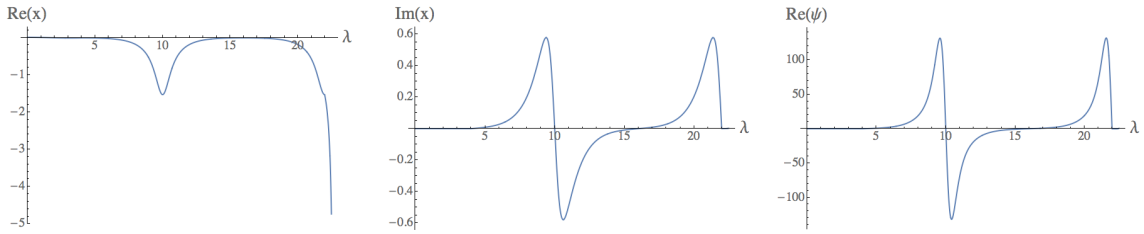

Figure 26: An example of an irrelevant solution. The path chosen here is indicated by the green line in Fig. 25. The perturbation function contains two nodes, indicating that there exist perturbations of this solution that increase the probability.

potential barrier. In this sense this vertical line of nodes is avoidable and therefore does not obstruct a contribution to the path integral.

5.3.3 Potential barrier with singularities

Our final example is also the most interesting one, namely a potential hill of the form

$$V = \frac{1}{x^2 + 1}\,. \tag{5.26}$$

For real x values this potential is everywhere finite (see Fig. 27), but in the complex plane there are singularities at $x(t) = \pm i$. In classical physics these would not play any role, but in our treatment of quantum tunneling using complex time paths the singularities are important. They imply that there now exist possible tunneling paths that are distinct in the sense that they can encircle the singularities in various ways. It is then crucial to have a way of assessing which such paths truly contribute to the tunneling amplitude, and which do not. As in our previous discussion, we will approach this question by looking at the solutions of

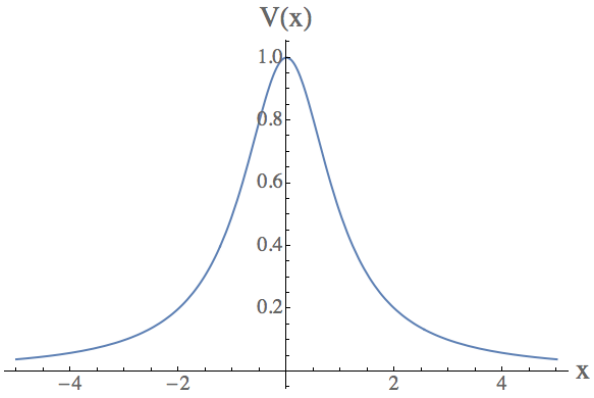

Figure 27: A potential hill $V = \frac{1}{x^2+1}$, which is entirely regular for real field values but contains singularities in the complex plane.

both the background and perturbation equations over extended regions in the complex time plane. For a first look see Fig. 28. Given that we are now in the presence of singularities, we must be a little more precise in specifying how we obtained these figures. In Fig. 28 we have solved the equations of motion by taking paths that start at the original classical solution (on the real time axis), then run up the Euclidean time direction in between the two vertical lines of periodically spaced singularities (which can clearly be seen in the left panel, along with their attached outwards-running branch cuts), and from there branch out again parallel to the real time axis to the left and to the right. We see that in this way we can reach other classical solutions at periodically spaced lines of classicality parallel to the real time axis. Also, the right panel shows that nodes reside along the same lines. Thus we have a situation very similar to that of the simple inverted harmonic oscillator of section 5.3.1: adjacent lines of classicality may be joined by node-less, and thus relevant tunneling solutions, while tunneling paths between further separated lines necessarily cross at least one node and must be discarded. Thus the relevant paths pass just beyond the closest singularity right of the center.

But now we have other possibilities too. In particular, we would like to know what happens when one chooses a path that passes by a singularity on the left. For this case, see Fig. 30. Here we are choosing paths in the following manner: from the classical solution on the real time axis let the path run up on the left hand side of the closest singularity left of the center. Having passed that singularity, we continue parallel to the real time axis, and then branch out from there up and down along the Euclidean time direction. In practice this means that we have chosen the branch cut emanating from the singularity to run straight down perpendicular to the real time axis. We see something interesting: to the right of the

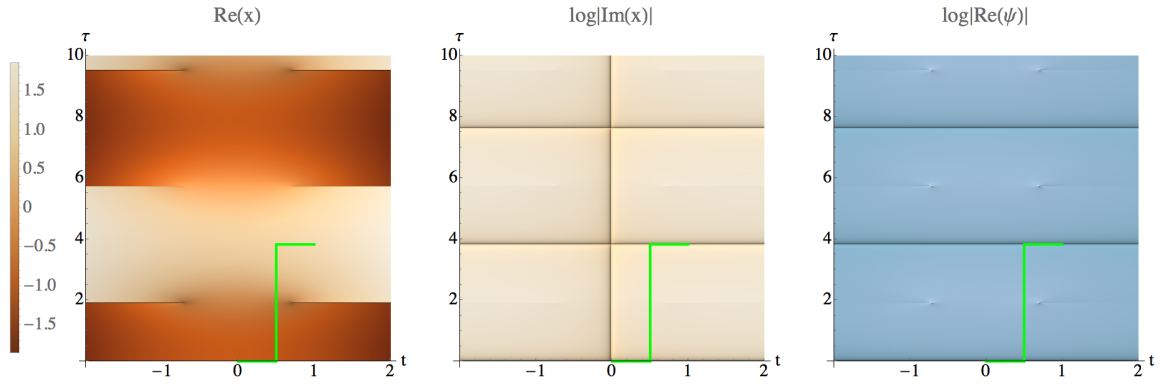

Figure 28: A first look at the solutions to the hill potential. The plots have been obtained with the initial condition that the particle is at rest at $x = -1$. For a complete description, see the main text.

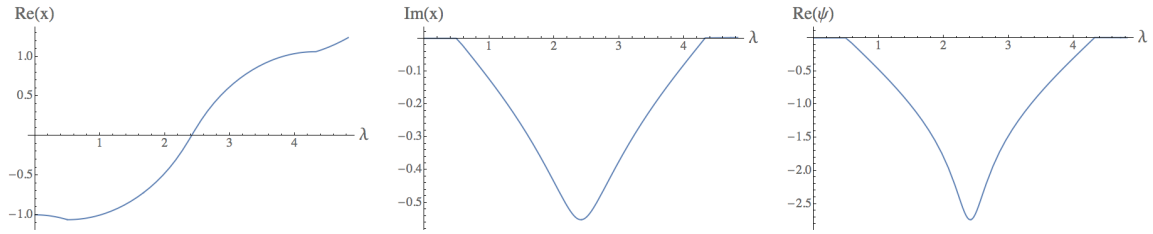

Figure 29: Solution along the green path in figure 28.

branch cut, the solution becomes real again on the real time axis. Note that this real solution is now not reachable via purely classical evolution from the original classical solution on the left, because of the branch cut residing in between. However, the path circling around the left singularity is a possible tunneling solution linking these two classical solutions. Is it also a relevant one? The right panel shows that unfortunately this is not the case. There is a line of nodes starting at the singularity and running straight up – any path joining the classical solution on the left to that on the right must necessarily intersect this line of nodes, and thus these solutions must all be discarded. One may wonder why the line of nodes is vertical in the present case. This is because the tunneling effectively occurs parallel to the real time axis, as opposed to the more usual situation where the tunneling is always along the Euclidean time direction. Here this occurs because of the presence of the singularity. As a consequence, near a node of a putative Euclidean solution the perturbation function could now be expanded in terms of $\sin(kt)$ functions, so that a line of nodes then emanates in the Euclidean time direction – this is simply the rotated version of the argument presented around Eq. (5.14).

Other paths passing by singularities left of the center and further removed from the

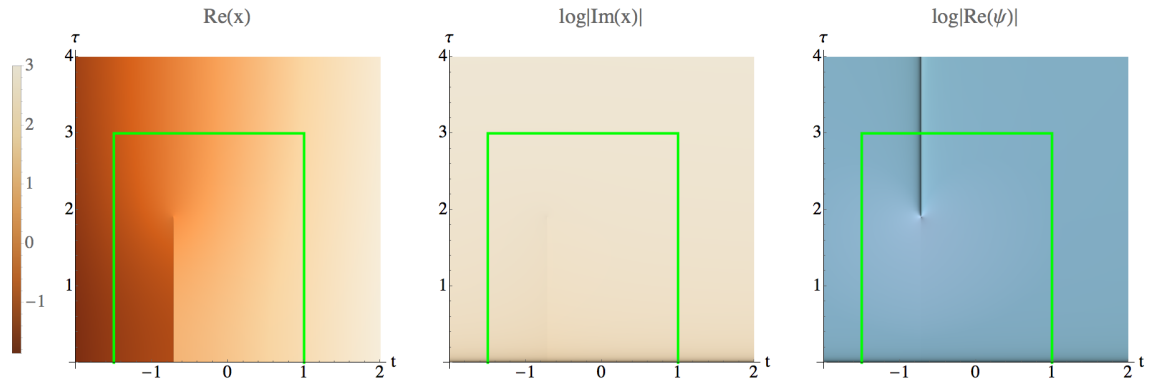

Figure 30: Investigating the left singularity. – for a description of how this plot was obtained, see the main text. A new feature is the straight line of nodes emanating from the left singularity and running vertically upwards along the Euclidean time direction.

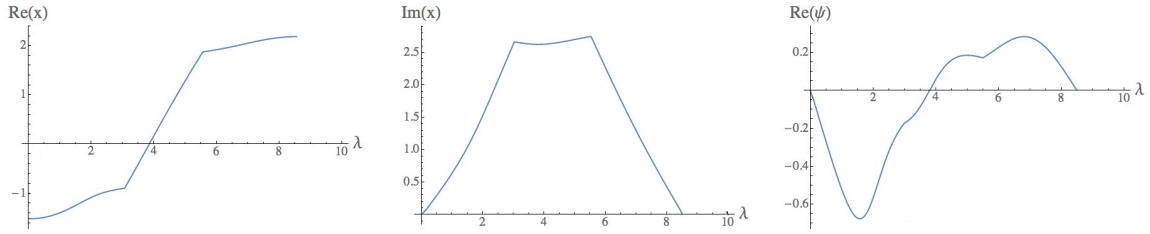

Figure 31: Solution along the green path in figure 30.

original classical solution will contain additional nodes, and hence all such paths are irrelevant. For the present potential, when we circle around the closest singularity left of the center by one additional full circle we essentially arrive back at the starting position, and thus no further paths need to be investigated. For other potentials, involving higher order singularities, additional non-trivial paths may exist, and our method will then allow one to determine all of the solutions relevant to quantum tunneling.

5.4 Discussion

Working in the semi-classical approximation, we have shown how complex time paths can mediate quantum tunneling between distinct classical histories. Both in order to find the location of the possible classical solutions and to determine the relevance of the solutions, we have shown that it is useful to solve the background and perturbation equations of motion over an extended region of the complexified time plane. This in particular enables one to find the nodes of the (real part of the) perturbation function, which, as we have argued, determine whether or not a given path contributes significantly to the tunneling amplitude. Our work

extends previous treatments where single complex solutions have been considered. Moreover, our analysis of the perturbation function and its nodes is new. The latter analysis provides a crucial new aspect, with the absence of nodes being the criterion selecting the relevant paths.

It might be useful to add further comments contrasting our work with earlier approaches. The closest related works are those of Cherman-Ünsal [109] and Turok [108], which both aim to develop a description of quantum tunneling in "real" time, essentially by choosing a path in the complex time plane that is aligned as closely as possible with the real time axis. However, as our approach makes clear, although the contour can be chosen to be essentially aligned with the real time axis in some parts, the overall shift in Euclidean time is essential to capture tunneling. A special case is provided by the presence of singularities, in which case there may exist paths that encircle a singularity and then return back to the real line (though actually on a new sheet of the solution function), as exemplified in section 5.3.3 – still, at some point a departure from the real line is unavoidable to capture quantum effects.

Bender [102, 103] and Turok advocate using solutions with a complex energy to describe tunneling. In describing an initial wavepacket, this is in fact required, as emphasized by Turok. However, when describing a quantum transition between histories that can to a good approximation be described classically, there is no need to use complex energy solutions. In all our examples, we have chosen the energy to be real, as determined by the starting classical history. This is in no way an obstacle to describing tunneling by complex time paths. It is simply the initial conditions that determine the value of the energy. Note furthermore that since energy is conserved, a complex energy does not allow one to obtain a purely classical history after tunneling – the best one can achieve is approximate classicality.

As shown by Cherman-Ünsal and Turok, the imaginary part of the field may reach very large values during tunneling. Turok has even proposed that these imaginary values may have a physical significance, and that they may be observable via weak measurements. We are skeptical about this claim, since the tunneling path may be deformed at will as long as one does not cross any singularities. Such deformations are allowed by Cauchy's theorem, and cannot result in any change in the physics. However, since the deformed paths reach different imaginary values of the field, these imaginary values cannot have a physical significance. It would however be fascinating if we were proven wrong about this point!

The advantage of our method is that it provides a rather general prescription for treating classical-to-quantum-to-classical transitions. This might be of great use in more complicated situations: we intend to extend our methods to quantum field theory, and also to semi-

classical quantum gravity. In this case, one may generally expect singularities to be present and classical histories to come to an end, most notably near black hole or big bang type singularities (see chapter 7 for our work in this direction). It is our (ambitious) hope that in such situations our method may be of use in identifying possible quantum transitions to other classical solutions.

5.5 False Vacuum Decay

If we try to describe tunneling in quantum field theory, many results from the simple quantum mechanical case carry over, but there are significant differences. In two seminal papers, Coleman and Callan [100, 110] outlined the process by which tunneling occurs in quantum field theory. The key assumption is that ϕ is a function of $\rho = (\tau^2 + |x|^2)^{1/2}$ only and hence is invariant under Euclidean rotational symmetry (i.e $O(4)$ symmetry). Indeed, it was later proved that if there are solutions which are not $O(4)$ symmetric, they will have higher Euclidean action and therefore will be sub-dominant. Since the significance of any solution will be suppressed exponentially by their Euclidean action, even solutions with only slightly larger action will be negligible in calculating the transition amplitude. Under the above assumption, the Euclidean equation of motion simplifies to

$$\frac{d^2\phi}{d\rho^2} + \frac{3}{\rho}\frac{d\phi}{d\rho} = U'(\phi) \tag{5.27}$$

which comes from the usual action of a scalar field in flat-space with potential U:

$$S_E = \int d\tau d^3x \left[\left(\frac{d\phi}{d\tau} \right)^2 + \frac{1}{2}(\nabla\phi)^2 + U \right] \tag{5.28}$$

The boundary conditions for the scalar field reduce to

$$\lim_{\rho\to\infty} \phi(\rho) = \phi_+ \tag{5.29}$$

$$\frac{d\phi}{d\rho}|_{\rho=0} = 0 \tag{5.30}$$

and the action B is found by evaluating

$$B = S_E[\text{bounce}] - S_E[\phi_f] = 2\pi^2 \int_0^\infty d\rho\rho^3 \left[\frac{1}{2}\phi'^2 + U(\phi) - U_f \right] \tag{5.31}$$

While it is not possible to solve this expression in general, when the width of the wall that separates the two vacua is small compared to the radius of the bubble, there is a very useful approximation - the aptly named thin-wall approximation. A thin wall means that we can write the field as a step function

$$\phi(\rho) = \begin{cases} \phi_t & \rho < \bar{\rho} - \Delta/2 \\ \phi_w & \bar{\rho} - \Delta/2 < \rho < \bar{\rho} + \Delta/2 \\ \phi_f & \rho > \bar{\rho} + \Delta/2 \end{cases} \tag{5.32}$$

where $\Delta\rho$ is the width of the wall. This significantly simplifies the action as we can now write

$$B = 2\pi^2\bar{\rho}^3 S_1 - \frac{1}{2}\pi^2\bar{\rho}^4\epsilon \tag{5.33}$$

where ϵ is the difference between true and false vacua $\epsilon = U(\phi_f) - U(\phi_t)$ and

$$S_1 = \int_{\bar{\rho}-\Delta\rho/2}^{\bar{\rho}+\Delta\rho/2} d\rho \left(\frac{1}{2}\phi'^2 + U(\phi)\right) \tag{5.34}$$

is the action on the wall. With all these quantities known, what is left to determine is $\bar{\rho}$ which is the size of the wall which maximizes the bounce solution. Hence it can be found by setting

$$\frac{\partial B}{\partial \bar{\rho}} = 6\pi^2\bar{\rho}^2 S_1 - 2\pi^2\bar{\rho}^3\epsilon = 0 \tag{5.35}$$

giving

$$\bar{\rho} = \frac{3S_1}{\epsilon} \tag{5.36}$$

5.5.1 Coleman DeLuccia Instantons

Generalizing the above to gravity is an important task as it allows describing early universe phenomena. In the weak gravity regime, which is the only regime where our description is valid, we can compute the corrections that gravity gives to the tunnelling rate. As a first step, one has to choose a metric to describe the system. While the $O(4)$ symmetric metric was proven to give the dominant contribution to the tunneling rate in the flat case, no such theorem exists in the curved case. Nevertheless, examples show that it is reasonable to assume that the $O(4)$ symmetric solution - termed the Coleman-De Luccia (CdL) instanton - is also the dominant contribution in the case with gravity. For example the Hawking-Moss instanton is an example of a different solution with $O(5)$ symmetry which can be shown to always have lower action than the CdL solution. Once one assumes $O(4)$ symmetry of the solution, the problem becomes very similar to the field theory, with the addition of an extra (gravitational) degree of freedom. The metric is

$$ds^2 = d\xi^2 + \rho(\xi)^2 d\Omega_3^2 \tag{5.37}$$

and the action is simply gravity minimally coupled to a scalar field. The equations of motion are

$$\dot{\rho}^2 = 1 + \frac{\rho^2}{3}\left(\frac{1}{2}\dot{\phi}^2 - U\right) \tag{5.38}$$

$$\ddot{\phi} + 3\frac{\dot{\rho}}{\rho}\dot{\phi} = U'(\phi) \tag{5.39}$$

and the action, upon substituting the equations of motion, takes on a very simple form

$$S_E = 4\pi^2 \int d\xi \left[\rho^3 U - 3\rho\right] \tag{5.40}$$

The boundary conditions are very similar to the no-boundary proposal of chapter 7. In order for the solution to be regular, we require

$$\dot{\rho}(\xi_0) = \pm 1 \tag{5.41}$$

$$\dot{\phi}(\xi_0) = 0 \tag{5.42}$$

where ξ_0 is the initial point of the instanton and hence $\rho = 0$ there. Of course we also require that the instanton interpolates between the two vacua.

5.6 The negative mode problem

Calculating the decay rate of metastable vacua while taking gravitational effects into account, has risen in importance upon the discovery that we might be living in a false vacuum. Using the Euclidean approach [100, 110, 23] for calculating the decay rate of metastable vacua to their true value, γ, the Arrhenius formula is given by

$$\gamma = \mathcal{A} e^{-\mathcal{B}} \,, \tag{5.43}$$

with

$$\mathcal{B} = S^{(cl)}(\varphi^b) - S^{(cl)}(\varphi^f) \,, \tag{5.44}$$

where the first term on the r.h.s. is the classical Euclidean action calculated along the bounce solution and the second term is the value of action evaluated at the false vacuum.

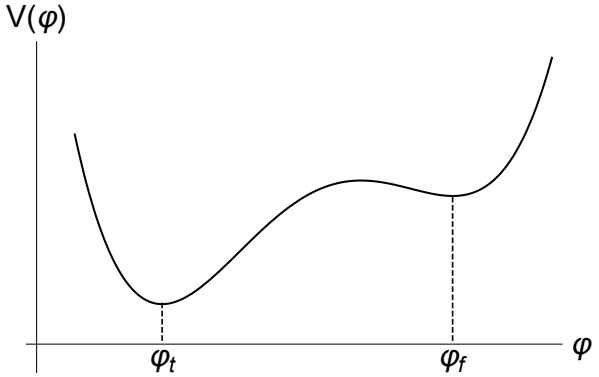

Figure 32: A typical potential in which false vacuum decay can occur. The bounce solution interpolates between the false vacuum φ_f and true vacuum φ_t.

The bounce solution is the lowest action $O(4)$ symmetric solution to the Euclidean equations of motion that interpolates between false and true vacua (see Fig. 32). Expanding around the bounce solution, gives the pre-exponential factor $\mathcal{A}$ as a Gaussian integral over

the linear perturbations. Proper bounces should have exactly one eigenfunction with a negative eigenvalue in the spectrum of linear perturbations, in order to make the decay picture coherent [111]. While this is always the case in flat space-time, generalizing to curved space-time results in some bounces getting infinitely many negative modes indicating a problem. Note that when gravity is involved, in addition to the basic bounce solution, there are oscillating instantons and an infinite tower of oscillating bounces [113, 124, 125], which, however, have more than one negative modes [114, 115] making their relation to tunneling questionable.

In the following sections based on [6] we aim to clarify the question of whether the negative mode problem is inherently related to Planck-scale physics and highlight differences between the Hamiltonian and Lagrangian approaches to the problem. Let us consider the theory of a single scalar field minimally coupled to gravity, which is defined by the following Euclidean action

$$S_E = \int d^4x\sqrt{g}\left(-\frac{1}{2\kappa}R + \frac{1}{2}\nabla_\mu\varphi\nabla^\mu\varphi + V(\varphi)\right), \tag{5.45}$$

where $\kappa = 8\pi G_N$ is the reduced Newton's gravitational constant. The most general $O(4)$ invariant metric is parametrised as

$$ds^2 = N^2(\eta)d\eta^2 + \rho^2(\eta)d\Omega_3^2\,, \tag{5.46}$$

where $N(\eta)$ is the lapse function, $\rho(\eta)$ is the scale factor and $d\Omega_3^2$ is metric of the unit three-sphere. In proper-time gauge, $N = 1$, the corresponding field equations are

$$\ddot{\varphi} + 3\frac{\dot{\rho}}{\rho}\dot{\varphi} = \frac{\partial V}{\partial\varphi}\,, \tag{5.47}$$

$$\ddot{\rho} = -\frac{\kappa\rho}{3}\left(\dot{\varphi}^2 + V(\varphi)\right)\,, \tag{5.48}$$

$$\dot{\rho}^2 = 1 + \frac{\kappa\rho^2}{3}\left(\frac{\dot{\varphi}^2}{2} - V(\varphi)\right)\,, \tag{5.49}$$

where $\dot{} = d/d\eta$. The leading exponential factor in the decay rate is determined by the bounce: A solution of these equations with appropriate boundary conditions. In order to calculate the pre-exponential factor $\mathcal{A}$ in Eq. (5.43) one should consider linear perturbations about the bounce solution. For this purpose we expand the metric and the scalar field over an $O(4)$ symmetric background as follows (compare to B):

$$ds^2 = (1 + 2A(\eta))d\eta^2 + \rho(\eta)^2(1 - 2\Psi(\eta))d\Omega_3^2\,, \qquad \varphi = \varphi(\eta) + \Phi(\eta)\,, \tag{5.50}$$

where ρ and φ are the background field values and A, Ψ and Φ are small perturbations. Note that under the infinitesimal shift $\eta \to \eta + \alpha$ the gauge transformations are

$$\delta\Psi = -\frac{\dot{\rho}}{\rho}\alpha\,, \qquad \delta\Phi = \dot{\varphi}\alpha\,, \qquad \delta A = \dot{\alpha}\ . \tag{5.51}$$

In what follows, we will be interested in the lowest (purely η-dependent, 'homogeneous') modes and consider only scalar metric perturbations. Expanding the total action to second order in perturbations and using the background equations of motion, we find

$$S = S^{(0)}[\rho, \varphi] + S^{(2)}[A, \Psi, \Phi] \, , \tag{5.52}$$

where $S^{(0)}$ is the action of the background solution and $S^{(2)}[A, \Psi, \Phi]$ is the quadratic action. An analysis of the equations of motion following from this quadratic action shows [116, 117] that there are constraints in this system and only one out of three variables is physical. The unconstrained quadratic action about Coleman - De Luccia bounces was first derived in [116] using the $\Psi = 0$ gauge in the Lagrangian approach. Integrating out A and expressing the quadratic action in terms of the remaining, physical perturbation Φ, one gets

$$S_L^{(2)} = 2\pi^2 \int \rho^3 d\eta \left[\frac{\dot{\rho}^2}{2Q_L} \dot{\Phi}^2 + \frac{1}{2} U_\Phi \Phi^2 \right] \tag{5.53}$$

with the potential being

$$U_\Phi = \frac{\dot{\rho}^2 V''}{Q_L} + \frac{\kappa \rho^2 \dot{\rho}^2 V'^2}{3 Q_L^2} + \frac{\kappa \rho \dot{\rho} \dot{\varphi} V'}{3 Q_L^2} \, , \tag{5.54}$$

where $' \equiv d/d\varphi$. In particular, it was noted that a factor termed Q appears in front of the kinetic term, which in the Lagrangian approach is the following combination of background quantities

$$Q_L = 1 - \frac{\kappa \rho^2 V(\varphi)}{3} = \dot{\rho}^2 - \frac{\kappa \rho^2 \dot{\varphi}^2}{6} \, . \tag{5.55}$$

This factor becomes negative for any bounce solution close to the point $\dot{\rho} = 0$. In addition, for some bounces it becomes negative a second time, in a regime where the last term dominates over $\dot{\rho}$. Despite its widespread use, the Lagrangian approach was criticized in [24] because of poor gauge fixing. Indeed, from the gauge transformations Eq. (5.51) it is clear that we cannot freely transform the variable Ψ. In particular the transformation breaks down at any point where $\dot{\rho} = 0$ making it impossible to impose a nonsingular gauge on Ψ. Unfortunately, there are not many alternatives in the Lagrangian approach since it only involves configuration space variables. Later, Lee and Weinberg [122] promoted Φ to a gauge invariant variable

$$\chi = \dot{\rho} \Phi + \rho \dot{\varphi} \Psi \, , \tag{5.56}$$

and obtained a pulsation equation, which exactly coincides with the earlier $\Psi = 0$ gauge fixed approach (see Appendix in [123]).

Therefore, we will use the Hamiltonian approach in this note which is more adequate for constrained dynamical systems. Using a Hamiltonian approach following Dirac the quadratic action has the form [118, 123]

$$S_H^{(2)} = \pi^2 \int d\eta \Phi \left[-\frac{d}{d\eta} \left(\frac{\rho^3(\eta)}{Q_H} \frac{d}{d\eta} \right) + \rho^3(\eta) U[\varphi(\eta), \rho(\eta)] \right] \Phi \,, \tag{5.57}$$

where the potential U is expressed in terms of the bounce solution as

$$U[\varphi(\eta), \rho(\eta)] \equiv \frac{V''(\varphi)}{Q_H} + \frac{2\kappa\dot{\varphi}^2}{Q_H} + \frac{\kappa}{3Q_H^2} \Big(6\dot{\rho}^2\dot{\varphi}^2 + \rho^2 V'^2(\varphi) - 5\rho\dot{\rho}\dot{\varphi}V'(\varphi) \Big) \,. \tag{5.58}$$

and again a factor $Q_H \equiv Q$ appears in quadratic action and this time it reads

$$Q = 1 - \frac{\kappa\rho^2\dot{\varphi}^2}{6} \,. \tag{5.59}$$

Unlike the previous prefactor in Eq. (5.55), this factor is positive definite for a wide class of bounces where one finds exactly one *tunneling* negative mode in the spectrum of the unconstrained action [118, 117, 119, 123]. When Q becomes negative along the bounce, the pulsation equation is regular and the tunneling negative mode persists, but on top of it one gets an infinite tower of negative modes that has support in the negative Q region. Furthermore, negative Q leads to catastrophic particle creation and instability of the quasiclassical approximation [116].

5.7 Negative mode problem for a polynomial potential

5.7.1 Numerical example of negative Q far from Planck scale

One might argue that the problematic behaviour of Q only appears close or above the Planck scale where classical General Relativity is no longer valid. Here with combined numerical and analytic methods we can show that this is not the case and Q may be negative even far away from the Planck scale. For definiteness we parameterize the quartic potential as

$$V(\varphi) = V_0 + \frac{\lambda}{8}(\varphi^2 - \mu^2)^2 + \frac{\epsilon}{2\mu}(\varphi + \mu) \tag{5.60}$$

and plot it in Fig. 33. The evolution of the scale factor and scalar field for the Coleman - De Luccia bounce solution and the evolution of the corresponding Q factor is shown in Fig. 34 and we can immediately see that even though the energy scale is significantly below the Planck scale, Q turns negative along the evolution. It might be argued that Q becomes negative because the curvature becomes huge close at the maximal radius of the instanton. However, the four-dimensional Ricci scalar R, given by

$$R = \frac{6}{\rho(\eta)^2} \left(1 - \dot{\rho}(\eta)^2 - \rho(\eta)\ddot{\rho}(\eta) \right) \tag{5.61}$$

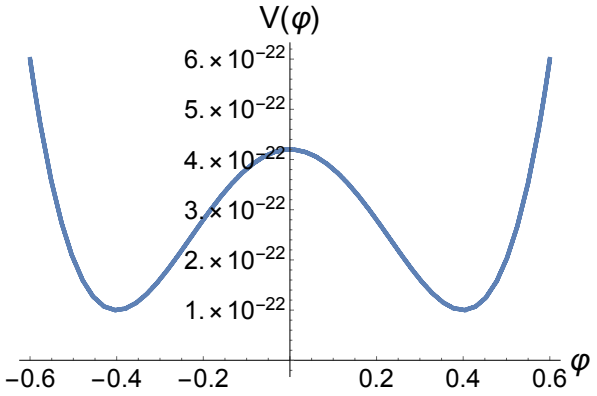

Figure 33: A plot of the potential Eq.(5.60) for the parameter values $V_0 = 10^{-22}$, $\lambda = 10^{-19}$, $\epsilon = 10^{-30}$, and $\mu = 0.4$. For these parameters we have $V(\varphi_{top})$ five orders of magnitude below the Planck scale. The minima for this potential are almost degenerate, a fact, which is reflected in the small value for ϵ, but there still is a true and a false vacuum.

is suppressed by a factor of $\frac{1}{\rho^2}$, where the scale factor ρ typically is large in the negative Q regime. Hence, the curvature is expected to be small as well which is demonstrated for the example above in Fig. 35. In general the intuitive reasoning of φ rolling in the inverted potential gives a good guideline for how to find solutions with negative Q at an arbitrary scale. In particular, taking $V(\varphi_{top})$ much bigger than $V(\varphi_{\pm})$ where $\varphi_{\pm}$ are the two deSitter vacua of the potential will give a fast rolling field with a large bubble radius which are the exact conditions for negative Q. In the next section we make this argument more precise.

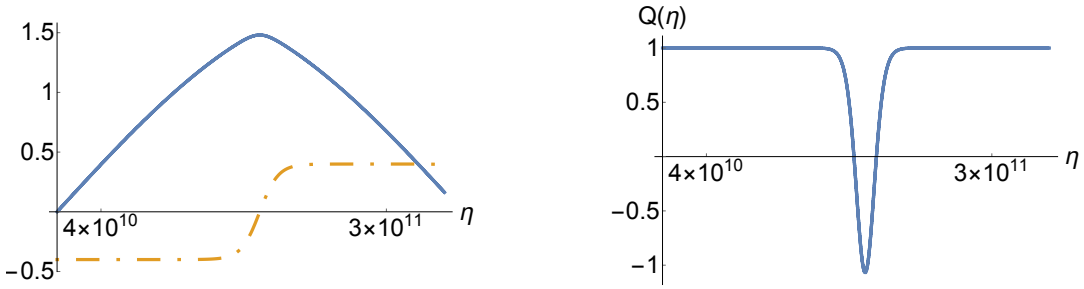

Figure 34: *Left:* The evolution of the scale factor $\rho(\eta)/10^{11}$ in blue and scalar field $\varphi(\eta)$ in orange as a function of Euclidean time η which ranges from 0 to approximately 3.6×10^{11} in this example. *Right:* The evolution of Q for this instanton clearly demonstrating that it becomes negative along the bounce solution.

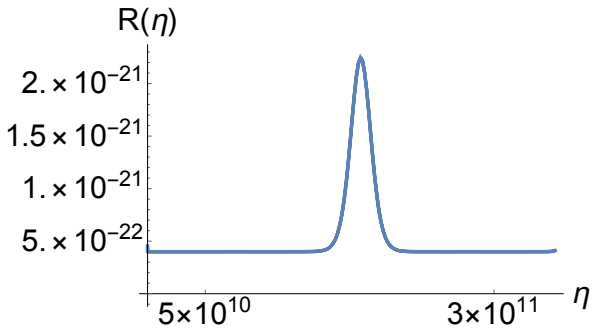

Figure 35: The four dimensional Ricci scalar for the instanton solution in Fig. 34

.

5.7.2 Negative Q in the thin wall approximation

We are interested in a formula for Q that depends only on the parameters of the potential. Critically we note that the smallest value of Q (see Eq. (5.59)) is obtained when $\rho^2\dot{\varphi}^2$ is maximized which, in the thin wall limit approximately happens when both ρ and $\dot{\varphi}$ are extremized. Thus, starting with ρ, the general formula for the bubble size [126] is

$$\rho^2 = \frac{\rho_0^2}{1 + 2(\rho_0^2/2\bar{\lambda})^2 + (\rho_0/2\bar{\Lambda})^4} \,, \tag{5.62}$$

where ϵ is the separation between the true and false vacuum $\epsilon = V_f - V_t$, ρ_0 is the critical bubble size without gravity and

$$\bar{\lambda}^2 = \frac{3}{\kappa(V_f + V_t)} = \frac{3}{\kappa(2V_f - \epsilon)}, \qquad \bar{\Lambda}^2 = \frac{3}{\kappa(V_f - V_t)} \,. \tag{5.63}$$

This provides a generalization of Coleman - De Luccia's earlier result which can be recovered by setting $\bar{\Lambda}^2/\bar{\lambda}^2 = \pm 1$ corresponding to $V_f = 0$ or $V_t = 0$ respectively. Using definitions Eq. (5.63), expression for bubble size Eq. (5.62) can be written as follows

$$\rho^2 = \frac{\rho_0^2}{\frac{\kappa\rho_0^2 V_f}{3} + \left(1 - \frac{\kappa\rho_0^2\epsilon}{12}\right)^2} \,. \tag{5.64}$$

This expression shows that in contrast to flat space-time, where bubble size grows indefinitely when $\epsilon \to 0$, in dS-dS transition it reaches maximum size and starts to decrease again. Hence this expression simplifies dramatically by taking a particular value for ϵ, namely

$$\epsilon = \frac{12}{\kappa\rho_0^2} = \frac{3}{4}\kappa\sigma^2 \,, \tag{5.65}$$

where σ is the bubble tension in the absence of gravity. Due to this choice the bubble size now takes on a particularly simple form

$$\rho^2 = \frac{3}{\kappa V_f} \,. \tag{5.66}$$

So far all the calculations were independent of the particular form of the potential. One can go one step further and obtain a concrete value for ϵ based on the parameters of the potential by choosing

$$V(\phi) = \frac{c^2}{8}(\varphi^2 - \mu^2)^2 + \frac{\epsilon}{2\mu}(\varphi + \mu) \ , \tag{5.67}$$

where $c^2 > 0, \mu > 0$ and $\epsilon \geq 0$, such that the wall tension σ can be solved for analytically, in the thin wall approximation

$$\sigma = \int_{\varphi_t}^{\varphi_f} \left[2\left(V_s(\varphi) - V_s(\varphi_t)\right)\right]^{1/2} d\varphi = \frac{2}{3} c\mu^3 \ , \tag{5.68}$$

where $V_s = \frac{\lambda}{8}(\varphi^2 - \mu^2)^2$ is the symmetric part of the potential and for this potential we have $\varphi_{t,f} = \pm\mu$. This implies that the critical value for ϵ is

$$\epsilon = \frac{1}{3}\kappa c^2 \mu^6 \ . \tag{5.69}$$

Returning to the definition of Q and making use of the Friedman equation

$$\dot{\rho}^2 = 1 + \frac{\kappa}{3}\rho^2 \left(\frac{1}{2}\dot{\varphi}^2 - V(\varphi)\right) \tag{5.70}$$

we obtain

$$Q = 2 - \dot{\rho}^2 - \frac{\kappa}{3}\rho^2 V(\varphi) \tag{5.71}$$

and consequently, if we restrict ϵ to be of the special form of Eq. (5.69), we have

$$Q_c = 2 - \dot{\rho}^2 - \frac{V(\varphi)}{V_f} \qquad \rightarrow \qquad Q_c \leq 2 - \frac{V(\varphi)}{V_f} \ . \tag{5.72}$$

Hence if we can find a ϕ such that this quantity is negative, we can be sure that Q will be negative somewhere. As a first guess we can take for example $\phi_c = 0$. Numerically we will see that this assumption leaves us very close to the extremal value for Q_c. Writing this in terms of the parameter of the potential given in Eq. (5.67), we obtain:

$$Q_c \leq 2 - \frac{V(\varphi)}{V_f} \approx 2 - \frac{V(0)}{V_f} \tag{5.73}$$

$$= 2 - \frac{1}{V_f}\left(\frac{c^2}{8}\mu^4 + \frac{\epsilon}{2}\right) \tag{5.74}$$

$$\approx \frac{3}{2} - \frac{c^2}{8}\frac{\mu^4}{\epsilon} \tag{5.75}$$

$$= \frac{3}{2}\left(1 - \frac{1}{4\kappa\mu^2}\right) \tag{5.76}$$

where in the last approximation we took $\varphi_t \approx \mu$ which implies $V_f \approx \epsilon$ and we have plugged in the critical value for epsilon in the second last line. All this implies that for $\mu^2 < \frac{1}{4\kappa}$ we expect

that Q is negative at some point. This confirms our intuition that for steeper potentials we expect Q to be more negative since the scalar field will roll faster in such a potential. Indeed, this choice of ϵ illustrates this beautifully since it eliminates the dependence on the height of the potential. Thus we can find transitions that have the problematic negative pre-factor for the kinetic term of the perturbations at *any* scale.

5.7.3 Existence of Coleman - De Luccia solutions

It is known [127], [113] that for the existence of Coleman - De Luccia bounce solution in a given potential $V(\varphi)$ following condition should be satisfied

$$|V''(\varphi_{top})| > 4H^2(\varphi_{top}) \,, \tag{5.77}$$

where $V''(\varphi) = \frac{d^2V(\varphi)}{d\varphi^2}$ and $H^2(\varphi) = \frac{\kappa V(\varphi)}{3}$. For the quartic potential defined in Eq. (5.67) we approximate $\varphi_{top} = 0$ and consequently must satisfy

$$\frac{c^2\mu^2}{2} > \frac{2}{3}\kappa\left(\frac{c^2\mu^4}{4} + \epsilon\right) \tag{5.78}$$

Choosing $\epsilon = \frac{1}{3}\kappa c^2\mu^6$, as above, we find that in order for Coleman - De Luccia instantons to exist we must have

$$\mu^2 < \frac{3}{8\kappa}(\sqrt{17} - 1) \approx \frac{9}{8\kappa} \tag{5.79}$$

Hence for $0 < \mu^2 < \frac{1}{4\kappa}$, Coleman - De Luccia solutions exist but are pathological as Q is negative for some part of the instanton. For $\frac{1}{4\kappa} < \mu^2 < \frac{9}{8\kappa}$, the Coleman - De Luccia instantons exist and are perfectly well behaved while for $\mu^2 > \frac{9}{8\kappa}$ no Coleman - De Luccia solutions exist.

5.7.4 Comparison with numerics

In deriving the analytic bounds for μ we took several approximations. Therefore it is useful to compare the approximate analytics to the full, numerical solutions. Here we choose $\kappa = c = 1$ for simplicity and without loss of generality and compare the two methods for various values of μ. Note that since ϵ scales like μ^6, the thin wall approximation is satisfied very rapidly as μ decreases from 1. Four sample geometries are shown in Fig. 36 while their corresponding Q values are plotted in Fig. 37. In table 5.7.4 we compare the analytics with the numerics, indicating that our approximation yields excellent results. In particular, the approximation of taking $\varphi_c = 0$ is a very good one while the largest uncertainty comes from neglecting the derivative of ρ. From Fig. (37) is also apparent that the Hamiltonian kinetic pre-factor Q

and its Lagrangian counterpart Q_L behave in a very similar fashion when μ is large but may differ qualitatively in other situations. In particular since Q_L always develops a negative region, the difference between the two grows as μ shrinks.

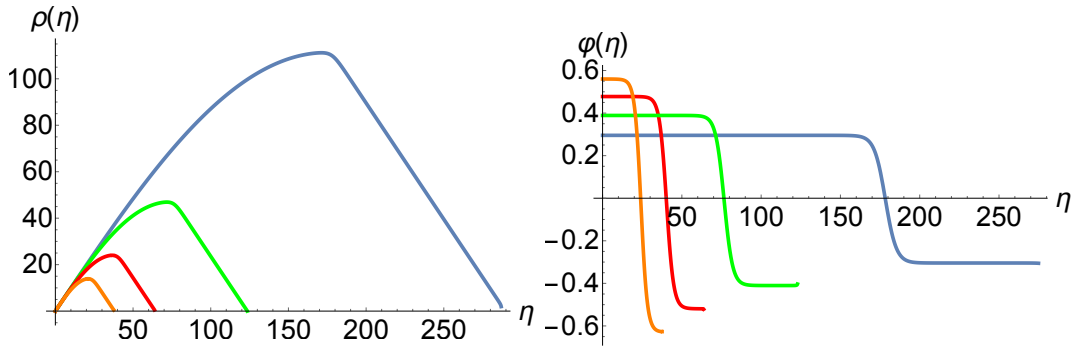

Figure 36: Plotted here is the evolution of four instantons in the potential given by equation (5.67) but for four different values of μ. The orange, red, green, and blue curves correspond to $\mu = 3/5, 1/2, 2/5$, and $3/10$ respectively. *Left:* The evolution of the scale factor in terms of Euclidean time η. *Right:* The evolution of the scalar field.

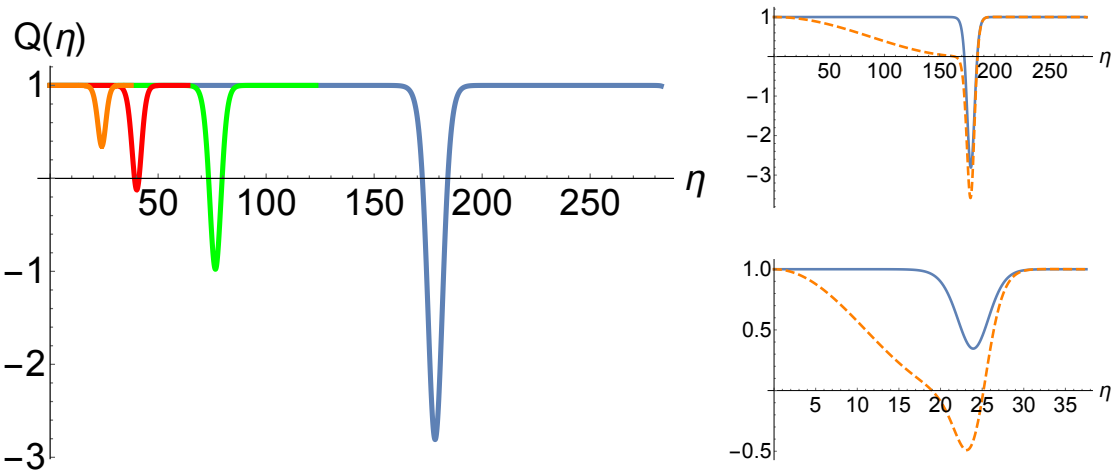

Figure 37: *Left:* The kinetic pre-factor Q for the bounces shown above. *Right:* Comparison of Q in blue and Q_L in dashed orange. At the top $\mu = 3/10$ while at the bottom $\mu = 3/5$.

These results are still of order one in μ which corresponds to a field excursion for ϕ of order one also which might be considered problematic. On the other hand, the approximations we are using work better for ever smaller values μ, hence even though it is numerically very hard to find Coleman - De Luccia instantons for these values, we can nevertheless rely on the analytical tools developed to analyze these solutions.

	$\mu = 3/5$		$\mu = 1/2$		$\mu = 2/5$		$\mu = 3/10$	
	Numerics	Analytics	Numerics	Analytics	Numerics	Analytics	Numerics	Analytics
ρ_c'	-0.4901	0	-0.4939	0	-0.4982	0	-0.4976	0
ϕ_c	0.0108	0	0.0037	0	-0.0001	0	0.0002	0
ρ_c	13.266	14.001	23.250	24.132	45.927	47.036	109.852	111.323
ρ_m	13.898	14.001	24.019	24.132	46.916	47.036	111.199	111.323
Q_{min}	0.3457	$\leq$ 0.4583	-0.1242	$\leq$ 0	-0.9768	$\leq$ -0.8437	-2.8087	$\leq$ -2.6667

Table 3: Comparison of various quantities in the analytic expression with the numerics. The ones with subscript c refer to the the values where Q takes the minimum. ρ_m is the maximum/critical bubble radius and Q_{min} is the minimum value for Q.

5.8 Negative mode problem for Higgs-like potentials

Taking into account the current experimental bounds of the standard model parameters, the instability scale of the Higgs potential, $\lambda(\mu_\Lambda) = 0$, depends sensitively on the top Quark and Higgs masses. The bounds at 1σ currently are [128]

$$1.16 \cdot 10^9 \text{ GeV} < \mu_\Lambda < 2.37 \cdot 10^{11} \text{ GeV} . \tag{5.80}$$

such that the top of the potential barrier lies at about

$$\varphi_{top} = 4.64 \cdot 10^{10} \text{ GeV} , \tag{5.81}$$

and the barrier height is

$$V_{top} = 3.46 \cdot 10^{38} \text{ GeV}^4 = (4.31 \cdot 10^9 \text{ GeV})^4 . \tag{5.82}$$

In Planck units $M_{Pl} = 1/\sqrt{8\pi G} \approx 2.435 \cdot 10^{18}$ GeV $= 1$, these numbers are:

$$4.76 \cdot 10^{-10} < \mu_\Lambda < 9.73 \cdot 10^{-8} , \varphi_{top} = 1.91 \cdot 10^{-8} , V_{top} = 9.84 \cdot 10^{-36} . \tag{5.83}$$

At high energies the Higgs potential can be modelled as [129]

$$V_H = V_0 + \frac{\lambda_H(\varphi)}{4}\varphi^4 , \tag{5.84}$$

$$\lambda_H = q\left[(\ln\varphi)^4 - (\ln\Lambda)^4\right] , \tag{5.85}$$

where q is a dimension-less fitting parameter and V_0 is the cosmological constant. An sample potential for specific values of q and Λ is given in Fig. (38). We can further mimic the Higgs potential by choosing $V_0 << V_{top}$ and

1. $\Lambda = 10^{-9}, q = 10^{-2}$ for the lower bound value of instability scale or

2. $\Lambda = 10^{-7}, q = 10^{-9}$ for the upper bound value of the instability scale, Eq. (5.83).

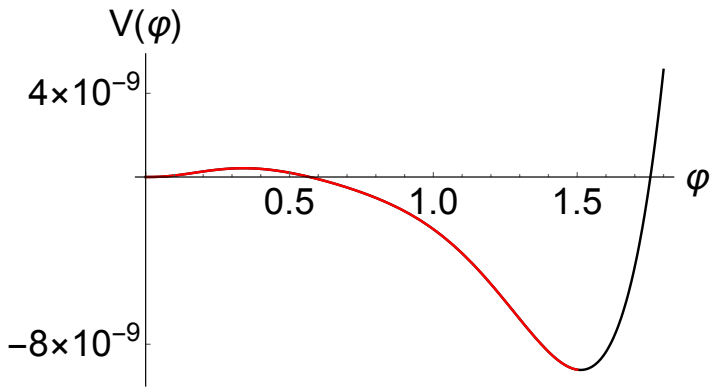

Figure 38: An example of the Higgs-like potential described in Eq. (5.84) for $q = 10^{-7}$ and $\Lambda = 0.57$. The bounce solution is marked in red and does not develop a problematic, negative Q, region.

Numerically, we found that for $\Lambda < \Lambda_*$ Q is positive everywhere while for $\Lambda > \Lambda_*$, Q develops a region with $Q < 0$. Choosing parameters $q = 10^{-7}$ and $V_0 = 10^{-12}$ we found $0.57 < \Lambda_* < 0.6$, see Figure 39. Therefore for a realistic Higgs like potential, the negative mode problem shows up only at the Planck values of the instability scale.

5.9 Discussion

Using the Hamiltonian approach to false vacuum decay [118, 119], we have shown that for generic polynomial potentials the negative mode problem is not related to Planck scale physics. At the same time we demonstrated that for a Higgs - like potential, a region with $Q < 0$ does not develop for realistic values of the potential's parameters. Instead, the problem only shows up if we assume the Higgs instability scale to be close to the Planck mass.

In the present analysis we used the Hamiltonian reduction scheme, which is based on Dirac's approach to constrained dynamical systems. Within this method, both, gauge fixed [118] and gauge invariant [119] approaches, are not problematic and give the same answer. Hence we think this reduction gives a more adequate description of the physical situation than the Lagrangian approach. Note that there is a similar controversy in the counting of the number of negative modes [130], [131] of axionic Euclidean wormholes [132, 133]. Recently it was advocated that the Hamiltonian approach discussed here, also gives the correct answer in the wormhole case [134]. On the other hand why Lagrangian and Hamiltonian reductions give

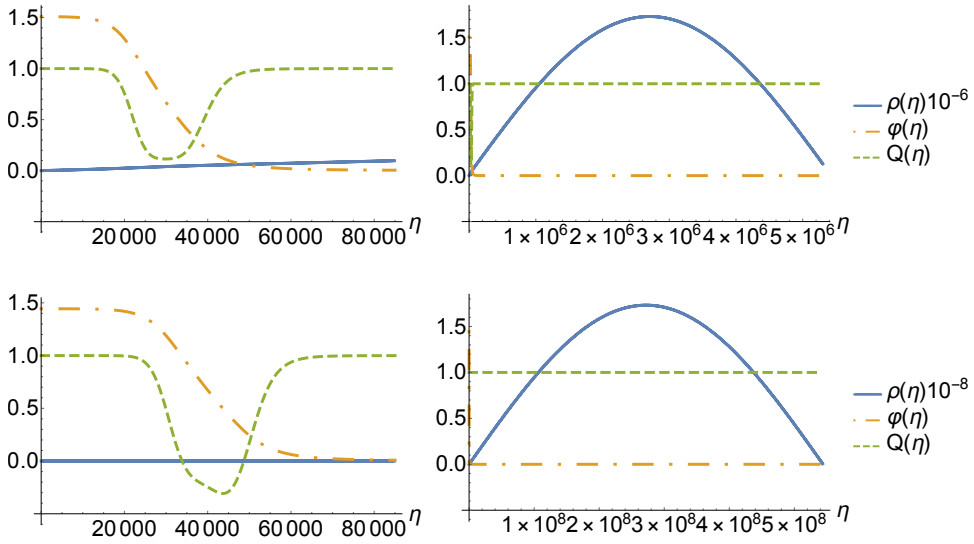

Figure 39: Here we show the values of the scalar field φ, scale factor ρ and the function Q for the Higgs like potential Eq. (5.84). The top figure shows the Coleman - De Luccia instanton for $\Lambda = 0.57$ while the bottom one has $\Lambda = 0.6$. The images on the left are zoomed in versions of the full instantons shown on the right. $M_{Pl} = 1$ units are used where we zoomed in on the part of the instanton where the scalar field tunnels and the problematic behaviour of Q might occur.

a different kinetic pre-factor Q for bounces in false vacuum decay and its physical relevance is still an open, puzzling question.

6 Quantum Cosmology

Quantum cosmology is the application of the principles of quantum mechanics to the universe as a whole. Although it might not seem fruitful to apply a theory describing the smallest objects to the largest object we know, quantum theory makes a strong argument for doing so. The reason is that most quantum systems are coupled to its environment which is again coupled to its environment and so forth until we reach the largest possible scales: The entire universe - the only closed quantum system. The universe then is fundamentally quantum but appears classical in most of its stages; a process known as decoherence. The most interesting periods are, of course, where decoherence has not yet happened and the quantum nature of the universe becomes apparent. Probing it is the goal of quantum cosmology which we will introduce following [19, 135] in the following sections.

6.1 The Hamiltonian Formulation of General Relativity

In order to commence with a general formalism for quantum cosmology we first have to turn our attention to the Hamiltonian formalism of General Relativity [74]. One considers an embedding of a three-surface with three-metric h_{ij} in a four-manifold with four-metric $g_{\mu\nu}$. In Arnowitt-Deser-Misner (ADM) variables this embedding leads to a (3+1) split of the four-metric

$$ds^2 = -(N^2 - N_i N^i)dt^2 + 2N_i dx^i dt + h_{ij}dx^i dx^j \tag{6.1}$$

where N is a scalar called the lapse and the three-vector N_i is called the shift vector. Both of these quantities are general functions of all coordinates. They describe how the coordinates on one three surface are related to the ones on an adjacent three-surface and are therefore arbitrary or pure gauge. Writing the standard Einstein-Hilbert action (2.4) in terms of the ADM variables, we obtain

$$S_{EH} = \frac{1}{2}\int d^3x dt \mathcal{L}_{ADM} \tag{6.2}$$

with

$$\mathcal{L}_{ADM} = N\sqrt{h}\left[K_{ij}K^{ij} - K^2 + {}^{(3)}R - 2\Lambda\right] \tag{6.3}$$

where in the extrinsic curvature in these variables reads

$$K_{ij} = \frac{1}{2N}\left[\dot{h}_{ij} - D_I h_j - D_j h_i\right] \tag{6.4}$$

Here we chosen to denote the time derivative with an over-dot $\dot{x} = \frac{\partial x}{\partial t}$ and D denotes the three-dimension covariant derivative on the hyper-surface. Now we are in a position to directly write down the Hamiltonian form of the action

$$S_{EH} = \int d^3x dt \left[\dot{h}_{ij}\pi^{ij} - N\mathcal{H} - N^i\mathcal{H}_i \right] \tag{6.5}$$

where the π^{ij} is the conjugate momentum to h_{ij} defined via

$$\pi^{ij} = \frac{\partial \mathcal{L}_{ADM}}{\partial \dot{h}_{ij}} \tag{6.6}$$

It is important to note that the momenta conjugate to the lapse and shift are identically zero

$$\pi = \frac{\partial \mathcal{L}_{ADM}}{\partial \dot{N}} = 0 \qquad \pi_i = \frac{\partial \mathcal{L}_{ADM}}{\partial \dot{N}^i} = 0 \tag{6.7}$$

implying that they act as Lagrange multipliers in the action, which is another way of saying that N and N^i are pure gauge variables. $\mathcal{H}$ and $\mathcal{H}_i$ are the constraints of the system. We have the momentum constraint

$$\mathcal{H}_i = -2D_j\pi^j_i = 0 \tag{6.8}$$

and the Hamiltonian constraint

$$\mathcal{H} = 2G_{ijkl}\pi^{ij}\pi^{kl} - \frac{1}{2}\sqrt{h}\left({}^{(3)}R - 2\Lambda\right) = 0 \tag{6.9}$$

where the DeWitt metric G_{ijkl} is given by

$$G_{ijkl} = \frac{1}{2\sqrt{h}}(h_{ik}h_{jl} + h_{il}h_{jk} - h_{ij}h_{kl}) \tag{6.10}$$

The constraints are equivalent to the time-time and time-space components of the classical Einstein equations and play a crucial role in the quantization of the system. The space of all three-metrics on a three-surface forms superspace (which is unrelated to supersymmetry's superspace) and comes equipped with the DeWitt metric as its natural metric. It is infinite dimensional since we have a finite number of coordinates h_{ij} at an infinite number of points in the three-space. This is why people often employ the so-called minisuperspace approach, restricting to certain metrics that make the system finite dimensional and thus more tractable.

6.2 Quantization

Quantizing by Dirac's method [136], the wave function of the universe Ψ, is taken to be a functional of the three-metric h_{ij} and the matter configuration on superspace. Note that

the wave function does not depend on the coordinate t, simply because GR is an example of a parametrized theory and time is already contained in the other dynamical variables of the system. Wave functions live in a Hilbert space on which quantum operators such as position and momentum space operators act. The observables of the theory are represented by Hermitian operators. According to Dirac's quantization procedure the wave function has to be annihilated by the quantum analogue of the classical constraints. In other words, assuming the usual substitution for the momenta

$$\pi^{ij} \to -i\frac{\delta}{\delta\hbar_{ij}} \tag{6.11}$$

one obtains the momentum constraint originating from the fact that the shift is a Lagrange multiplier

$$\mathcal{H}_i\Psi = 2iD_j\frac{\delta\Psi}{\delta\hbar_{ij}} = 0 \tag{6.12}$$

and the so-called Wheeler-DeWitt equation which comes from the lapse

$$\mathcal{H}\Psi = \left[-G_{ijkl}\frac{\delta}{\delta\hbar_{ij}}\frac{\delta}{\delta\hbar_{kl}} - \sqrt{h}({}^{(3)}R - 2\Lambda)\right]\Psi = 0 \tag{6.13}$$

In this discussion, and all subsequent ones in this thesis, we will ignore issues that arise due to operator orderings in the Wheeler-DeWitt equation. Notice that the momentum constraint is simply a quantum mechanical expression of the theory's invariance under three-dimensional diffeomorphisms [137]. That means that the wave function Ψ is the same under a change of coordinates on the three surface h_{ij}.

6.3 Minisuperspace

As we have touched on before, the fact that superspace is infinite dimensional makes it very hard to work with. In practice, therefore, all but a finite number of degrees of freedom are frozen out by choosing a specific, restrictive metric ansatz. Most commonly this is achieved by restricting the fields to be homogeneous, however, any model with a finite number of degrees of freedom may be called a minisuperspace model. Fortunately, this simplification seems to be a reasonable one. After all, the universe is homogeneous and isotropic on its largest scales. Conceptually, however, the minisuperspace simplification is dubious: the uncertainty principle clearly does not allow setting most fields and their conjugate momenta to zero simultaneously. Furthermore, there currently does not exist a systematic approximation scheme which represents the full theory increasingly better. Nevertheless, minisuperspace models allow the study of certain features of the full theory and most work in quantum

cosmology has been done in this setting.

Restricting to any of the cosmological models presented in table 3.5.2 with $s \geq 3$ and the Lemaitre-Tolman-Bondi family, reduce the theory from super- to minisuperspace. Upon substituting a metric ansatz into the general form of the metric, one obtains

$$S[h_{ij}, N, N^i] = S[q^\alpha(t), N(t)] = \int_0^1 dt N \left[\frac{1}{N^2} f_{\alpha\beta}(q) \dot{q}^\alpha \dot{q}^\beta - U(q) \right] \tag{6.14}$$

where $f_{\alpha\beta}$ is a reduced version of the DeWitt metric and the degrees of freedom are encoded in the variable q. The integration over t is from 0 to 1 which can be achieved by rescaling the lapse N and $U(q)$ depends on the details of the metric ansatz. We now study the quantization of minisuperspace.

6.3.1 Canonical Quantization

The most important feature of the action (6.14) is that it is of the form of a relativistic point particle moving in n dimensional, curved space-time under the influence of the potential $U(q)$. After varying with respect to the variables q^α and N we obtain the field equations

$$\frac{1}{N} \frac{d}{dt} \left(\frac{\dot{q}^\alpha}{N} \right) + \frac{1}{N^2} \Gamma^\alpha_{\beta\gamma} \dot{q}^\beta \dot{q}^\gamma + f^{\alpha\beta} \frac{\partial U}{\partial q^\beta} = 0 \tag{6.15}$$

$$\frac{1}{2N^2} f_{\alpha\beta} \dot{q}^\alpha \dot{q}^\beta + U(q) = 0 \tag{6.16}$$

These should be equivalent to the Einstein equations. Unfortunately, this is not guaranteed - instead one has to check in every case separately. In models that are equivalent, the canonical Hamiltonian is given by

$$H_c = p_\alpha \dot{q}^\alpha - L = N \left[\frac{1}{2} f_{\alpha\beta} p^\alpha p^\beta + U(q) \right] = NH \tag{6.17}$$

where, just like in the general case, we defined the canonical momenta

$$p_\alpha = \frac{\partial L}{\partial \dot{q}^\alpha} \tag{6.18}$$

Finally the Hamiltonian form of the action is given by

$$S = \int_0^1 dt \left[p_\alpha \dot{q}^\alpha - NH \right] \tag{6.19}$$

which unsurprisingly indicates that N is simply a Lagrange multiplier, enforcing the Hamiltonian constraint $H = 0$. The wave function is then found by demanding that it is annihilated by H. This gives rise to the minisuperspace Wheeler-DeWitt equation.

$$H\Psi = 0 \rightarrow \left[-\frac{1}{2} \nabla^2 - \frac{1}{8} \frac{n-2}{n-1} K_f + U(q) \right] \Psi = 0 \tag{6.20}$$

where K_f and ∇^2 are the curvature and Laplacian of the minisuperspace metric respectively. Note that this, minisuperspace, form of the WDW equation does not have operator ordering issues since the order is resolved by demanding that it is covariant in minisuperspace.

6.3.2 Path Integral Quantization

An equivalent but very useful way of quantizing the system is via the path integral; a formalism we have already discussed in the context of quantum mechanics. Unlike quantum mechanics, however, we first need to fix the remaining redundancy in the description of the system. It can be shown that all the remaining gauge symmetry of minisuperspace is fixed by imposing the condition

$$\dot{N} - \chi(p_\alpha, q^\alpha, N) = 0 \tag{6.21}$$

where χ is an arbitrary function. The path integral representing the wave function is then given by

$$\Psi = \int Dp_\alpha Dq^\alpha DN \Delta_G e^{iS[p,q,N]} \tag{6.22}$$

where $S[p, q, N]$ is the Hamiltonian form of the action (6.19) and Δ_G is the so-called Faddeev-Popov measure guaranteeing that the path integral does not depend on any particular gauge choice. Heuristically, we integrate over all paths ($q^\alpha(t)$,$p_\alpha(t)$,$N(t)$) that satisfy the boundary conditions $q^\alpha(0) = q_0^\alpha$ and $q^\alpha(1) = q_1^\alpha$. In practice the only realistic gauge choice is $\dot{N} = 0$ for which $\Delta_G =$ constant. Then the functional integral over the lapse reduced to an ordinary one

$$\Psi = \int dN \int Dp_\alpha Dq^\alpha e^{iS[p,q,N]} \tag{6.23}$$

Often, in order to evaluate the integral, one rotates to Euclidean time in analogy with Quantum Field Theory in which case it is customary to write

$$\Psi = \int dN \int Dq^\alpha e^{-I[q,N]} \tag{6.24}$$

where I is the Euclidean action and the momenta have already been integrated out[11]

6.4 Boundary Conditions

There is an old, simple idea illustrating the problem of initial conditions: take any state that the universe might be in and evolve it back in time to some primordial epoch – you will

[11] There are problems with defining the path integral in this way that only appear when gravity is included. We take a closer look at these problems and their possible resolution in chapter 8.

obtain a possible set of "initial" conditions for the universe. Considering that our current universe is in many ways special (and certainly non "generic"), this argument makes it very clear that we will need a theory of initial conditions if we are to understand the history of the universe. In a sense the task is to pick out just one wave function from the all the ones which are allowed by the dynamics (i.e the WDW equation). Initially, the hope was that mathematical consistency would single out just one solution. Unfortunately, this seems to not be true and in lieu proposals for the initial conditions were developed. The most famous ones are the no-boundary proposal of Hartle and Hawking [138, 69, 139, 140], and the closely related tunnelling prescription of Vilenkin [21, 29, 141, 142] which we will focus on for the remainder of the thesis. The no-boundary proposal is most easily expressed in terms of the Euclidean path integral formulation of quantum cosmology. The idea is to restrict the class of manifolds being summed over to ones that only have a single boundary at the final surface. In practice, the simplest way of describing the no-boundary proposal as well as the tunnelling prescription is by considering a Euclidean, closed FLRW metric non-minimally coupled to a scalar field. In that case, the equations of motion reduce to the ones presented in eqs. (3.48) - (3.52) with the anisotropies set to zero and crucially $N = i$. In the saddle point approximation to the path integral, the integral is approximated by a sum of the integrand's saddle points

$$\Psi(b, \chi) \approx \sum e^{-S_E(b,\chi)} \tag{6.25}$$

where b and χ are the values of the scale factor a and scalar field ϕ on the final three-surface. S_E is the Euclidean action of a, typically complex, instanton solution for a and ϕ which satisfy the no boundary conditions

- $a(0) = 0$ and the solution does *not* have a singularity there. This condition is the one that required a Euclidean solution and closed spatial slices in the first place. It also implies that at $t = 0$ we must have $a'(0) = 1$ and $\phi'(0) = 0$.

- At some point τ_f in the complex τ plane, $(a, \phi) = (b, \chi)$. The solution then needs to interpolate between $\tau = 0$ and $\tau = \tau_f$. Note that τ_f can also be rescaled to 1 in which case, the lapse is no longer set to $N = i$ but generally becomes complex.

Notably the no-boundary proposal can smoothly lead to both inflationary and ekpyrotic cosmologies [143] and predict a classical universe as we observe it today.

6.5 Classicality

What does it mean for the universe to be classical in quantum cosmology? Let us choose a semi-classical ansatz for the wavefunction

$$\Psi = e^{(-A+i\tilde{S})/\hbar} \tag{6.26}$$

with $A(q^\alpha)$ and $\tilde{S}(q^\alpha)$ real functions. Plugging this ansatz into the WdW equation and expanding in powers of $\hbar$ gives to leading order:

$$-\frac{1}{2}G^{\alpha\beta}\left(-\frac{\partial A}{\partial q^\alpha}+i\frac{\partial \tilde{S}}{\partial q^\alpha}\right)\left(-\frac{\partial A}{\partial q^\beta}+i\frac{\partial \tilde{S}}{\partial q^\beta}\right)+\mathcal{U}=0 \tag{6.27}$$

Thus if

$$\frac{\partial \tilde{S}}{\partial q^\alpha} \gg \frac{\partial A}{\partial q^\alpha}, \tag{6.28}$$

i.e. if the phase of the wavefunction varies much faster than its amplitude for all degrees of freedom, we obtain the Lorentzian Hamilton-Jacobi equation (which specifies the classical dynamics)

$$\frac{1}{2}G^{\alpha\beta}\frac{\partial \tilde{S}}{\partial q^\alpha}\frac{\partial \tilde{S}}{\partial q^\beta}+\mathcal{U}=0\,, \tag{6.29}$$

as long as we identify $\tilde{S}$ with the classical action. With this identification, we also obtain the classical relation between the momenta and the action,

$$p_A = \frac{\partial \tilde{S}}{\partial q^\alpha}\,, \tag{6.30}$$

and the behaviour of the wavefunction can be said to be classical since it is strongly peaked around classical solutions to the equations of motion. A possible probabilistic interpretation of the wavefunction has been described by Vilenkin [144] and relies on the conserved Klein-Gordon current

$$J_B = -\frac{i}{2}(\Psi^*\nabla_B\Psi - \Psi\nabla_B\Psi^*)\,. \tag{6.31}$$

Evaluating this current for the semi-classical form of the wavefunction yields $J_B = e^{-2A}\nabla_B\tilde{S}$ and consequently

$$\nabla^B\left(e^{-2A}\nabla_B\tilde{S}\right)=0\,. \tag{6.32}$$

Vilenkin's prescription then is to specify a spacelike hypersurface in field space, and define approximately conserved relative probabilities $e^{-2A}\,n^B\nabla_B\tilde{S}$ where n^B is the unit normal to the surface.

7 Quantum Singularity Resolution

In a universe that is fundamentally quantum mechanical, classical cosmological evolution may not be predicted by the universe's quantum state for all times and in all regions of the configuration space on which the wave function Ψ is defined. Instead one expects histories of the universe to behave classically in limited patches only. Regions of our universe where classical evolution likely breaks down include the high curvature realm of the early universe and the interior of black holes.

Classical evolution emerges when the quantum probabilities are high for histories with deterministic correlations in time. These quantum probabilities are given by the quantum state and cannot be reliably diagnosed from the classical equations of motion for cosmology any more than this can be done for any other quantum system. This means in particular that classical evolution can break down without the breakdown of the classical equations of motion. An example of this is the universe's evolution near the de Sitter like throat in the inflationary histories in the no-boundary wave function [145].

Histories of the universe do not simply end when they cease to behave classically. Rather classical evolution is replaced by quantum evolution. In this chapter we apply the framework of minisuperspace quantum cosmology to study what happens when classical cosmological evolution breaks down in the early universe, in the context of four dimensional Einstein gravity coupled to a scalar field.

In particular, we will explore two approaches to resolving the initial, cosmological, singularity: The first is an extension of the no-boundary proposal and the closely related tunnelling prescription to anisotropic (Bianchi IX) models of the universe, in the context of an inflationary model following [5] closely.

In the second approach we find saddle point solutions of the Lorentzian path integral for this model that describe transitions connecting two patches where the universe behaves classically, according to Einsteins equations. In that sense quantum mechanics aids in resolving the cosmological singularity. This part follows [4].

7.1 The Anisotropic Minisuperspace Model

In the following sections we will extend the no-boundary proposal of Hartle and Hawking [138, 69, 139, 140], and the closely related tunnelling prescription of Vilenkin [21, 29, 141, 142] to include anisotropies. Our focus is on the saddle point geometries that approximate the path integral, and on the classicality of the wavefunction - these are issues that apply equally

to both proposals. The inclusion of anisotropies is of interest because it provides the first step in going beyond the often-employed restriction to spatially homogeneous and isotropic minisuperspace models. In that sense these models are already a good deal more realistic than the isotropic ones. Also, it is known that in the approach of a cosmological singularity, the spacetime metric can locally be described to better and better accuracy by precisely a Bianchi IX metric [51]. Thus we may reasonably hope that the Bianchi IX models studied here capture certain salient features of a full superspace analysis.

Anisotropic models have been studied repeatedly in quantum cosmology, starting from the more qualitative works of Hawking and Luttrell [146], and Moss and Wright [147]. Various approximate solutions to the Wheeler-DeWitt equation were given by Del Campo and Vilenkin [148], by Amsterdamski [149] and by Duncan and Jensen [150]. These works provided valuable first insights into the existence and properties of anisotropic instantons. More recently, Fujio and Futamase instigated a more systematic numerical study, in which they found an obstruction to constructing instantons with large anisotropies [151].

Here we wish to extend these studies. We will show that Bianchi IX instantons satisfying the no-boundary regularity conditions may actually be constructed with arbitrary anisotropies. A non-trivial feature is however that care must be taken in choosing a contour of integration in the complex time plane, as for increasing anisotropies singularities start to appear, and the standard contour (originally employed by Hawking since the earliest works [138]) becomes inappropriate. The visual methods developed in [143, 152, 3] are well suited to reveal this feature, and readily suggest better contours.

Even though we do not find any limit to how large the anisotropies can be at a given instant, all classical histories implied by the instantons undergo inflationary dynamics, just as is the case for isotropic models [140], and thus the anisotropies are quickly diluted away. Nevertheless, we find an interesting effect induced by the anisotropies: they cause the wavefunction of the universe to become classical, in a WKB sense, more slowly than in the isotropic case. More specifically, isotropic inflationary universes satisfy the WKB conditions (that the amplitude of the wavefunction should vary slowly compared to the phase) approximately in inverse proportion to the amount of volume created, while anisotropic universes do so only in inverse proportion to the linear size of the universe. We show this result numerically, and prove it analytically for constant equation of state.

We will consider the scalar field potential to be of exponential form,

$$V(\phi) = V_0 e^{c\phi}, \tag{7.1}$$

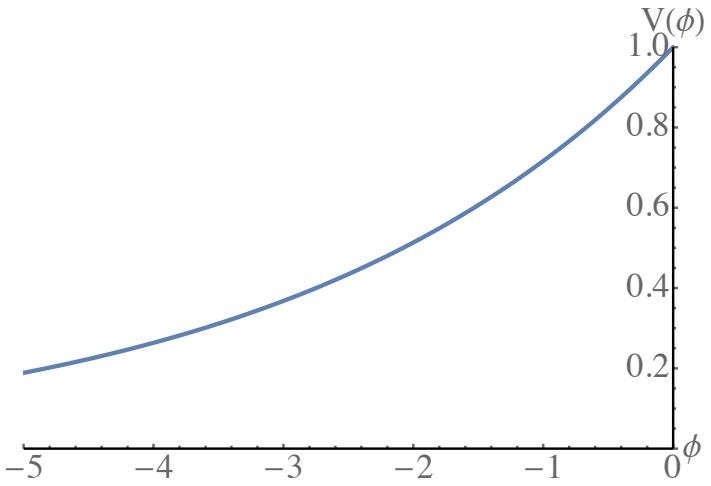

Figure 40: The scalar field potential $V(\phi) = e^{c\phi}$. For our numerical examples, we chose $c = 1/3$ and correspondingly $\epsilon = 1/18$.

as shown in Fig. 40 and with c taken to be a positive constant. We will set $V_0 = 1$, which can be achieved by shifting the origin of ϕ. The reason for choosing an exponential is that for such potentials the slow-roll parameter $\epsilon = c^2/2$ is constant (though it need not be small – only the condition $\epsilon < 1$ is required for inflation to take place). Furthermore, with this potential, the theory has a classical scaling/shift symmetry. Indeed, if one performs the following transformations, with $\Delta\phi$ constant,

$$\phi \equiv \bar{\phi} + \Delta\phi \ , \quad g_{\mu\nu} \equiv e^{-c\Delta\phi}\bar{g}_{\mu\nu} \ , \tag{7.2}$$

one finds that the action changes only by an overall constant

$$S = e^{-c\Delta\phi}\int d^4x\sqrt{-\bar{g}}\left(\frac{\bar{R}}{2} - \frac{1}{2}\bar{g}^{\mu\nu}\partial_\mu\bar{\phi}\partial_\nu\bar{\phi} - e^{c\bar{\phi}}\right) \ . \tag{7.3}$$

This symmetry of the equations of motion is of great value in obtaining analytic approximations.

7.2 The Anisotropic No-Boundary Proposal

7.2.1 No-Boundary Conditions

The WdW equation admits many solutions. In order to know which one to pick, we need a theory of initial conditions. First recall that the path integral construction of the wavefunction,

$$\Psi(b,\chi,b_+,b_-) = \int_{\mathcal{C}} \mathcal{D}N\mathcal{D}a\mathcal{D}\phi\mathcal{D}\beta_+\mathcal{D}\beta_-\, e^{\frac{i}{\hbar}\int \mathrm{d}t\left[p_A\dot{q}^A - N\mathcal{H}\right]} \ , \tag{7.4}$$

is equivalent to canonical quantisation, in the sense that the wavefunction thus constructed automatically solves the WdW equation (see e.g. [153]). Here the arguments of the wavefunction correspond to the specified field values on the final hypersurface. If we denote the time coordinate at the final hypersurface by τ_f, then the arguments are

$$a(\tau_f) = b, \quad \phi(\tau_f) = \chi, \quad \beta_+(\tau_f) = b_+, \quad \beta_-(\tau_f) = b_- \,. \tag{7.5}$$

In the definition (7.4) the no-boundary proposal then restricts the class $\mathcal{C}$ of metrics over which the path integral is performed to be the class of compact, regular metrics admitting regular field configurations and having no boundary other than the final boundary just described. This restriction selects particular solutions of the WdW equation – this is the sense in which the no-boundary proposal is indeed a theory of initial conditions. Below we will evaluate the path integral in the saddle point approximation, i.e. we will look for finite action solutions of the classical equations of motion satisfying the required boundary conditions. As is well known [154], with the "no-boundary" boundary conditions, these solutions must in fact be complex, although of course at the final boundary all field vales in (7.5) are required to be real. Given one saddle point, one can obtain others rather trivially, by taking either the complex conjugate or the time reverse (or both) of a particular saddle point geometry. Hartle and Hawking then have a proposal as to which of these saddle points should be retained [138, 69, 139, 140]. A second well-known theory of initial conditions is Vilenkin's tunnelling proposal. In that theory, the universe is also envisaged to tunnel from "nothing", and the regular tunnelling geometries satisfy the same no-boundary regularity condition. The difference with the approach of Hartle and Hawking is that the tunnelling boundary conditions select a different saddle point to be retained [21, 29, 141, 142]. Since the various saddle points in question can be trivially obtained from one another, we will not dwell on distinguishing the two proposals below - our focus is on obtaining and characterising the saddle point geometries in the first place, and on the classicality properties of the wavefunction, which are issues that apply equally to both theories of initial conditions.

The no-boundary condition demands regularity at the so-called South Pole of the solution (i.e. where the volume of the universe is zero). In our case this corresponds to $a = 0$, which we can set to be at $t = 0$. From the Friedman equation it is clear that at the South Pole

$$\dot{a}^2 = \frac{N^2}{3} U(\beta_+, \beta_-) \tag{7.6}$$

must be satisfied. For small anisotropies, Eq. (3.47) implies that $U < 0$, and thus we see that the Friedman constraint forces us to complexify the fields (we will shortly see that in fact we

need to take $U(\beta_+(t=0),\beta_-(t=0)) = U(0,0) = -3$. The ϕ equation (3.52) enforces

$$\dot{\phi} = 0\,. \tag{7.7}$$

The β equations (3.50),(3.51) give $U_{,\beta_+} = U_{,\beta_-} = 0$ which correspond respectively to

$$2e^{2\beta_+} - e^{-\beta_+ - \sqrt{3}\beta_-} - e^{-\beta_+ + \sqrt{3}\beta_-} + 2e^{-4\beta_+} - e^{2\beta_+ - 2\sqrt{3}\beta_-} - e^{2\beta_+ + 2\sqrt{3}\beta_-} = 0\,, \tag{7.8}$$

$$-e^{-\beta_+ - \sqrt{3}\beta_-} + e^{-\beta_+ + \sqrt{3}\beta_-} - e^{2\beta_+ - 2\sqrt{3}\beta_-} + e^{2\beta_+ + 2\sqrt{3}\beta_-} = 0\,. \tag{7.9}$$

These equations allow six complex solutions given by

$$(e^{\beta_+}, e^{\sqrt{3}\beta_-}) = \Big\{(1,1),(-1,-1),(-(-1)^{1/3},1),((-1)^{1/3},-1),((-1)^{2/3},1),(-(-1)^{2/3},-1)\Big\}\,. \tag{7.10}$$

It is instructive to analyse the form of the metric near the South Pole for these values. Inserting the values of the first two solutions yields

$$ds^2_{SP} \approx -N^2dt^2 + a^2\left(\sigma_1^2 + \sigma_2^2 + \sigma_3^2\right)\,. \tag{7.11}$$

Solutions 3 and 4 give

$$ds^2_{SP} \approx -N^2dt^2 - \left(\frac{1}{2} + i\frac{\sqrt{3}}{2}\right)a^2\left(\sigma_1^2 + \sigma_2^2 + \sigma_3^2\right)\,, \tag{7.12}$$

while the last pair of solutions give

$$ds^2_{SP} \approx -N^2dt^2 + \left(-\frac{1}{2} + i\frac{\sqrt{3}}{2}\right)a^2\left(\sigma_1^2 + \sigma_2^2 + \sigma_3^2\right)\,. \tag{7.13}$$

Since we are allowing for complex scale factors a when searching for instanton solutions, all these cases are in fact equivalent, and we may simply use (7.11).

Even though we defined the path integral in real/Lorentzian time, we just saw that the boundary conditions force us to consider complex solutions as saddle points of the action. This means that from here on we should consider the time variable to be complex. To make contact with the existing literature on no-boundary instantons, we will take our complexified time variable to be given by τ, such that $Im(\tau) = t$. Thus one may think of the real part of τ as denoting the Euclidean time direction, and the imaginary part as real time. The regularity of the field equations near the South Pole then translates into the following series expansions

up to $\mathcal{O}(\tau^5)$

$$a = \tau - \frac{1}{18}V_0 e^{c\phi_{SP}}\tau^3 + \frac{1}{8640}((-216(\beta''_{SP+})^2 - 216(\beta''_{SP-})^2 + (8-27c^2)V_0^2 e^{2c\phi_{SP}})\tau^5 + \cdots \tag{7.14}$$

$$\phi = \phi_{SP} + \frac{c}{8}V_0 e^{c\phi_{SP}}\tau^2 + \frac{c(2+3c^2)}{576}V_0^2 e^{2c\phi_{SP}}\tau^4 + \cdots \tag{7.15}$$

$$\beta_+ = \frac{1}{2}\beta''_{SP+}\tau^2 + \frac{1}{144}(45(\beta''_{SP-})^2 + \beta''_{SP+}(-45\beta''_{SP-} + 7V_0 e^{c\phi_{SP}}))\tau^4 + \cdots \tag{7.16}$$

$$\beta_- = \frac{1}{2}\beta''_{SP-}\tau^2 + \frac{1}{144}\beta''_{SP-}(90\beta''_{SP+} + 7V_0 e^{c\phi_{SP}})\tau^4 + \cdots \tag{7.17}$$

These series expansions are needed to form a well-defined numerical problem. We can see that the instantons are characterised by the three complex numbers

$$\phi_{SP}, \quad \beta''_{SP+}, \quad \beta''_{SP-}\,, \tag{7.18}$$

representing the scalar field value, and the values of the second derivatives of the anisotropy functions, at the South Pole. The no-boundary condition forces the anisotropy functions and their first derivatives to be zero at the no-boundary point, but allow for a non-trivial second derivative. In this way anisotropies can develop.

7.2.2 Classicality

In section 6.5 we have already specified what classicality means in the general context of quantum cosmology. Now we investigate what these conditions reduce to in the context of the Bianchi IX metric since we are interested in how the classicality conditions behave when anisotropies are introduced.

$$S = 6\pi^2 \int dt N \left[\frac{1}{2}G_{AB}\left(\frac{1}{N}\frac{dq^A}{dt}\right)\left(\frac{1}{N}\frac{dq^B}{dt}\right) - \mathcal{U}(q^A)\right] \tag{7.19}$$

with $q^A = (a, \phi, \beta_+, \beta_-)$ and

$$G_{AB} = \mathrm{diag}\left(-2a, \frac{1}{3}a^3, \frac{1}{2}a^3, \frac{1}{2}a^3\right). \tag{7.20}$$

Then the associated Hamiltonian is given by

$$\mathcal{H} = \frac{1}{2}G^{AB}p_A p_B + \mathcal{U}\,, \tag{7.21}$$

with the canonical momenta $p_a = -2a\dot{a}$, $p_\phi = \frac{1}{3}a^3\dot{\phi}$, $p_{\beta_+} = \frac{1}{2}a^3\dot{\beta}_+$, $p_{\beta_-} = \frac{1}{2}a^3\dot{\beta}_-$, and where the total effective potential is given by

$$\mathcal{U}(q^A) = a\,U(\beta_+, \beta_-) + a^3 V(\phi). \tag{7.22}$$

In the end, we then require that

$$\frac{\partial \tilde{S}}{\partial q^A} \gg \frac{\partial A}{\partial q^A}, \tag{7.23}$$

holds for any A i.e. for all variables $q^A = (a, \phi, \beta_+, \beta_-)$.

7.2.3 Existence and Basic Features of Anisotropic Instantons

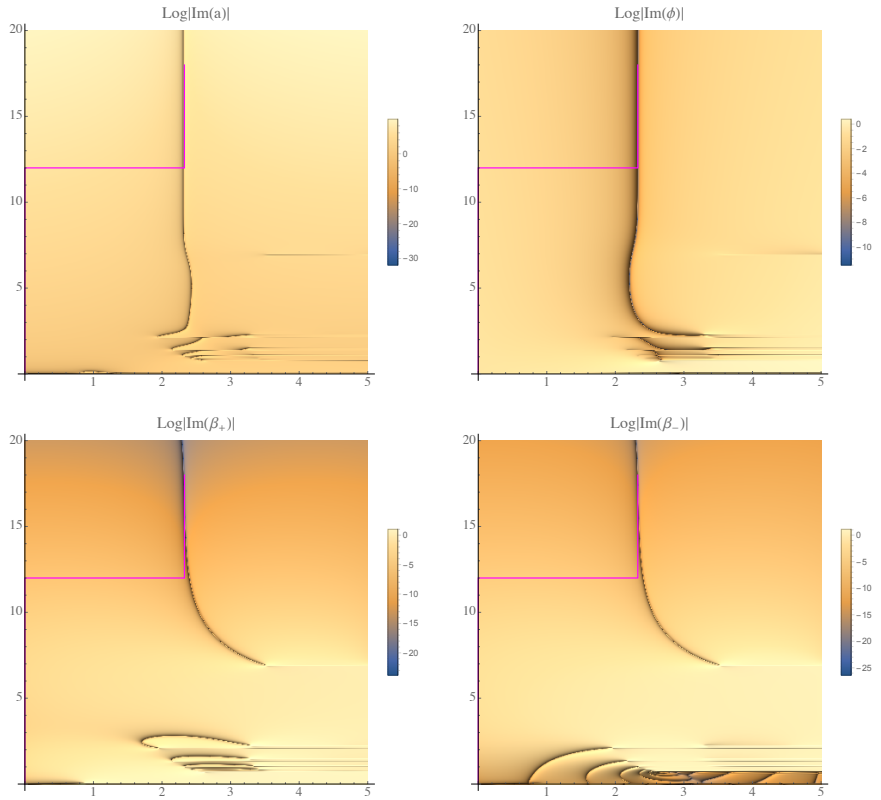

Figure 41: An example of an anisotropic instanton, optimised to reach the real values $b = 10000, \chi = -2, b_+ = 1, b_- = 1$ on the final boundary. These values are reached at $\tau_f = 2.32705 + 17.9932\,i$, with the South Pole values $\phi_{SP} = 0.942081 - 0.554398\,i, \beta''_{SP+} = -0.926417 + 0.173177\,i, \beta''_{SP-} = -0.00373004 + 0.000697265\,i$. We have drawn an example of a "good" contour of integration in magenta, which avoids the singularities and their associated branch cuts visible in the lower right part of the figures. For a detailed description of the figure, see the main text.

We can now look for solutions satisfying the no-boundary conditions (7.14) - (7.17) while approaching the desired real values of b, χ, b_+, b_- on the final hypersurface at some τ_f. In order to find such solutions we have the freedom of adjusting the contour and the South Pole values (7.18). We find these values by implementing a numerical Newtonian optimisation

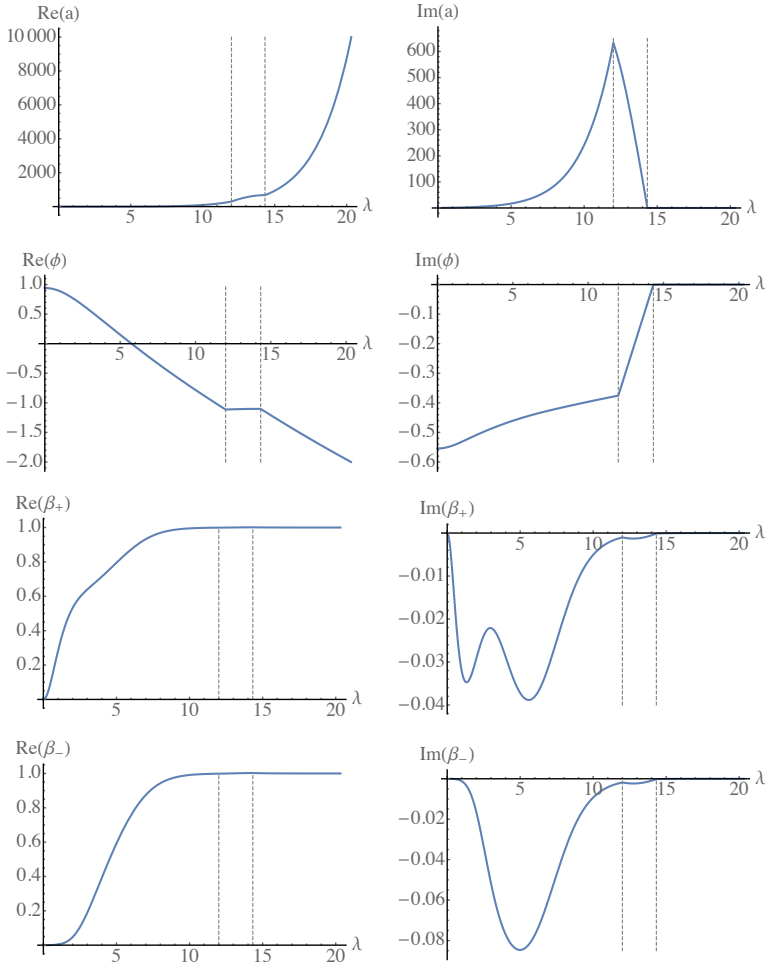

Figure 42: The evolution of the fields $a, \phi, \beta_+, \beta_-$ along the contour shown in magenta in Fig. 41. The contour has been parameterised with a monotonically increasing parameter λ, and the dashed lines indicate the locations where the contour changes direction. Note that the fields approach real values on the final, vertical part of the contour. The inflationary attractor ensures that this is possible simultaneously for all fields. Also note that the anisotropy functions $\beta_\pm$ start out at zero, as they must to satisfy the no-boundary conditions, then grow to complex values and and eventually settle at the desired real values.

algorithm. An example of an anisotropic instanton, optimised to reach the values ($b = 10000, \chi = -2, b_+ = 1, b_- = 1$) on the final boundary is shown in Fig. 41. What we show in the figure are relief plots of the imaginary parts of the functions $a(\tau), \phi(\tau), \beta_\pm(\tau)$ over the complex time plane τ with $\tau = 0$ corresponding to the South Pole where the no-boundary conditions are implemented. More precisely, we are plotting the logarithm of the absolute value of the imaginary part of these functions, such that small imaginary part corresponds to very negative values and thus very dark points. The dark lines thus represent the locus

where the fields are essentially real. These plots are obtained by solving the equations of motion, starting from the South Pole, going upwards along the imaginary τ axis to a fixed height first, and then branching out horizontally to a dense series of points on a horizontal line. Then this procedure is repeated for a slightly higher horizontal line, until a dense grid of points is obtained, covering the desired region of the complex time plane.

Our procedure thus implicitly entails a choice of contour along which the equations of motion are solved. This contour is different from the type of contour usually employed for no-boundary instantons, see Fig. 43. The usual contour runs out horizontally along the real τ axis (along which the solution is approximately that of a Euclidean sphere) and then up, parallel to the imaginary τ axis, to the final location τ_f where the desired field values are reached. In the isotropic case, the solution along this last contour then corresponds to a portion of de Sitter space. However, when significant anisotropies are included, this standard type of contour is no longer viable, as singularities develop and the standard contour would in fact take us to a different sheet of the solution function. Along this new sheet we have checked and found that the final real values $(b, \chi, b_\pm)$ are not reached. But we can avoid the singularities by running the contour first up along the imaginary τ axis, and then horizontally across. An example of such a "good" contour is shown by the magenta line in Fig. 41, and the evolution of the fields along this contour is shown in Fig. 42.

Note that the presence of additional singularities is not really surprising: the anisotropies lead to an increased energy density, which favours a decelerating scale factor (see Eq. (3.53)) and thus favours gravitational collapse. In regions where the scale factor a shrinks, a singularity can only be avoided if the homogeneous curvature dominates over the anisotropies, since the homogeneous curvature can induce a bounce analogous to that present in the closed slicing of de Sitter space. This however will generically not occur, as the energy density of the homogeneous curvature scales as $1/a^2$ while that of the anisotropies scales as $1/a^6$. Thus we may generically expect singularities to form in regions where the scale factor shrinks, and consequently it is only natural that we see many additional singularities in the anisotropic case. (See also [4] for tunnelling solutions which circumvent singularities in a similar manner.)

With the right contour, we can now construct anisotropic instantons over large ranges of values, where we only seem to be limited in the range by the computational time it takes to optimise the instantons. As an example, we show the South Pole values and values of the action for instantons optimised to reach $(b = 100, \chi = -1/2)$, with the anisotropy parameters ranging from $-7/10 \leq b_+ \leq +1/2$ and $-1/2 \leq b_- \leq +1/2$. These ranges coincide with

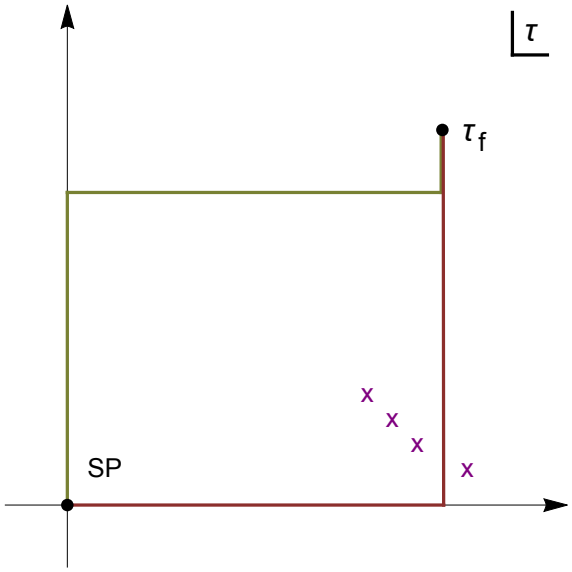

Figure 43: Due to the presence of singularities (marked by purple crosses), we cannot choose the standard "Hawking" contour in the complex time plane (in red), as this contour would not have yielded a solution with the desired boundary conditions. Instead we have to use a modified contour such as the one in green. Shown here is the complexified Euclidean time plane τ, with the South Pole at $\tau = 0$ and the final boundary conditions imposed at τ_f.

the ranges for the potential $U(\beta_+, \beta_-)$ shown in Fig. 4. The optimised South Pole values $\phi_{SP}, \beta''_{SP+}, \beta''_{SP-}$ are shown in Figs. 44 - 46, while the action is shown in Fig. 47. The figures clearly reflect the expected $b_- \to -b_-$ symmetry that comes with this choice of coordinates. Note that the South Pole values of the scalar field vary little as the anisotropies are increased, and in particular the imaginary part stays essentially constant. Note also that for a pure b_+ deformation the values of β''_{SP-} stay close to zero, and to a somewhat lesser extent this is also true for the β''_{SP+} values when considering pure b_- deformations. This indicates that there is not much "rotation" (or mixing between β_+ and β_-) of the instantons between the South Pole and the final hypersurface. Regarding the action in Fig. 47, we can see that the real part of the action is very large, which is as expected since a classical history has been reached. The imaginary part of the action, which can be thought of as the "quantum" part, is much smaller but increases steeply for larger anisotropies. We note also that it changes sign: the minimum is located at $b_+ = b_- = 0$ where $Im(S) = -79.769844$, while for large anisotropies the imaginary part of the action becomes large and positive. We will further comment on this feature in the discussion section.

Having constructed anisotropic instantons over a significant range of anisotropy parame-

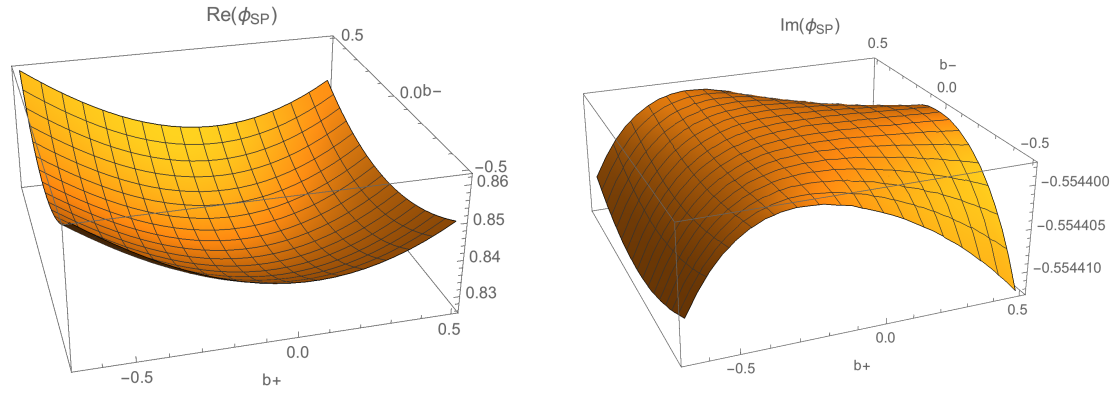

Figure 44: Real and imaginary parts of ϕ_{SP} at the South Pole, in terms of the final, real values of $b_\pm$ indicated, and for $b = 100$, $\chi = -1/2$. Note that $Im(\phi_{SP})$ varies only over a very small range.

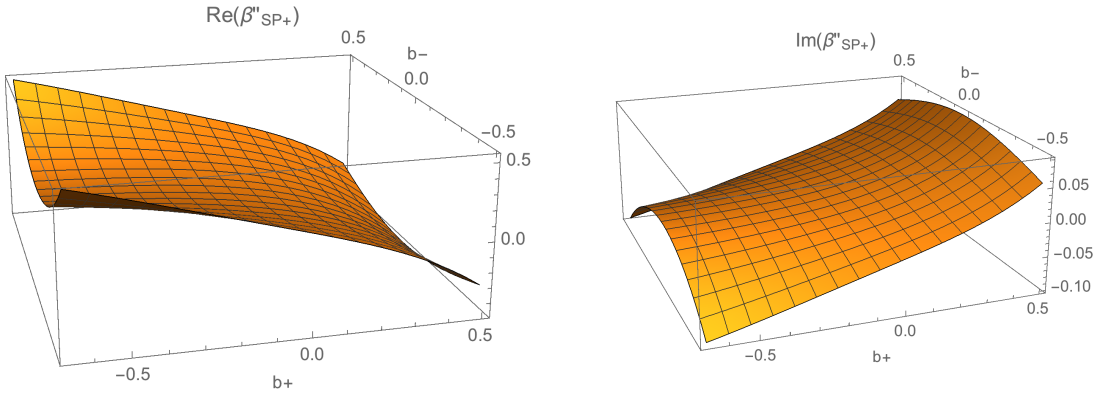

Figure 45: Real and imaginary parts of β''_{SP+} at the South Pole, in terms of the final, real values of $b_\pm$ indicated, and for $b = 100$, $\chi = -1/2$.

ters, we should note an interesting consequence of the shift/scaling symmetry (7.2). Given a solution such as the ones we have just described, a shifted instanton with final values

$$b \to b\, e^{-\frac{c}{2}\Delta\chi}, \quad \chi \to \chi + \Delta\chi, \quad b_+ \to b_+, \quad b_- \to b_-\,, \tag{7.24}$$

can be obtained from the following South Pole values

$$\phi_{SP} \to \phi_{SP} + \Delta\chi \tag{7.25}$$

$$\beta''_{SP+} \to \beta''_{SP+}\, e^{c\Delta\chi} \tag{7.26}$$

$$\beta''_{SP-} \to \beta''_{SP-}\, e^{c\Delta\chi} \tag{7.27}$$

$$\tau_f \to \tau_f\, e^{-\frac{c}{2}\Delta\chi}\,, \tag{7.28}$$

where we also included the shifted time coordinate of the final hypersurface. Here $\Delta\chi$ is

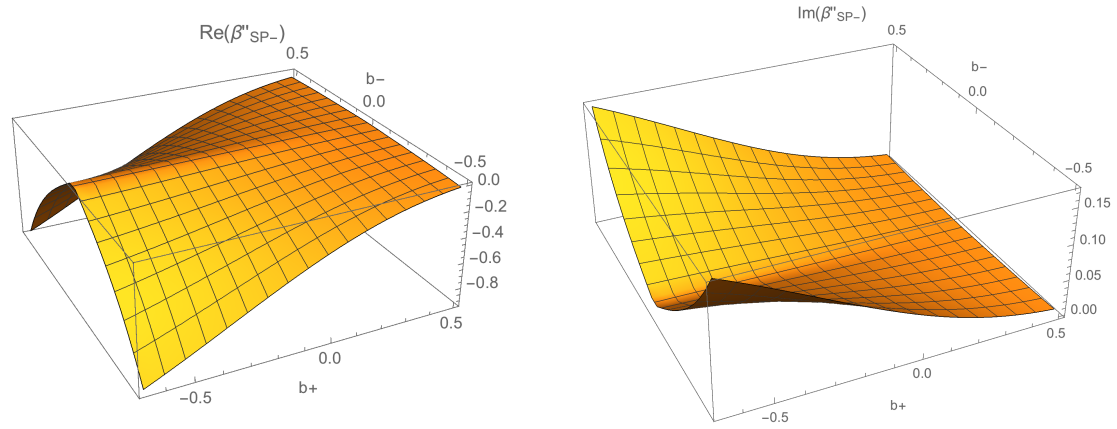

Figure 46: Real and imaginary parts of β''_{SP-} at the South Pole, in terms of the final, real values of $b_\pm$ indicated, and for $b = 100$, $\chi = -1/2$.

an arbitrary real number, und thus a one-parameter family of instantons with the same anisotropy parameters, but different scale factor and scalar field values can be obtained. These shifted instantons belong to different classical histories. Interestingly, starting from a specific instanton, one can use these relations to construct an instanton with the same anisotropies but with a much larger value of the scale factor. But evolving that new history back in time to the original scale factor one realises that this has shifted to a history with much larger anisotropies (as measured at a reference scale factor value). Given that using the formulae above we can shift the scale factor by an arbitrary amount, this means that we can obtain histories with an arbitrarily large anisotropies, along a one-parameter set of deformations. Together with our grids in Figs. 44, 45 and 46 this strongly suggests that, at least in the case of a constant equation of state, there is no limit to how large the anisotropies can be.

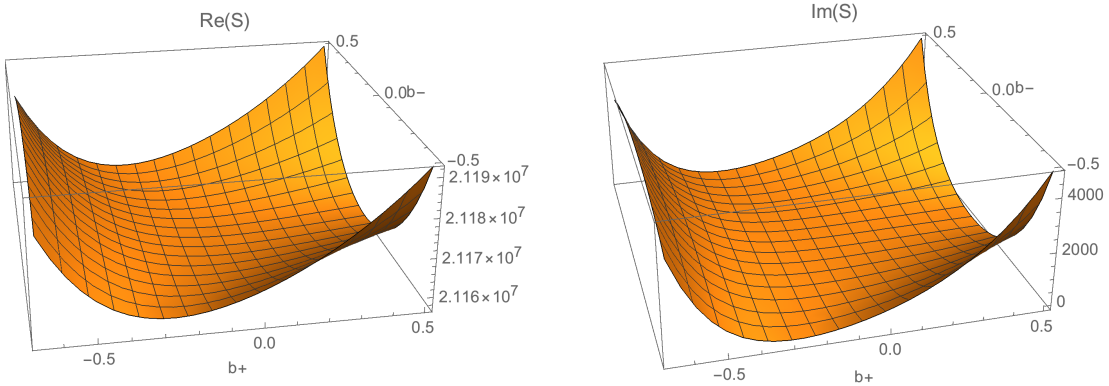

Figure 47: Real and imaginary parts of the action S, in terms of the final, real values of $b_\pm$ indicated, and for $b = 100$, $\chi = -1/2$.

The visual methods employed here, and which were developed in [143, 152, 3], have the great advantage of allowing one to see by eye where the singularities are located, and thus clearly show in what manner the choice of contour is crucial. With the right contour, we have been able to construct anisotropic instantons with any desired final anisotropy parameters. Thus we suspect that the obstruction to constructing instantons with large anisotropies reported in [151] might have been due to the fact that the authors used the standard contour, and thus inadvertently landed on a wrong sheet of the solution function.

7.2.4 Scaling of the classicality conditions

So far, we have discussed the instanton solutions that are required to approximate the wavefunction (7.4) in the saddle point approximation. But it is important to realise that the instantons themselves do not represent the physical spacetime (which is also why it is unproblematic that they are complex valued) – rather all the physics must be deduced from the wavefunction itself. The most basic question we can ask is whether the wavefunction thus calculated predicts a classical spacetime. We can analyse this question using the WKB classicality conditions reviewed in section 7.2.2. To evaluate whether the amplitude of the wavefunction evolves slowly compared to its phase, we must first find out how the action changes as the boundary conditions $(b, \chi, b_\pm)$ of the wavefunction are varied, i.e. we must evaluate the wavefunction along a classical history. Moreover, to evaluate the partial derivatives w.r.t the fields we must also evaluate the wavefunction with small changes in the individual fields, so that we may approximate the derivatives by finite differences. Thus we must evaluate $\Psi[b(\lambda), \chi(\lambda), b_+(\lambda), b_-(\lambda)]$ for a sequence of time steps, where $[b(\lambda), \chi(\lambda), b_+(\lambda), b_-(\lambda)]$ denotes a classical history parameterised by a time coordinate λ, and also the slightly shifted instantons $\Psi[b+\delta b, \chi, b_+, b_-]$, $\Psi[b, \chi+\delta\chi, b_+, b_-]$, $\Psi[b, \chi, b_++\delta b_+, b_-]$ and $\Psi[b, \chi, b_+, b_-+\delta b_-]$ at each time step. Then we can form the WKB conditions

$$\mathcal{WKB}_{q^A} \equiv \frac{\partial_A Im(S)}{\partial_A Re(S)}\,, \quad q^A = (b, \chi, b_+, b_-)\,, \tag{7.29}$$

which are shown in Fig. 48. The numerical results for the WKB conditions are given by the blue lines, while the red dashed lines indicate fitting functions. There are a few points to note: the most obvious feature is that the WKB conditions become better and better satisfied as the universe expands. Thus the wavefunction really does predict a classical spacetime at large values of the scale factor. The seond point to note is that the WKB conditions approach a scaling law, since the log-log plots approach straight lines. Interestingly however, the four conditions do not all approach the same scaling. The conditions involving derivatives of the

scale factor b and the scalar field χ approach the scaling relation

$$\mathcal{WKB}_{b,\chi} \propto \frac{1}{b^{3-\epsilon}} \propto e^{-\frac{3-\epsilon}{1-\epsilon}\mathcal{N}}\,, \tag{7.30}$$

which is the same scaling that one obtains for isotropic inflationary universes (here $\mathcal{N}$ denotes the number of e-folds of evolution, $\mathrm{d}\mathcal{N} \equiv \mathrm{d}\ln(aH)$). This is perhaps not so surprising, since the anisotropies are diluted away at late values of the scale factor. For a small slow-roll parameter ϵ, one has $\mathcal{WKB}_{b,\chi} \sim b^{-3}$, i.e. the classicality conditions are satisfied in inverse proportion to the volume generated by inflation. These relations were proven analytically for the isotropic case in [155].

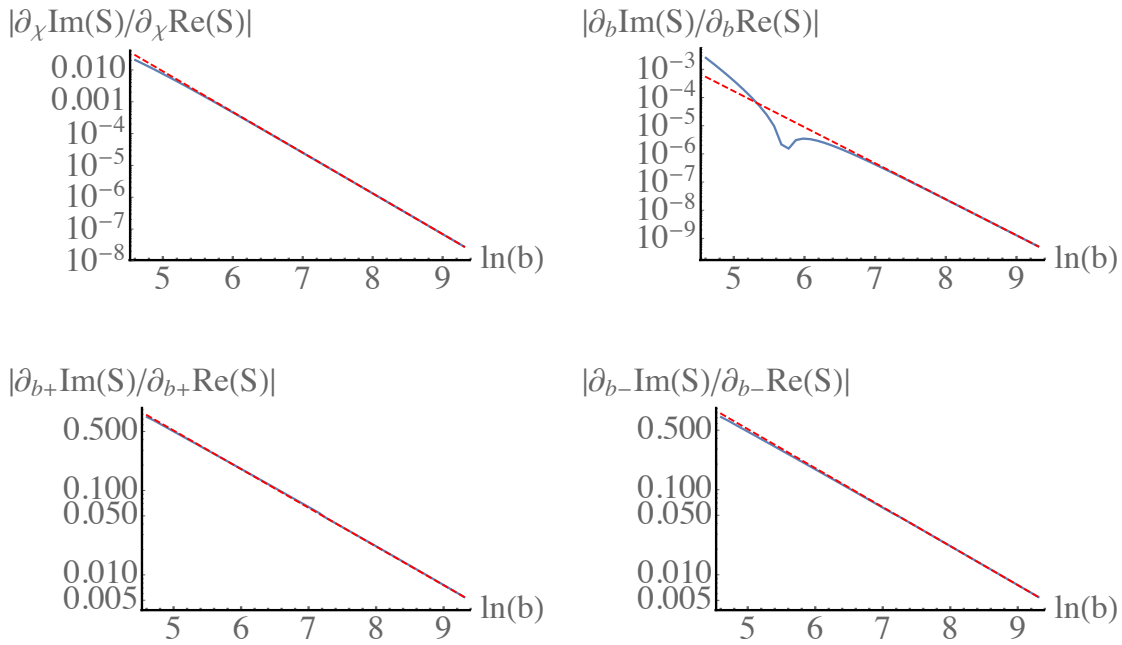

Figure 48: Plots of the WKB classicality conditions (in blue) and their asymptotic scaling behaviour (red dashed lines). For the classicality conditions involving the scale factor b and the scalar field χ the red dashed lines are proportional to $b^{-3+\epsilon}$, while for the relations involving the anisotropy functions $b_\pm$ the fitted red dashed lines are proportional to $b^{-1-\epsilon}$. Thus the anisotropies cause the wavefunction to become classical more slowly than in the isotropic case.

For the WKB conditions involving derivatives of the anisotropy functions $b_\pm$, we obtain a different scaling law, namely

$$\mathcal{WKB}_{b_+,b_-} \propto \frac{1}{b^{1+\epsilon}} \propto e^{-\frac{1+\epsilon}{1-\epsilon}\mathcal{N}}\,. \tag{7.31}$$

This is a substantially slower fall-off than that in Eq. (7.30), and for small slow-roll parameter ϵ one approximately finds $\mathcal{WKB}_{b_\pm} \sim b^{-1}$, that is to say the classicality conditions only become satisfied in inverse proportion to the linear size of the universe. Thus the anisotropies slow down the approach to classicality.

We can derive this asymptotic scaling analytically. For this we need to derive the behaviour of the fields at large scale factor. At late times, the inflationary attractor is reached, and the energy density in the anisotropies is diluted as $1/a^6$. Thus the anisotropies will only act as a small perturbation. Because of the attractor, successive constant time slices of a single instanton will correspond with great accuracy to a series of subsequent instantons for a wavefunction evaluated on the corresponding classical history. In an exponential scalar potential the scale factor will approach the inflationary attractor solution

$$b = b_0 t^{1/\epsilon}\,, \tag{7.32}$$

where t is the Lorentzian time coordinate and b_0 is a constant. At large scale factor, we can consider the anisotropy equations of motion at linear order in the anisotropy functions,

$$\ddot{b}_\pm + \frac{3}{\epsilon t}\dot{b}_\pm + \frac{8}{b_0^2 t^{2/\epsilon}} b_\pm = 0\,. \tag{7.33}$$

These equations can be solved asymptotically in a series expansion, giving

$$b_\pm(t) = b_{\infty\pm}\left(1 + \frac{4\epsilon^2}{b_0^2(1-\epsilon^2)} t^{2-\frac{2}{\epsilon}} + \cdots\right)\,. \tag{7.34}$$

Here $b_{\infty\pm}$ are the asymptotic values of the anisotropy parameters reached at $t \to \infty$.

It is interesting to see how this solution transforms under the shift-scaling symmetry (7.24) that arises for exponential potentials. This symmetry only affects the time coordinate t and the scale factor b in the metric, and not the anisotropy parameters $b_\pm$, so that we have

$$\bar{b}_\pm(\bar{t}) = b_\pm(e^{-\frac{c}{2}\Delta\chi} t) \tag{7.35}$$

$$= b_{\infty\pm}\left(1 + \frac{4\epsilon^2}{b_0^2(1-\epsilon^2)} e^{-\frac{c}{2}\Delta\chi(2-\frac{2}{\epsilon})} \bar{t}^{2-\frac{2}{\epsilon}} + \cdots\right)\,, \tag{7.36}$$

which, using the transformation of the integration constant $\bar{b}_0^2 = b_0^2 e^{\frac{\epsilon-1}{\epsilon} c\Delta\chi}$ [155], leads to

$$\bar{b}_\pm(\bar{t}) = b_{\infty\pm}\left(1 + \frac{4\epsilon^2}{\bar{b}_0^2(1-\epsilon^2)} \bar{t}^{2-\frac{2}{\epsilon}} + \cdots\right)\,. \tag{7.37}$$

Thus the solution for the anisotropy parameters is indeed unchanged in form, and in particular the value of the anisotropies at infinity is unchanged.

We are now in a position to determine how the action changes along a classical history. As argued above, at sufficiently late times the anisotropies will act as small perturbations, and

hence we can treat them perturbatively without loss of generality. Then, to leading order, the $b_\pm$ dependent changes in the action (3.54) will be reflected solely in the term

$$\int \mathrm{d}t N a\, U(\beta_+, \beta_-)\,. \tag{7.38}$$

Successive instantons are obtained in the late time limit by evolving in the Lorentzian time direction, hence the lapse function is $N = 1$ and the asymptotic scaling of the anisotropy parameters in Eq. (7.34) implies that they will reach constant values,

$$\begin{aligned}
\Delta Re(S) &= \int \mathrm{d}t a\, U(\beta_+, \beta_-) && (7.39)\\
&\approx \int \mathrm{d}t\, b_0\, t^{\frac{1}{\epsilon}} U(b_+, b_-) && (7.40)\\
&\approx b_0\, t^{\frac{1}{\epsilon}+1} U && (7.41)\\
&\propto b\, V^{-1/2} U\,. && (7.42)
\end{aligned}$$

Thus $\partial_{b_\pm} Re(S) \propto b\, V^{-1/2} U_{,b_\pm}$. In order to determine the change in the imaginary part of the action, we can use the scaling/shift symmetry described above. As shown in [155], for isotropic instantons with constant ϵ this symmetry implies that $\Delta Im(S) \propto b^{\frac{2\epsilon}{\epsilon-1}} V^{\frac{1}{\epsilon-1}}$. But we have just seen that the symmetry does not affect the anisotropy parameters. Hence we must have

$$\Delta Im(S) \propto f(b_+, b_-)\, b^{\frac{2\epsilon}{\epsilon-1}} V^{\frac{1}{\epsilon-1}}\,, \tag{7.43}$$

for some function $f(b_+, b_-)$ which we cannot determine from these arguments. However, we also do not need to know its precise functional form. This is because asymptotically, both the function f and its derivatives $f_{,b_\pm}$ will reach the constant values $f(b_{\pm\infty})$ and $f_{,b_\pm}(b_{\pm\infty})$ respectively, and we are only interested in the overall scaling. Putting the above results together, we arrive at the scaling law for the WKB classicality conditions associated with the anisotropy parameters,

$$\mathcal{WKB}_{b_\pm} = \frac{\partial_{b_\pm} Im(S)}{\partial_{b_\pm} Re(S)} \propto \frac{f_{,b_\pm}(b_{\pm\infty})\, b^{\frac{2\epsilon}{\epsilon-1}} V^{\frac{1}{\epsilon-1}}}{U_{,b_\pm}(b_{\pm\infty}) b\, V^{-1/2}} \propto \frac{1}{b^{1+\epsilon}}\,. \tag{7.44}$$

A final feature seen in Fig. 48 is the little dip in the plot of $\mathcal{WKB}_b$. This feature shows that the scaling law has not been reached yet, and thus suggests that the wavefunction has not really reached classicality yet at this stage. It is instructive to look at an early instanton just before the dip – such an instanton is shown in Fig. 49. The instanton has been optimised to reach the values $(b = 100, \chi = -1/2, b_+ = 1, b_- = 1)$. Interestingly, the vertical lines emanating from τ_f for the plots of the imaginary values of the scale factor and scalar field

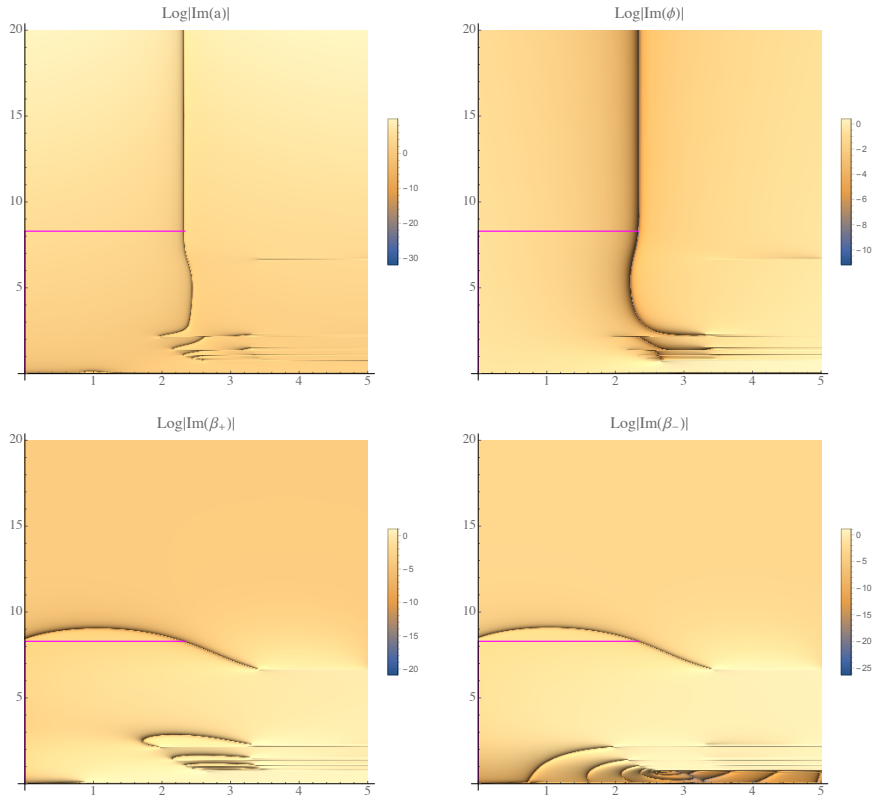

Figure 49: An "early" instanton with a smaller scale factor, optimised for $b = 100, \chi = -1/2, b_+ = 1, b_- = 1$. These values are reached at $\tau_f = 2.33345 + 8.29691\,i$, with the South Pole values $\phi_{SP} = 0.905134 - 0.554599\,i, \beta''_{SP+} = -0.909196 + 0.164990\,i, \beta''_{SP-} = -0.00369960 + 0.000726549\,i$. The magenta contour runs from the South Pole at $\tau = 0$ to the final hypersurface at τ_f. We have solved the equations of motion over a larger time domain in order to show that the fields (especially the anisotropy functions) do not retain approximately real values beyond τ_f yet.

show that these fields are already very nearly real in the Lorentzian time direction, while the ansiotropy parameters do not remain as close to real beyond τ_f, compare also to Fig. 41 This is in agreement with the fact that the classicality conditions involving the anisotropy functions are satisfied more slowly than those involving the scale factor and scalar field. Thus, at that stage, one cannot yet say that a classical spacetime is predicted, and several more e-folds of expansion are needed before classicality is reached.

To conclude this section we recap that the no-boundary proposal is a method that avoids the initial cosmological singularity by regularizing the metrics under consideration. Using novel numerical techniques we could refute earlier claims in the literature that large anisotropies do not allow for no-boundary configurations. However, we do note that the presence of

anisotropies delays the classicalization of the space-time.

7.3 Quantum Transitions of the Universe

In the last section the cosmological singularity has been resolved by using the no-boundary proposal which sums only over non-singular metrics. Here we present an alternative resolution of cosmological singularities: Quantum transitions that interpolate between classical histories [4]. The classical behaviour of the boundary configurations means that the saddle points obey boundary conditions corresponding to real values of the scalar field and scale factor on both ends of the transition (cf. Fig. 50). The solutions are complex in the interior, however, as is common for gravitational instantons. The action of the saddle points specifies probabilities for quantum transitions through the region of breakdown of classical evolution, thereby connecting a classical history in a given patch with a classical history in another patch. One history typically branches into many histories [145].

We investigate two qualitatively different cosmological scenarios that are of special interest: quantum transitions between inflationary histories on both ends, and transitions from ekpyrosis to inflation. The classical extrapolation of the histories beyond its domain of validity can produce a curvature singularity in both cases. In inflation the singularity lies in the past, whereas ekpyrotic histories contain a singularity in their future. The quantum transitions we find can thus be viewed as a resolution – albeit in minisuperspace – of the cosmological singularity in these models.

Transitions between inflationary histories may be argued to be somewhat academic in that the opposite side of the bounce is unlikely to lead to testable predictions on our side of the bounce. This is because the physical arrows of time point away from the bounce on both sides in all quantum states, such as the no-boundary state [22], that implies perturbations are in their vacuum state near the bounce [156]. By contrast, transitions from ekpyrosis to inflation are central to the theory because the arrow of time does not reverse in ekpyrotic cosmology, where the detailed spectral properties of the perturbations on our side generally depend on the conditions before and at the bounce.

The plan of this section is as follows: we start by briefly describing the general framework that we will work with, namely the semiclassical path integral for quantum gravity in the minisuperspace approximation. We find saddle points of the path integral describing transitions between inflationary histories in Section 7.3.1. In section 7.3.2 we find transitions between an ekpyrotic contracting phase and an inflationary expanding phase. We conclude in section 7.4 and provide further technical details in the appendix.

We work in a minisuperspace model in which the Lorentzian four-geometries are homo-

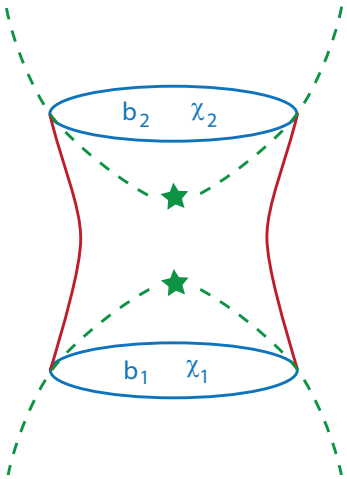

Figure 50: We will study quantum transitions (in red) between real, classical boundaries (in blue), here shown for the situation in which the classical evolution (in green) would lead to singularities.

geneous, isotropic, and spatially closed on the manifold $M = \mathbf{R} \times S^3$. For the matter content we take a single homogeneous scalar field ϕ moving in a potential $V(\phi)$. Thus we can simply take the metric of section (3.5.4) with the anisotropies set to zero.

Quantum states of the universe are represented by wave functions Ψ on the superspace spanned by the three-geometries and the field configurations on a spacelike surface Σ. Taking Σ to be a surface of homogeneity, useful coordinates on minisuperspace are the scale factor of the three-geometry which we denote by b and the homogeneous value of the scalar field ϕ denoted by χ. Histories are specified by functions $(a(\lambda), \phi(\lambda))$ that define curves in configuration space $(b(\lambda), \chi(\lambda))$ and vice versa. Thus $\Psi = \Psi(b, \chi)$. When there is a need to be more compact we will write $x^A = (b, \chi),\ A = 1, 2$. Then $\Psi = \Psi(x^A)$.

Classical histories are specified by functions $\hat{a}(\lambda)$ and $\hat{\phi}(\lambda)$ that are real valued and satisfy the classical Einstein equations and the dynamical equation for the scalar field. Classical histories are predicted in regions of superspace where the wave function is well approximated by a semiclassical ("WKB") form as reviewed in section 6.5.

This semiclassical algorithm for classical prediction has been extensively used in quantum cosmology to extract predictions for cosmological observables from a wave function of the universe in domains where the classicality conditions hold. But histories need not be all quantum or all classical. Instead the classicality conditions (6.28) may hold in some regions of configuration space but not in other regions. Histories $(a(\lambda),\ \phi(\lambda))$ do not end when the classicality conditions break down. After all, histories are defined on the whole of the

manifold $M = \mathbf{R} \times S^3$. Instead when the classicality conditions fail deterministic classical evolution is replaced by quantum evolution. This allows for *quantum transitions* through the region of semiclassical breakdown that connect different parts of histories in the classical region of superspace [145]. Tunneling through a barrier is a well known example of this.

In minisuperspace quantum cosmology, the quantum transition amplitude between two classical histories is specified by the propagator between an initial spatial hypersurface where $(b, \chi) = (b_1, \chi_1)$ and a final one with data (b_2, χ_2),

$$T(b_2, \chi_2 | b_1, \chi_1) \equiv \int_{(b_1,\chi_1)}^{(b_2,\chi_2)} \delta N \delta a \delta \phi \exp\left\{ i\mathcal{S}[a,\phi]/\hbar \right\} . \tag{7.45}$$

We show below that the transition probabilities derived from this stabilise as the boundary surfaces are moved further into the classical domain of the histories. Hence we obtain a transition matrix $T(b_2, \chi_2 | b_1, \chi_1)$ between classical histories, that in many ways is analogous to an S-matrix. The transition probabilities between specified classical histories are then proportional to

$$p_{\text{trans}}(b_2, \chi_2 | b_1, \chi_1) \propto |T(b_2, \chi_2 | b_1, \chi_1)|^2 . \tag{7.46}$$

Below we calculate this propagator (7.45) in the semiclassical approximation in two different cosmological models.

7.3.1 Quantum Transitions: from Inflation to Inflation

In this section we consider a positive scalar potential and evaluate the propagator (7.45) in its saddle point approximation to compute quantum transitions connecting classical, inflationary histories across a de Sitter like throat or a classical singularity. In Section 7.3.2 we will return to the propagator (7.45) in models with more general potentials that allow for transitions between ekpyrotic contraction and inflationary expansion.

We first consider the semiclassical approximation to the propagator (7.45) interpolating between two identical inflationary histories on both ends. This amounts to finding (complex) 'bounce' solutions of the Euclidean equations of motion of gravity coupled to a scalar field,

$$a'' + \frac{a\kappa^2}{3}\left(V(\phi) + \phi'^2 \right) = 0 , \tag{7.47a}$$

$$\phi'' + 3\frac{a'}{a}\phi' - \frac{\partial V(\phi)}{\partial \phi} = 0 , \tag{7.47b}$$

$$a'^2 - 1 + \frac{\kappa^2 a^2}{3}\left(-\frac{1}{2}\phi'^2 + V(\phi) \right) = 0 , \tag{7.47c}$$

where a prime denotes a derivative w.r.t. Euclidean time.

The symmetry of the problem means it is natural to consider saddle points that are symmetric around the bounce which translates into the boundary condition that, at the point τ_s of symmetry,

$$a'(\tau_s) = 0 \ , \qquad \phi'(\tau_s) = 0 \ , \tag{7.48}$$

where we are free to choose $\tau_s = 0$. The complex value $\phi(\tau_s)$ of the scalar field at the surface of symmetry can be varied to obtain the required boundary values (b, χ) of the fields. The bounce value of the (complex) scale factor in turn is determined by the Hamiltonian constraint. Hence we have,

$$\phi(\tau_s) = \phi_s e^{i\theta_s} \ , \qquad a(\tau_s) = \sqrt{\frac{3}{V(\phi(\tau_s))}} \ . \tag{7.49}$$

These constitute a sufficient set of boundary conditions to determine saddle point solutions to the propagator path integral. The bounce solutions can be viewed as solutions in the complex τ-plane, with the bounce located at $\tau = \tau_s = 0$ and the boundaries where $(a, \phi) = (b, \chi)$ at some complex value $\pm\upsilon$, with $\upsilon = X + it$.

To find the saddle points we must tune the three free parameters ϕ_s, θ_s and X such that the desired boundary values are reached. Fig. 51 shows an example, for a quadratic potential with $m = \sqrt{2} \cdot 10^{-2}$. The top panels show the logarithm of the absolute value of $\mathrm{Im}(\phi)$ and $\mathrm{Im}(a)$ in the complex τ-plane for $\phi_s = 10$ and $\theta_s = -0.0637813$. Black lines correspond to large negative values of the logarithm, indicating where the fields become real. Loosely speaking, a classical history corresponds to having vertical black lines (vertical is the Lorentzian time direction) for a and ϕ at the same location in the complex τ-plane. It turns out that the scale factor has in general multiple lines parallel to the y-axis where its imaginary part becomes zero. This is because in a slowly changing potential, the solution for the scale factor is sinusoidal, $a \sim \sqrt{\frac{3}{V(\phi(\tau_s))}} \sin(\sqrt{\frac{V(\phi(\tau_s))}{3}}\tau)$. Then, by tuning the phase θ_s one can ensure the lines of real a and real ϕ coincide. In fact, given there are multiple vertical lines where a is real for a given ϕ_0, one can find several symmetric bouncing saddle points connecting different classical solutions. In Fig. 51 we have taken θ such that the scalar field becomes real on the first branch in the upper right quadrant.

The action of the complex bouncing saddle points determines the quantum transition amplitude between the two classical histories at the endpoints. We have chosen to integrate the action along a contour that is not only symmetric, as required by the NBWF, but which also provides the dominant contribution to the quantum transition. In appendix D.1 we

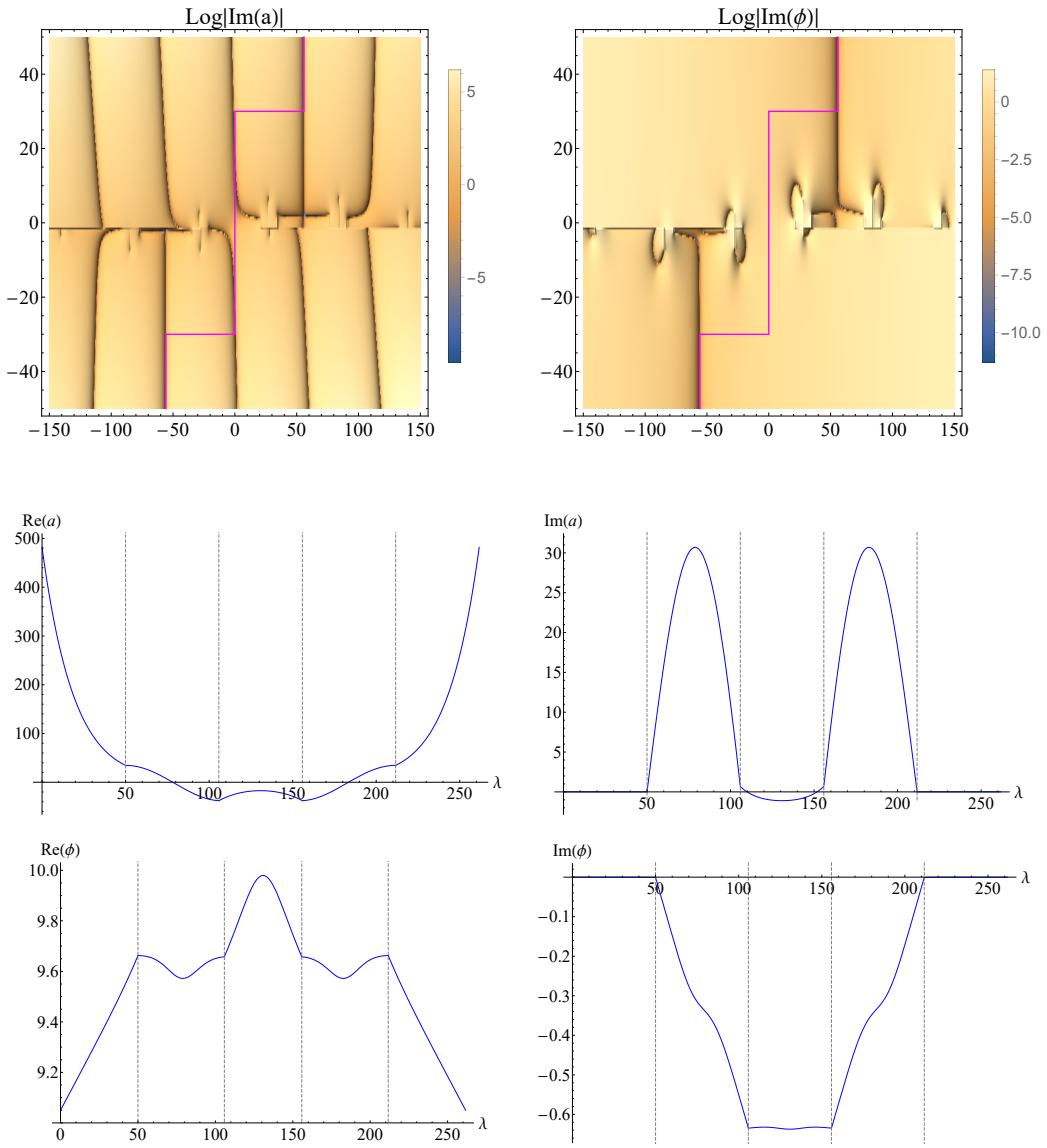

Figure 51: For $\phi_s = 10, \theta_s = -0.0637813$ we show on the left side $|\log(\mathrm{Im}(a))|$ and on the right $|\log(\mathrm{Im}(\phi))|$ in the complex τ-plane. These plots show where the the scale factor and scalar field become real. The phase θ_s is fine-tuned such that the lines of real values of ϕ and a overlap on the first branch of a to the right of the origin. The contour we chose is drawn in magenta, and the lower panels show the evolution of the fields along this contour as a function of λ, which is related to τ by $\tau = \int N d\lambda$. Here we took $\lambda = 0$ in the bottom left corner and evaluated the fields from this point to the upper right corner where $\lambda = 261.6$. For the present solution, we have $b_1 = b_2 = 500$, $\chi_1 = \chi_2 = 9.04196$ and at (b_2, χ_2) we have $a_{,\tau} = -4.00006 \times 10^{-7} - 26.1886i$, $\phi_{,\tau} = 2.18152 \times 10^{-8} + 0.0115247i$.

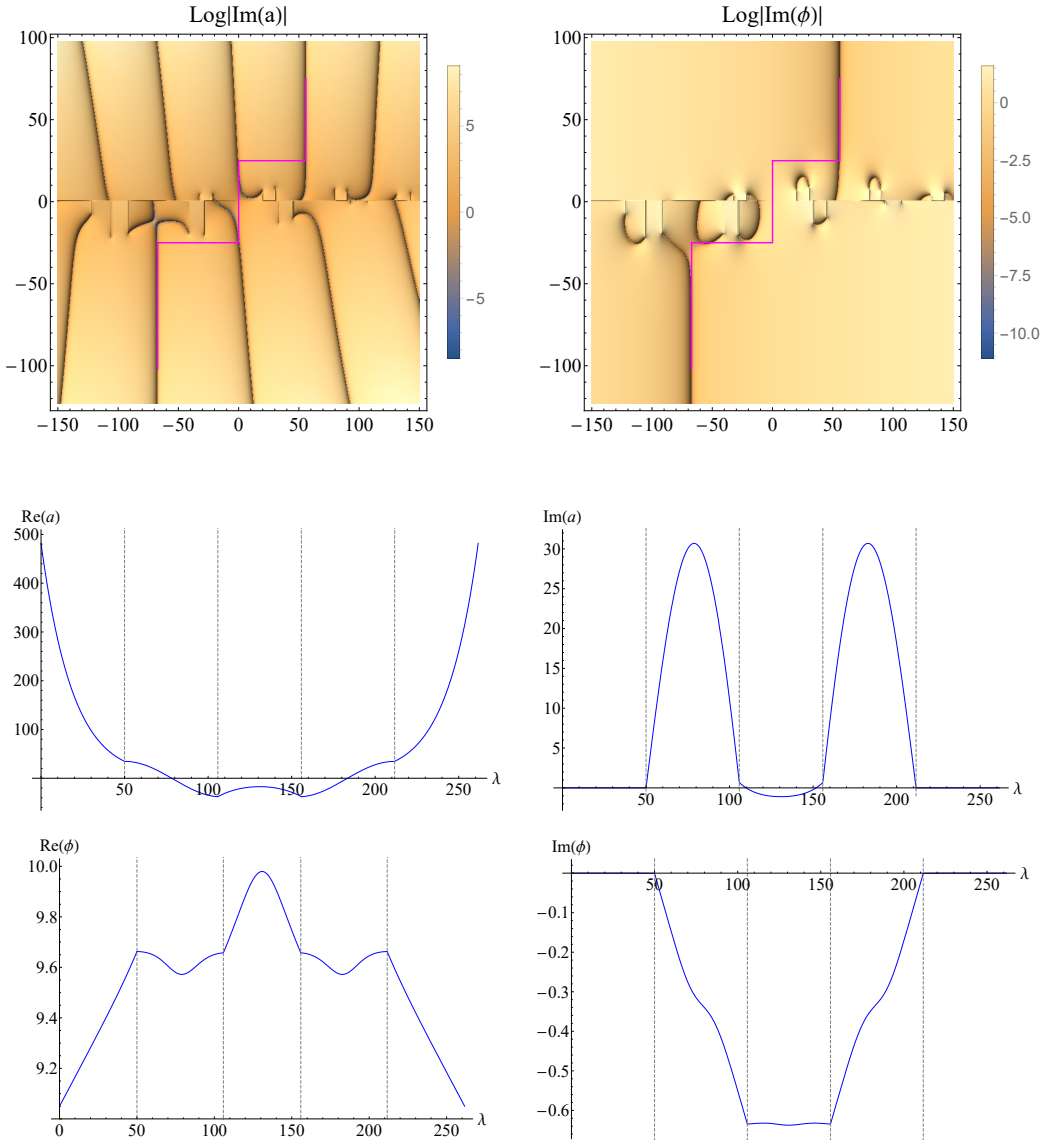

Figure 52: An example of an asymmetric bounce with $(b_1 = 500, \chi_1 = 7)$ and $(b_2 = 500, \chi_2 = 9.04196)$. In the upper panel we show the behaviour of the imaginary parts of the fields in the complex τ-plane, together with the contour we chose in magenta. In the lower panels we show the field values along this magenta path. This solution is obtained with the following derivatives imposed at the final boundary: $a_{,\tau} = 6.93303 \times 10^{-6} - 26.1886i$, $\phi_{,\tau} = -3.78052 \times 10^{-7} + 0.0115265i$.

discuss our choice of contour in more detail. We also discuss approximate analytic solutions in appendix D.2.

The contour we selected is shown in Fig. 51 in magenta in the upper panel. The evolution of the fields along this contour is shown in the lower panels of the figure. The fields indeed

become real along the last vertical leg out to the end points, where the saddle points coincide with a classical history. The upper panel shows there are singularities in the complex τ-plane, especially along the real τ axis. Had we chosen a contour encircling one of these singularities, we would have obtained either a different solution or no solution at all.

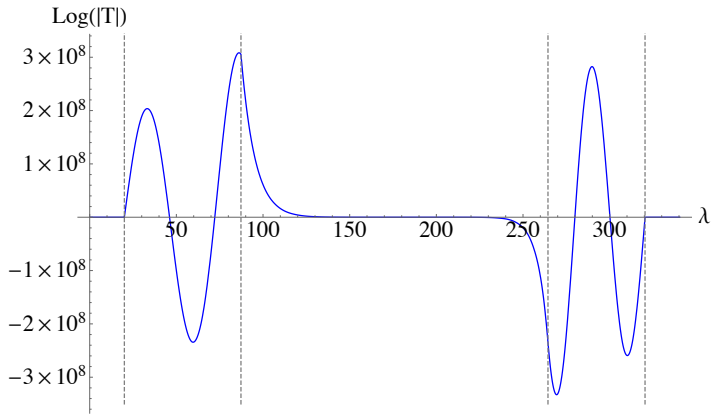

Figure 53: The real part of the interpolating saddle point action along the magenta contour shown in Fig. 52. This tends to a constant near the boundaries of the instanton, indicating that the quantum transition probabilities between given classical histories rapidly stabilise in the classical domain away from the bounce.

Evidently the symmetric bounce solutions can equally well be obtained by integrating the equations of motion from one of the boundaries, instead of starting at the point of symmetry. This proves to be a more useful setup to find interpolating saddle points between different classical histories on both ends. Fig. 52 shows an example of such an asymmetric bounce, connecting two inflationary histories with a different number of efolds. The contour we selected to compute this asymmetric transition is the one which smoothly changes into the original symmetric contour, without crossing any singularities, when the data on both boundaries are taken to be equal again.

At this point one may wonder whether the quantum transition probabilities (7.46) depend on the boundary value that is taken for the scale factor in the calculation of the propagator (7.45). Clearly this should not be the case as long as the classicality conditions hold on the boundary, since classical evolution preserves the real part of the Euclidean action.

It is therefore a useful consistency check of our method to verify whether the resulting transition probabilities stabilise if we take the boundary surfaces to larger scale factor, deeper into the classical domain of the histories. A first indication that this will indeed be the case for our solutions is provided in Fig. 53 which shows, for the solution plotted in Fig. 52, that the real part of the Euclidean action of the interpolating saddle point tends to a constant

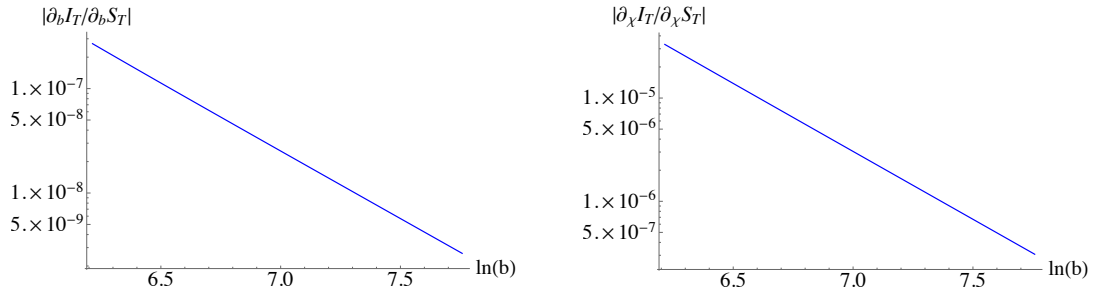

Figure 54: Classicality conditions derived from a saddle point describing a quantum bounce, assuming a classical incoming history, as a function of $\ln(b)$. The smallness of these ratios shows that the transition probability stabilises along the outgoing classical history.

near both boundaries. A more precise assessment is given in Fig. 54 where the WKB ratio $\nabla_A I_T/\nabla_A S_T$ is plotted as a function of b. We defined here I_T and S_T as respectively the real and imaginary part of the Euclidean action. The derivatives are estimated from taking finite differences, obtained by calculating successive interpolating instantons matching onto a classical history $(b(\lambda), \chi(\lambda))$, as well as slightly displaced instantons $(b + \delta b, \chi)$ and $(b, \chi + \delta\chi)$. The fact that the WKB conditions are small means the real part of the action is conserved. Thus the transition probability is independent of the slice at which the interpolating instanton is matched onto a given classical history. This also means that to compute asymmetric transitions we can fix b to a convenient value, and let the boundary values of the scalar field vary.

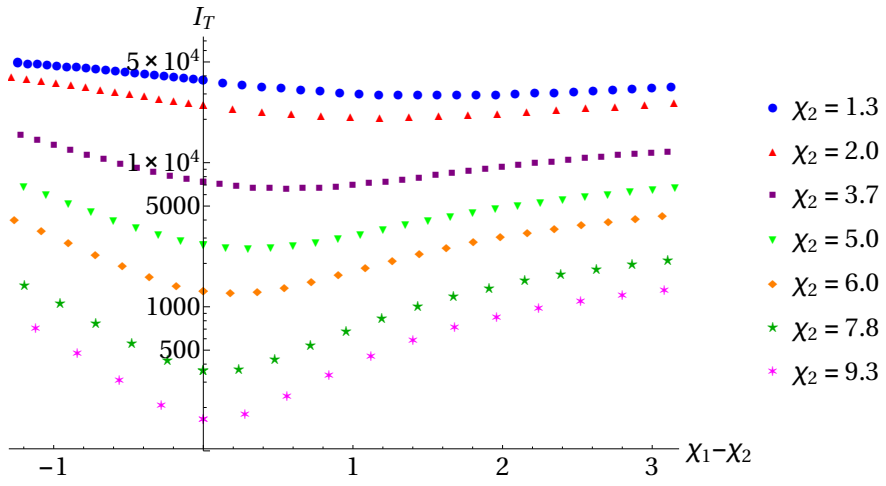

Figure 55: Logplot of the real part of the transition actions I_R as a function of the difference $\chi_1 - \chi_2$ for seven different initial values χ_2 shown in the legend. On both sides of the transition we fixed $b = 500$, well into the classical regime.

Our results for the semiclassical quantum transitions between inflationary histories in a

quadratic potential are summarized in Figures 55 and 56. Shown in Fig. 55 are the real part of the saddle point actions interpolating to different final values of $\chi_2 = 9.3, 7.8, 6.0, 5.0, 3.7, 2.0, 1.3$, as a function of the difference $\chi_2 - \chi_1$ with fixed $b = 500$ on both sides of the bounce. For large initial scalar field values χ_2 the most probable transition is the symmetric one. If we decrease χ_2 the instanton actions increase, giving a lower overall probability for a transition to occur. This behaviour is similar to that of probability distributions resulting from the tunneling wave function in cosmology [29], which one might have expected since the transitions we compute are not unlike tunneling events. This is illustrated in Fig. 56 where we integrated over all initial values χ_1 to obtain the total probability to transition as a function of χ_2. Finally we note that the minima shift slightly towards larger values of $\chi_1 - \chi_2$, implying that transitions to universes with a slightly longer period of inflation are preferred.

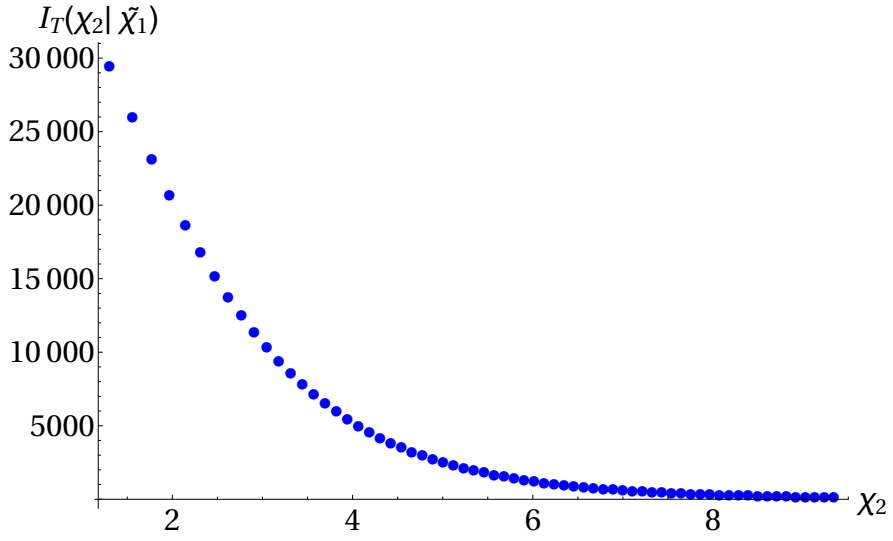

Figure 56: The real part of the transition action, as a function of χ_2, for the most probable history on the other side of the bounce. The values $\tilde{\chi}_1$ thus correspond for each χ_2 to the minimum of the curves in Fig. 55. This shows that transitions are more likely for larger χ_2.

Transition probabilities of this kind can be used to compute probabilities for entire four-dimensional histories in any quantum state that predicts classical inflationary patches.

7.3.2 Quantum Transitions: from Ekpyrosis to Inflation

The methods we have developed are not confined to the case of inflationary dynamics. In fact, the inflationary case is slightly special in that the transitions relate classical histories with opposite arrows of time. As a separate road to pursue, one may also consider big crunch singularities, and ask whether it is possible to tunnel out of them into an expanding universe,

thereby avoiding the big crunch. The best understood example of a big crunch is that of an ekpyrotic phase, which is a phase of high-pressure contraction during which anisotropies are suppressed [16, 17]. Thus, during such a phase the universe is driven towards a spatially flat crunch, and this justifies our minisuperspace approach.

We should note that various models for transitions from the contracting into an expanding phase have been investigated to date: in the original ekpyrotic model, the big crunch was modelled as the collision of higher-dimensional branes [16, 157]. At the classical level, the crunch was still singular (even though the singularity is much milder from a higher-dimensional point of view [158]), and thus the precise evolution across such a transition rests on assumptions of how to match a contracting with an expanding universe across a singular surface, see e.g. [159, 160]. To improve the calculational reliability, non-singular bouncing models were also constructed [161, 162, 47, 163] (for an implementation within the NBWF see [164]). Such models have the great advantage that one can calculate explicitly and unambiguously what happens to the background evolution and to cosmological perturbations (and it was found, for instance, that long-wavelength cosmological perturbations evolve across the bounce without being altered [63, 84]). However, all of the currently known models include hypothetical forms of matter, such as ghost condensates [165] or Galileons [61, 62], with unusual properties and no clear origin in fundamental physics.

Here we will be concerned with a more direct, and in fact more conservative approach: namely we want to see if one can transition out of an ekpyrotic contraction phase via a quantum transition[12]. As we will demonstrate, this is indeed possible, and in the particular example that we have studied, the ekpyrotic universe performs a quantum transition into an expanding inflationary phase. The reason for transitioning to inflation rather than, say, a kinetic dominated phase, is that the inflationary attractor guarantees a transition to another phase of classical evolution.

The model that we study again contains gravity coupled to a scalar field with a potential. We take the potential to be of the form

$$V(\phi) = V_0 \left(1 - e^{-c\phi}\right) + 2\tanh(-\phi) \ , \tag{7.50}$$

with the constants chosen to be $V_0 = c = 3$. The potential is shown in Fig. 57. It contains a steep negative region for negative values of ϕ, separated by a barrier from a region where the potential is positive and flat for positive ϕ. This potential allows for two types of attractor

[12]See e.g. [166, 167, 168, 169, 170] for some earlier work on the quantum resolution of cosmological singularities mostly in the context of the holographic approach to quantum gravity.

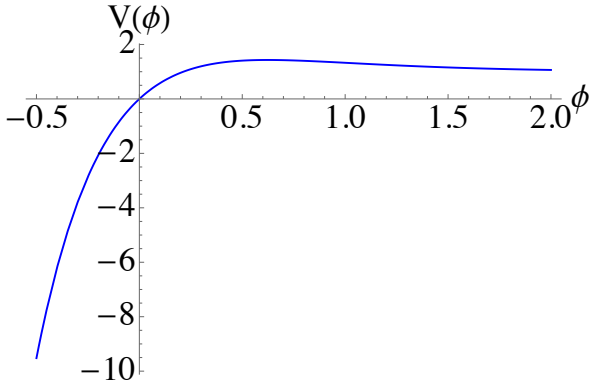

Figure 57: The potential $V(\phi) = 3\left(1 - e^{-3\phi}\right) + 2\tanh(-\phi)$ that we are considering in this section. It allows for ekpyrotic contracting solutions on the left, and for inflationary expanding solutions to the right of the maximum. We wish to show that quantum transitions between these two types of solutions are possible.

solutions: inflationary slow-roll solutions at positive ϕ, and ekpyrotic contracting solutions at negative ϕ. Let us be slightly more specific about the ekpyrotic solutions: for $\phi \lesssim -1$, we can approximate $V(\phi) \approx -3e^{-3\phi}$. Assuming a standard flat Robertson-Walker metric $\mathrm{d}s^2 = -\mathrm{d}t^2 + a^2(t)\mathrm{d}\mathbf{x}^2$, this model allows for the scaling solutions [143]

$$a(t) = a_0(-t)^{1/\epsilon}\left(1 + \frac{\sqrt{2\epsilon}}{3}\alpha\,(-t)^{1-3/\epsilon} + \ldots - \frac{1-3\epsilon}{3(1-\epsilon)}\frac{1}{\sqrt{2\epsilon}}\beta\,(-t)^{2-2/\epsilon} + \ldots\right) \quad (7.51)$$

$$\phi(t) = \sqrt{\frac{2}{\epsilon}}\ln\left(-\sqrt{\frac{\epsilon^2 V_0}{\epsilon - 3}}t\right) + \alpha\,(-t)^{1-3/\epsilon} + \ldots + \beta\,(-t)^{2-2/\epsilon} + \ldots\,, \quad (7.52)$$

where a_0 is a constant and where we have included the leading correction terms. The parameters α, β are fixed by initial conditions. Here $\epsilon = c^2/2 = 9/2$ is the fast-roll parameter, which by definition is always larger than 3 during an ekpyrotic phase. This expression clearly shows that the scaling solution is an attractor, as all correction terms die off in the approach to an eventual big crunch at $t = 0$. Note that the approximation of a spatially flat metric is justified since both the energy of expansion $H^2 \propto t^{-2} \propto a^{-2\epsilon} = a^{-9}$ and the energy density of the scalar field $\dot{\phi}^2 \propto a^{-9}$ grow much faster than the energy density in anisotropic fluctuations (which scales as a^{-6}) as the universe contracts.

The question now is whether, while classically headed for disaster, the big crunch can be avoided by a quantum transition to the other attractor solution, namely the inflationary one at positive scalar field values. Semi-classically, such a quantum transition can be described by a complex saddle point of the path integral, i.e. we will once again look for a complex solution of the equations of motion, this time interpolating between an ekpyrotic starting

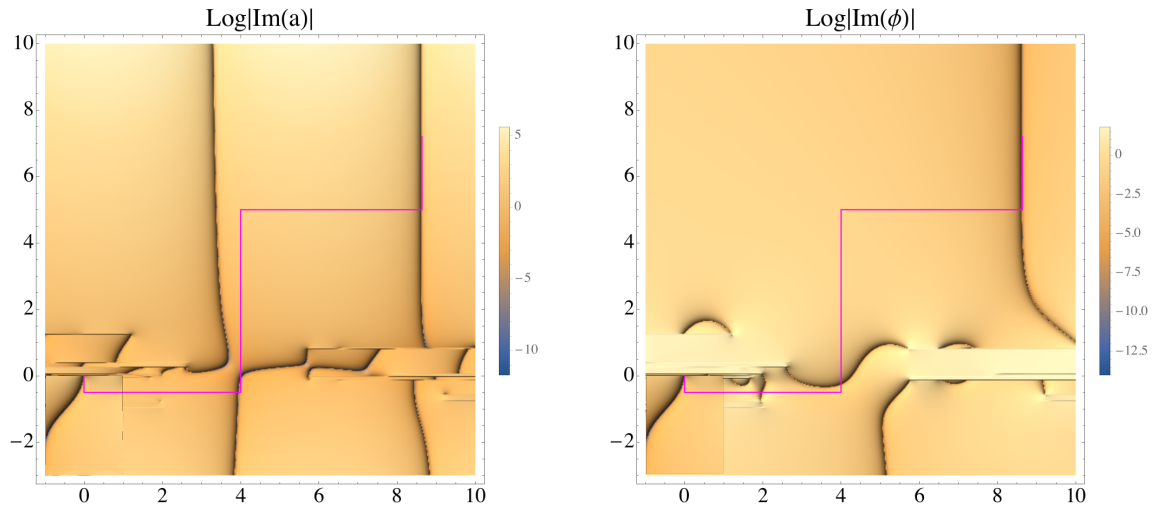

Figure 58: These relief plots show our solution interpolating between a contracting ekpyrotic phase and an expanding inflationary phase over a region of the complex time plane. More specifically, the plots show (the logarithm of the absolute value of) the imaginary part of the scale factor (left panel) and scalar field (right panel), with darker colours corresponding to smaller imaginary parts. Thus the dark lines show the locus where the fields take real values. The bottom left part of the figures show an ekpyrotic history headed for a big crunch at $t = 0$, while the upper right part shows the final inflationary history with coincident lines of real scale factor and scalar field. On the ekpyrotic side, the lines of real a and ϕ also become coincident in the approach to the crunch, but this occurs over a very small time interval just before the crunch – this is as expected from studies of ekpyrotic instantons [152]. The graph necessarily only shows one sheet of the full solution function, while one can clearly distinguish several singular points and the associated branch cuts.

point and an inflationary final point. Finding such a solution is complicated in this case by the presence of numerous singularities, which arise because along the ekpyrotic part of the potential a singularity can be reached within a finite time. Because of these singularities, it is not obvious what the appropriate contour in the complex time plane ought to be, and some trial and error is inevitable. An example of an interpolating solution is shown in Fig. 58, and the evolution of the fields along the contour drawn as a pink line in Fig. 58 is shown in Fig. 59. The many singularities mentioned above are immediately apparent in Fig. 58, which shows only the relevant sheet of the solution function. Encircling the singularities in different ways typically leads to an entirely different solution, usually containing no region

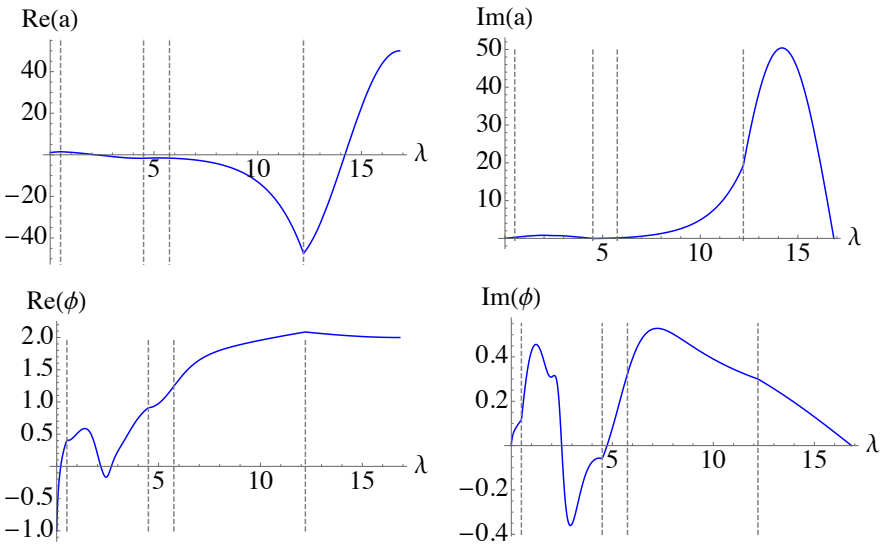

Figure 59: These graphs show the evolution of the scale factor $a$and the scalar field ϕ along the contour (parameterised by λ) shown by a pink line in Fig. 58. Note that the fields are real at the end points, as required. In fact, for this particular solutions, we have $b_1 = 1$, $\chi_1 = -1$ and $b_2 = 50$, $\chi_2 = 2$. The solution corresponds to imposing $\chi_{1,\tau} = -1.40549 + 14.1652i$ and $b_{1,\tau} = -0.582476 + 5.69670i$, with $b_{1,\tau}$ being determined by the Hamiltonian constraint. At small λ, the contour first runs down, and accordingly along this first segment the fields undergo a reverse ekpyrotic contraction. Along the middle segments, the evolution is fully complex, and along the final vertical segment a real inflationary expanding history has been reached. At large λ, it is also obvious from the plots of the action that the imaginary part varies fast compared to the variation in the real part, which shows that the WKB classicality conditions will be satisfied there. More prosaically, this can already be guessed from the fact that the imaginary parts of a and ϕ are tiny there, compared to the real parts. At small λ, it is less obvious that the ekpyrotic starting history is indeed classical in a WKB sense, which is why we have performed a more detailed WKB analysis as shown in Fig. 60.

of classicality. This solution is a showcase example of the use of complex time paths in describing quantum tunneling, as described in more detail in [108, 3] and in chapter 5.

As one can see from the figures, our solution indeed interpolates between an ekpyrotic and an inflationary history, with a fully complex evolution in between. It is obvious that a classical inflationary solution is reached near the final boundary, since the scale factor and scalar field remain real in the Lorentzian direction for an extended period of time. On the ekpyrotic side, although at the starting point the fields are real, they rather quickly develop imaginary parts too. This is because the ekpyrotic contraction occurs over a very short time

period, and thus appears compressed in the figure. In order to show unambiguously that we are indeed starting from a classical ekpyrotic contraction history, we have evaluated the WKB classicality conditions (6.28) on the ekpyrotic side, keeping the final field values on the inflationary end fixed (while allowing the field derivatives to vary). Corresponding plots are shown in Fig. 60. As the figures show, the WKB conditions are better and better satisfied as the universe contracts towards a big crunch, which is just as expected for the ekpyrotic attractor [152, 155]. This result also implies that the probability for tunnelling out of an ekpyrotic phase is constant along a classical ekpyrotic contracting solution, analogously to the inflationary case treated in section 7.3.1.

The solution that we have just presented may be considered as a proof of principle that quantum transitions out of an ekpyrotic contracting phase and into an expanding inflationary phase are possible.

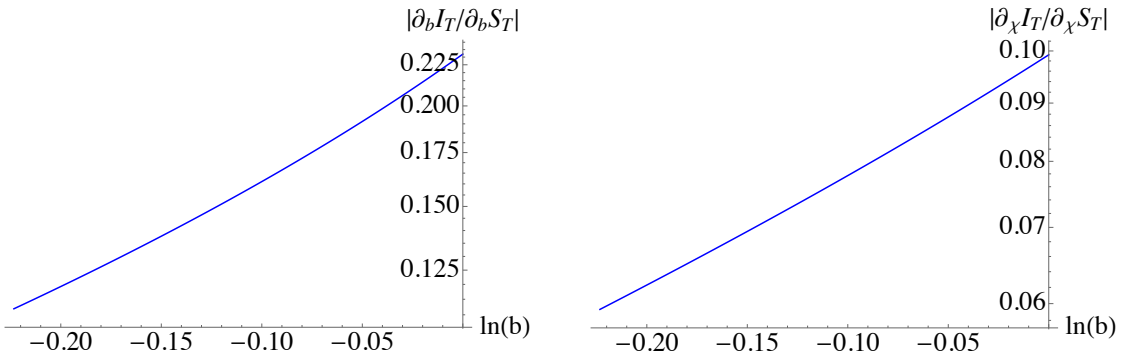

Figure 60: A graph of the WKB classicality conditions (6.28). These become small as the universe contracts, i.e. as b decreases, thus demonstrating that the approach to a big crunch is accurately described by a classical ekpyrotic phase.

7.4 Discussion

We have provided two ways of resolving classical singularities through quantum means. Firstly, anisotropic (Bianchi IX) no-boundary inflationary instantons may be constructed with arbitrary values of the anisotropy functions. A novel feature is that the construction of these instantons requires a different contour in the complex time plane than the one usually employed for no-boundary inflationary instantons, due to the presence of singularities caused by the anisotropies. A further implication of the anisotropies is that the wavefunction of the universe becomes classical in a WKB sense less fast than in the isotropic case. More precisely, the classicality conditions are satisfied only in inverse proportion to the linear size of the universe, as opposed to inversely to the volume, which would have been the case for

isotropic instantons. Thus the anisotropies keep the wavefunction fully quantum for longer, and it will be interesting to explore possible implications of this feature.

Our results imply that for a scalar field model with an inflationary potential the no-boundary state predicts classical histories with arbitrarily large anisotropies. In all cases that we have constructed we found that an inflationary phase is reached, and thus at late times these anisotropies decay away. In general, due to the presence of the anisotropies, the classical histories reached at late times contain a big bang singularity when extrapolated into their past. This singularity is then resolved by the no-boundary proposal in the sense that the description in terms of a classical space-time becomes untenable at small scale factor values, since the wavefunction does not yet describe a classical universe at that point.

A further extension concerns the construction of anisotropic ekpyrotic instantons. Here also we are naively faced with a puzzle: the new $\mathcal{WKB}_{b_\pm}$ classicality conditions that we have derived here scale as $b^{-1-\epsilon}$. In ekpyrotic models the universe is contracting and moreover $\epsilon > 3$. Then, if the same scaling were to hold, it would appear that the classicality conditions would blow up and not be satisfied as b shrinks. This is however hard to believe as an ekpyrotic phase is an attractor and suppresses anisotropies in much the same way as inflation does. It will therefore be interesting to clarify this puzzle.

Secondly, we have shown that classical cosmological singularities can be resolved in minisuperspace semi-classical quantum gravity and replaced by quantum bounces interpolating between contracting and expanding branches of cosmological histories.

We have focussed on two cases of special interest where classical cosmological evolution often involves a singularity: transitions from inflation to inflation, and transitions from ekpyrosis to inflation. Let us summarise our findings.

The quantum bounces that we have found are mediated by complex saddle points of the action of gravity coupled to a scalar field, interpolating between specified real initial and final classical configurations. For the case of inflationary-to-inflationary transitions, the symmetry of the problem selects the appropriate contour of integration in the complex plane. This provides a clean starting point to identify more general instantons describing asymmetric transitions obtained by smoothly deforming away from the symmetric case. Interestingly, at large values of the inflaton potential, the most likely transition turns out to be the symmetric one whereas at low values of the potential – the regime where the classical extrapolation produces a singularity – tunnelling to a slightly larger value of the potential is preferred.

Combined with the no-boundary wave function, which provides a measure on inflationary

cosmology, our results for the quantum bounces yield probabilities for an ensemble of complete inflationary histories exhibiting a quantum transition that connects two classical inflationary patches on either side. The quantum transitions identified here allow one to refine and differentiate between different possible pasts of the inflationary histories in the NBWF, which are coarse grained over in the usual treatment.

We have also analysed a potential that contains both ekpyrotic contracting and inflationary expanding solutions. In this case, we have demonstrated the existence of similar quantum transitions from the contracting phase into the expanding one, avoiding the big crunch singularity that in a purely classical context would follow the ekpyrotic contraction.

8 Lorentzian Quantum Cosmology

So far in this thesis we have used a somewhat ad-hoc notion of the path integral. For example in chapter 7, we approximated the path integral by the saddle point with the lowest Euclidean action. However, because we could not solve the theory analytically, we could not systematically list all saddle points and then choose the lowest action one. Therefore, it is not entirely clear whether we found the correct one. Furthermore, we have, so far, relied primarily on the Euclidean path integral. This framework is motivated by the no-boundary proposal - which is more naturally formulated in the Euclidean theory - and developed in analogy to quantum field theory where the Euclidean (so-called Wick rotated) theory has nicer convergence properties. This is because the Lorentzian path integral is highly oscillatory and thus its convergence not guaranteed. When gravity is included, however, the Euclidean path integral faces more serious trouble than in the usual field theory case: The Euclidean action is unbounded from below. Ever larger gradients of the universe's overall scale-factor lead to an increasingly negative action rendering the entire theory unstable. This is the so-called conformal factor problem [25, 171]. Indeed, upon a conformal transformation of the metric

$$\tilde{g}_{\mu\nu} = \Omega^2 g_{\mu\nu} \tag{8.1}$$

the Ricci scalar transforms as

$$\tilde{R} = \Omega^{-2} R - 6\Omega^{-3}\Omega_{,\mu}\Omega^{,\mu} \tag{8.2}$$

and the bulk of the Euclidean gravitational action becomes

$$S_E[\tilde{g}] = -\frac{1}{2}\int_{\mathcal{M}} \sqrt{\tilde{g}}\tilde{R} \tag{8.3}$$

$$= -\frac{1}{2}\int_{\mathcal{M}} \left[\Omega^2 R + 6\Omega_{,\mu}\Omega^{,\mu}\right]\sqrt{g}d^4x \tag{8.4}$$

Thus S_E can be as negative as desired by simply choosing a very rapidly varying conformal factor Ω. In practice this means that the Euclidean path integral by itself does not define the theory uniquely but additional input in the form of a complex integration contour is required. It is for these reason that recently there has been a trend to return to a purely Lorentzian definition of the path integral, defined over real, Lorentzian metrics [28, 172]. Causality and unitarity are immediate and natural consequences of this choice. Furthermore, any ambiguities that appear in the wavefunction of Wheeler and DeWitt are eliminated as the boundary conditions are specified in terms of initial and final three-geometries. The question raised in the beginning still remains however: How does one deal with the oscillatory

integral? It turns out that in simple examples, the integral is conditionally convergent. There exists a mathematical framework which rigourously prescribes how to deform the integral's integration contour in the complex plane such that it becomes absolutely convergent: Picard-Lefschetz theory[13]. In the following sections, we will first introduce Picard-Lefschetz Theory as a mathematical tool and illustrate its use with a simple example. Consequently, we will apply it in a cosmological context by identifying minisuperspace models for which the path integral can be solved completely. This allows us to re-examine the no-boundary proposal and provide the basis for an analysis of eternal inflation that goes beyond what is typically found in the literature.

8.1 Picard-Lefschetz Theory

The main idea of Picard-Lefschetz theory is to complexify the integral of interest and then deform the original contour of integration (here the contour for the lapse integral) in such a way as to render the resulting integral manifestly convergent. It may be useful to consider a simple example, say $\tilde{I} = \int_{\mathbb{R}} dx e^{ix^2}$. Along the defining contour, namely the real line, this is a highly oscillating integral. But now we can deform the contour by defining $x = e^{i\pi/4}y$, such that $\tilde{I} = e^{i\pi/4}\int dy e^{-y^2}$. Along the new contour, the integral has stopped oscillating, and in fact the magnitude of the integrand decreases as rapidly as possible. The integral is now manifestly convergent, and one may check that the arcs at infinity linking the original contour to the new one yield zero contribution. Note that along the steepest descent path, there is an overall constant phase factor (here $e^{i\pi/4}$) – this is a general feature of such paths.

More formally, we can write the exponent $iS[x]/\hbar$ and its argument, taken to be x here, in terms of their real and imaginary parts, $iS/\hbar = h + iH$ and $x = u^1 + iu^2$ – see Fig. 61 for an illustration of the concepts. Downward flow of the magnitude of the integrand is then defined by

$$\frac{\mathrm{d}u^i}{\mathrm{d}\lambda} = -g^{ij}\frac{\partial h}{\partial u^j}\,, \tag{8.5}$$

with λ denoting a parameter (along the flow) and g_{ij} denoting a metric on the complexified plane of the original variable x (here we can take this metric to be the trivial one, $ds^2 = d|u|^2$). The real part of the exponent h is also called the Morse function. It decreases along the flow, since $\frac{\mathrm{d}h}{\mathrm{d}\lambda} = \sum_i \frac{\partial h}{\partial u^i}\frac{\mathrm{d}u^i}{\mathrm{d}\lambda} = -\sum_i \left(\frac{\partial h}{\partial u^i}\right)^2 < 0$. The downward flow Eq. (8.5) can be rewritten as

$$\frac{\mathrm{d}u}{\mathrm{d}\lambda} = -\frac{\partial\bar{\mathcal{I}}}{\partial\bar{u}}, \quad \frac{\mathrm{d}\bar{u}}{\mathrm{d}\lambda} = -\frac{\partial\mathcal{I}}{\partial u}\,, \tag{8.6}$$

[13]While we complexify the integral in the process of evaluating it, the fundamental definition of the path integral is still over real, Lorentzian metrics.

and this form of the equations is useful in that it straightforwardly implies that the phase of the integrand, $H = \mathrm{Im}[iS/\hbar]$, is conserved along a flow,

$$\frac{\mathrm{d}H}{\mathrm{d}\lambda} = \frac{1}{2i}\frac{\mathrm{d}(\mathcal{I}-\bar{\mathcal{I}})}{\mathrm{d}\lambda} = \frac{1}{2i}\left(\frac{\partial\mathcal{I}}{\partial u}\frac{\mathrm{d}u}{\mathrm{d}\lambda} - \frac{\partial\bar{\mathcal{I}}}{\partial\bar{u}}\frac{\mathrm{d}\bar{u}}{\mathrm{d}\lambda}\right) = 0\,. \tag{8.7}$$

Thus, along a flow the integrand does not oscillate, rather its amplitude decreases as fast as possible. Such a downwards flow emanating from a saddle point σ is denoted by $\mathcal{J}_\sigma$ and is often called a "Lefschetz thimble".

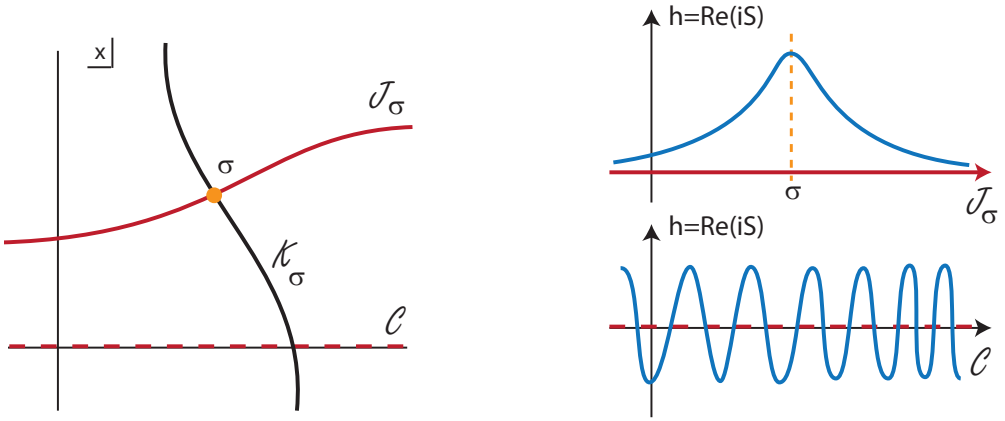

Figure 61: Picard-Lefschetz theory instructs us how to deform a contour of integration such that an oscillating integral along a contour $\mathcal{C}$ gets replaced by a steepest descent contour (or in general a sum thereof) along a Lefschetz thimble $\mathcal{J}_\sigma$ associated with a saddle point σ. Only those saddle points contribute for which the flow of steepest ascent $\mathcal{K}_\sigma$ intersects $\mathcal{C}$.

In much the same way one can define an upwards flow

$$\frac{\mathrm{d}u^i}{\mathrm{d}\lambda} = +g^{ij}\frac{\partial h}{\partial u^j}\,, \tag{8.8}$$

with H likewise being constant along such flows. Upwards flows are denoted by $\mathcal{K}_\sigma$, and they intersect the thimbles at the saddle points. Thus we can write

$$\mathrm{Int}(\mathcal{J}_\sigma, \mathcal{K}_{\sigma'}) = \delta_{\sigma\sigma'}\,. \tag{8.9}$$

Our goal then is to express the original integration contour $\mathcal{C}$ as a sum over Lefschetz thimbles,

$$\mathcal{C} = \sum_\sigma n_\sigma \mathcal{J}_\sigma\,. \tag{8.10}$$

Multiplying this equation on both sides by $\mathcal{K}_\sigma$ we obtain that $n_\sigma = \mathrm{Int}(\mathcal{C}, \mathcal{K}_\sigma)$. Thus a saddle point, and its associated thimble, are relevant if and only if one can reach the original integration contour via an upwards flow from the saddle point in question. Intuitively, this

makes sense: we are replacing an oscillating integral, with many cancellations, by one which does not contain cancellations, and thus the amplitude along the non-oscillating path must be lower. Putting everything together, we can then re-express the conditionally convergent integral by a sum over convergent integrals,

$$\int_{\mathcal{C}} \mathrm{d}x\, e^{iS[x]/\hbar} = \sum_{\sigma} n_\sigma \int_{\mathcal{J}_\sigma} \mathrm{d}x\, e^{iS[x]/\hbar} \tag{8.11}$$

$$= \sum_{\sigma} n_\sigma\, e^{i\,H(x_\sigma)} \int_{\mathcal{J}_\sigma} e^{h} \mathrm{d}x \tag{8.12}$$

$$\approx \sum_{\sigma} n_\sigma\, e^{iS(x_\sigma)/\hbar}\,. \tag{8.13}$$

The last line expresses the fact that the integral along each thimble may easily be approximated via the saddle point approximation, the leading term being the value at the saddle point itself. If required, one can then evaluate sub-leading terms by expanding in $\hbar$, but in the present work this will not be necessary. This concludes our mini-review of Picard-Lefschetz theory – for a detailed discussion see [27], and for applications in a similar context than the present one see [28, 173, 174].

8.2 Exactly Soluble Scalar Field Minisuperspace Models

8.2.1 The Simplest Case: Pure Gravity

We consider an FLRW metric of any curvature coupled to a cosmological constant. Because the theory has gauge symmetry, quantization implies extra difficulty. The usual treatment, pioneered by Batalin, Fradkin, and Vilkovisky (BFV), is to introduce a ghost term which breaks the reparametrization symmetry and fixes the proper time gauge $\dot{N} = 0$ [175, 153, 176]. After integrating over the ghost and momentum fields, one obtains

$$G[a_1; a_0] = \int_{0^+}^{\infty} dN \int_{a_0}^{a_1} Da e^{iS(a,N)/\hbar} \tag{8.14}$$

The path integral over the scale factor represents the quantum mechanical amplitude for the universe to evolve from having a_0 as its radius to a_1 in a proper time N. Integrating over the lapse implies that we consider all possible paths of positive proper time. In [176] it was shown that this choice means that a_0 lies in the causal past of a_1. The resulting action reads

$$S = 2\pi^2 \int_0^1 dt N \left(-\frac{3}{N} a\dot{a}^2 + 3ka - a^3\Lambda \right) \tag{8.15}$$

The path integral simplifies significantly upon the following change of variables [177]

$$N(t) \to N(t)/a(t)q(t) = a^2(t) \tag{8.16}$$

which means that the action now reads

$$S = 2\pi^2 \int_0^1 dt \left(-\frac{3}{4N}\dot{q}^2 + N(3k - \Lambda q \right) \tag{8.17}$$

and we can solve the equation of motion for q exactly and the path integral over it is Gaussian. Hence the expression for the propagator reduces to

$$G[q_1; q_0] = \sqrt{\frac{3\pi i}{2\hbar}} \int_0^\infty \frac{dN}{N^{1/2}} e^{2\pi^2 i S_0/\hbar} \tag{8.18}$$

where S_0 is the on-shell action for q but *not* for N. We are now dealing with a highly oscillating integral and ought to apply Picard-Lefschetz theory to approximate it by its saddle points. S_0 can be explicitly evaluated and is given by

$$S_0 = N^3 \frac{\Lambda^2}{36} + N\left(-\frac{\Lambda}{2}(q_0 + q_1) + 3k \right) - \frac{1}{N}\frac{3}{4}(q_1 - q_0)^2 \tag{8.19}$$

which has four, generally complex, saddle points which are solutions of

$$\frac{\partial S_0}{\partial N} = N_s^4 \Lambda^2 + N_s^2 \left(-6\Lambda(q_0 + q_1) + 36k \right) + 9(q_1 - q_0)^2 = 0 \tag{8.20}$$

The saddle points themselves are

$$N_s = c_1 \frac{3}{\Lambda} \left[\left(\frac{\Lambda}{3} q_0 - k \right)^{1/2} + c_2 \left(\frac{\Lambda}{3} q_1 - k \right)^{1/2} \right] \tag{8.21}$$

c_0 and c_1 can be either -1 or 1 and thus four solutions are obtained. When $k = 1$ these can be complex while for flat or hyperbolic geometries they are purely real. The closed $k = 1$ case is interesting because within it, the no-boundary proposal can be analyzed. In particular, depending on the boundary conditions, four qualitatively different scenarios occur

- Classical boundary conditions $q_1 \geq q_0 > 3/\Lambda$ where all saddle points are real.
- The no-boundary proposal $q_1 > 3/\Lambda > q_0$ where one of the roots becomes imaginary.
- Quantum boundary conditions $3/\Lambda > q_1 > q_0$ where both roots become imaginary.

This analysis has led to the finding that the no-boundary proposal's amplitude is well approximated by the propagator $G_{nb}[q_1, 0] \approx e^{-12\pi^2/\hbar\Lambda}$. However, extending this result to include perturbations yields catastrophic results: Ever larger perturbations are favoured and the no-boundary proposal is rendered unstable [173, 172]. One possible resolution is by changing the no-boundary proposal altogether and choosing a saddle point by introducing suitable boundary conditions. In this case the saddle point with suppressed perturbations can be selected by introducing Robin boundary conditions [178] which we introduced in appendix A.1.

8.2.2 Gravity and a Scalar Field

For gravity minimally coupled to a scalar field with a potential, the Feynman propagator in minisuperspace is given by

$$G[a_1, \phi_1; a_0, \phi_0] = \int_{0^+}^{\infty} dN \int_{a_0}^{a_1} \int_{\phi_0}^{\phi_1} DaD\phi e^{iS(a,\phi,N)/\hbar} \,. \tag{8.22}$$

This propagator describes the amplitude to go from an initial 3-surface with scale factor a_0 and scalar field ϕ_0 to a final 3-surface specified by a_1 and ϕ_1. The action here is given by the Einstein-Hilbert functional with a minimally coupled scalar field and the Gibbons-Hawking-York boundary term. Note that the last term is crucial to make the variational principle compatible with the mentioned Dirichlet boundary conditions. The full action reads

$$S = 6\pi^2 \int dt_p N \left(-\frac{a\dot{a}^2}{N^2} + a + \frac{a^3}{3} \left(\frac{1}{2} \frac{\dot{\phi}^2}{N^2} - V \right) \right) \tag{8.23}$$

where we used the usual metric of a closed FLRW universe with lapse N

$$ds^2 = -N^2 dt_p^2 + a(t_p)^2 d\Omega_3^2 \,. \tag{8.24}$$

We take the range of integration of the lapse function to be over strictly positive and real values only - in line with the definition of the Lorentzian path integral. While the path integral is a very intuitive tool in computing amplitudes for the universe's, it is not used very much because in most situations it is difficult or impossible to compute it explicitly. In particular one cannot solve the above analytically for generic potentials of the scalar field $V(\phi)$. For certain specific forms of $V(\phi)$, however, exact solutions may be obtained. One class has been studied in [179] and we shall review their approach here. Our goal is to transform the action (8.23) into a form that is quadratic in its variables such that we can solve the resulting path integral exactly. To do this, first consider a rescaling of the time coordinate,

$$ds^2 = -\frac{N^2}{a(t)^2} dt^2 + a(t)^2 d\Omega_3^2, \tag{8.25}$$

followed by a redefinition of the fields [179],

$$x(t) \equiv a^2(t) \cosh\left(\sqrt{\frac{2}{3}} \phi(t) \right) \,, \tag{8.26}$$

$$y(t) \equiv a^2(t) \sinh\left(\sqrt{\frac{2}{3}} \phi(t) \right) \,. \tag{8.27}$$

The inverse transformations are given by

$$a(t) = \left(x^2(t) - y^2(t) \right)^{1/4} \,, \qquad \phi(t) = \sqrt{\frac{3}{2}} \tanh^{-1}\left(\frac{y(t)}{x(t)} \right) \,. \tag{8.28}$$

Then, for a potential of the form

$$V(\phi) = \alpha \cosh \sqrt{\frac{2}{3}}\phi \,, \tag{8.29}$$

the action reduces to the remarkably compact form [179]

$$S = V_3 \int_0^1 dt N \left[\frac{3}{4N^2} \left(y'(t)^2 - x'(t)^2 \right) + 3 - \alpha x(t) \right] , \tag{8.30}$$

where a prime refers to derivation with respect to the coordinate time t, and we are choosing the range of the time coordinate between the initial and final hypersurface to be $0 \leq t \leq 1$. Here we wrote the coordinate volume of the three-dimensional spatial slice as V_3 – for the standard three-sphere we have $V_3 = 2\pi^2$ but here, for notational simplicity, we will use re-scaled coordinates such that $V_3 = 1$ (since we will be interested in situations where the scale factor is large, our calculations also apply with good accuracy to FLRW metrics with flat spatial slices, as long as the spatial volume is regulated to a finite value). The resulting equations of motion are

$$x''(t) = \frac{2\alpha}{3} N^2 \,, \qquad y''(t) = 0 \,. \tag{8.31}$$

Imposing Dirichlet boundary conditions $x(0) = x_0$, $x(1) = x_1$, and $y(0) = y_0$, $y(1) = y_1$ (where these boundary values are related to the original boundary conditions $a_{0,1}, \phi_{0,1}$ via the definitions (8.26) and (8.27)), the resulting solutions are given by

$$\bar{x}(t) = \frac{\alpha}{3} N^2 t^2 + (x_1 - x_0 - \frac{\alpha}{3} N^2) t + x_0 \,, \tag{8.32}$$

$$\bar{y}(t) = (y_1 - y_0) t + y_0 \,. \tag{8.33}$$

A general path that is summed over in the path integral can now be written as $x(t) = \bar{x}(t) + X(t)$ and similarly for $y(t)$. The path integral over x can then be performed by shifting variables to X, where the integral over X is a simple Gaussian that can be evaluated exactly. After solving the x and y integrals in this manner we are left with an ordinary one-dimensional integral over the lapse only,

$$G[x_1, y_1; x_0, y_0] = \int_{0^+}^{\infty} dN P(N) e^{iS_0(x_0, x_1, y_0, y_1, N)/\hbar} \tag{8.34}$$

where $P(N)$ is a non-exponential prefactor (scaling as $1/N$), and the action S_0 is obtained by substitution of the solutions (8.32) and (8.33), yielding

$$S_0 = \frac{\alpha^2}{36} N^3 + N \left(3 - \frac{1}{2} \alpha (x_0 + x_1) \right) + \frac{3}{4N} \left((y_1 - y_0)^2 - (x_1 - x_0)^2 \right) \,. \tag{8.35}$$

In order to evaluate the above integral, which is a conditionally convergent integral, we will make use of Picard-Lefschetz theory. The first step in evaluating the propagator (8.34) then is to identify the saddle points of the integrand. Since we will be interested in the leading semi-classical approximation, we can neglect the prefactor $P(N)$ from this point onwards, as it will not affect the saddle points of the integrand at leading order in $\hbar$. The saddle points obey the condition

$$\frac{\partial S_0}{\partial N} = \frac{\alpha^2}{12}N^2 + \left(3 - \frac{1}{2}\alpha(x_0 + x_1)\right) - \frac{3}{4N^2}\left((y_1 - y_0)^2 - (x_1 - x_0)^2\right) = 0\,, \tag{8.36}$$

which has four solutions

$$N_{c_1,c_2} = c_1\sqrt{\frac{3}{\alpha^2}}\sqrt{-6 + \alpha(x_0 + x_1) - c_2\sqrt{I}}\,, \tag{8.37}$$

where

$$I = \alpha^2\left((y_1 - y_0)^2 - (x_1 - x_0)^2\right) + (6 - \alpha(x_0 + x_1))^2 \tag{8.38}$$

and $c_1, c_2 \in \{-1, 1\}$. As we will see below, for the cases of interest to us, these saddle points will either be all real, or two real and two pure imaginary. The subsequent analysis based on [7] depends on the boundary conditions that are chosen.

8.3 Homogeneous Transitions During Inflation

A beautiful idea of modern cosmology is that the origin of the largest structures in the universe may lie in primordial quantum fluctuations [180, 38]. Inflation and ekpyrosis provide concrete mechanisms that can amplify quantum fluctuations into essentially classical density perturbations, which can then act as seeds for the formation of structure via gravitational collapse [38, 181, 39, 40, 41, 182, 183, 184, 185, 186, 187, 188, 189]. The amplification itself is calculated within the framework of quantum field theory (QFT) in curved spacetime. In this formalism, one fixes a classical background spacetime (and a classical background matter configuration) and then quantises small fluctuations around this background [190]. This approach is reminiscent of the Born-Oppenheimer approximation, where light electronic excitations are quantised around a heavy atomic nucleus which to a first approximation is treated classically. This analogy suggests that for many applications this approximation scheme should be valid and yield precise results. However, there are also good reasons to try to go beyond this first approximation: conceptually, it makes little sense to think of the background as classical and the fluctuations as quantum. All of nature should be described by the same theory, and thus the background should be thought of as being just as much

part of the quantum wavefunction as the fluctuations. Beyond this conceptual consideration, it is important to gain an understanding of the quantisation of the entire system in order to assess under what circumstances the approximation of QFT in curved spacetime breaks down, and to see what might replace it in such a regime. In the context of inflation, which we will focus on in this chapter, the calculation of quantum fluctuations is used not only for small fluctuations, but also for large fluctuations deep in the tails of the distribution. This is especially relevant for eternal inflation, where it is assumed that the quantum fluctuations of the inflaton can be larger than its changes due to classical evolution [191, 29]. Although such large fluctuations are rare, they may play an important role in the cosmological context as they can alter the global structure of spacetime: in a region where the inflaton jumps up the potential, the expansion rate of the universe will be larger than before, and this will cause that region to grow significantly more than the classical evolution would have suggested. It is notoriously hard to make predictions for observables under these circumstances (see e.g. [192, 193] and references therein), and this provides further motivation for trying to understand such large quantum fluctuations in more detail.

In this work we will undertake a first step in the direction of understanding inflationary fluctuations in semi-classical gravity, where the background is quantised alongside the fluctuations. We achieve this by working with the path integral formulation of gravity and, more specifically, with the Lorentzian path integral [26, 175]. Moreover, we will make use of an exactly solvable minisuperspace model in which gravity is coupled to a scalar field with a specific inflationary potential [179]. The fact that we are working in minisuperspace, and that we consequently only consider homogeneous fluctuations of the fields, is a restriction that we hope to improve on in future work. However, on super-Hubble scales such an approximation should be rather accurate by simple virtue of causality (cf. also the stochastic picture of super-Hubble fluctuations [43]).

Our goal then is to describe homogeneous inflationary transitions, both small and large, in a fully quantum manner. The framework that we employ allows us to see how the fields evolve "during" a quantum transition, and we will see how the transition amplitude depends not only on the change in the scalar field, but also (though to a lesser extent) on the change in the scale factor. The key feature of our calculation is the use of Robin boundary conditions. This allows us to follow the semiclassical evolution of a universe which has a large enough initial size and is initially inflating. In order for these requirements to be compatible with Heisenberg's uncertainty principle, the initial size and velocity are specified only with some

uncertainty. This is implemented by the Robin condition which is in fact equivalent to an initial coherent state. A general feature that we observe is that the transition amplitude is governed by contributions from two saddle points when the uncertainty in the initial value of the scalar field is small, but with large uncertainty in the inflaton velocity. In this case a description in terms of QFT in curved spacetime in fact breaks down, as two separate backgrounds contribute significantly. However, as soon as the uncertainty in the field value is increased to the expected level ($H/(2\pi)$) while the uncertainty in the field momentum is correspondingly reduced, we generically see that a so-called Stokes phenomenon happens: this is a topological change in the (steepest descent) flow lines, beyond which only a single saddle point remains relevant to the path integral, and where consequently the approximation in terms of QFT in curved spacetime is vindicated. However, in the flattest region of the potential even this is not quite enough, and some additional uncertainty in the size of the universe is required in order to obtain consistent results.

The plan of this chapter (based on [7]) is as follows: We will test the model presented in section 8.2.2 by applying it to boundary conditions that correspond to a scalar field classically rolling down an inflationary potential in section 8.3.1. This example turns out to be non-trivial already, in that it demonstrates the need for, and the use of, an appropriate initial state. Equipped with these realisations we then explore transitions during which the scalar field evolves up the potential, in section 8.3.2. A further constraint on the validity of our calculations is analysed in section 8.3.3. We conclude with a discussion of our results in section 8.4.

One motivation for the present study is to verify the intuitions from QFT in curved spacetime (briefly summarized in section 3.1.4): does quantum cosmology, where the scale factor of the universe is also quantised, support the view that the scalar field fluctuations evolve in a fixed background spacetime. Does this picture become better or worse as the potential becomes flatter? Is there a qualitative difference between the eternal and non-eternal regimes?

We will be interested in inflationary evolution, in two distinct cases: first, to set up our calculation and to check its validity, we will investigate the description of purely rolling down the potential. Afterwards, we will consider the case where the universe inflates, and then we will demand that the scalar field jump up the potential.

Before continuing, we should add a note about the potential we are using, namely $V(\phi) = \alpha \cosh\left(\sqrt{\frac{2}{3}}\phi\right)$. In Fig. 62 we have plotted the flatness of the potential (more specifically, we

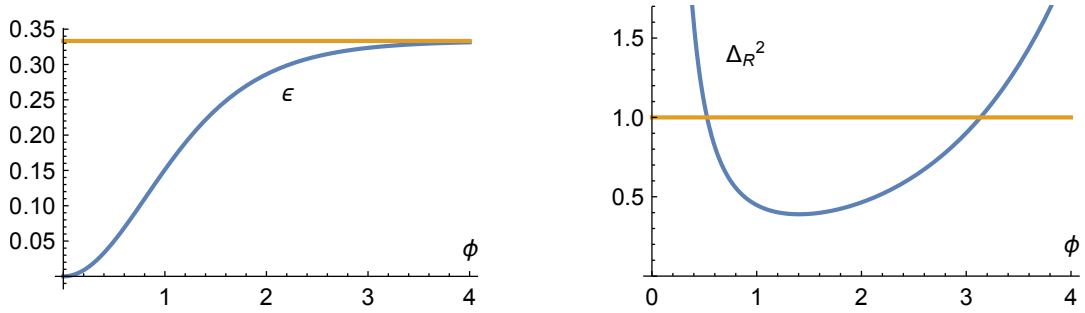

Figure 62: These plots show the flatness $V_{,\phi}^2/(2V^2)$ (left panel) and the variance of the curvature perturbation (right panel) for our potential (8.29) with $\alpha = 1/10$. Slow-roll is achieved only for small values of ϕ, and for small ϕ we are also in the conjectured regime of eternal inflation. There is a second regime of large variance at larger values of $\phi \gtrapprox 3$, but here the potential quickly exceeds the Planck energy density, so that we will ignore this region in the present work. The yellow line on the left indicates the asymptotic value of ϵ for large ϕ. On the right the yellow line separates the regimes where eternal inflation is expected from those where it is not.

have plotted $V_{,\phi}^2/(2V^2)$ which in the slow-roll limit coincides with ϵ) as well as the variance of the curvature perturbation, for $\alpha = 1/10$. Here we can see that inflationary solutions can be achieved throughout, but slow roll is only applicable for very small $\phi \lessapprox 0.2$. Meanwhile the variance becomes large both for small field values $\phi \lessapprox 0.5$ and for very large values $\phi \gtrapprox 3$, although these specific numbers will change for other choices of α.

8.3.1 Inflation - Rolling Down the Potential

Now that we have set up our model, we can evaluate transition amplitudes with various boundary conditions. In fact, in the present chapter we will only look at homogeneous configurations. This is because on the one hand, this restriction brings about a significant technical simplification, and on the other hand it is suggested as a reasonable approximation (in a suitably sized patch of the universe) by the calculations of stochastic inflation, as discussed in the introduction. In order to test our formalism, we will start with a situation in which the universe is expanding while the scalar field is rolling down the potential, i.e. we start with a situation in which we expect there to exist a classical inflationary solution. Thus at first we will pick Dirichlet boundary conditions with

$$a_1 > a_0\,, \qquad \phi_1 < \phi_0\,, \tag{8.39}$$

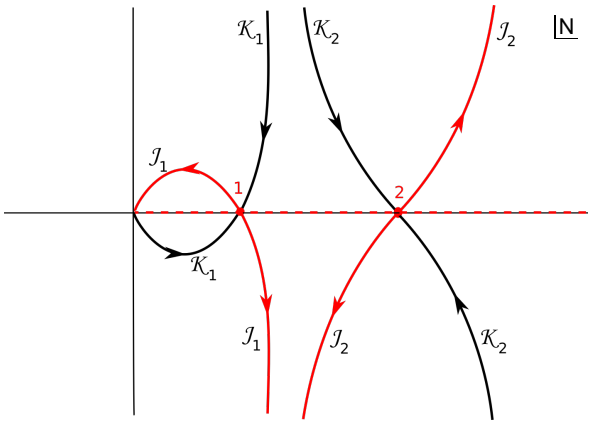

Figure 63: The figure shows a typical example of the saddle points and the flow lines in the complex N plane. The $\mathcal{J}_s/\mathcal{K}_s$ lines are the steepest descent/ascent paths associated with the saddle point s, where arrows indicate downwards flow. The integral along the positive real N line (dashed line) is equivalent to the integral along the path $\mathcal{J}_1 + \mathcal{J}_2$ (full red line). Both saddle points are relevant to the path integral.

where we will stick to the $\phi \geq 0$ side of the potential, and we will assume that the scale factors are larger than the de Sitter radius implied by the potential, $a_{0,1} > \sqrt{3/V(\phi_{0,1})}$. For boundary conditions such as these, the action (8.35) admits four real saddle points, two at positive values of the lapse function, and two at negative values, as given by Eq. (8.37). The two saddle points at positive N are trivially relevant to our path integral, since they lie on the original integration contour – see Fig. 63 for an illustration. The figure also shows the associated paths of steepest descent, and the original integration contour along $\mathbb{R}^+$ can indeed be deformed into the sum of these two steepest descent contours. Superficially, it may be surprising that there are *two* relevant saddle points because we expect only the inflationary solution, but upon analysing the saddle point geometries it becomes clear what is happening.

The first solution, for smaller N, corresponds to an inflationary universe (an example of which is given in Fig. 64). The second solution, the one for larger N, corresponds to a bouncing universe (see Fig. 65). Note that due to the blue-shifting that occurs during contraction, the scalar field can initially roll up the potential, and then roll down again during the expanding phase. From these geometrical properties it also becomes clear why there are two solutions: the path integral simply finds all solutions corresponding to the given boundary conditions. It does not know about the prior evolution of the universe and hence picks out solutions consistent both with initial expansion and contraction. Note that a classical bouncing solution exists because we took the spatial sections of the metric to be

closed, and hence the solution can be thought of as being a deformation of the de Sitter hyperboloid with the waist sitting in between the initial and final hypersurfaces. We should emphasise that in this situation, where two (real) saddle points contribute, an approximation in terms fo QFT in curved spacetime does *not* hold, since we are in the presence of *two* relevant background spacetimes (cf. the analogous discussion regarding pure de Sitter space in [194]).

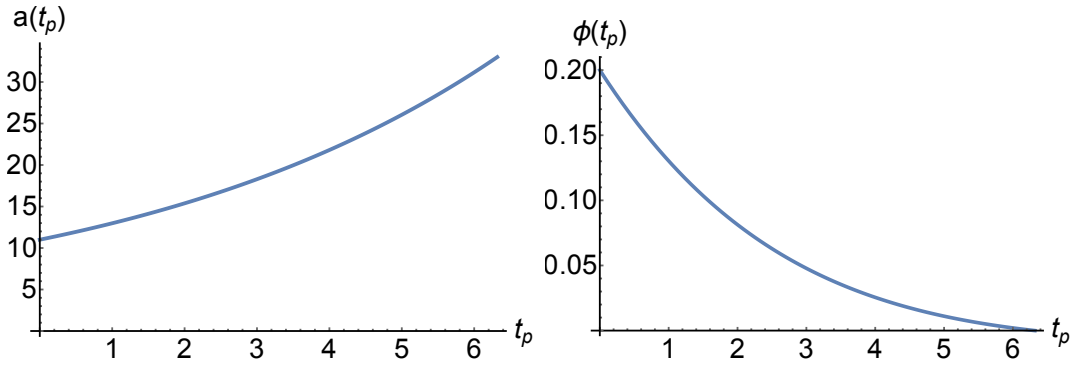

Figure 64: A typical example of the geometry at the saddle point N_1. In particular, here we have $\phi_0 = 2/10$, $\phi_1 = 0$, $a_0 = 11$, and $a_1 = 33$ corresponding to 1 e-fold of inflation and, as expected, we find inflationary behaviour of the scale factor and scalar field.

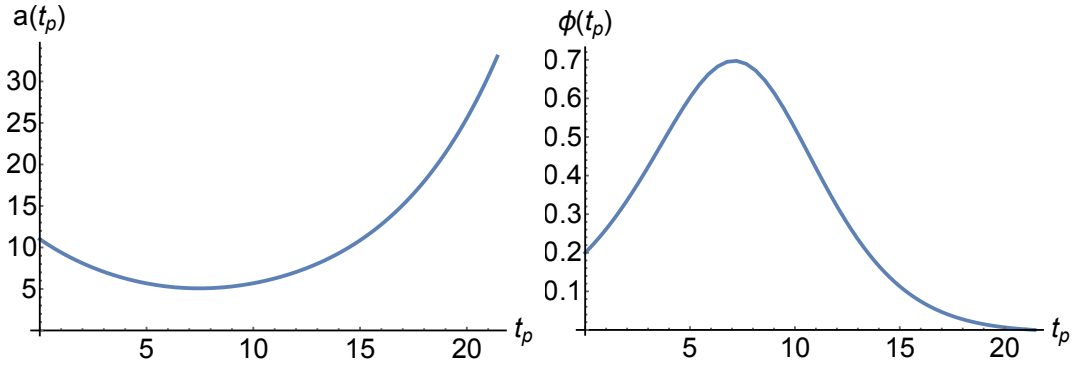

Figure 65: A typical example of the geometry of the saddle point N_2. In particular, here we have $\phi_0 = 2/10$, $\phi_1 = 1/10$, $a_0 = 11$, and $a_1 = 33$ corresponding to bouncing behaviour of the scale factor and scalar field.

If we would like to single out the purely expanding inflationary solution we have to impose that the universe was already expanding with the scalar field rolling down the potential before we consider the transition computed through the path integral. In other words we need to include information not only about the initial values of the fields but also about their initial

velocities. So far we have calculated the propagator with Dirichlet boundary conditions

$$G[x_1, y_1; x_0, y_0] = \int_{0^+}^{\infty} dN e^{iS(x_0,x_1,y_0,y_1,N)/\hbar} \,. \tag{8.40}$$

In this description we have complete certainty of the initial and final values of x and y or correspondingly of a and ϕ. On the other hand, the uncertainty principle implies that we have no knowledge of the initial and final velocities.

We would now like to spread the uncertainty between positions and momenta imposing initial conditions where neither the value of the fields nor their conjugate momenta are specified but rather a linear combination of the two:

$$c_1 x(0) + c_2 P_x(0) = c_3 \,, \tag{8.41}$$

$$c_4 y(0) + c_5 P_y(0) = c_6 \,. \tag{8.42}$$

These are initial conditions of Robin type which require boundary terms in the action different from the Gibbons-Hawking-York one. To this effect, we will augment the action by additional boundary terms [194, 178],

$$S_R = S + p_x x_0 + p_y y_0 + \frac{i\hbar}{4\sigma_x^2}(x_0 - x_i)^2 + \frac{i\hbar}{4\sigma_y^2}(y_0 - y_i)^2 \,, \tag{8.43}$$

where p_x, p_y, σ_x and σ_y are constants. The variation of the action now reads

$$\begin{aligned}\delta S_R = &\int_0^1 N \left[\frac{3}{2N^2}\left(x''(t)\delta x - y''(t)\delta y\right) - \alpha \delta x\right] dt \\ &- \frac{3}{2N} x'(t)\delta x\Big|_0^1 + \frac{3}{2N} y'(t)\delta y\Big|_0^1 + \left(p_x + \frac{i\hbar}{2\sigma_x^2}(x_0 - x_i)\right)\delta x_0 + \left(p_y + \frac{i\hbar}{2\sigma_y^2}(y_0 - y_i)\right)\delta y_0 \,.\end{aligned} \tag{8.44}$$

Substituting the definitions of the momenta $P_x = -\frac{3}{2N}x'(t)$ and $P_y = \frac{3}{2N}y'(t)$, the variational principle is satisfied if

$$x_0 - \frac{2\sigma_x^2}{i\hbar} P_x(0) = x_i - \frac{2\sigma_x^2}{i\hbar} p_x \,, \tag{8.45}$$

$$y_0 - \frac{2\sigma_y^2}{i\hbar} P_y(0) = y_i - \frac{2\sigma_y^2}{i\hbar} p_y \tag{8.46}$$

at the initial boundary and if $x(1) = x_1, y(1) = y_1$ at the final boundary. Hence, comparing to the conditions (8.42), the action S_R defines a mixed boundary value problem with a Dirichlet condition at $t = 1$ and a Robin one at $t = 0$. The Robin condition interpolates between Dirichlet (where the positions are known exactly) and Neumann (where the momenta are known exactly) as the parameters σ_x and σ_y are changed. For $\sigma_x, \sigma_y \to 0$ the boundary condition reduces to Dirichlet while for $\sigma_x, \sigma_y \to \infty$ it reduces to Neumann.

In the following we will evaluate the path integral

$$\int dN \int \delta x \int \delta y \, e^{iS_R/\hbar} \tag{8.47}$$

with the mixed boundary conditions defined by S_R for various values of σ_x and σ_y and explore the consequences in terms of the structure of the flow lines. Notice that the propagator (8.47) can be interpreted as a convolution with an initial state

$$G[x_1, y_1; \psi_0] = \int \int G[x_1, y_1; x_0, y_0] \psi_0(x_0, y_0) dx_0 dy_0 \tag{8.48}$$

where $G[x_1, y_1; x_0, y_0]$ is the propagator evaluated with Dirichlet boundary conditions and the initial wave function reads

$$\psi_0(x_0, y_0) = e^{\frac{i}{\hbar}(p_x x_0 + p_y y_0) - \frac{(x_0 - x_i)^2}{4\sigma_x^2} - \frac{(y_0 - y_i)^2}{4\sigma_y^2}} \,. \tag{8.49}$$

The functional form of this initial state is that of a coherent, Gaussian state, which allows us to express our knowledge of the initial uncertainty in the field values and their momenta[14]. By construction the initial positions are peaked around the values x_i,y_i, with a Gaussian spread around them. In the limit where $\sigma_x = \sigma_y = 0$ the initial positions simply become x_i and y_i by construction. We are then back to the position representation which we were (implicitly) using up to now. Performing the Gaussian integrals over x_0 and y_0 gives us the saddle point solutions

$$\bar{x}_0 = \frac{\hbar N x_i - \alpha i N^2 \sigma_x^2 + 2iN p_x \sigma_x^2 + 3x_1 i \sigma_x^2}{\hbar N + 3i\sigma_x^2} \,, \tag{8.50}$$

$$\bar{y}_0 = \frac{\hbar N y_i + 2iN p_y \sigma_y^2 - 3y_1 i \sigma_y^2}{\hbar N - 3i\sigma_y^2} \,. \tag{8.51}$$

For small spreads σ, we have $\bar{x}_0 \approx x_i, \bar{y}_0 \approx y_i$, while for very large σ we obtain

$$\bar{x}_0 \approx x_1 - \frac{\alpha}{3} N^2 + \frac{2N}{3} p_x \,, \qquad \bar{y}_0 \approx y_1 - \frac{2N}{3} p_y \qquad (\sigma_{x,y} \gg 1) \,. \tag{8.52}$$

Thus at large spreads x_i, y_i disappear from the formula, which is an indication that the position is less well known. In fact at large σ the momentum is determined with increasing precision. To show this in more detail we focus on one of the momenta and variables (p_x and x respectively) but the result holds for both. Hamilton's equations give

$$P_x(t) = -\frac{3}{2N} x'(t) = -N\alpha t - \frac{3}{2N} \left(x_1 - x_0 - \frac{1}{3} N^2 \alpha \right) \tag{8.53}$$

[14] A detailed discussion of the use of initial and final (off-shell) states will be published in upcoming work by Angelika Fertig, Job Feldbrugge, Laura Sberna and Neil Turok [**?**].

where the last line was obtained by plugging in the solution of the equations of motion for x. Thus, at the saddle points the initial momentum simply reduces to

$$P_x(0) = -\frac{3}{2N}\left(x_1 - x_0 - \frac{1}{3}N^2\alpha\right), \tag{8.54}$$

which agrees with Eq. (8.52). We may also find the sub-leading terms by making use of Eq. (8.50), plugging it into the general expression for the momentum and expanding for large σ_x, to obtain

$$P_x(0) = p_x + \frac{i\hbar}{\sigma_x^2}\frac{1}{6}\left(3x_1 - 3x_i + 2Np_x - \alpha N^2\right) + O\left(\frac{1}{\sigma_x^4}\right), \tag{8.55}$$

which confirms that in the large σ_x limit we reach the pure momentum representation.

Let us now return to our inflationary example. We choose initial momenta p_x and p_y such that a is expanding and ϕ is rolling down the potential. The values of p_x and p_y are fixed such that they correspond to the classical inflationary solution that links our initial and final boundary conditions. After performing the integrals over x_0 and y_0, we are again left with an integral over the lapse function N,

$$G[x_1, y_1; \psi_0] \approx \int_{0^+}^{\infty} dN e^{i\tilde{S}(x_i,x_1,y_i,y_1,p_x,p_y,\sigma_x,\sigma_y,N)/\hbar} \tag{8.56}$$

This new action results from having replaced x_0 and y_0 with their saddle point values $\bar{x}_0, \bar{y}_0$ in Eq. (8.35) and including the contributions from the initial state. More explicitly, we have

$$\begin{aligned}
\frac{i}{\hbar}\tilde{S} &= \frac{i}{\hbar}S_0 + \frac{i}{\hbar}(p_x x_0 + p_y y_0) - \frac{1}{4\sigma_x^2}(x_0 - x_i)^2 - \frac{1}{4\sigma_y^2}(y_0 - y_i)^2 \\
&= \frac{i}{\hbar}\left[\frac{\alpha^2}{36}N^3 + N\left(3 - \frac{\hbar\alpha N(x_i + x_1) - \alpha^2 i N^2\sigma_x^2 + 2i\alpha N p_x\sigma_x^2 + 6\alpha x_1 i\sigma_x^2}{2(\hbar N + 3i\sigma_x^2)}\right)\right. \\
&\qquad \left. + \frac{3N}{4}\left(\frac{\hbar(y_i - y_1) + 2ip_y\sigma_y^2}{\hbar N - 3i\sigma_y^2}\right)^2 - \frac{3N}{4}\left(\frac{\hbar(x_i - x_0) - \alpha i N\sigma_x^2 + 2ip_x\sigma_x^2}{\hbar N + 3i\sigma_x^2}\right)^2\right] \\
&\quad + \frac{i}{\hbar}(p_x x_i + p_y y_i) + \frac{\alpha N^2\sigma_x^2 p_x - 2Np_x^2\sigma_x^2 - 3x_1 p_x\sigma_x^2}{\hbar(\hbar N + 3i\sigma_x^2)} + \frac{-2Np_y^2\sigma_y^2 + 3y_1\sigma_y^2 p_y}{\hbar(\hbar N - 3i\sigma_y^2)} \\
&\quad + \left(\frac{-\alpha N^2 + 2Np_x + 3(x_1 - x_i)}{4(\hbar N + 3i\sigma_x^2)}\right)^2 + \left(\frac{2Np_y - 3(y_1 - y_i)}{4(\hbar N - 3i\sigma_y^2)}\right)^2
\end{aligned} \tag{8.57}$$

The replacements of x_0 and y_0 have as a consequence that the dependence of the action on the lapse function N has become more complicated. But once again we can solve this integral using Picard-Lefschetz theory. Let us start from small values of σ_x and σ_y and investigate what happens as the spreads $\sigma_{x,y}$ are increased, see Fig. 66. At zero spread, we are in the pure position representation, with two relevant saddle points (upper left panel in the figure). But as soon as the spreads are turned on, the situation changes: we now have six complex

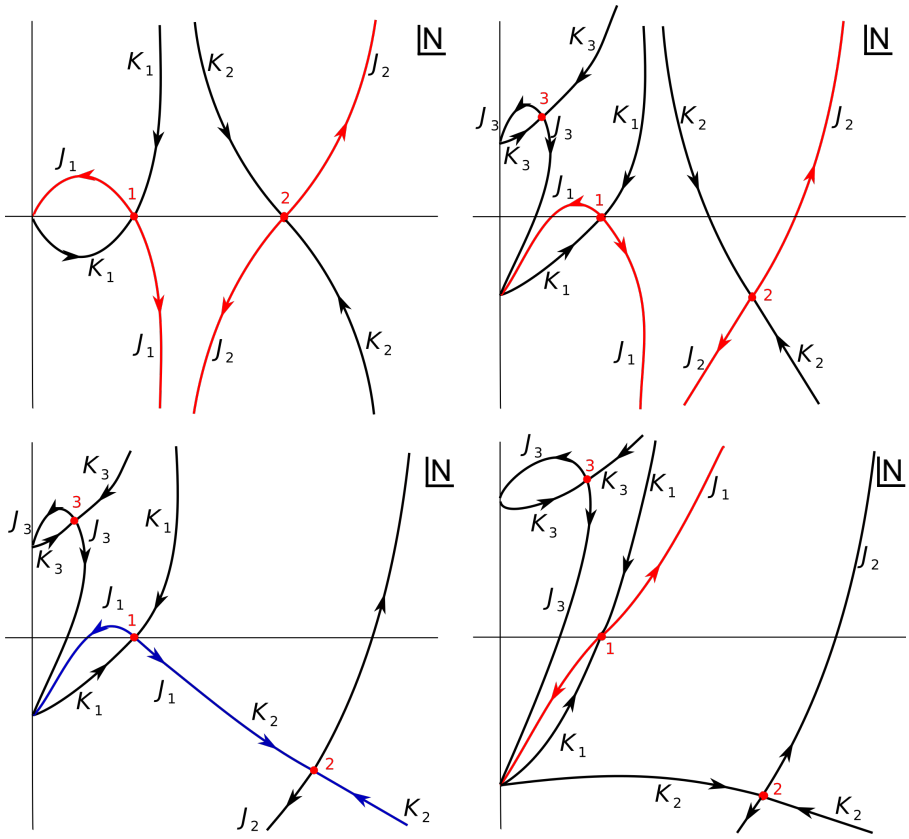

Figure 66: The structure of the flow lines is shown as a function of the uncertainty σ_ϕ for inflationary boundary conditions, with $\sigma_{x,y}$ determined via Eqs. (8.66), (8.67). In order to draw these graphs we have used the boundary conditions $a_0 = 100, \phi_0 = 1/10, a_1 = 200, \phi_1 = 1/100$ and $\alpha = 1/10$, with the corresponding momenta being given by $(\dot{a}(t_p), \dot{\phi}(t_p)) = (1.7953, -0.0820864)$. The numerically determined flow lines would have been difficult to put on a legible graph due to the large distances between saddle points, hence we have re-drawn these graphs to show the qualitative behaviour of the flow lines. Only the saddle points with $Re(N_i) > 0$ are considered, being the only ones relevant for the flow analysis. Top left panel: For $\sigma_\phi = 0$ both the expanding and the bouncing solutions are relevant to the path integral (corresponding to the saddle points N_1 and N_2). Top right panel: For non-zero σ a new saddle point appears, the saddle point N_2 moves off the real line while N_1 maintains its original position (here $\sigma_\phi = 0.0100$). For small enough σ the original integration contour is deformed to the Lefschetz thimble $\mathcal{J}_1 + \mathcal{J}_2$. Bottom left panel: For a critical value of $\sigma = \sigma_c$ a Stokes phenomenon happens (here $\sigma_c \approx 0.0154$). The steepest descent path associated to N_1 ($\mathcal{J}_1$) coincides now with the steepest ascent through N_2 ($\mathcal{J}_2$). This is the Stokes line, the blue line in the figure. Bottom right panel: For $\sigma > \sigma_c$ the bouncing solution (N_2) no longer contributes to the path integral and only the inflating one (N_1) survives (here $\sigma_\phi = 0.0200$).

saddle points (three with positive real part, and three with negative real part) out of which two are relevant to the Lorentzian path integral, see the upper right panel in Fig. 66. As we increase our certainty about the values of the initial momenta, the saddle points and flow lines change their location in the complex plane. Eventually a drastic transition occurs where the topology of the flow lines changes. This, so-called Stokes phenomenon, happens when a flow line connects two saddle points, for example in this case when

$$Im(\tilde{S}(N_1)) = Im(\tilde{S}(N_2)) \tag{8.58}$$

for two distinct saddle points N_1 and N_2. After this transition only one saddle point (N_1) remains relevant to the path integral, while the second one (N_2) has become irrelevant. The saddle point N_1, the only relevant critical point after the Stokes phenomenon, does not move at all as a function of σ_x and σ_y. Furthermore the behaviour of the scale factor and scalar field at this location is inflationary as desired (see Fig. 64), while the bouncing solution (Fig. 65) has become irrelevant. This is entirely consistent with our interpretation of the initial state: as we increase our knowledge of the initial momentum (chosen to represent an expanding universe), only the expanding solution survives. Thus we see that the path integral gives sensible results for transitions in which the scale factor expands and the scalar field rolls down the potential. At the same time, we can appreciate the importance of the Robin initial condition in determining the outcome of future evolution.

8.3.2 Jumping Up the Potential

Inflation may be able to sustain itself indefinitely if the scalar field can jump up the potential, thus inducing a phase of enhanced accelerated expansion. In order to understand the true consequences of eternal inflation, it seems likely that a more fully quantum understanding of such transitions, and the associated issues of measures, must be developed. Here we take a step in that direction, by investigating the semi-classical geometries of such up-jumps. Thus we will now consider boundary conditions of the form

$$a_1 > a_0 > \sqrt{\frac{3}{V(\phi_0)}}\,, \qquad\qquad \phi_1 > \phi_0\,. \tag{8.59}$$

Again we must find the relevant saddle points, so that we can look at their geometries. Just as in the previous case in the Dirichlet limit $\sigma_{x,y} = 0$ we have four saddle points out of which two will be relevant for the path integral (the other two being the time reverses of the relevant two).

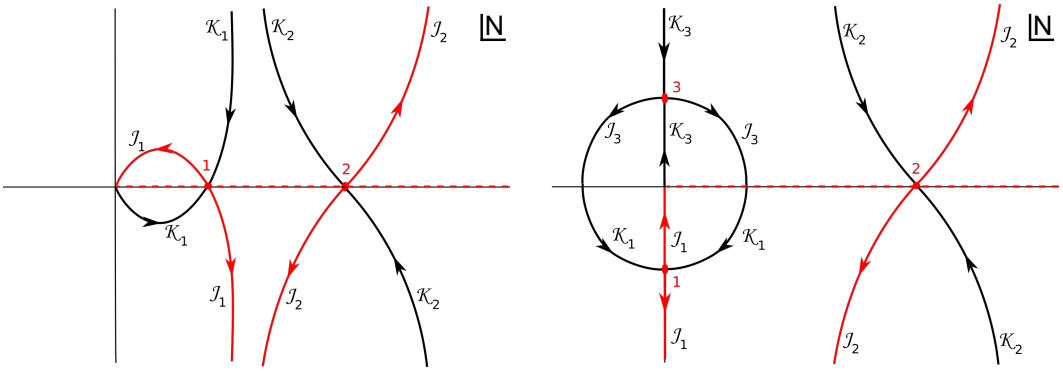

Figure 67: The figures show the structure of the steepest ascent and descent path ($\mathcal{J}_s$ and $\mathcal{K}_s$) for $\sigma_{x,y} = 0$ and $\phi_1 > \phi_0$. The left (case A) and the right (case B) panels show the only two inequivalent qualitative structures allowed for by up-jumping boundary conditions. In both cases the action has 4 critical points but only those with $Re(N_s) \geq 0$ are plotted. The original integration contour (dashed red line) can be deformed smoothly to the Lefschetz thimble $\mathcal{J}_1 + \mathcal{J}_2$ so that two saddle points contribute to the path integral. The geometries of these saddle points are plotted in Figs. 68 and 69 for case B.

In fact, for different values of the initial conditions the saddle point N_1 can be either purely real or purely imaginary: we call these two possibilities case A and case B respectively. Case A is obtained for $a_1 \geq a_0 e^{\sqrt{6}(\phi_1 - \phi_0)}$, otherwise we have case B. The second relevant saddle point (N_2) always turns out to be real. Fig. 67 shows the flow lines for the two possible inequivalent cases, while Figs. 68 and 69 show the associated geometries for case B.

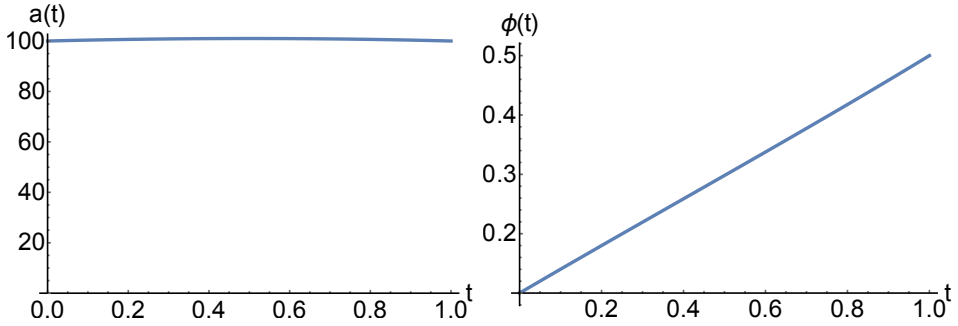

Figure 68: Geometry of saddle point number 1 in the right panel of Fig. 67. Plotted here are the scale factor and scalar field with respect to coordinate time where we have chosen $\alpha = 1/10$, $\phi_i = 1/10$, $\phi_1 = 1/2$, $a_0 = 100$, $a_1 = 100$ and $\sigma_\phi = 0$. The saddle point is purely imaginary, and consequently the scale factor is Euclidean here.

Note that the field values for all saddle points are strictly real, although for case B the saddle point N_1 is at a purely imaginary value, implying that the geometry is in fact

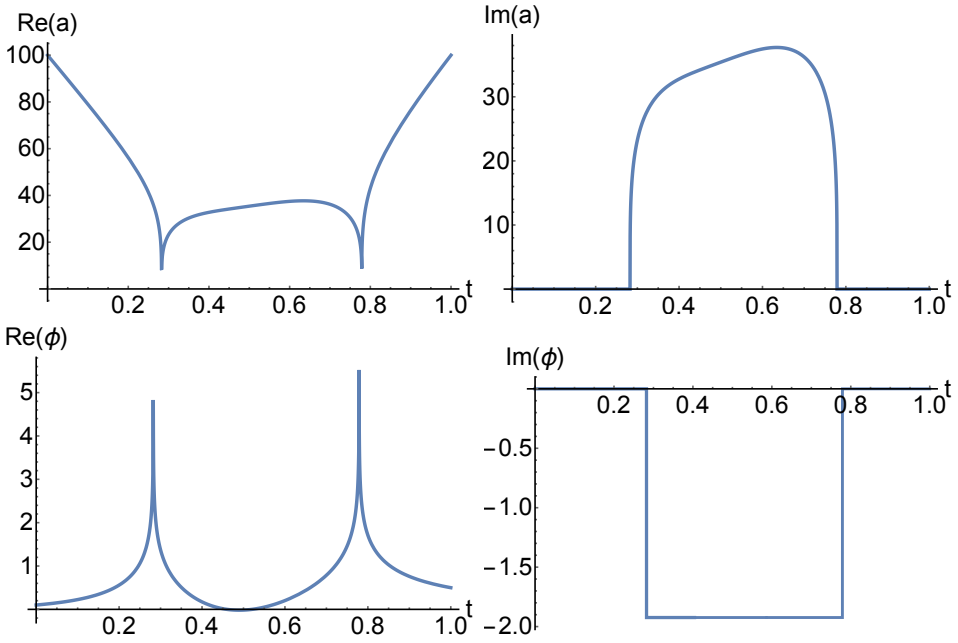

Figure 69: Geometry of saddle point number 2 in the right panel of Fig. 67. The scalar field passes through zero twice, and at these singularities the scalar field blows up. Moreover, the scalar field starts out rolling up the hill, so that this geometry could only be relevant for a physical situation in which the scalar field would already have a large initial velocity up the hill, while we are interested in a prior state with the scalar slowly rolling down the potential.

Euclidean. This also means that the action at this saddle point is imaginary, and consequently the contribution to the path integral will be significantly suppressed compared to the saddle point N_2. This second saddle point also has some peculiarities: it contains two singularities where the scale factor $a(t)$ passes through zero and where the scalar field blows up. On top of this difficulty, the scalar field starts out by rolling up the potential. Thus such a geometry may not be smoothly linked to a prior phase of inflation where the field is rolling down the potential. We can in fact show that no saddle point exists for which the scalar field is initially rolling down, but where it ends up higher in the potential. To see this consider the physical time derivatives of the scalar field and scale factor,

$$\dot{\phi}(t_p) = \frac{\phi'(t)a(t)}{N} = \sqrt{\frac{3}{2}}\frac{x(t)y'(t) - y(t)x'(t)}{N\left(x(t)^2 - y(t)^2\right)^{3/4}}\,, \tag{8.60}$$

$$\dot{a}(t_p) = \frac{a'(t)a(t)}{N} = \frac{x(t)x'(t) - y(t)y'(t)}{2N\left(x(t)^2 - y(t)^2\right)^{1/2}}\,, \tag{8.61}$$

which at $t = 0$ reduce to

$$\begin{aligned}\dot{\phi}_0 &= \frac{\alpha N^2 y_0 + 3x_0 y_1 - 3x_1 y_0}{\sqrt{6}N\left(x_0^2 - y_0^2\right)^{3/4}} \\ &= \frac{1}{\sqrt{6}Na_0}\left(N^2\alpha\sinh\left(\sqrt{\frac{2}{3}}\phi_0\right) + 3a_1^2\sinh\left(\sqrt{\frac{2}{3}}(\phi_1 - \phi_0)\right)\right),\end{aligned} \tag{8.62}$$

$$\begin{aligned}\dot{a}_0 &= \frac{x_0(3(x_1 - x_0) - \alpha N^2) - 3y_0(y_1 - y_0)}{6N((x_0 - y_0)(x_0 + y_0))^{1/2}} \\ &= \frac{1}{6N}\left(3a_1^2\cosh\left(\sqrt{\frac{2}{3}}(\phi_1 - \phi_0)\right) - 3a_0^2 - \alpha N^2\cosh\left(\sqrt{\frac{2}{3}}\phi_0\right)\right).\end{aligned} \tag{8.63}$$

Since we assume a transition up the potential, $\phi_1 - \phi_0 > 0$ and this makes the second term in (8.62) positive. Thus $\dot{\phi}_0$ can never be real and positive for the considered boundary conditions. The reason for this stumbling block is simply that we are working in the pure position representation here, where we have not included any information about the momenta of the fields. But we are actually interested in the situation in which we have a prior inflationary state, with the scale factor growing and the inflaton rolling down the potential. Once we include this information, we will see that much more sensible results are obtained.

Thus we must repeat the same procedure as in the last section, i.e. we introduce Robin boundary conditions or, equivalently, convolve the propagator with an initial wavefunction as in Eq. (8.49), yielding the effective action (8.57), where the momenta are chosen to correspond to an inflating universe. Let us be more specific about which form of the spreads $\sigma_{x,y}$ we will consider. From the definitions of the variables x, y we have to leading order

$$\sigma_x = 2a_0\cosh\left(\sqrt{\frac{2}{3}}\phi_0\right)\sigma_a + \sqrt{\frac{2}{3}}a_0^2\sinh\left(\sqrt{\frac{2}{3}}\phi_0\right)\sigma_\phi\,, \tag{8.64}$$

$$\sigma_y = 2a_0\sinh\left(\sqrt{\frac{2}{3}}\phi_0\right)\sigma_a + \sqrt{\frac{2}{3}}a_0^2\cosh\left(\sqrt{\frac{2}{3}}\phi_0\right)\sigma_\phi\,. \tag{8.65}$$

While these relations are only accurate for small spreads, we will simply use them as definitions, even when the spread is large. Our discussion in section 3.1.4 indicated that we can expect that for flat potentials the metric changes little, and most of the perturbation is expressed as a change in the scalar field value. This would suggest the choice $\sigma_a = 0$ with the entire spread relegated to ϕ. In this case

$$\sigma_x = \sqrt{\frac{2}{3}}a_0^2\sinh\left(\sqrt{\frac{2}{3}}\phi_0\right)\sigma_\phi\,, \tag{8.66}$$

$$\sigma_y = \sqrt{\frac{2}{3}}a_0^2\cosh\left(\sqrt{\frac{2}{3}}\phi_0\right)\sigma_\phi\,. \tag{8.67}$$

Note that this case corresponds to a specific choice of initial state, a choice that is motivated by the calculations of section 3.1.4. If not specified otherwise, this will be our default choice of initial state. Thus when we quote results in terms of σ_ϕ alone, this should be understood as shorthand for $\sigma_{x,y}$ given by Eqs. (8.66) and (8.67). However, we will also be led to consider other choices, with both σ_a and σ_ϕ turned on.

The evolution of the saddle point locations and their associated flow lines as a function of σ_ϕ is illustrated in Fig. 70. For $\sigma_\phi = 0$, two of the four critical points of the action are relevant to the Lorentzian propagator. As we turn on σ_ϕ, the four saddle points smoothly change their location in the complex N plane and two extra saddle points appear, which however turn out to never give a dominant contribution to the path integral. For a critical value of the uncertainty $\sigma_\phi = \sigma_c$, a Stokes phenomenon happens which changes the topology of the flow lines. The process is shown in Fig. 70 for case A. The final result is entirely analogous for case B, the only difference lying in the fact that in that case the saddle point N_1 travels from the imaginary line to the real line as σ_ϕ increases. After the Stokes phenomenon ($\sigma > \sigma_c$), the only relevant saddle point is N_1 and this saddle point becomes more and more real as σ_ϕ is further increased. The geometry of the relevant saddle point N_1 after the Stokes phenomenon has occurred, i.e. for $\sigma_\phi > \sigma_c$, is shown in Fig. 71. An interesting aspect is that the initial position of the scalar field $\bar{x}_0$ is no longer close to the original initial position x_0, but is significantly larger – in fact it has become larger than the final value x_1 (and ϕ also contains a small imaginary part, which is a reflection of the transition being a quantum transition).

What does this mean? In the Dirichlet formulation of the Feynman propagator we calculate a transition between two fixed geometries and matter content. In that setting it is not possible to continuously link an inflationary evolution with an evolution where the scalar field tunnels up the potential. However, by introducing Robin boundary conditions, thus allowing for a spread in field values and momenta, we do find solutions. Analysing them in more detail, we find that the scalar field *already* starts higher up the potential and then simply rolls down according to an inflationary solution. Thus, instead of choosing a solution that rolls up the potential, the system has picked out a (comparatively unlikely) configuration contained within the initial state in which the inflaton is already higher up in the potential than required, so as to allow a slow-roll solution to the final configuration. In complete analogy, the scale factor starts out at a smaller value and then grows as the scalar field rolls down.

This result can be further quantified by analysing probabilities of the geometry and scalar field undergoing transitions to various values of ϕ_1 and a_1 as depicted in Fig. 72. It is obvious

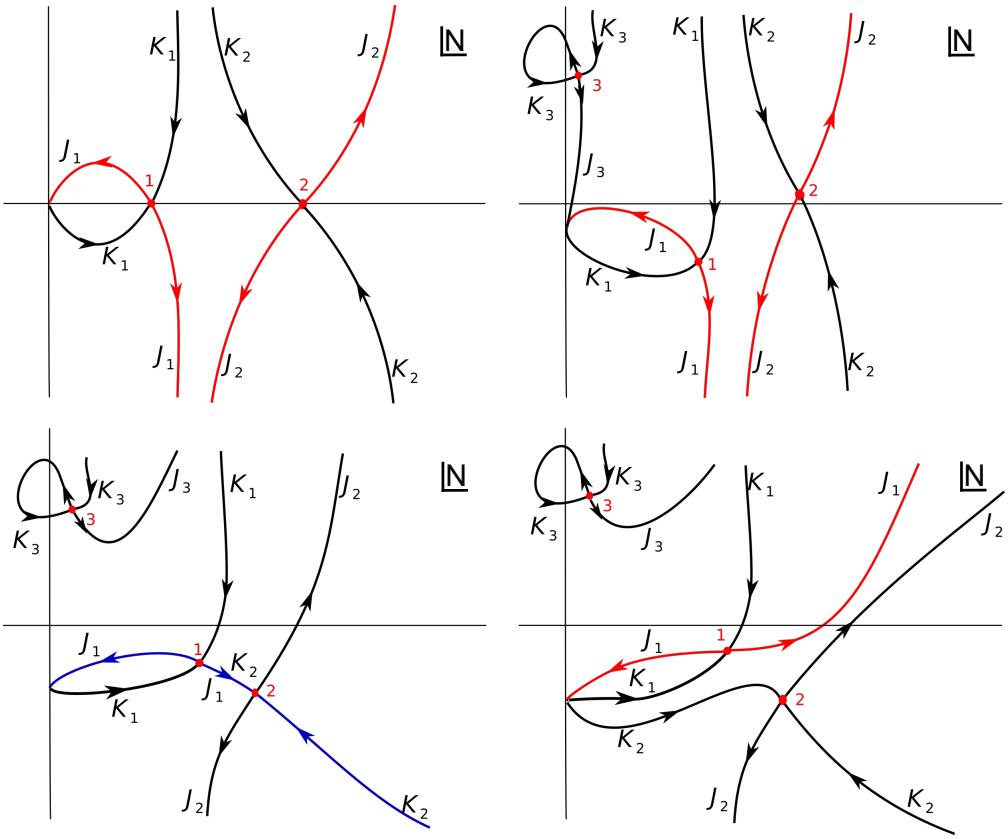

Figure 70: Evolution of the saddle points and their associated flow lines in the complex N plane as σ_ϕ is increased. The original integration contour (positive real line) can be smoothly deformed to the complex Lefschetz thimble (the red line) leaving the value of the path integral unchanged. The Lefschetz thimble runs through one or more saddle points of the action. One of the initially relevant saddle points (N_1) is relevant for all values of σ_ϕ but its position and therefore the geometry associated to it changes. The other saddle point becomes irrelevant after the Stokes phenomenon (the Stokes line is the blue line in the bottom left panel). The third saddle point never contributes to the path integral. In order to draw these graphs, we have used the boundary conditions $a_0 = 100, \phi_0 = 1/10, a_1 = 200, \phi_1 = 1/2$, while the values of the spread for these four plots are respectively $\sigma_\phi = 0, 0.0100, \sigma_c \approx 0.0154, 0.0700$.

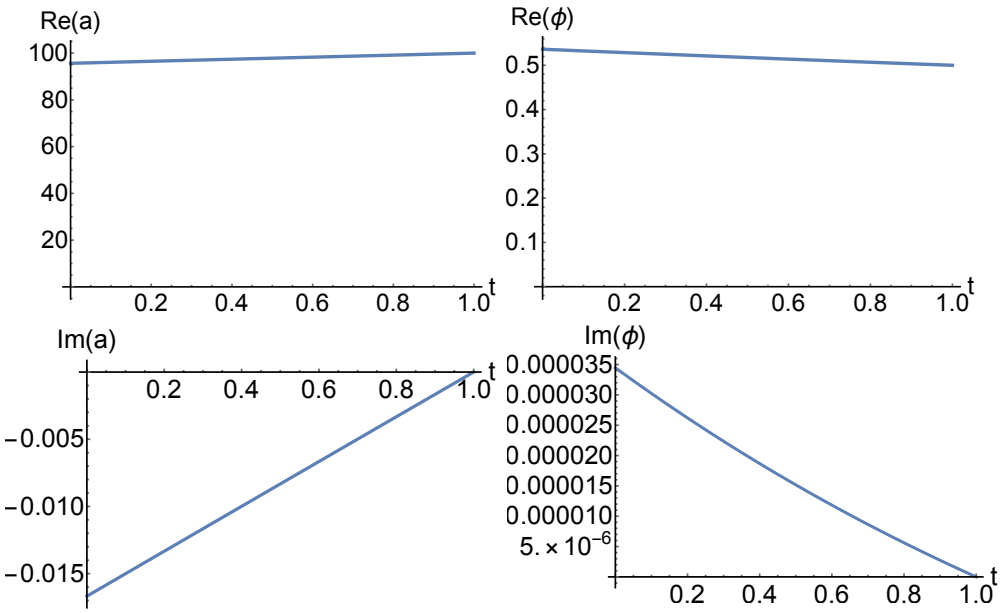

Figure 71: Geometry of the relevant saddle point for $\sigma > \sigma_c$. Plotted here are the real and imaginary parts of the scale factor and scalar field with respect to coordinate time where we have chosen $\alpha = 1/10$, $\phi_0 = 1/10$, $\phi_1 = 1/2$, $a_0 = 100$, $a_1 = 100$ and $\sigma_\phi = 2/100$. The final relevant solution is seen to be a slightly complexified version of an ordinary inflationary solution, with the scale factor expanding and the scalar field rolling *down* the potential, even though our boundary conditions are such that we consider an up-jump from the central value of the inflaton.

that for larger values of a_1 and ϕ_1, transitions become less and less likely. In fact, the most likely transitions occur for a tiny increase in the scale factor, in our example from $a_0 = 100$ to $a_1 \approx 101$. This confirms the expectation from QFT in curved spacetime that the geometry ultimately changes very little when the scalar field jumps up the potential. Here we should note that when we impose a final scale factor value that is equal to or smaller than the initial one, then transitions to certain values of the scalar field are impossible (semi-classically). This is reflected in some of the curves in Fig. 72 having gaps in them. What happens in these cases is that the relevant saddle point moves to the region where $Re(N) < 0$, i.e. these solutions then actually correspond to time-reversed solutions. This is consistent with the fact that the system prefers to choose inflationary, expanding solutions and requiring the final scale factor to be small then clashes with this preference. In line with this observation is the fact that if we look at increasing values of the final scale factor, then the spread is actually reduced due to the inflationary attractor. In fact, the final weighting remains Gaussian to a good approximation, with only the peak value having shifted and the spread shrinking. We

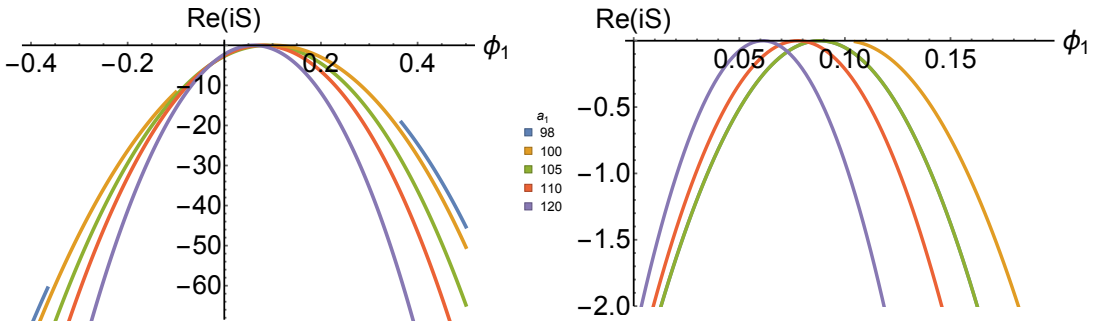

Figure 72: The logarithm of the transition amplitude going from $(a_0, \phi_0) = (100, 1/10)$ to various values of a_1 and ϕ_1. Here the x-axis represents ϕ_1 while the different colours refer to different values of a_1, ranging between 98 and 120. The action was evaluated for a spread of $\sigma_\phi = \frac{H}{2\pi}$. Interestingly, for $a_1 \leq 100$ there are areas where no transition is possible and hence there are gaps in the parabola. This is because the usually relevant saddle point has negative real N for these transitions, and no other saddle point is relevant. In such cases, the transition would be more than exponentially suppressed. The picture on the right is the same as on the left except zoomed in onto the top of the curves. As the final scale factor value a_1 is increased, the peak of the distribution shifts and the spread in ϕ narrows.

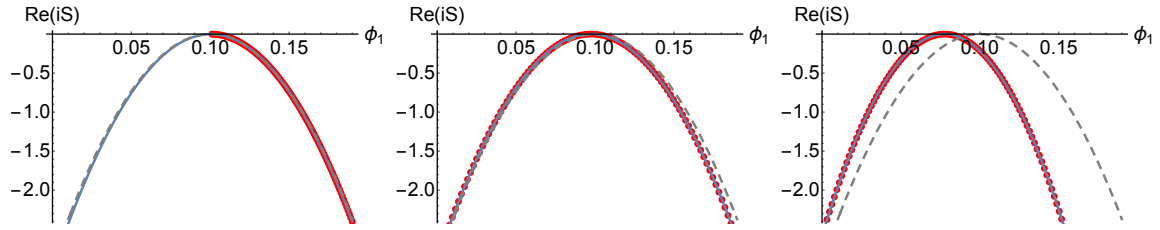

Figure 73: An example of the distribution of fluctuations after the quantum transition in red with a fitted parabola in blue. In all three graphs $\alpha = 1/10$, $\phi_0 = 1/10$, $a_0 = 100$. However $a_1 = 100, 101, 110$ in the left, centre and right graphs respectively. In dashed grey we have plotted the initial spread in $\sigma_\phi = H/(2\pi)$ centred around the classical value ϕ_{top}. From the picture it is clear that the peak of the distribution shifts and the spread in ϕ narrows as we increase the final scale factor – see also Fig. 74 for more details.

can see this more quantitatively in Fig. 73, where we plot the final weighting alongside a fitted parabola with final width Σ_f, defined via

$$Re(i\tilde{S}/\hbar) = h(\phi_1) = h(\phi_{top}) - \frac{(\phi_1 - \phi_{top})}{4\Sigma_f^2} + \cdots , \tag{8.68}$$

where ϕ_{top} denotes that value of ϕ at which the weighting (Morse function h) is maximal for a given final scale factor value a_1. From the figure we can see that the parabola provides an excellent fit. The decrease in the width as the universe expands is plotted in Fig.74.

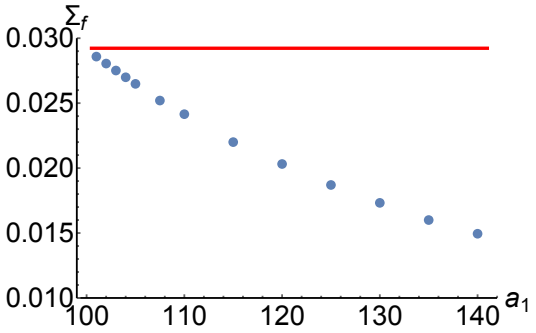

Figure 74: For transitions in which the final scale factor is only slightly larger than the initial one, the weighting for different final configurations is essentially equal to the weighting implied by the initial state. But as the final scale factor value a_1 increases the spread (of the weighting) is reduced as a result of the inflationary attractor. The numerical example shown here is the same one as in Fig.72. The red line is the spread in the inflaton value imposed before the transition occurs.

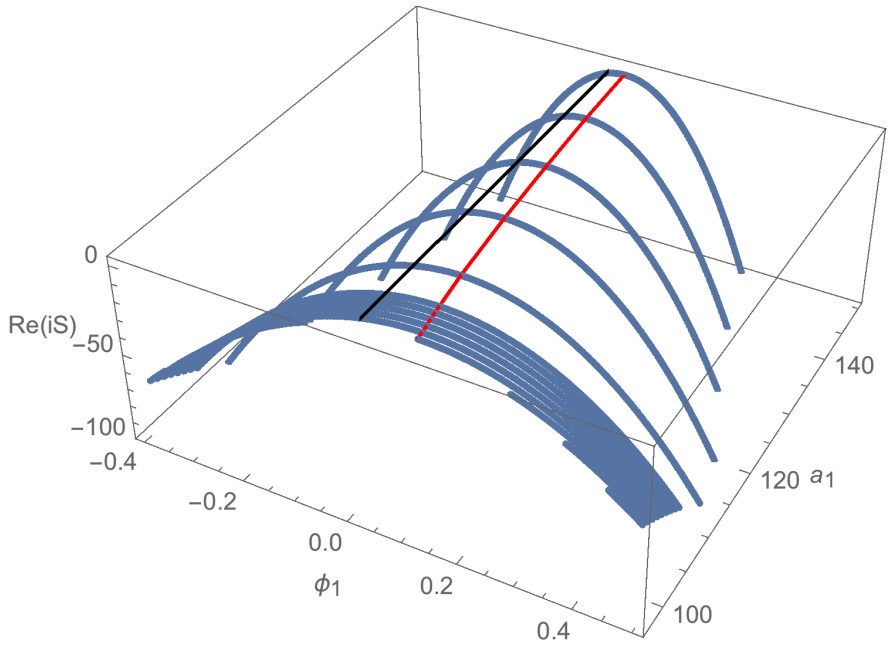

Figure 75: A 3-dimensional version of Fig. 72 illustrating how the peak of the weighting (red line) follows a slow-roll solution down towards the minimum of the potential at $\phi = 0$ (black line), while large excursions of the inflaton away from the classical solution become less and less likely as the universe expands.

All this is nicely visible in a 3-dimensional version of these plots in Fig. 75. Accompanied with this shrinking of the width is a displacement of the peak of the weighting. The 3-dimensional picture shows that the peak slowly approaches $\phi = 0$ as the universe expands –

in other words, the peak of the weighting follows the classical slow-roll trajectory associated with the initial central values of the fields and their momenta that we imposed via the initial state. As the universe expands, the wavefunction narrows around this classical solution, and we attribute this feature to the inflationary attractor. Thus, starting from a fixed initial state and as the universe grows larger, inflaton excursions away from the classical solution become less likely.

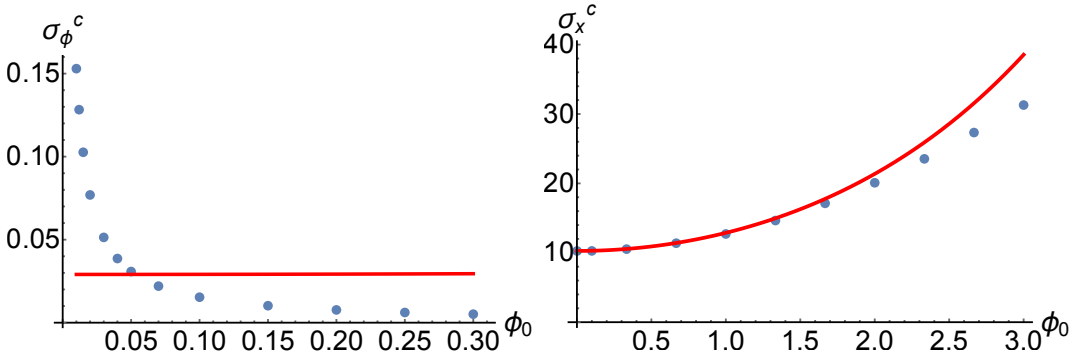

Figure 76: *Left panel:* The blue dots indicate the value of σ_ϕ at which the Stokes phenomenon appears while the value of $H/(2\pi)$ is given by the red line. Here $\alpha = 1/10$ and $a_0 = 100$. The critical value of σ depends only on the initial value ϕ_0 and not on the final values a_1 and ϕ_1. This graph shows that for a sufficiently large initial scalar field value, only one saddle point is relevant at $\sigma = H/(2\pi)$. *Right panel:* The critical spread expressed in terms of the canonical variables. This figure shows the critical value σ_x^c as a function of the initial inflaton value ϕ_0. Near $\phi_0 = 0$ we recover the exact value for de Sitter space given in Eq. (8.69). The red curve shows the expected value if one were to assume only an uncertainty in the initial scale factor, and not in the inflaton value. For larger ϕ_0 we can see that the critical value lies below this curve, implying that for sufficiently large ϕ_0, where the potential is less flat, the uncertainty in the inflaton value can induce an earlier Stokes phenomenon. To calculate the points, we have fixed $a_0 = a_1 = 100$ with varying ϕ_0 and a ϕ_1 that corresponds to the field jumping up the potential. The initial state's momenta were calculated by keeping ϕ_0' fixed, finding the corresponding a_0' via the Friedmann equation and then converting to the momenta in x and y.

An important effect that we saw earlier was that beyond some critical value of the spread a Stokes phenomenon happens and only a single saddle point remains relevant. When this occurs, we automatically obtain a situation in which quantum field theory in curved spacetime is a reasonable approximation, as only a single background geometry is relevant to the path integral. We can now make this discussion more quantitative – see Fig. 76. An important

aspect of this discussion concerns the relationship between the original variables a, ϕ and the canonical variables x, y, expressed via the transformations Eqs. (8.26) - (8.27) and the relations between the spreads (8.64) and (8.65). We argued in section 3.1.4 that the standard calculation in a fixed background suggests that the inflaton should have a significant spread, of order $H/(2\pi)$, with the scale factor being kept essentially fixed. This would amount to setting $\sigma_a = 0$. The left panel in Fig. 76 shows the critical value of σ_ϕ that is required under those circumstances in order to obtain the Stokes phenomenon, as a function of the initial inflaton value ϕ_0. (An important point is that the critical spread does not depend on the final inflaton value ϕ_1.) What the figure shows is that for large enough ϕ_0 the Stokes phenomenon always occurs before the spread is increased to $H/(2\pi)$. Thus, in regions where the potential is not too flat (but including regions where the density perturbations that are generated may be large), the standard intuition is vindicated.

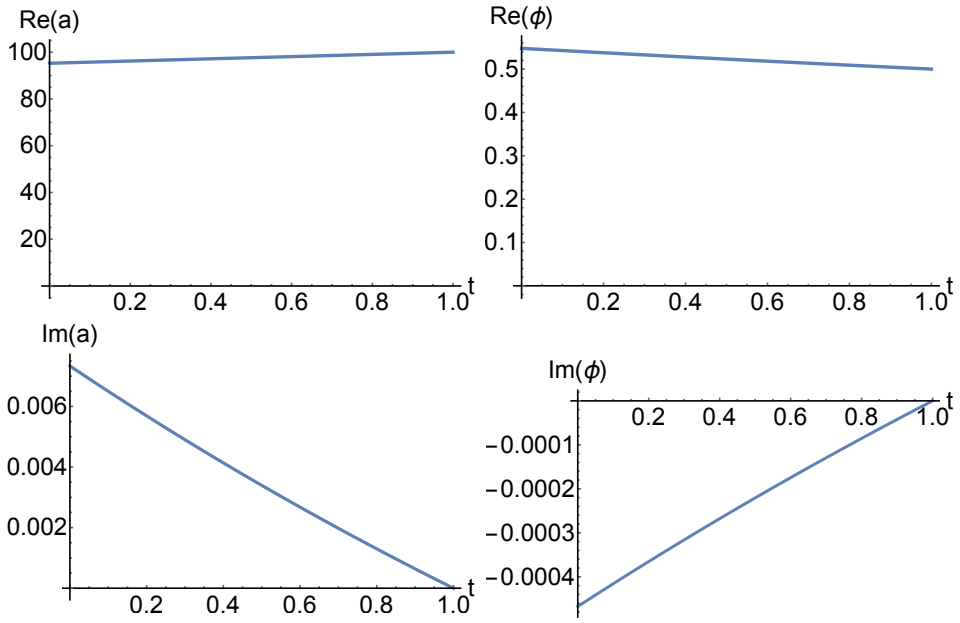

Figure 77: Geometry of the relevant saddle point where the scale factor is kept constant $a_0 = a_1 = 100$ and the scalar field transitions from $\phi_0 = 1/1000$ to $\phi_0 = 1/2$. The initial state's momenta were chosen to be $p_x \approx -54.7$ and $p_y \approx -0.0134$ with uncertainties $\sigma_x = 11$ and $\sigma_y = 100$ which implies that the Stokes phenomenon has already happened. Notice that this geometry closely resembles the one of Fig. 71, where ϕ_0 is larger.

For small values of ϕ_0 however we see a departure from this behaviour, in that the minimum value of σ_ϕ that would be required to obtain a Stokes phenomenon becomes larger and larger. At this point it is advantageous to switch to a description in terms of the canonical variables x, y. Note that when $\sigma_a = 0$, we have that $\sigma_x \propto \sinh\left(\sqrt{2/3}\phi_0\right)\sigma_\phi$ and thus, for

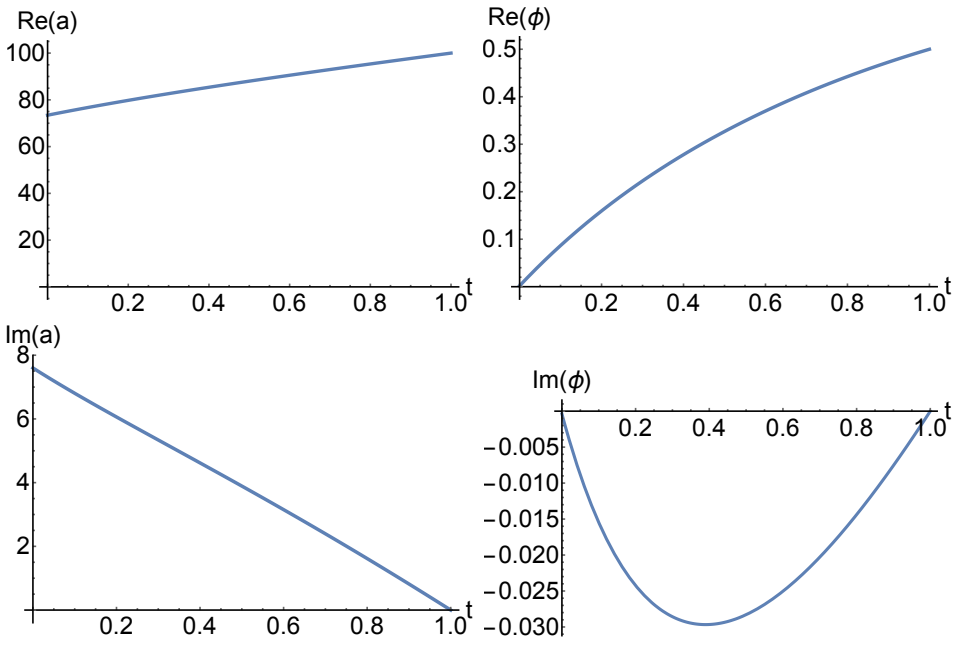

Figure 78: Geometry of the relevant saddle point where the numerical values are identical to the ones of Fig. 77 except that now $\sigma_y = 0$.

small ϕ_0 a large inflaton uncertainty σ_ϕ may still correspond to a much smaller spread σ_x. The right panel in Fig. 76 now shows the critical spread expressed in terms of σ_x as a function of ϕ_0. Here we are departing from the assumption that $\sigma_a = 0$, and in fact in the plot we have chosen a constant value for σ_y.[15] What we see is that for small initial scalar field values the critical spread is reduced, rather than enhanced, compared to larger ϕ_0. Moreover, the limiting value at $\phi_0 = 0$ corresponds exactly to the critical value calculated for pure de Sitter space in [194], and where the scale factor of the universe was the only degree of freedom,

$$\sigma_x^c(\phi_0 = 0) = \left(\frac{a_0^2}{9\alpha}\right)^{1/4} . \tag{8.69}$$

Thus we see that in the region where the potential is flattest, we *require* a minimum uncertainty in the size of the universe $\sigma_a \neq 0$, and it appears not to be sufficient to only have a large enough uncertainty in the inflaton value. Based on the formula (8.69), we might guess that the critical uncertainty should be given, as long as the slow-roll approximation holds, by replacing α by $V(\phi_0)$, and taking into account the transformation formula (8.64). Hence, if we assumed that now on the contrary σ_ϕ was set to zero, and we would consider only an

[15] It turns out that the precise value of σ_y is not so important, except when σ_y is very small (a case which we will discuss below). We believe that the relative insensitivity to σ_y, and the importance of σ_x, are simply a reflection of the fact that the potential depends solely on x.

initial spread in the scale factor, then we might expect the critical spread to be given by

$$\sigma_x^c(\sigma_a \neq 0, \sigma_\phi = 0) = \cosh\left(\sqrt{\frac{2}{3}}\phi_0\right)\left(\frac{a_0^2}{9V(\phi_0)}\right)^{1/4}. \tag{8.70}$$

The corresponding curve is plotted in red in the right panel of Fig. 76. We can see that the true critical spread in fact lies somewhat below this curve. This can be understood in terms of the previous discussion where we showed that for large enough ϕ_0 even a small σ_ϕ is already enough to cause the Stokes phenomenon. Thus, away from the very flat region of the potential near $\phi_0 = 0$ we find that an inflaton uncertainty $\sigma_\phi \lessapprox H/(2\pi)$ is sufficient to lead to a consistent description of quantum transitions, both down and up the potential. However, in the flattest region of the potential (where the slow-roll parameter is smaller than $\epsilon \lesssim 5 \times 10^{-4}$), which may be the region of most interest in terms of applications to eternal inflation, this is not enough, and the initial quantum state must contain a significant uncertainty in the scale factor too, of a magnitude indicated by the de Sitter result (8.69).

As discussed above and shown in Fig. 71, the relevant saddle point geometry is typically similar to a standard slow-roll inflationary solution, albeit one with slightly complexified field values. This is certainly the case whenever the initial inflaton value ϕ_0 is large enough, and σ_ϕ has been chosen to lie above the critical value σ_c. However, as we just saw, in the flattest part of the potential a significant uncertainty in the size of the universe is also required in order to achieve a Stokes phenomenon. We may thus expect the relevant saddle point geometry to change character, and in closing this discussion we will briefly illustrate this effect. Near $\phi_0 = 0$ we still have the possibility of having a large uncertainty in the inflaton value too, i.e. we may still have a large σ_ϕ and thus, in combination with σ_a, we may still have large values of both σ_x and σ_y. In this case we still have a roughly slow-roll saddle point geometry, where as before the inflaton starts with a comparatively unlikely value high up on the potential and slowly rolls down - see Fig. 77. However, the uncertainty in the inflaton value could also be small, with a correspondingly well determined initial expansion rate, so that once again a Stokes phenomenon is achieved. This corresponds to having a very small (or vanishing) value for σ_y. In this case the scalar field is forced to roll up the potential, since its initial and final values are specified with great certainty. But we showed in Eq. (8.62) that it is not possible for the inflaton to roll up, as long as the field values are real. The resolution is that in this case the saddle point becomes highly complex, and the field evolution also correspondingly complex - see Fig. (78). Moreover, at the end of the transition the scalar field is still rolling up the potential. These two cases thus nicely illustrate the importance of the initial Robin conditions, or equivalently the initial state, in determining the most likely

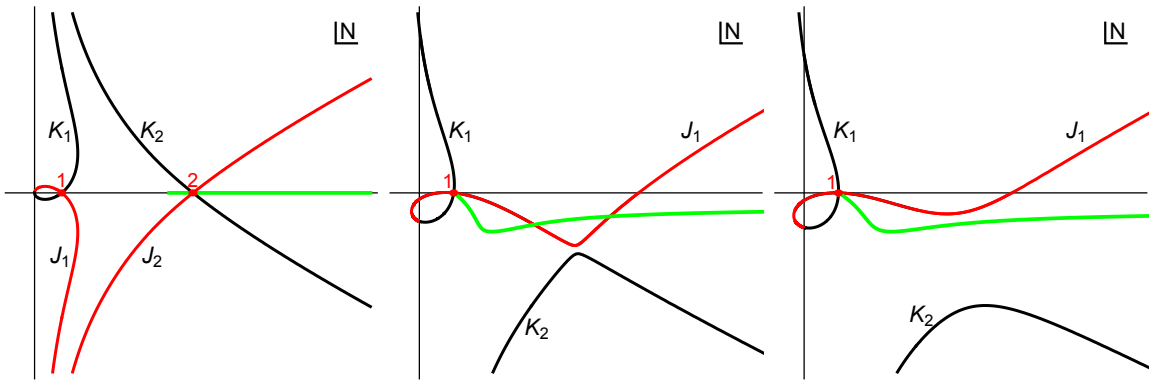

Figure 79: The plots show the flow lines (in black) and the scale factor's curve of zeros (in green) for increasing values of σ_ϕ. The left, middle and right panels correspond to $\sigma_\phi = 0$, $\sigma_\phi = \sigma_c = 0.0154$, and $\sigma_\phi = 0.0170 > \sigma_z$ respectively. The other parameters read $a_0 = 100$, $a_1 = 200$, $\phi_0 = 1/10$, $\phi_1 = 1/2$, $\alpha = 1/10$, $p_x = -54.79$, and $p_y = -1.34$ similar to the previous examples. The curves of zeros still crosses the Lefschetz thimble when the Stokes phenomenon happens, but after a further, modest increase in the spread to $\sigma_\phi \approx 0.0164$, the lines do not cross anymore, and the path integral is well defined.

subsequent evolutions. The most appropriate form of the initial state will of course depend on the physical situation under consideration, and determining the appropriate form of the initial state will be the most important ingredient in applying our results to situations of interest, such as eternal inflation.

8.3.3 Avoiding Off-Shell Singularities

For every value of σ_ϕ there are regions in the complex N plane where the scale factor $a(t)$ vanishes for some $t \in [0, 1]$ and the scalar field $\phi(t)$ correspondingly diverges [194]. These configurations are irregular in terms of the physical variables a and ϕ and as a consequence the action functional diverges. Note that this irregularity has no counterpart in terms of the canonical variables x, y and the corresponding action is analytic. In fact, what becomes singular when the scale factor vanishes is the map which connects the two sets of variables. Thus, these singularities would appear in the Jacobian factor the we have been ignoring in the saddle point approximation, because it usually plays a sub-leading role. However, in the special case where the map becomes singular, the Jacobian would render the path integral ill-defined. Therefore, in order to deal with a well defined path integral we will require that such a curve of zeros (of the scale factor) in the complex N plane does not lie on the defining integration contour, the Lefschetz thimble nor region in between the two.

The curve of zeros, just like the flow lines associated with the various saddle points, changes as a function of σ_ϕ. The typical behaviour is shown in Fig. 79. For $0 \leq \sigma_\phi \leq \sigma_c$, the curve of zeros crosses the Lefschetz thimble but there is no more crossing starting from $\sigma > \sigma_z > \sigma_c$. For larger values of the uncertainty, the path integral is well approximated by one saddle point and the variables a and ϕ are well defined. From our numerical studies we found that σ_z is only modestly larger than σ_c, leading to a small increase of the spread required to recover QFT in curved space-time.

8.4 Discussion

In this work we have taken the first steps in analysing inflationary quantum transitions in semi-classical gravity, more specifically in the path integral formulation of gravity. Such an analysis is of interest since inflationary fluctuations are regularly considered as having momentous implications: they may be the source of the primordial density fluctuations, and they are thought to be able to alter the global structure of spacetime. Since they are typically treated using the framework of QFT in curved spacetime, an important question is whether this approximate treatment is justified. We have analysed this question making use of a specific minisuperspace model containing a scalar field ϕ in a potential of the form $V(\phi) = \alpha \cosh\left(\sqrt{\frac{2}{3}}\phi\right)$, where the potential is chosen such that a transformation of variables is possible that enables the action to become quadratic. This potential has the interesting feature of interpolating between a very flat region near $\phi = 0$, where the potential is approximately constant, and a region with a larger slow-roll parameter $\epsilon \approx 1/3$.

Our results, which only deal with the simplified case of homogeneous transitions, in fact largely support the results of QFT in curved spacetime, under the assumption that an appropriate initial state of the universe is considered. The way in which the "standard" results are recovered is however rather surprising: for instance, we are led to think of a transition up the inflationary potential not so much as involving the inflaton rolling up the potential, but rather as the selection of an unlikely, but otherwise perfectly ordinary, inflationary solution that was already "hidden" in the initial state (our results share some conceptual similarities with the framework of Braden et al. in [37]). In other words, the semi-classical picture that is emerging is that an unlikely large value of the scalar field is picked out (typically containing a small imaginary part as well), such that the desired final value of the scalar field can be reached from it by ordinary slow-roll down the potential.

In order to obtain consistent results, it is crucial however that an appropriate initial state

is imposed. We have done this by using Robin initial conditions, which may equivalently be seen as the imposition of an initial coherent state for the canonical variables of the model. We find that in potential regions that are not too flat, the initial state must contain a sufficient uncertainty in the inflaton value in order for a single saddle point to be relevant to the transition amplitude, implying that an approximate description in terms of QFT in curved spacetime is justified. The critical minimal uncertainty in such potential regions is moreover below the expected scale $H/(2\pi)$, where H denotes the Hubble rate at the start of the transition. More surprising is perhaps our finding that in very flat potential regions (in our model where the slow-roll parameter ϵ is smaller than about 5×10^{-4}), considering only an uncertainty in the inflaton is not sufficient: one must also allow for a sufficiently large uncertainty in the size of the universe. This may have consequences for models of eternal inflation, since it remains to be demonstrated that an appropriate state is generated prior to the up-jumping transitions that are usually considered in this framework. The generation of an appropriate initial state remains an interesting topic for future work.

There are in fact many other avenues for future work. An important extension of the present work will be to add inhomogeneous perturbations. Another aspect that will be worth studying will be the difference between transitions that occur while inflation is already underway, compared to transitions right at the beginning of inflation. This latter study will of course require the additional input from a theory of initial conditions, such as the no-boundary proposal [195, 178]. In addition, it may be of interest to clarify what goes wrong when two saddle points remain relevant to a particular transition. Based on the earlier study in pure de Sitter space [194] we expect fluctuations around the two saddle point geometries to be incompatible with each other and to lead to problematic interference effects or instabilities. Understanding such interference may help in clarifying what happens for transitions in very flat potential regions when the uncertainty in the size of the universe is insufficient. Finally, one can use the semi-classical techniques employed here to investigate other physical setups, such as quantum transitions across the big bang [196, 4]. We hope to report on progress along those lines in the future.

9 Conclusion

In this thesis we highlighted and made progress on a variety of open issues with the standard model of cosmology and its extensions. A main goal was to have minimal assumptions which is why we only used ingredients that are known to exist in our universe. Beginning with classical gravity, we found an analytic solution to Einstein's equations for classically bouncing cosmologies that may contain anisotropies, inhomogeneities and electro-magnetic fields. This solution is a re-interpretation of a familiar family of black hole interiors which signifies an exciting duality; the extent of which is yet to be seen. In a more general setting, we extended our analysis to the full Bianchi IX metric where we showed that bounces still persist within a narrow but open set of parameters. It is interesting that their dynamics leaves the universe in a state that is well suited for inflation as during the bouncing phase the scalar field rolls up the potential. As such, a hybrid model that contains both a contracting phase and an expanding, inflationary phase seems natural and attractive. Importantly, these bounces occur without the need for exotic matter and serve as a fantastic proof of principle for their usefulness.

Moving on to the quantum realm, we have shown the specifics of how quantum mechanics effects the evolution of the universe near cosmological singularities. Employing the path integral framework as a step beyond the usual QFT in curved space-time treatment we were able to finally ask the right question in order to begin addressing eternal inflation. In the path integral it was difficult to even ask the question of how the scalar field can tunnel up the potential during inflation. Now this is possible as we have furthered the development of the Lorentzian path integral which provides a more consistent framework - free from pathologies - than the Euclidean one.

We have further presented two distinct ways of resolving cosmological singularities. First, we showed that at the level of the background instanton solution, the no-boundary proposal is still meaningful when anisotropies are involved. This is contrary to previous claims in the literature and result of our development of novel visualization techniques that allow analyzing the singularity structure of the saddle point geometry. The second method of resolution is another application of these methods. Formulated in an entirely complex language, we found that quantum transitions provide a consistent and plausible way of avoiding cosmological singularities in the early universe.

The wide breadth of topics offers many directions for promising research and many new questions emerged. For the classical bounces, there are two further avenues for future research that seem particularly promising: the first is related to the question as to what happens when the anisotropy becomes larger than the allowed bound in order to have a classical bounce, i.e. what happens when the anisotropy potential $U(\beta_+, \beta_-)$ becomes positive? Here, no classical non-singular bounce solutions remain, but perhaps there exist quantum transitions between a contracting and an expanding phase of the universe. In the absence of anisotropies, we have started an exploration of such solutions in chapter 7, but it would be important to extend this analysis to the more rigorous approach using Picard-Lefschetz theory to define and evaluate the gravitational path integral, while also including anisotropies.

This applies equally well to the ekpyrotic-to-inflationary transitions described in chapter 7, where we do not have any guidelines as to what the appropriate contour of integration should be, and thus we do not know yet whether the solutions that we have found are the dominant ones. An important question for future work is to clarify this, perhaps by generalising the treatment of quantum mechanical tunnelling described in [3] to include gravity. Another question is whether one can transition to other phases of classical evolution, such as a radiation or matter dominated universe. Beyond these questions, our work opens up the possibility to place ekpyrotic cosmology on firmer footing. Specifically it provides a starting point to address the central open question of the evolution of perturbations through a classically singular bounce, and possible observational signatures of the pre-bounce era. This will require a generalisation of our treatment that includes cosmological perturbations. We leave this question for upcoming work.

Finally, as emphasized by Anabalón and Oliva [70], bouncing universe solutions as presented in chapter 4 with positive vacuum energy are closely related to wormholes in the presence of negative vacuum energy. Hence our results suggest the existence of many new anisotropic wormhole solutions, including multi-wormhole solutions with arbitrarily large numbers of throats. It will be interesting to construct and study these solutions, which we hope to do in the near future.

The negative mode problem of chapter 5, however, remains elusive. It is puzzling why La-

grangian and Hamiltonian reductions give a different kinetic pre-factor Q for bounces in false vacuum decay and what its physical relevance is. It will be exciting to see if the implementation of a more general framework by not only considering Euclidean but a fully complex lapse as we proposed in section 5 could resolve this issue. Another interesting issue is to investigate in which realistic cosmological or astrophysical set up a situation with negative Q could occur and what the physical consequences might be.

Ultimately, we are interested in furthering the development of a consistent and powerful framework to describe quantum effects in the early universe and what the observational consequences are. This is important because many puzzling and exciting phenomena such as the cosmological singularity, eternal inflation or the no-boundary proposal crucially rely on it. It will certainly be interesting to see what impact combining ingredients presented here such as implementing the anisotropic no-boundary proposal followed by a contracting, classically bouncing solution has for cosmological predictions. Continuing the work presented in this thesis provides a promising and fruitful avenue to better understand and resolve our uncertainties about early universe cosmology.

A The Variational Principle

A.1 Dirichlet Conditions

In section 2.1 we state that the variational principle for the Einstein-Hilbert action is only well-defined if the Gibbons-Hawking-York (GHY) boundary term is added. Here we present the standard argument in detail following [197], which derives the GHY term. Afterwards we will generalize this argument to more general boundary conditions which yield different boundary terms as well. The variational principle or principle of least action states that the path followed by physical system is the one for which the action is stationary. As a consequence of minimizing the value of the action integral, one obtains the classical equations of motion. In the case of General Relativity the variational principle requires the variation of the Einstein Hilbert action to be zero.

$$0 = \delta S_{EH} = \delta \left[\frac{1}{2} \int_{\mathcal{M}} \sqrt{-g} R d^4x \right] \tag{A.1}$$

$$= \delta \left[\frac{1}{2} \int_{\mathcal{M}} \sqrt{-g} g^{\rho\sigma} R_{\mu\nu} d^4x \right] \tag{A.2}$$

$$= \frac{1}{2} \int_{\mathcal{M}} \left[g^{\mu\nu} R_{\mu\nu} \delta\sqrt{-g} + \sqrt{-g} R_{\mu\nu} \delta g^{\mu\nu} + \sqrt{-g} g^{\mu\nu} \delta R_{\mu\nu} \right] d^4x \tag{A.3}$$

Hence we need to compute the variations of the determinant of the metric and of the Ricci scalar. Considering the first term we write

$$\delta\sqrt{-g} = -\frac{1}{2} \frac{1}{\sqrt{-g}} \delta g \tag{A.4}$$

which puts us in a position to apply Jacobi's rule for differentiating invertible matrices

$$\delta g = g g^{\mu\nu} \delta g_{\mu\nu} \tag{A.5}$$

and obtain

$$\delta\sqrt{-g} = -\frac{1}{2} \frac{1}{\sqrt{-g}} g g^{\mu\nu} \delta g_{\mu\nu} = \frac{1}{2} \sqrt{-g} g^{\mu\nu} \delta g_{\mu\nu} = -\frac{1}{2} \sqrt{-g} g_{\mu\nu} \delta g^{\mu\nu} \tag{A.6}$$

where the last line follows from the fact that

$$0 = \delta(g_{\mu\nu} g^{\mu\nu}) = \delta g_{\mu\nu} g^{\mu\nu} + g_{\mu\nu} \delta g^{\mu\nu} \tag{A.7}$$

Hence Eq. (A.3) turns into

$$\delta S_{EH} = \frac{1}{2} \int_{\mathcal{M}} d^4x \sqrt{-g} \left[R_{\mu\nu} - \frac{1}{2} g_{\mu\nu} R \right] \delta g^{\mu\nu} + \frac{1}{2} \int_{\mathcal{M}} d^4x \sqrt{-g} g^{\mu\nu} \delta R_{\mu\nu} d^4x \tag{A.8}$$

$$= \frac{1}{2} \int_{\mathcal{M}} d^4x \sqrt{-g} G_{\mu\nu} \delta g^{\mu\nu} + \frac{1}{2} \int_{\mathcal{M}} \sqrt{-g} g^{\mu\nu} \delta R_{\mu\nu} d^4x \tag{A.9}$$

$$\tag{A.10}$$

and the first term is exactly satisfied by the left-hand side of the Einstein equations. Next we need to compute the remaining second term. We can re-express it in terms of the Christoffel symbols, via Palatini's identity

$$\delta R_{\mu\nu} = \nabla_\rho(\delta\Gamma^\rho_{\mu\nu}) - \nabla_\mu(\delta\Gamma^\rho_{\rho\nu}) \tag{A.11}$$

as

$$g^{\mu\nu}\delta R_{\mu\nu} = \nabla_\rho(g^{\mu\nu}\delta\Gamma^\rho_{\mu\nu} - g^{\rho\nu}\delta\Gamma^\mu_{\mu\nu}) \tag{A.12}$$

where we could commute the metric and covariant derivative because of metric compatibility $\nabla_\sigma g^{\mu\nu} = 0$. We now have an expression that is of the form

$$\int_{\mathcal{M}} \sqrt{-g}\nabla_\mu X^\mu d^4x = \int_{\mathcal{M}} \partial_\mu \left(\sqrt{-g}X^\mu\right) d^4x \tag{A.13}$$

where the integrand is a total derivative and does not contribute to the equations of motion and

$$X^\rho = g^{\mu\nu}\delta\Gamma^\rho_{\mu\nu} - g^{\rho\nu}\delta\Gamma^\mu_{\mu\nu} \tag{A.14}$$

. We want to see the precise form of the boundary term, however, and thus apply Stokes' theorem

$$\int_{\mathcal{M}} \partial_\mu \left(\sqrt{-g}X^\mu\right) d^4x = \int_{\partial\mathcal{M}} \epsilon\sqrt{h}X^\mu n_\mu d^3y \tag{A.15}$$

This implies that we have to find the value of X^μ on the boundary of the manifold $\partial\mathcal{M}$. Expanding the Christoffel symbols in terms of the metric and recalling that the variation of the metric at the boundary is zero, we obtain

$$g^{\mu\nu}\delta\Gamma^\rho_{\mu\nu} = \frac{1}{2}g^{\mu\nu}g^{\rho\sigma}\left(\delta g_{\mu\sigma,\nu} + \delta g_{\sigma\nu,\mu} - \delta g_{\mu\nu,\sigma}\right) \tag{A.16}$$

$$g^{\rho\nu}\delta\Gamma^\mu_{\mu\nu} = \frac{1}{2}g^{\rho\nu}g^{\mu\sigma}\left(\delta g_{\mu\sigma,\nu} + \delta g_{\sigma\nu,\mu} - \delta g_{\mu\nu,\sigma}\right) \tag{A.17}$$

Therefore, upon relabeling indices in the second line via $\nu \leftrightarrow \sigma$, we end up with the simple expression

$$X^\rho|_{\partial\mathcal{M}} = g^{\mu\nu}g^{\rho\sigma}\left(\delta g_{\mu\sigma,\nu} - \delta g_{\mu\nu,\sigma}\right) \tag{A.18}$$

Multiplying by the normal vector we get

$$n_\rho X^\rho|_{\partial\mathcal{M}} = n^\sigma g^{\mu\nu}\left(\delta g_{\mu\sigma,\nu} - \delta g_{\mu\nu,\sigma}\right) \tag{A.19}$$

$$= n^\sigma\left(\epsilon n^\mu n^\nu + h^{\mu\nu}\right)\left(\delta g_{\mu\sigma,\nu} - \delta g_{\mu\nu,\sigma}\right) \tag{A.20}$$

$$= n^\sigma h^{\mu\nu}\left(\delta g_{\mu\sigma,\nu} - \delta g_{\mu\nu,\sigma}\right) + \epsilon n^\sigma n^\mu n^\nu\left(\delta g_{\mu\sigma,\nu} - \delta g_{\mu\nu,\sigma}\right) \tag{A.21}$$

where we have expanded the four metric in terms of the ADM variables. In the last line we arranged the terms in a suggestive way. Indeed, upon, exchanging ν and σ, we find that the last term is anti-symmetric in these indices and therefore vanishes. The first term, on the other hand, contains a tangential derivative $\delta g_{\mu\nu,\rho} e^\rho_a$ because of the three-metric's form (2.6). Hence we are left with

$$n_\rho X^\rho|_{\partial\mathcal{M}} = n_\rho \left(g^{\mu\nu}\delta\Gamma^\rho_{\mu\nu} - g^{\rho\nu}\delta\Gamma^\mu_{\mu\nu} \right) = -n^\sigma h^{\mu\nu}\delta g_{\mu\nu,\sigma} \tag{A.22}$$

This term is not zero because the derivative points along the normal to the boundary and not along the tangent. Putting it all together, the variation of the Einstein-Hilbert action gives

$$\begin{aligned}
\delta S_{EH} &= \frac{1}{2}\int_{\mathcal{M}} d^4x\sqrt{-g}G_{\mu\nu}\delta g^{\mu\nu} + \frac{1}{2}\int_{\mathcal{M}} \sqrt{-g}g^{\mu\nu}\delta R_{\mu\nu}d^4x && \text{(A.23)}\\
&= \frac{1}{2}\int_{\mathcal{M}} d^4x\sqrt{-g}G_{\mu\nu}\delta g^{\mu\nu} + \frac{1}{2}\int_{\partial\mathcal{M}} \sqrt{h}\epsilon X^\mu n_\mu d^3y && \text{(A.24)}\\
&= \frac{1}{2}\int_{\mathcal{M}} d^4x\sqrt{-g}G_{\mu\nu}\delta g^{\mu\nu} - \frac{1}{2}\int_{\partial\mathcal{M}} \epsilon\sqrt{h}n^\sigma h^{\mu\nu}\delta g_{\mu\nu,\sigma}d^3y && \text{(A.25)}
\end{aligned}$$

All that is left to show is that the variation of the GHY term (as given in Eq. (2.4)) precisely cancels this term. Essentially this reduces to taking the variation of the extrinsic curvature's trace K. We start by rewriting K as

$$K = n^\mu_{;\mu} = g^{\mu\nu}n_{\mu;\nu} = \left(\epsilon n^\mu n^\nu + h^{\mu\nu}\right) n_{\mu;\nu} \tag{A.26}$$

Now we notice that the definition of the unit normal vector n_μ implies that $n_\mu n^\mu = 0$ and hence $(n_\mu n^\mu)_{;\rho} = 0$. This, in turn, implies that $n^\mu n_{\mu;\rho}$ which means that the expression for K simplifies dramatically

$$K = n^\mu_{;\mu} = h^{\mu\nu}n_{\mu;\nu} = h^{\mu\nu}\left(n_{\mu,\nu} - \Gamma^\rho_{\mu\nu}n_\rho\right) \tag{A.27}$$

Taking the variation of this expression is straight-forward

$$\begin{aligned}
\delta K &= -h^{\mu\nu}\delta\Gamma^\rho_{\mu\nu}n_\rho && \text{(A.28)}\\
&= -h^{\mu\nu}n_\rho\frac{1}{2}g^{\rho\sigma}\left(\delta g_{\mu\sigma,\nu} + \delta g_{\sigma\nu,\mu} - \delta g_{\mu\nu,\sigma}\right) && \text{(A.29)}\\
&= h^{\mu\nu}\frac{1}{2}g^{\rho\sigma}\delta g_{\mu\nu,\sigma}n_\rho && \text{(A.30)}\\
&= \frac{1}{2}h^{\mu\nu}\delta g_{\mu\nu,\sigma}n^\sigma && \text{(A.31)}
\end{aligned}$$

which is exactly what we wanted to show.

A.2 Neumann Conditions

In this section, following [32], we will derive an alternative boundary term which allows specifying the momenta instead of positions. In the standard derivation of the variational principle presented above, we saw that the total variation of the Einstein-Hilbert action together with the GHY term gives

$$\delta S_D = \delta S_{EH} + \delta S_{GHY} \tag{A.32}$$

$$= \frac{1}{2}\int_{\mathcal{M}} d^4x\sqrt{-g}G_{\mu\nu}\delta g^{\mu\nu} - \frac{1}{2}\int_{\partial\mathcal{M}} \epsilon\sqrt{h}(K^{ij} - Kh^{ij})\delta h_{ij}d^3y \quad = \frac{1}{2}\int_{\mathcal{M}} d^4x\sqrt{-g}G_{\mu\nu}\delta g^{\mu\nu} - \frac{1}{2}\int_{\partial\mathcal{M}} \pi^{ij}\delta h_{ij}d^3 \tag{A.33}$$

where we defined the canonical momentum of the boundary metric as

$$\pi^{ij} = \epsilon\sqrt{h}(K^{ij} - Kh^{ij}) \tag{A.34}$$

The second term in the action's variation vanished since we set δh_{ij}, evaluated at the boundary, to zero. Usually this is done implicitly, but here we stress it in order to point out that this implies Dirichlet boundary conditions. It furthermore suggests a strategy for implementing other ones. To obtain Neumann conditions we set $\delta\dot{h}_{ij}$ or equivalently π_{ij} to zero at the boundary which means that we need a term different from the GHY term that will make the variational principle well-defined for this condition. Eq. (A.33) suggests that the appropriate Neumann action is

$$S_N = S_D - \int_{\partial\mathcal{M}} d^3y\pi^{ij}h_{ij} \tag{A.35}$$

since the variation yields

$$\delta S_N = \frac{1}{2}\int_{\mathcal{M}} d^4x\sqrt{-g}G_{\mu\nu}\delta g^{\mu\nu} - \frac{1}{2}\int_{\partial\mathcal{M}} \delta\pi^{ij}h_{ij}d^3y \tag{A.36}$$

Explicitly, the Neumann action reads

$$S_N = S_{EH} + S_{\partial N} \tag{A.37}$$

$$= S_{EH} \tag{A.38}$$

Curiously, evaluating the Einstein-Hilbert action without a boundary term is equivalent to imposing Neumann boundary conditions. Note that this is only true in 4 space-time dimensions as the boundary term is dimension dependent [32].

A.3 Robin Conditions

The most general boundary conditions one can impose are Robin conditions which specify a linear combination of positions and momenta. Explicitly, this implies setting

$$\pi^{ij} + \zeta\sqrt{|h|}h^{ij} = 0 \tag{A.39}$$

where ζ is left as a free choice. Upon adding an appropriate term to the Neumann action we get

$$S_R = S_{EH} - \zeta \int_{\partial\mathcal{M}} d^3\sqrt{|h|} \tag{A.40}$$

Upon varying this action we obtain

$$\delta S_R = \frac{1}{2}\int_{\mathcal{M}} d^4x\sqrt{-g}G_{\mu\nu}\delta g^{\mu\nu} - \frac{1}{2}\int_{\partial\mathcal{M}} \delta\left(\pi^{ij} + \zeta\sqrt{|h|}h^{ij}\right) d^3y \tag{A.41}$$

where we used the relation $\sqrt{|h|}h^{ij}\delta h_{ij} = 2\delta(\sqrt{|h|}h^{ij})h_{ij}$.

B Cosmological Perturbation Theory

Here we give a brief review of a few salient features of the theory of cosmological perturbations. Readers familiar with this material may skip to the next section. We will consider theories of gravity minimally coupled to a scalar field ϕ with a potential $V(\phi)$. Thus the action is given by

$$S = \int d^4x\sqrt{-g}\left[\frac{R}{2} - \frac{1}{2}(\partial\phi)^2 - V(\phi)\right], \tag{B.1}$$

where we have set $8\pi G = 1$. In the cosmological context we are interested in Friedmann-Lemaître-Robertson-Walker (FLRW) solutions and perturbations around them. In this section we will focus on spatially flat backgrounds, $\mathrm{d}\bar{s}^2 = -\mathrm{d}t^2 + a^2(t)\delta_{ij}\mathrm{d}x^i\mathrm{d}x^j$, where $a(t)$ denotes the background scale factor and $H = \dot{a}/a$ characterises the expansion rate. An inflationary phase then corresponds to a phase of accelerated expansion, $\ddot{a} > 0$, which can also be formulated as the requirement that $\epsilon < 1$, where we have introduced the slow-roll parameter $\epsilon \equiv -\dot{H}/H^2 = \dot{\phi}^2/(2H^2)$. The condition for inflation can be met when the potential is sufficiently flat. For a very flat potential, we have the approximate relation $\epsilon \approx V_{,\phi}^2/(2V^2)$, which is valid when $\epsilon \ll 1$.

Now we can consider perturbations of this background space-time. Retaining only scalar perturbations, we can write the metric as

$$\mathrm{d}s^2 = -(1+2A)\mathrm{d}t^2 + 2a(t)B_{,i}\mathrm{d}x^i\mathrm{d}t + a^2(t)[(1+2\psi)\delta_{ij} + 2\partial_i\partial_j E]\mathrm{d}x^i\mathrm{d}x^j\,, \tag{B.2}$$

where A, B, ψ, E are the perturbations. One additional scalar perturbation arises from the perturbation of the scalar field, $\delta\phi$. A small local change in the coordinates can be written as $x^\mu \to x'^\mu = x^\mu + \xi^\mu$, where the vector ξ^μ can be decomposed as $\xi^\mu = (\xi^0, \xi^i)$ with $\xi^i = \xi^i_T + \partial^i\xi$. Here ξ is a scalar and $\partial_i\xi^i_T = 0$ is a divergence free 3-vector. Thus ξ^0 and ξ are the two scalar transformation parameters. The associated gauge transformations of the metric perturbations are given by

$$A \to A + \dot{\xi}_0 \tag{B.3}$$

$$B \to B + \frac{1}{a}(-\xi_0 - \dot{\xi} + 2H\xi) \tag{B.4}$$

$$\psi \to \psi + H\xi_0 \tag{B.5}$$

$$E \to E - \frac{1}{a^2}\xi, \tag{B.6}$$

while the scalar field perturbation transforms as $\delta\phi \to \delta\phi - \dot{\phi}\xi^0$.

We will perform our calculation in flat gauge where the spatial metric $h_{ij} = a(t)^2\delta_{ij}$ is kept fixed as the spatial section of a flat FLRW universe (ξ^0 can be chosen to eliminate ψ and ξ to eliminate E). At linear order the constraints, which can be thought of as the 00 and $0i$ Einstein equations, are given by (see e.g. [198])

$$A = \frac{\dot{\phi}}{2H}\,\delta\phi = \sqrt{\frac{\epsilon}{2}}\delta\phi \tag{B.7}$$

$$\partial^i\partial_i B = -\frac{1}{2H}(V_{,\phi} + \frac{\dot{\phi}}{H}V)\delta\phi - \frac{\dot{\phi}}{2H}\dot{\delta\phi} = -\epsilon\frac{\mathrm{d}}{\mathrm{d}t}\left(\frac{\delta\phi}{\sqrt{2\epsilon}}\right), \tag{B.8}$$

where in the constraint for B we have already used (B.7) to replace A.

C Kantowski-Sachs bounces

An easier toy model for non-singular cosmological bounces than the axial Bianchi IX model of section 4.5.3 can be found in the Kantowski-Sachs (KS) class of metrics [72]. These metrics contain a two-sphere in their spatial directions, and the line element is given by

$$ds^2_{KS} = -dt^2 + \frac{a^2(t)}{4} e^{-2\beta(t)} dr^2 + \frac{a^2(t)}{4} e^{\beta(t)} d\Omega_2^2 \,, \tag{C.1}$$

where the factor of $1/4$ was included in analogy with the Bianchi IX case. Again, a represents the spatial volume while β quantifies an anisotropic deformation. In this case there is only one a deformation parameter. In the presence of a cosmological constant Λ, the equations of motion and constraint are given by

$$3\frac{\ddot{a}}{a} + \frac{3}{2}\dot{\beta}^2 = N^2\Lambda \tag{C.2}$$

$$\ddot{\beta} + 3H\dot{\beta} + \frac{2N^2}{3a^2} U_{,\beta} = 0 \tag{C.3}$$

$$3H^2 = \frac{3}{4}\dot{\beta}^2 + N^2(\Lambda + \frac{1}{a^2}U) \tag{C.4}$$

where the constraint has been used to simplify the acceleration equation. The effective potential is

$$U(\beta) = -4e^{-\beta} \,. \tag{C.5}$$

It is very similar to the axial Bianchi IX potential in Eq. 4.55, except that the $e^{-4\beta}$ term is absent. At large positive β the two models are essentially equivalent, but at negative β the KS potential remains negative, causing a runaway of the solutions asymptotically.

Now we may look for actual bounce solutions. A perturbative expansion around a would-be bounce leads to the expansions

$$a = a_b(1 + \frac{\Lambda}{6}t^2 + \cdots) \tag{C.6}$$

$$\beta = \beta(0) - \frac{1}{3}\Lambda t^2 + \cdots \tag{C.7}$$

where the scale factor at the bounce is given by $a_b = a(t=0) = \frac{1}{\sqrt{\Lambda} e^{\beta(0)/2}}$ and we have fixed the time of the bounce to be at $t = 0$. The above expansions suggest that one might try an ansatz $a \propto e^{-\beta/2}$ and this indeed solves the equations of motion exactly,

$$a = \frac{1}{\sqrt{\Lambda}} e^{-\beta/2} = c_1 \left(\cosh(\sqrt{\Lambda} t + c_2)\right)^{1/3} \tag{C.8}$$

where c_1, c_2 are integration constants. Thus analytic bounce solutions exist for every possible value of β at the bounce, while asymptotically the anisotropy parameter β always runs off

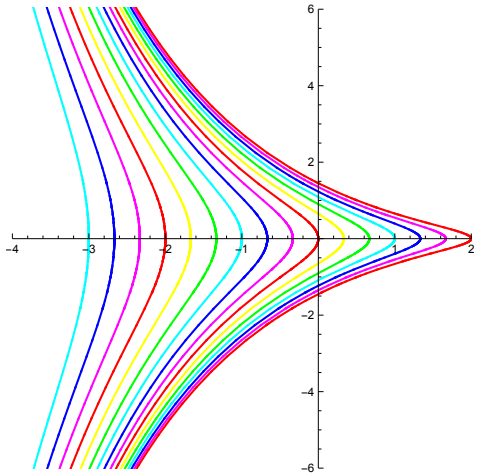

Figure 80: Evolution of the anisotropy parameter β as a function of time for Kantowski-Sachs bounces. For all βs there exists a bounce (here with $\dot{\beta} = 0$ at the bounce).

to minus infinity. For these solutions, in fact only the r direction bounces while the 2-sphere remains constant throughout. These solutions are plotted in Fig. 80, and may be recognised as $dS_2 \times S^2$ (and we note that closely related wormhole solutions also exist [199]).

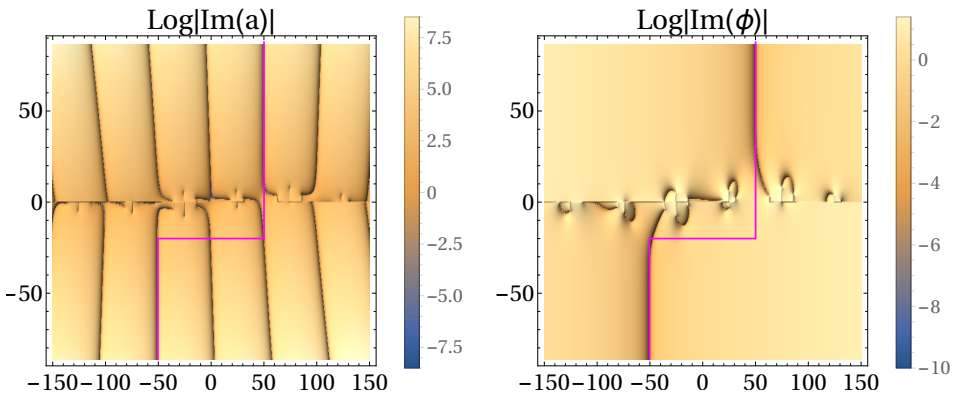

Figure 81: An instanton with an L-shaped path connecting $\chi_1 = 10$ to $\chi_2 = 10$.

D Quantum Bounces

D.1 Contours of Integration

For inflationary-to-inflationary transitions, apart from the specific symmetric contour used in the main part of the text, other paths are possible which also lead to potentially valid interpolating solutions. One example is an L-shaped path, as shown in Fig. 81. From the final classical history, this path runs straight down through the point where the big bang singularity would have been, had the solution been real. The fact that the solution is complex now allows one to continue through this point, and connect with an incoming classical history in the bottom left quadrant. However, as shown in Fig. 82, if we look at transitions to different scalar field values, then for the L-shaped path the implied probability distribution would be non-normalisable, indicating that this class of solutions may not be physical. Similar results are obtained for other L-shaped paths that connect with further-removed loci of real a values, and with upside-down L-shaped paths that run through the would-be singularity from the bottom up. For this reason we focus on the symmetric contour.

But even for the symmetric contour, we have further possibilities, as we can use it to connect classical histories that are further separated in Euclidean time. Fig. 83 shows the real part of the action for such transitions between increasingly separated "branches" where the scale factor is real, each time with field derivatives optimised such that the locus of real scalar field asymptotically overlaps with the line of real scale factor. For these higher branches, the action increases monotonically, indicating that these transitions, though also normalisable, are further suppressed. We may thus safely ignore these.

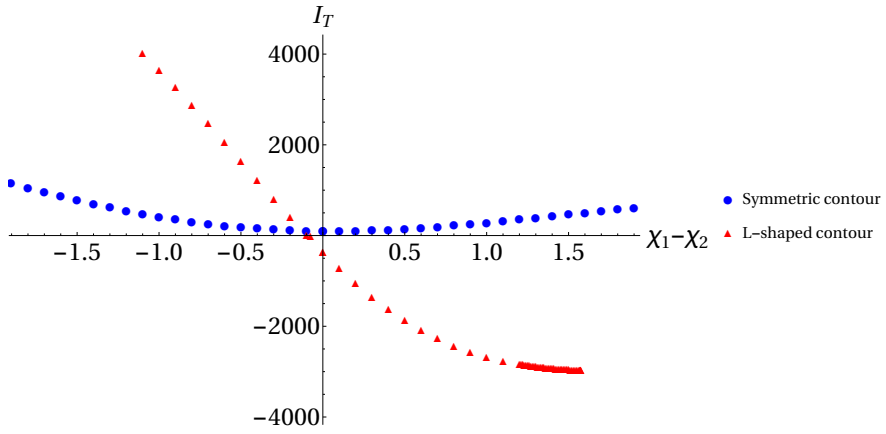

Figure 82: The real part of the action for transition from $\chi_1 = 10$ to various values of χ_2, plotted as a function of $\chi_1 - \chi_2$ and for two types of integration contour: the L-shaped one (in blue dots) and the symmetric one (in red squares).

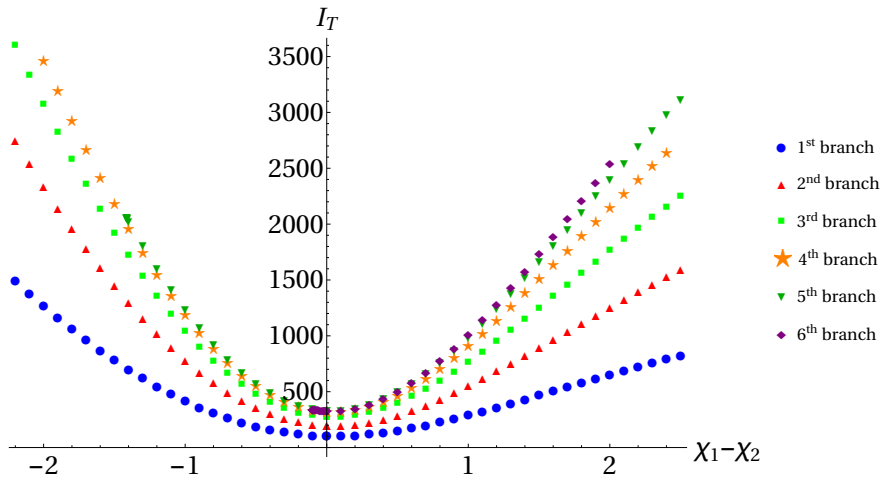

Figure 83: The real part of the action for symmetric contours connecting classical histories that are ever further separated in Euclidean time, and which we refer to as different branches. These solutions have higher actions and are thus further suppressed.

D.2 Perturbative Results

For inflationary-to-inflationary transitions, the equations of motion can be solved analytically in various approximate regimes, allowing us to provide approximate analytic descriptions of the quantum transitions.

D.2.1 Large scalar field

At large field values we will be in the slow-roll regime, $\phi'^2 \ll V(\phi)$ and $\phi'' \ll \frac{\partial V(\phi)}{\partial \phi}$. If the scale factor is also large, then the spatial curvature can be ignored and the equations of motion simplify to

$$3\frac{a'}{a} = m^2\frac{\phi}{\phi'} \ , \tag{D.1a}$$

$$a'' + \frac{a\kappa^2 m^2\phi^2}{6} = 0 \ , \tag{D.1b}$$

$$\left(\frac{a'}{a}\right)^2 = -\frac{\kappa^2 m^2\phi^2}{6} \ . \tag{D.1c}$$

These can be solved explicitly, for example by substituting the first equation into the last,

$$\phi'^2 = -\frac{2}{3}\frac{m^2}{\kappa^2} \ , \tag{D.1d}$$

which can be easily solved to give

$$\phi(\tau) = \phi(0) \pm i\frac{m}{\kappa}\sqrt{\frac{2}{3}}\tau \ . \tag{D.2}$$

Notice that again we took the point of symmetry $\tau_s = 0$. This result for ϕ can be plugged into (D.1a), from which we then obtain the sale factor

$$\frac{a'}{a} = \mp i\frac{\kappa m}{\sqrt{6}}\left(\phi(0) \pm i\sqrt{\frac{2}{3}}\frac{m\tau}{\kappa}\right) \Rightarrow a(\tau) = Ce^{\mp i\frac{\kappa m\phi(0)\tau}{\sqrt{6}} + \frac{m^2\tau^2}{6}} \ . \tag{D.3}$$

To find the value of C, we will follow Lyons [154], who states that when $\mathrm{Re}(\phi(0)) > 0$ in the upper half $\tau-$plane the solutions with the upper sign are valid while in the lower half τ-plane the ones with the lower sign are valid. This means that around $\tau = 0$ both solutions should be matched to one solution,

$$\phi(\tau) \approx \phi(0) \ , \tag{D.4}$$

$$a(\tau) \approx C\cos\left(\frac{\kappa m\phi(0)}{\sqrt{6}}\tau\right) \ . \tag{D.5}$$

Notice that it is clear that these solutions obey the bounce boundary conditions that we impose. To find C we plug a into the Hamiltonian constraint, giving $C = \sqrt{\frac{3}{2}}\frac{1}{\kappa m\phi(0)}$. Collecting

our results, the solution is approximately given by

$$\phi(\tau) = \phi(0) + i\sqrt{\frac{2}{3}}\frac{m\tau}{\kappa} \ , \tag{D.6}$$

$$a(\tau) = \sqrt{\frac{3}{2}}\frac{1}{\kappa m\phi(0)} \exp\left(-i\frac{\kappa m\phi(0)}{\sqrt{6}}\tau + \frac{m^2\tau^2}{6}\right) \ . \tag{D.7}$$

From this we can understand the behaviour in our numerics. It is clear that ϕ is real along $\tau = X_{TP} + it$ with $X_{TP} = -\phi_{sI}\frac{\kappa}{m}\sqrt{\frac{2}{3}}$. Here we have split $\phi(0)$ in its real and imaginary components $\phi(0) = \phi_{sR} + i\phi_{sI}$. It is also interesting to write $\phi(0) = \phi_s e^{i\theta_s}$, from which we can see that a change in phase, keeping ϕ_s fixed, shifts the line of real $\phi(\tau)$:

$$X_{TP} = -\phi_s \sin(\theta_s)\sqrt{\frac{3}{2}}\frac{\kappa}{m} \ . \tag{D.8}$$

Let us now take a closer look at the scale factor. To see where it becomes real, we will try to write it as an amplitude times a phase,

$$\begin{aligned} a(\tau) =& \sqrt{\frac{3}{2}}\frac{1}{\kappa m\phi_s} \exp\left[\frac{m^2}{6}(x^2 - t^2) + \frac{\kappa m\phi_s}{\sqrt{6}}(\cos(\theta_s)t + \sin(\theta_s)x)\right] \\ & \times \exp\left[i\left(\frac{m^2 xt}{3} - \theta_s - \frac{\kappa m\phi_s}{\sqrt{6}}(\cos(\theta_s)x - \sin(\theta_s)t)\right)\right] \ . \end{aligned} \tag{D.9}$$

This becomes real when the phase is a multiple of π. If t is not too big, the only relevant term is the one without t, therefore we expect that a is real along

$$X = \frac{n\pi\sqrt{6}}{\kappa m\phi_s \cos(\theta_s)} \ , \tag{D.10}$$

with $n \in \mathbb{Z}$. This explains why we see different lines in the complex $\tau-$plane along which a is real. In the numerical results there are singularities around $\tau = 0$, though these do not appear in our analytic results. The lines of real a and ϕ will coincide if

$$-\phi_{sI}\frac{\kappa}{m}\sqrt{\frac{3}{2}} = \frac{n\pi\sqrt{6}}{\kappa m\phi_{sR}} \Rightarrow \phi_{sI} = -\frac{2n\pi}{\kappa^2\phi_{sR}} \ , \tag{D.11}$$

or written in terms of the absolute value and the phase of $\phi(0)$

$$\theta_s = \frac{1}{2}\sin^{-1}\left(\frac{4n\pi}{\kappa^2\phi_s^2}\right) \ . \tag{D.12}$$

Thus we expect no obstruction to finding such interpolating solutions numerically.

D.2.2 Small scalar field

Another region where analytic results are possible is the region where the scalar field is a small perturbation, without backreaction on the metric. Starting with the case for which there is no scalar field at all, the equation of motion for a is solved by

$$a''(\tau) = 0 \Rightarrow a(\tau) = A + B\tau \ . \tag{D.13}$$

Because we demand $a'(0) = 0$ we can conclude that without a scalar field the scale factor is constant, $a(\tau) = A$. If we now add a small scalar field to this background, we get an equation of motion for ϕ:

$$\phi'' - m^2\phi = 0 \ . \tag{D.14}$$

The solution for this, obeying the appropriate boundary condition $\phi'(0) = 0$, is

$$\phi(\tau) = \phi_s e^{i\theta_s} \cosh(m\tau) \ . \tag{D.15}$$

Plugging this together with a into the Hamiltonian constraint gives $a(\tau) = \pm\frac{\sqrt{6}}{\kappa m \phi_s e^{i\theta_s}}$.

Now we can look for regions where both a and ϕ are real. The only values of θ_s for which a is real are $\theta = n\pi$. ϕ can then only be real along the imaginary axis, i.e. $X_{TP} = 0$. This explains why we can not find complex bounce solutions for very small ϕ_s, the only possible solutions are those that are real.

E Horava Lifshitz Gravity

This chapter, based on [8] stands in contrast to the rest of this thesis insofar as that we do not consider ordinary General Relativity but an alternative theory of gravity: Horava-Lifshitz gravity. Here we are interested in showing that alternative theories of gravity might not suffer from some of the problems that occur in the standard model according to GR. In GR a homogeneous and isotropic universe is described by the Friedmann equation

$$3H^2 = 8\pi G\rho - \frac{3K}{a^2} + \Lambda\,, \tag{E.1}$$

where H is the Hubble expansion rate, G is Newton's constant, ρ is the energy density, $K = 0, 1, -1$ is the curvature constant of a maximally symmetric 3-space, a is the scale factor and Λ is the cosmological constant. The asymptotic value, of ρ at late time can be set to zero by redefinition of Λ. In the standard cosmology, ρ then includes energy densities of radiation ($\propto 1/a^4$) and pressure-less matter ($\propto 1/a^3$). The fact that all but Λ decay as the universe expands is the source of the cosmological constant problem. The present chapter does not intend to solve the cosmological constant problem and we simply assume that Λ has the observed value. The slowest decaying component on the right hand side of the Friedmann equation is the spatial curvature term $-3K/a^2$ and is the source of the flatness problem in the standard cosmology.

Inflation, once it occurs, makes ρ almost constant for an extended period in the early universe so that even the curvature term decays faster than ρ. The initial condition of the standard cosmology is thus set at the end of inflation in such a way that the curvature term is sufficiently smaller than $8\pi G\rho$. Subsequently, the ratio of the curvature term to $8\pi G\rho$ grows but the initial value of the ratio at the end of inflation is so small that the universe reaches the current epoch before the ratio becomes order unity. This is how inflation solves the flatness problem.

If a theory of quantum gravity predicts that the ratio $(3K/a^2)/(8\pi G\rho)$ be sufficiently small at the beginning of the universe then this could be an alternative solution to the flatness problem. The purpose of the present chapter is to propose such a solution based on the projectable version of Hořava-Lifshitz (HL) gravity [31, 200], which has recently been proved to be renormalizable [201, 202] and thus is a good candidate for a quantum gravity theory. Since our proposal is solely based on a fundamental principle called the anisotropic scaling, which is respected by all versions of the HL theory, it is expected that the same idea can be implemented in other versions of HL gravity.

One of the fundamental principle of HL gravity is the so-called *anisotropic scaling*, or Lifshitz scaling,

$$t \to b^z t\,, \quad \vec{x} \to b\vec{x}\,, \tag{E.2}$$

where t is the time coordinate, $\vec{x}$ are the spatial coordinates and z is a number called dynamical critical exponent. In $3+1$ dimensions the anisotropic scaling with $z = 3$ is realized in the ultraviolet (UV) regime which is the essential reason for renormalizability. The anisotropic scaling with $z = 3$ also leads to a novel mechanism of generating scale-invariant cosmological perturbations, solving the horizon problem without inflation [203].

In the context of quantum cosmology, the initial conditions of the universe are typically set by quantum tunneling described by an instanton, i.e. a classical solution to Euclidean equations of motion with suitable boundary conditions. In relativistic theories, where $z = 1$, quantum tunneling is thought to be dominated by an $O(4)$ symmetric instanton, implying that $T = L$, where T and L are the Euclidean time and length scales, respectively. After analytic continuation to the real time evolution, this causes the flatness problem unless inflation follows.

Setting $z = 3$, however, the story is completely different. An instanton should lead to $T \propto L^3$ and thus

$$T \simeq M^2 L^3\,, \tag{E.3}$$

where T and L are again the Euclidean time and length scales, respectively, and M is the scale above which the anisotropic scaling (E.2) with $z = 3$ becomes important. If the theory is UV complete then the scaling (E.3) is expected to apply to any kind of instantons deep in the UV regime, i.e. for $L \ll 1/M$. If the size of the instanton L is indeed much smaller than $1/M$ then this implies that $T \ll L$ and thus the instanton has a highly anisotropic shape. We thus call this kind of instanton an *anisotropic instanton*. If the creation of the universe is dominated by a small anisotropic instanton then in the real time universe after analytic continuation, the spatial curvature length scale will be much greater than the cosmological time scale. In this way the anisotropic instanton may solve the flatness problem without inflation.

The rest of the present chapter is organized as follows. In Section E.1 we review projectable HL theory, obtaining the equivalent of Friedmann's equation (E.1) in this theory. New curvature-dependent terms are found, which will be essential for the solution to the flatness problem proposed here. In Section E.2 we examine a quantum state inspired by the no-boundary proposal: the idea that the universe nucleated from nothing, as represented

by Euclidean evolution replacing the Big Bang singularity. We find that under anisotropic scaling and the semi-classical evolution of HL theory, the curvature is sufficiently suppressed to solve the flatness problem without the need for inflation. The solution may be more general than the concrete model presented here, as argued in Section E.3, where we show that on dimensional grounds we can always predict the modifications to (E.1) from the modified dispersion relations of the theory. Together with equipartition of energy at the initial point evolution in this regime enforces the necessary suppression of the curvature.

E.1 Projectable HL gravity

The basic variables of the projectable version of HL gravity are:

$$\text{lapse} : N(t)\,,\ \text{shift} : N^i(t,\vec{x})\,,\ \text{3d metric} : g_{ij}(t,\vec{x}) \tag{E.4}$$

The theory respects the so-called foliation preserving diffeomorphism,

$$t \to t'(t)\,, \quad \vec{x} \to \vec{x}'(t,\vec{x})\,. \tag{E.5}$$

Adopting the notation of [204], the action of the gravity sector is then given by

$$I_g = \frac{M_{\rm Pl}^2}{2}\int N dt\sqrt{g}d^3\vec{x}\left(K^{ij}K_{ij} - \lambda K^2 - 2\Lambda + R + L_{z>1}\right)\,, \tag{E.6}$$

where

$$\begin{aligned}\frac{M_{\rm Pl}^2}{2}L_{z>1} &= (c_1 D_i R_{jk} D^i R^{jk} + c_2 D_i R D^i R + c_3 R_i^j R_j^k R_k^i \\ &\quad + c_4 R R_i^j R_j^i + c_5 R^3) + (c_6 R_i^j R_j^i + c_7 R^2)\,.\end{aligned} \tag{E.7}$$

Here, $K_{ij} = (\partial_t g_{ij} - D_i N_j - D_j N_i)/(2N)$ is the extrinsic curvature of the constant t hypersurfaces, $K^{ij} = g^{ik}g^{jl}K_{kl}$, $K = g^{ij}K_{ij}$, $N_i = g_{ij}N^j$, g^{ij} is the inverse of g_{ij}, D_i and R_i^j are the coveriant derivative and the Ricci tensor constructed from g_{ij}, $R = R_i^i$ is the Ricci scalar of g_{ij}, $M_{\rm Pl} = 1/\sqrt{8\pi G}$ is the Planck scale, and λ and c_n $(n = 1, \cdots, 7)$ are constants.

In HL gravity, as already stated in (E.4), a spacetime geometry is described by a family of spatial metrics parameterized by the time coordinate t, together with the lapse function and the shift vector. 3D space at each t can have non-trivial topology and may consist of several connected pieces, Σ_α $(\alpha = 1, \cdots)$, each of which is disconnected from the others. In this situation, we have a common lapse function and a set of shift vectors and a set of spatial metrics parameterized by not only (continuous) t but also (discrete) α, as

$$N^i = N^i_\alpha(t,\vec{x})\,, \quad g_{ij} = g^\alpha_{ij}(t,\vec{x})\,, \quad (\vec{x} \in \Sigma_\alpha)\,. \tag{E.8}$$

The equation of motion for $N(t)$ then leads to a global Hamiltonian constraint of the form,

$$\sum_\alpha \int_{\Sigma_\alpha} d^3\vec{x}\, \mathcal{H}_{g\perp} = 0\,, \tag{E.9}$$

where

$$\mathcal{H}_{g\perp} = \frac{M_{\rm Pl}^2}{2}\sqrt{g}(K^{ij}p_{ij} + 2\Lambda - R - L_{z>1})\,, \tag{E.10}$$

and $p_{ij} = K_{ij} - \lambda K g_{ij}$. Because of the summation over mutually disconnected pieces of the space $\{\Sigma_\alpha\}$ in (E.9),

$$\int_{\Sigma_\alpha} d^3\vec{x}\, \mathcal{H}_{g\perp} \neq 0 \tag{E.11}$$

is possible, provided that the sum of them over all α is zero. Therefore, if we are interested in a universe in one of $\{\Sigma_\alpha\}$ then there is neither a local nor a global Hamiltonian constraint that needs to be taken into account. On the other hand, the equation of motion for $N^i(t,\vec{x})$ and $g_{ij}(t,\vec{x})$ are local and thus must be imposed everywhere. The absence of a Hamiltonian constraint introduces an extra component that behaves like dark matter [205, 206], as we shall see below explicitly for a homogeneous and isotropic universe.

We now consider a homogeneous and isotropic universe in each connected piece of the space Σ_α ($\alpha = 1, \cdots$), described by

$$N_\alpha^i = 0\,, \quad g_{ij}^\alpha = a_\alpha(t)^2\Omega_{ij}\,, \tag{E.12}$$

where Ω_{ij}^α is the metric of the maximally symmetric three-dimensional space with the curvature constant $K_\alpha = 0, 1, -1$ and the Riemann curvature $R^{ij}{}_{kl}[\Omega^\alpha] = K_\alpha(\delta_k^i\delta_l^j - \delta_l^i\delta_k^j)$. The action is then

$$\begin{aligned} I_g &= 6\pi^2 M_{\rm Pl}^2 \int N dt \sum_\alpha \int_{\Sigma_\alpha} d^3\vec{x} a_\alpha^3 \mathcal{L}_\alpha\,, \\ \mathcal{L}_\alpha &= \frac{1-3\lambda}{2}H_\alpha^2 + \frac{\alpha_3 K_\alpha^3}{3a_\alpha^6} + \frac{\alpha_2 K_\alpha^2}{a_\alpha^4} + \frac{K_\alpha}{a_\alpha^2} - \frac{\Lambda}{3}\,, \end{aligned} \tag{E.13}$$

where $H_\alpha = (\partial_t a_\alpha)/(N a_\alpha)$, $\alpha_2 = 4(c_6 + 3c_7)/M_{\rm Pl}^2$ and $\alpha_3 = 24(c_3 + 3c_4 + 9c_5)/M_{\rm Pl}^2$. The variation of the action with respect to a_α leads to the dynamical equation,

$$\frac{3\lambda - 1}{2}\left(2\frac{\partial_t H_\alpha}{N} + 3H_\alpha^2\right) = \frac{\alpha_3 K_\alpha^3}{a_\alpha^6} + \frac{\alpha_2 K_\alpha^2}{a_\alpha^4} - \frac{K_\alpha}{a_\alpha^2} + \Lambda\,. \tag{E.14}$$

Integrating this equation once, we obtain

$$\frac{3(3\lambda-1)}{2}H_\alpha^2 = \frac{C_\alpha}{a_\alpha^3} - \frac{\alpha_3 K_\alpha^3}{a_\alpha^6} - \frac{3\alpha_2 K_\alpha^2}{a_\alpha^4} - \frac{3K_\alpha}{a_\alpha^2} + \Lambda\,, \tag{E.15}$$

where C_α is an integration constant. The first term on the right hand side behaves like a pressureless dust and thus is called *dark matter as integration constant* [205, 206]. The

equation of motion for $N(t)$ then to the global Hamiltonian constraint of the form (E.9). For example, if $K_\alpha = 1$ for $^\forall\alpha$ then the global Hamiltonian constraint is simply

$$\sum_\alpha C_\alpha = 0\,. \tag{E.16}$$

For the reason already explained in the previous paragraph, we do not need to consider this equation, if we are interested in a universe in one of $\{\Sigma_\alpha\}$.

E.2 Anisotropic instanton

Suppressing the subscript α, as we have shown in the previous section, a homogeneous and isotropic universe in the projectable HL gravity is described by

$$\frac{3(3\lambda-1)}{2}H^2 = \frac{C}{a^3} - \frac{\alpha_3 K^3}{a^6} - \frac{3\alpha_2 K^2}{a^4} - \frac{3K}{a^2} + \Lambda\,. \tag{E.17}$$

For simplicity, we set $\alpha_2 = 0$ and $\Lambda = 0$ giving

$$\frac{3(3\lambda-1)}{2}H^2 = \frac{C}{a^3} - \frac{\alpha_3 K^3}{a^6} - \frac{3K}{a^2}\,. \tag{E.18}$$

We assume that there is a UV fixed point of the renormalization group (RG) flow with a finite value of λ larger than 1, as in the case of $2+1$ dimensions [207]. Since we are interested in quantum tunneling in the UV, it is ideal to set λ to a constant value (> 1) at the UV fixed point. However, since the RG flow in $3+1$-dimensions has not yet been investigated, we shall consider λ as a free parameter (> 1). We shall adopt units in which $M_{\rm Pl} = 1$.

Hereafter in this section, we consider the creation of a closed ($K = 1$) universe. Switching to Euclidean time $\tau = i\int^t N(t')dt' + const.$, we obtain

$$\frac{3(3\lambda-1)}{2}\frac{(\partial_\tau a)^2}{a^2} = -\frac{C}{a^3} + \frac{\alpha_3}{a^6} + \frac{3}{a^2}\,. \tag{E.19}$$

Supposing that $a \to +0$ as $\tau \to +0$, the leading behavior of a for small τ is $a \simeq a_1\tau^{1/3}$, where a_1 is a constant. Hence, expanding a around $\tau = 0$ as

$$a = a_1\tau^{1/3} + a_2\tau^{2/3} + a_3\tau + \cdots\,, \tag{E.20}$$

and plugging this into the Euclidean equation of motion (E.19), we obtain

$$a_1 = \left(\frac{6\alpha_3}{3\lambda-1}\right)^{1/6},\ a_2 = 0\,,\ a_3 = \frac{3\alpha_2}{10}\sqrt{\frac{6}{\alpha_3(3\lambda-1)}}\,. \tag{E.21}$$

By using this formula, it is easy to solve (E.19) numerically from $\tau = \epsilon$ towards larger τ, where ϵ is a small positive number. The solution is unique for a given value of the integration

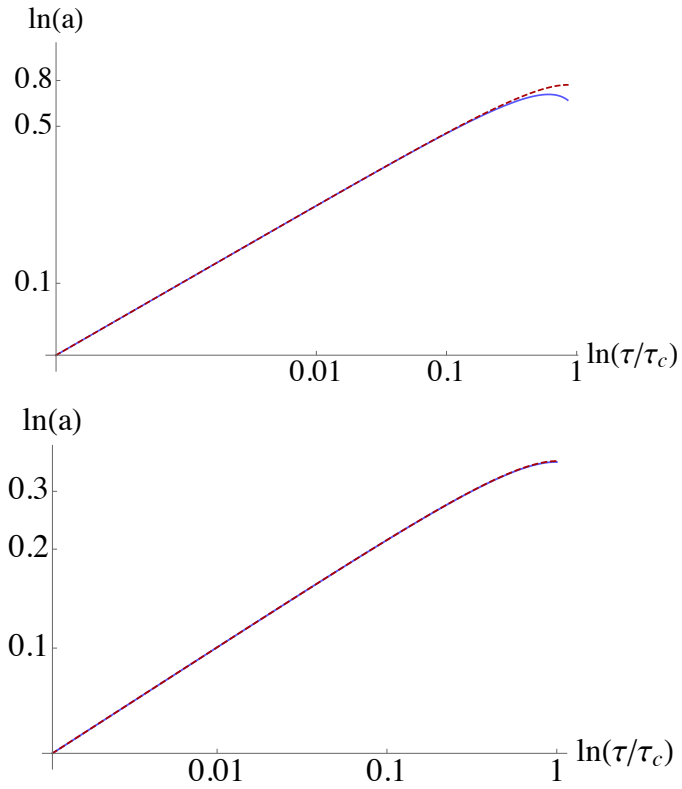

Figure 84: Loglog plots of $\ln a$ vs. $\ln \tau/\tau_c$ in blue with the analytic solution (E.26) superimposed in red. We have $\lambda_{HL} = 2$, $\alpha_3 = 1$, $\alpha_2 = 0$ for both plots, however on the left we have $C = 3$ while on the right $C = 20$. This confirms the validity of the analytic solution in the large C limit.

constant C as we have already fixed another integration constant corresponding to a constant shift of τ. Some numerical solutions are shown in figure 84. For a positive α_3 and a large enough positive C, one finds that $\partial_\tau a$ vanishes at a finite value of τ, which we call τ_c, i.e.

$$\partial_\tau a|_{\tau=\tau_c} = 0\,. \tag{E.22}$$

The Lorentzian evolution of the unvierse after the quantum tunneling is then obtained by Wick rotating the Euclidean solution at $\tau = \tau_c$ as $\tau = \tau_c + i\int^t N(t')dt'$, meaning that the instanton is represented by the solution in the range $\epsilon \leq \tau \leq \tau_c$ with $\epsilon \to +0$. The contribution of the connected piece of the space of interest to the Euclidean action iI_g is then

$$\begin{aligned} S_{\rm E} &= 6\pi^2 \lim_{\epsilon\to+0}\int_\epsilon^{\tau_c} d\tau \left[\frac{1-3\lambda}{2}a(\partial_\tau a)^2 - \frac{\alpha_3}{3a^3} - a\right] \\ &= 6\pi^2 \lim_{\epsilon\to+0}\int_\epsilon^{\tau_c} d\tau \left[\frac{C}{3} - \frac{2\alpha_3}{3a^3} - 2a\right], \end{aligned} \tag{E.23}$$

where we have used the equation of motion (E.19).

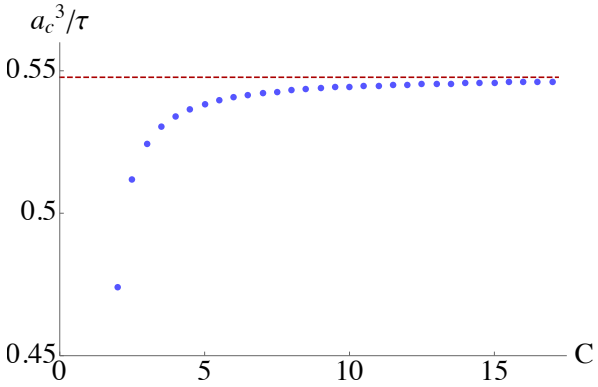

Figure 85: The plot shows a_c^3/τ_c as a function of C and confirms the expected analytic scaling behavior in the large C limit shown in red. To obtain the plot, we kept $\lambda_{HL} = 2$, $\alpha_3 = 1$, $\alpha_2 = 0$ and integrated the Euclidean equation of motion from $\tau = 0$ to $\tau = \tau_c$ for various values of the integration constant C.

For large positive C, we expect a to be small in the whole interval $0 \leq \tau \leq \tau_c$. Hence in this limit we can safely ignore the last term on the right hand side of (E.19):

$$\frac{3(3\lambda-1)}{2}\frac{(\partial_\tau a)^2}{a^2} \simeq -\frac{C}{a^3} + \frac{\alpha_3}{a^6}\,. \tag{E.24}$$

We then have an approximate analytic solution given by

$$\sqrt{\frac{2}{3(3\lambda-1)}}\tau \simeq \frac{2\sqrt{\alpha_3}}{3C}\left(1-\sqrt{1-\frac{C}{\alpha_3}a^3}\right)\,, \tag{E.25}$$

or equivalently

$$a \simeq \left[3\sqrt{\alpha_3}\mathcal{T} - \frac{9}{4}C\mathcal{T}^2\right]^{1/3}\,, \quad \mathcal{T} = \sqrt{\frac{2}{3(3\lambda-1)}}\tau\,. \tag{E.26}$$

As a result, we have

$$\tau_c \simeq \frac{2\sqrt{\alpha_3}}{3C}\sqrt{\frac{3(3\lambda-1)}{2}}\,, \quad a_c \simeq \left(\frac{\alpha_3}{C}\right)^{1/3}\,, \tag{E.27}$$

where $a_c \equiv a(\tau_c)$. This implies that

$$\frac{a_c^3}{\tau_c} \simeq \frac{3\sqrt{\alpha_3}}{2}\sqrt{\frac{2}{3(3\lambda-1)}} = \text{const}\,. \tag{E.28}$$

For a positive α_3 and a large positive value of C, $a_c \equiv a(\tau_c)$ is small as seen in (E.27). As expected from the scaling argument (E.3) in the Introduction and as confirmed numerically in figure 85, we have the scaling relation (E.28). These results support the claim that a small anisotropic instanton may solve the flatness problem in HL gravity.

To see if the small instanton dominates the creation of the universe, we need to estimate the tunneling rate, which in the regime of validity of the semi-classical approximation, is

given by the exponential of the Euclidean action (E.23). This however turns out to be a difficult task. First, both the (Euclidean) extrinsic curvature $K^i_{\mathrm{E}\,\mathrm{j}} = \delta^i_j \partial_\tau \ln a$ and the spatial curvature $R^i{}_j = 2\delta^i_j/a^2$ diverges in the limit $\tau \to +0$, indicating that the semi-classical description should break down near $\tau = 0$. We are thus unable to rely on the semi-classical formula for the tunneling rate. Indeed, the dominant term in the integrand of (E.23) for small τ is $\propto \alpha_3/a^3 \propto \sqrt{\alpha_3(3\lambda-1)}/\tau$, whose integral over the small τ region exhibits a divergence of order $\sqrt{\alpha_3(3\lambda-1)}\ln\epsilon$. Thus the quantum state employed in this paper while inspired by the no-boundary proposal, does not have a regular beginning. Quantum effects such as the RG flow of coupling constants might somehow ameliorate the log divergence but this is beyond the scope of the present paper. Second, based on a formulation of the Lorentzian path integral for quantum cosmology, it was recently suggested that the semi-classical formula for the tunneling rate may have to be drastically modified [28, 173, 172]. This may pose some doubts on the no-boundary proposal [138, 139, 69, 140] in general relativity. It is certainly worthwhile investigating whether a similar argument applies to HL gravity or not.

E.3 General argument

Although we have proposed a concrete framework for solving the flatness problem within HL gravity, the arguments presented are more general and may be valid for any UV complete theory with an anisotropic scaling of spacetime on purely dimensional grounds. This can be suspected from the simple argument presented in Section E, but we now take the dimensional argument further. All that we shall need from the concrete model presented are its dispersion relations (as in HL theory) and equipartition at the starting point (as imposed by the anisotropic instanton).

Let a general UV complete theory have modified dispersion relations for its massless particles (including gravitons) of the form:

$$E^2 = M^2 f(p^2/M^2)\,, \tag{E.29}$$

where f is a smooth function with the following asymptotic behavior,

$$f(x) = \begin{cases} x\,, & (0 \le x \ll 1) \\ x^z\,, & (x \gg 1) \end{cases}\,, \tag{E.30}$$

and the mass scale M may be taken to be of the order of the Planck scale or not. This is a Hamiltonian constraint for particles, so we may expect that in a FLRW setting a corresponding Hamiltonian constraint for vacuum solutions may result from replacing $E^2 \to H^2$

and $p^2 \to |K|/a^2$. Even when such a constraint does not strictly exist (as is the case with our model), an effective one may be present, resulting in a Friedmann-like equation. On dimensional grounds we therefore expect the Friedmann equation in vacuum to read:

$$H^2 = \pm M^2 f(|K|/a^2 M^2)\,. \tag{E.31}$$

The sign on the right hand side may be either positive or negative and the following argument does not rely on the choice of the sign. Addition of matter energy density ρ (or some component that stems from gravity but that behaves like matter, such as the term C/a^3 in (E.17)) then leads to:

$$H^2 = \frac{1}{3}\rho \pm M^2 f(|K|/a^2 M^2)\,, \tag{E.32}$$

where we have set $8\pi G = 1$. To complete the system we have to specify the second Friedmann equation (which indeed was the starting point for our concrete model), or alternatively, the conservation equation for ρ. Let us first assume conservation (this is in fact not needed: see Appendix E.7 for details.). With a general equation of state $w = p/\rho$ we then have:

$$\dot{\rho} + 3H(1+w)\rho = 0\,, \tag{E.33}$$

integrating into:

$$\rho \propto \frac{1}{a^{3(1+w)}}\,. \tag{E.34}$$

In our concrete model we have $z = 3$ and $w = 0$, but this set up is more general.

Let us now assume that at some time, deep in the UV regime far beyond the scale M, the Lorentzian signature universe is created, after which it is subject to (semi-) classical evolution. We assume that the theory we are considering is UV complete, so there is no need to fear going beyond the scale M. This "initial time" of creation can be seen as the result of tunneling from vacuum, via an instanton, similar to our concrete model, or it can be the result of any other process, e.g. a phase transition from a disordered quantum geometry. The point is that the Universe undergoes a transition *into* (semi-) classical evolution in the UV complete theory at a density ρ_{in}, assumed to be $\rho_{\text{in}} \gg M^4$.

Let us now also assume that an equipartition principle is in action, that is, we assume roughly equal amounts of energy for different types of contributions that enter the Hamiltonian. In our setting there are just two contributions: matter (with a general equation of state w) and curvature. Curvature can be seen as a fluid with energy density:

$$\rho_K = \pm 3M^2 f(|K|/a^2 M^2)\,, \tag{E.35}$$

and we can tweak this formula as appropriate, to contain the concrete model. Equipartition then implies:

$$\rho \approx \rho_K \,, \tag{E.36}$$

which is equivalent to the suppression of curvature K/a^2 derived from the anisotropic instanton presented in Section III. However, defined in terms of ρ_K there is no suppression. Indeed $\rho \sim \rho_K \sim \rho_{\rm in}$ initially and the subsequent evolution takes care of the suppression. Whether we phrase things in terms of K/a^2 or ρ_K the final result is the same.

Let the curvature be measured by

$$\Omega_K = \frac{\rho_K}{\rho + \rho_K} \,. \tag{E.37}$$

Using (E.34) and (E.35) we see that for $M^4 \ll \rho \ll \rho_{\rm in}$ we have:

$$\Omega_K \propto a^{3(1+w)-2z} \,, \tag{E.38}$$

whereas for $\rho \ll M^4$ we have the standard flatness problem instability:

$$\Omega_K \propto a^{3(1+w)-2} \,. \tag{E.39}$$

So that Ω_K may be suppressed in the first stage of evolution we see that a necessary condition for solving the flatness problem in an expanding universe is:

$$z > \frac{3(1+w)}{2} \,. \tag{E.40}$$

In our concrete model this is satisfied since $z = 3$ and $w = 0$, but in fact for the $z = 3$ HL theory this would work with any $w < 1$. With standard gravity (i.e. $z = 1$) we would need $w < -1/3$, i.e. inflation.

The above is a necessary but not sufficient condition. The exact condition will involve M and $\rho_{\rm in}$ as well as z and w. Assuming the universe exits the UV phase around $\rho \sim M^4$ to enter a standard hot big bang model, then curvature must be suppressed at $\rho \sim M^4$ by:

$$\Omega_K \ll \Omega_{\rm sup} = z_{\rm eq} \left(\frac{T_{\rm CMB}}{M_{\rm Pl}}\right)^2 \left(\frac{M_{\rm Pl}}{M}\right)^2 \,, \tag{E.41}$$

where we have used (E.39) and $z_{\rm eq}$ is the redshift of matter radiation equality. If $M \sim M_{\rm Pl}$, with standard assumptions we have roughly $\Omega_{\rm sup} \sim 10^{-60}$, as is well known.

In order to obtain this suppression while $M^4 < \rho < \rho_{\rm in}$ we should therefore impose the condition:

$$\frac{\rho_{\rm in}}{M^4} \gg \Omega_{\rm sup}^{-\frac{3(1+w)}{2z-3(1+w)}} \,, \tag{E.42}$$

where we have used (E.38) in conjunction with ρ conservation (and solution (E.34)), even though the latter is not strictly necessary. Equation E.42 is the general condition for solving the flatness problem in the vast class of models considered here. For the concrete model proposed in this paper ($z = 3$ and $w = 0$) we have:

$$\frac{\rho_{\rm in}}{M^4} \gg \Omega_{\rm sup}^{-1}\,, \tag{E.43}$$

so that with $M = M_{\rm Pl}$ this amounts to

$$\frac{\rho_{\rm in}}{M_{\rm Pl}^4} \gg 10^{60}\,. \tag{E.44}$$

Eq. (E.42) establishes the general condition for a solution of the flatness problem in general UV complete theories with anisotropic scaling. In summary, they must start operating sufficiently above the Planck scale and satisfy equipartition in some form at this initial point. This applies to our concrete model with a starting point defined by an anisotropic instanton. However, the formal mechanism is more general.

E.4 Summary and discussions

In the context of the renormalizable theory of gravity called Hořava-Lisfhitz (HL) theory, we have proposed a possible solution to the flatness problem without relying on inflation, supposing that the initial condition of the universe respects the so-called anisotropic scaling (E.2) with $z = 3$. This scaling is isotropic in space but anisotropic in spacetime, and is the essential reason for the renormalizability of HL theory. Because of this scaling, any physical system in the deep ultraviolet (UV) regime tends to possess the scaling property $T \simeq M^2 L^3$, where T and L are the time scale and the length scale of the system and M is the mass scale characterizing the anisotropic scaling. If the universe started in the deep UV regime then the initial condition is expected to satisfy this scaling property with $L \ll 1/M$, meaning that the curvature length scale of the universe is much longer than the expansion time scale. This is exactly what we need for solving the flatness problem.

Based on the projectable version of the HL theory for concreteness, we have found a family of instanton solutions parameterized by an integration constant C. This family of solutions is unique under the FLRW ansatz for the pure gravity system, i.e. without any matter fields, for a given set of parameters in the action. For positive and large enough C, the spatial size $a_{\rm in}$ and the (Euclidean) temporal size $\tau_{\rm in}$ of the instanton are decreasing functions of C. We confirmed the scaling relation $a_{\rm in}^3/\tau_{\rm in} \simeq const.$ in the large C limit, both numerically and analytically. We call those instantons with anisotropy in 4-dimensional Euclidean spacetime

(but with isotropy in 3-dimensional space) *anisotropic instantons*. The anisotropic instanton provides a concrete example of physical systems that realize the scaling property $T \simeq M^2 L^3$ and thus may solve the flatness problem in cosmology.

We have also given a more general argument for the solution of the flatness problem, based on the assumption of equipartition among different contributions of energy density to the Hamiltonian of the system. The equipartition between the highest time derivative term and the highest spatial gradient term can be considered as a restatement of the anisotropic scaling and thus is expected to be universally applicable to many physical systems in any possible UV complete theories with anisotropic scaling.

E.5 Scale-invariant perturbation

In the projectable Hořava-Lifshitz gravity, the number of physical degrees of freedom is three: two from the tensor graviton and one from the scalar graviton. Actually, one can consider the scalar graviton as perturbation of the "dark matter as integration constant", i.e. the C/a^3 term in (E.17). In other words, the "dark matter as integration constant" is a coherent condensate of scalar gravitons. Both tensor and scalar gravitons obey the $z = 3$ anisotropic scaling and thus it is expected that the quantum tunneling comes with scale-invariant cosmological perturbations of both of them, following exactly the same logic as the one proposed in [203].

After quantum tunneling, the universe is still in the UV regime and thus the stress-energy tensor of matter fields $T_{\mu\nu}$ does not have to satisfy the usual four-dimensional conservation equation, $\nabla^\mu T_{\mu\nu} \neq 0$, where ∇^μ is the four-dimensional covariant derivative. In this situation, matter fields and the scalar graviton exchange energies [205]. It is therefore possible that the scale-invariant perturbations of the scalar graviton may be transferred to matter fields. As a result of such transfer processes a part of the coherent condensate of scalar gravitons, i.e. the "dark matter as integration constant", may be converted to a gas/dust of scalar graviton particles, which may also behave as dark matter. If energy densities in the matter sector are initially small compared with that in the "dark matter as integration constant" then the resulting perturbations after such transfer of energies will inevitably be almost scale-invariant and adiabatic.

E.6 Evolution after instanton

In Sec. E.2, we have shown that for a large positive value of the *dark matter as integration constant*, C, there is an instanton solution near the origin of the Euclidean time τ, given by (E.20) with (E.21). After the Lorentzian universe emerges as the analytical continuation of the instanton, this "dark matter" dominates the energy density of the universe for some time. For the subsequent evolution, we assume a minimal scenario as a demonstration in this appendix. Since C interacts with matter (and thus in fact is not constant in its presence) [204], it can decay and populate the universe with matter and radiation some time after the instanton tunneling. Under the assumption that the continuity equation is respected in the matter sector, the relevant part of (E.17) after the transition reads, with addition of matter and radiation,

$$\frac{3(3\lambda-1)}{2}H^2 = \frac{C}{a^3} - \frac{3K}{a^2} + \rho_{\rm mat} + \rho_{\rm rad} + \Lambda \,, \tag{E.45}$$

where $M_{\rm Pl}$ is again set to unity, and $\rho_{\rm mat}$ and $\rho_{\rm rad}$ are the energy densities of radiation and matter, respectively. We have recovered the cosmological constant Λ to account for the late-time accelerated expansion, whose potential dynamics, which is an interesting topic on its own, is beyond the scope of this section. We further assume an instantaneous reheating by the decay of C for simplicity, and that the values of C, $\rho_{\rm rad}$ and $\rho_{\rm mat}$ shift before and after reheating as

$$t_c < t < t_{\rm reh}: \quad \rho_{\rm mat} = \rho_{\rm rad} = 0 \,, \tag{E.46}$$

$$t_{\rm reh} < t: \quad \frac{C}{a^3} + \rho_{\rm mat} = \frac{a_0^3}{a^3}\rho_{\rm mat}^0 \,,\ \rho_{\rm rad} = \frac{a_0^4}{a^4}\rho_{\rm rad}^0 \,, \tag{E.47}$$

where "c," "reh" and "0" denote the values at the instanton transition, reheating and present time, respectively.

The universe undergoes the standard cosmic history of the hot big bang cosmology after the reheating, namely nucleosynthesis followed by radiation-, matter- and then Λ-dominated periods. The fractional curvature "density," defined as $\Omega_K(t) \equiv (3K/a^2)/\rho_{\rm tot}$, evolves as

$$\frac{|\Omega_K(t_c)|}{|\Omega_K(t_0)|} = \frac{\rho_0}{\rho_{\Lambda m}} \left(\frac{a_{\rm reh}}{a_0}\right) \left(\frac{a_0}{a_{\Lambda m}}\right)^4 \left(\frac{a_{\Lambda m}}{a_{\rm eq}}\right) \left(\frac{a_c}{a_0}\right) \,, \tag{E.48}$$

where the subscript "eq" and "Λm" denote the values at the time of matter-radiation and Λ-matter equalities, respectively. The values of $\rho_0/\rho_{\Lambda m}$, $a_{\rm reh}/a_0$, $a_0/a_{\Lambda m}$ and $a_{\Lambda m}/a_{\rm eq}$ are given in the same way as the standard cosmological evolution. On the other hand, by setting

$K = 1$, (E.28) gives

$$\frac{a_c}{a_0} = \frac{s^{1/2}}{a_0}\left(\frac{\tau_c}{a_c}\right)^{1/2} = \sqrt{\frac{s}{3}\left|\Omega_K(t_0)\right|\rho_0}\left(\frac{\tau_c}{a_c}\right)^{1/2} , \tag{E.49}$$

where $s \equiv \sqrt{\frac{3\alpha_3}{2(3\lambda-1)}}$. The fractional density Ω_K at the time $t = t_c$ is approximately given by

$$|\Omega_K(t_c)| \simeq \frac{3/a_c^2}{\alpha_3/a_c^6} = \frac{3s^2}{\alpha_3}\left(\frac{\tau_c}{a_c}\right)^2 . \tag{E.50}$$

Hence (E.48) reduces to

$$\begin{aligned}\frac{\tau_c}{a_c} &\simeq \frac{\alpha_3^{2/3}|\Omega_K(t_0)|\,\rho_{\rm eq}^{2/9}\,\rho_0^{1/9}}{2^{8/9}\,3\,s\,\Omega_m^{8/9}\,(1+z_{\rm reh})^{2/3}} \\ &\simeq 1.80\cdot 10^{-47}\alpha_3^{1/6}\left(\frac{3\lambda-1}{2}\right)^{1/2} \\ &\qquad\times\left(\frac{10^{10}}{1+z_{\rm reh}}\right)^{2/3}\frac{|\Omega_K(t_0)|}{0.005} ,\end{aligned} \tag{E.51}$$

where in the last approximate equality we have used the observed values to plug in $\rho_{\rm eq} \simeq \left(5.67\cdot 10^{-28}M_{\rm Pl}\right)^4$, $\rho_0 \simeq \left(1.01\cdot 10^{-30}M_{\rm Pl}\right)^4$ and $\Omega_m \simeq 0.308$.

As we learn from (E.51), we need an anisotropic instanton with the level of anisotropy of order $T/L \lesssim 10^{-47}$ in order to respect the observational upper bound $|\Omega_K(t_0)| \lesssim 0.005$ [34], provided that the reheating occurs before BBN ($z_{\rm reh} \gtrsim 10^{10}$), that λ at the time of tunneling does not deviate much from its (expected) IR value $\lambda_{\rm IR} = 1$, and that $\alpha_3 \sim \mathcal{O}(1)$ in the Planck units. This small value is to account for the present flatness of the universe by the proposed mechanism in Sec. E.2, which in the inflationary cosmology would be compensated by the duration of inflation $\sim 50-60$ e-foldings. This also sets the lower bound on the energy scale that the instanton tunneling has to occur. At the time of this transition, (E.17) gives

$$\begin{aligned}\frac{3(3\lambda-1)}{2}H_c^2 &\sim \frac{C}{a_c^3} \sim \frac{\alpha_3}{a_c^6} \simeq \frac{\alpha_3}{s^3}\left(\frac{a_c}{\tau_c}\right)^3 \\ &\simeq \frac{\left(1.28\cdot 10^{35}\right)^4}{\alpha_3}\left(\frac{1+z_{\rm reh}}{10^{10}}\right)^2\left(\frac{0.005}{|\Omega_K(t_0)|}\right)^3 ,\end{aligned} \tag{E.52}$$

where H_c is the value of Hubble parameter at the time of instanton transition (in Planck units), and this corresponds to the energy scale at the transition to be $E_c \equiv \sqrt{H_c} \gtrsim 10^{35}M_{\rm Pl}$, recovering the Planck units at the last inequality.

E.7 A more general solution to the flatness problem

In Section E.3 we showed how the concrete model presented in this chapter may be part of a more general class of solutions. In the paper's appendix [8] we expand further on this

argument, both in scope and in terms of interpretation.

There is a simple interpretation of the general argument presented in Section E.3. It is known that modified dispersion relations (MDR) may lead to an energy dependent speed of propagation for massless particles. This falls under the general umbrella term of "varying speed of light" (see [208] for an early review). In the guise of MDRs, such theories lead to several astrophysical and cosmological implications (e.g. [209, 210]). The phenomenon may be quantified by the phase speed $c_p = E/p$ or the group speed $c_g = dE/dp$. In the case of (E.29) and (E.30), in the UV we have:

$$c_p \propto c_g \propto \left(\frac{p}{M}\right)^{z-1}. \tag{E.53}$$

In view of this, it is tempting to map the Friedmann equation (E.32) into the standard-looking Friedmann equation:

$$H^2 = \frac{1}{3}\rho - \frac{Kc_h^2}{a^2} \tag{E.54}$$

also with a time dependent c, and where we have reinstated K as the culprit for the sign ambiguity of the curvature term (relevant in what follows). Assuming $K \neq 0$ we have $c_h^2 = a^2M^2f$, so that in the UV:

$$c_h \approx \left(\frac{1}{Ma}\right)^{z-1}. \tag{E.55}$$

We see that in the deep UV we have $c_h \propto c_g \propto c_p$, (with the understanding that comparisons assume the replacements $E^2 \to H^2$ and $p^2 \to |K|/a^2$). Thus in the deep UV the various c may be used interchangeably. The transition from UV to IR may be different, but this is not important here.

This interpretation at once connects the solution of the flatness problem presented here to that in [211]. This is particularly relevant if we wish to consider the implication of non-conservation of energy mentioned above. As shown in [211] such violations actually help solving the flatness problem, reinforcing the argument.

As is well known, violations of Lorentz invariance may bring about non-conservation. This depends on how we close the system started by (E.54). In the concrete model presented in this chapter, conservation of ρ is assumed (or rather, one starts from the second Friedmann equation and then integrates it into the first, building conservation into the model). An alternative is to assume no modifications to the second Friedmann equation:

$$\frac{\ddot{a}}{a} = -\frac{1}{6}\rho(1+3w). \tag{E.56}$$

This implies violations of the Bianchi identities and energy conservation. Specifically, in combination with (E.54) we find:

$$\dot{\rho} + 3\frac{\dot{a}}{a}\rho(1+w) = \frac{6Kc^2}{a^2}\frac{\dot{c}}{c}. \tag{E.57}$$

Merely looking at the sign of the RHS is very informative. Defining $\rho_c = 3H^2$ we see at once that if $\dot{c}/c < 0$ the violations of energy conservation act so as to push the Universe towards flatness. If the universe is closed ($K = 1$ and thus supercritical, $\rho > \rho_c$) then energy is removed from the universe; if the universe is open ($K = -1$ and $\rho < \rho_c$) then energy is inserted into the universe; no violations occur for a flat model. Thus ρ is pushed to ρ_c.

This does not mean that these violations are needed, or indeed relevant in all regimes. As in [211] we can combine (E.54) and (E.56) to obtain:

$$\dot{\Omega}_K = (1-\Omega_K)\Omega_K\frac{\dot{a}}{a}(1+3w) + 2\frac{c}{c}\Omega_K. \tag{E.58}$$

If $\Omega_K \ll 1$ this integrates to:

$$\Omega_K \propto a^{1+3w}c^2 \tag{E.59}$$

leading to (E.38), obtained ignoring violations of energy conservation. Thus these violations are not very important in the solution to the flatness problem, as long as curvature is already sufficiently suppressed.

Where these violations may be interesting is in situations in which the universe does not start from exact equipartition. Let us consider an extreme case. Suppose that initially $\rho = 0$ and $K = -1$, that is a Milne Universe beginning. Then the Universe starts with $\Omega_K = 1$ and no matter. This would be hopeless if energy were conserved (the Universe would simply remain empty). However inserting this condition into (E.58), we see that the first term initially vanishes, but the second term leads to $\Omega_K \propto c^2$. Hence curvature is still suppressed (at this rate) while matter is being dumped into the Universe. $\rho = 0$ is also pushed to $\rho = \rho_c$. Eventually $\Omega_K \ll 1$, after which violations of energy conservation become irrelevant, and suppression of curvature proceeds according to (E.59).

References

[1] S. F. Bramberger and J.-L. Lehners, "Nonsingular bounces catalyzed by dark energy," *Phys. Rev.* **D99** (2019) no. 12, 123523, arXiv:1901.10198 [hep-th].

[2] A. Anabalon, S. F. Bramberger, and J.-L. Lehners, "Kerr-NUT-de Sitter as an Inhomogeneous Non-Singular Bouncing Cosmology," arXiv:1904.07285 [hep-th].

[3] S. F. Bramberger, G. Lavrelashvili, and J.-L. Lehners, "Quantum tunneling from paths in complex time," *Phys. Rev.* **D94** (2016) no. 6, 064032, arXiv:1605.02751 [hep-th].

[4] S. F. Bramberger, T. Hertog, J.-L. Lehners, and Y. Vreys, "Quantum Transitions Through Cosmological Singularities," *JCAP* **1707** (2017) no. 07, 007, arXiv:1701.05399 [hep-th].

[5] S. F. Bramberger, S. Farnsworth, and J.-L. Lehners, "Wavefunction of anisotropic inflationary universes with no-boundary conditions," *Phys. Rev.* **D95** (2017) no. 8, 083513, arXiv:1701.05753 [hep-th].

[6] S. F. Bramberger, M. Chitishvili, and G. Lavrelashvili, "Aspects of the negative mode problem in quantum tunneling with gravity," arXiv:1906.07033 [gr-qc].

[7] S. F. Bramberger, A. Di Tucci, and J.-L. Lehners, "Homogeneous Transitions during Inflation: a Description in Quantum Cosmology," arXiv:1907.05782 [gr-qc].

[8] S. F. Bramberger, A. Coates, J. Magueijo, S. Mukohyama, R. Namba, and Y. Watanabe, "Solving the flatness problem with an anisotropic instanton in Horava-Lifshitz gravity," *Phys. Rev.* **D97** (2018) no. 4, 043512, arXiv:1709.07084 [hep-th].

[9] **Planck** Collaboration, P. A. R. Ade *et al.*, "Planck 2013 results. XXIII. Isotropy and statistics of the CMB," *Astron. Astrophys.* **571** (2014) A23, arXiv:1303.5083 [astro-ph.CO].

[10] **Planck** Collaboration, P. A. R. Ade *et al.*, "Planck 2015 results. XX. Constraints on inflation," *Astron. Astrophys.* **594** (2016) A20, arXiv:1502.02114 [astro-ph.CO].

[11] **WMAP** Collaboration, E. Komatsu *et al.*, "Seven-Year Wilkinson Microwave Anisotropy Probe (WMAP) Observations: Cosmological Interpretation," *Astrophys. J. Suppl.* **192** (2011) 18, arXiv:1001.4538 [astro-ph.CO].

[12] A. D. Linde, "A New Inflationary Universe Scenario: A Possible Solution of the Horizon, Flatness, Homogeneity, Isotropy and Primordial Monopole Problems," *Phys. Lett.* **108B** (1982) 389–393.

[13] A. H. Guth, "The Inflationary Universe: A Possible Solution to the Horizon and Flatness Problems," *Phys. Rev.* **D23** (1981) 347–356. [Adv. Ser. Astrophys. Cosmol.3,139(1987)].

[14] A. Albrecht and P. J. Steinhardt, "Cosmology for Grand Unified Theories with Radiatively Induced Symmetry Breaking," *Phys. Rev. Lett.* **48** (1982) 1220–1223.

[15] D. Baumann, "Inflation," in *Physics of the large and the small, TASI 09, proceedings of the Theoretical Advanced Study Institute in Elementary Particle Physics, Boulder, Colorado, USA, 1-26 June 2009*, pp. 523–686. 2011. arXiv:0907.5424 [hep-th].

[16] J. Khoury, B. A. Ovrut, P. J. Steinhardt, and N. Turok, "The Ekpyrotic universe: Colliding branes and the origin of the hot big bang," *Phys. Rev.* **D64** (2001) 123522, arXiv:hep-th/0103239 [hep-th].

[17] J.-L. Lehners, "Ekpyrotic and Cyclic Cosmology," *Phys. Rept.* **465** (2008) 223–263, arXiv:0806.1245 [astro-ph].

[18] A. Ijjas, P. J. Steinhardt, and A. Loeb, "Inflationary schism," *Phys. Lett.* **B736** (2014) 142–146, arXiv:1402.6980 [astro-ph.CO].

[19] J. J. Halliwell, "INTRODUCTORY LECTURES ON QUANTUM COSMOLOGY," in *7th Jerusalem Winter School for Theoretical Physics: Quantum Cosmology and Baby Universes Jerusalem, Israel, 27 December 1989 - 4 January 1990*, pp. 159–243. 1989. arXiv:0909.2566 [gr-qc].

[20] R. P. Feynman, "Space-time approach to nonrelativistic quantum mechanics," *Rev. Mod. Phys.* **20** (1948) 367–387.

[21] A. Vilenkin, "Creation of Universes from Nothing," *Phys. Lett.* **117B** (1982) 25–28.

[22] J. Hartle and S. Hawking, "Wave Function of the Universe," *Phys.Rev.* **D28** (1983) 2960–2975.

[23] S. R. Coleman and F. De Luccia, "Gravitational Effects on and of Vacuum Decay," *Phys. Rev.* **D21** (1980) 3305.

[24] T. Tanaka and M. Sasaki, "False vacuum decay with gravity: Negative mode problem," *Prog. Theor. Phys.* **88** (1992) 503–528.

[25] G. W. Gibbons, S. W. Hawking, and M. J. Perry, "Path Integrals and the Indefiniteness of the Gravitational Action," *Nucl. Phys.* **B138** (1978) 141–150.

[26] C. Teitelboim, "Quantum Mechanics of the Gravitational Field," *Phys. Rev.* **D25** (1982) 3159.

[27] E. Witten, "Analytic Continuation Of Chern-Simons Theory," *AMS/IP Stud. Adv. Math.* **50** (2011) 347–446, `arXiv:1001.2933 [hep-th]`.

[28] J. Feldbrugge, J.-L. Lehners, and N. Turok, "Lorentzian Quantum Cosmology," *Phys. Rev.* **D95** (2017) no. 10, 103508, `arXiv:1703.02076 [hep-th]`.

[29] A. Vilenkin, "The Birth of Inflationary Universes," *Phys. Rev.* **D27** (1983) 2848.

[30] A. D. Linde, "Eternally Existing Selfreproducing Chaotic Inflationary Universe," *Phys. Lett.* **B175** (1986) 395–400.

[31] P. Horava, "Quantum Gravity at a Lifshitz Point," *Phys. Rev.* **D79** (2009) 084008, `arXiv:0901.3775 [hep-th]`.

[32] C. Krishnan and A. Raju, "A Neumann Boundary Term for Gravity," *Mod. Phys. Lett.* **A32** (2017) no. 14, 1750077, `arXiv:1605.01603 [hep-th]`.

[33] C. Krishnan, S. Maheshwari, and P. N. Bala Subramanian, "Robin Gravity," *J. Phys. Conf. Ser.* **883** (2017) no. 1, 012011, `arXiv:1702.01429 [gr-qc]`.

[34] **Planck** Collaboration, P. A. R. Ade *et al.*, "Planck 2015 results. XIII. Cosmological parameters," *Astron. Astrophys.* **594** (2016) A13, `arXiv:1502.01589 [astro-ph.CO]`.

[35] S. W. Hawking and R. Penrose, "The Singularities of gravitational collapse and cosmology," *Proc. Roy. Soc. Lond.* **A314** (1970) 529–548.

[36] A. H. Guth, "Eternal inflation," arXiv:astro-ph/0101507 [astro-ph]. [Annals N. Y. Acad. Sci.950,66(2001)].

[37] J. Braden, M. C. Johnson, H. V. Peiris, A. Pontzen, and S. Weinfurtner, "A New Semiclassical Picture of Vacuum Decay," arXiv:1806.06069 [hep-th].

[38] V. F. Mukhanov and G. V. Chibisov, "Quantum Fluctuations and a Nonsingular Universe," *JETP Lett.* **33** (1981) 532–535. [Pisma Zh. Eksp. Teor. Fiz.33,549(1981)].

[39] A. H. Guth and S. Y. Pi, "Fluctuations in the New Inflationary Universe," *Phys. Rev. Lett.* **49** (1982) 1110–1113.

[40] S. W. Hawking, "The Development of Irregularities in a Single Bubble Inflationary Universe," *Phys. Lett.* **115B** (1982) 295.

[41] J. M. Bardeen, P. J. Steinhardt, and M. S. Turner, "Spontaneous Creation of Almost Scale - Free Density Perturbations in an Inflationary Universe," *Phys. Rev.* **D28** (1983) 679.

[42] M. Noorbala, V. Vennin, H. Assadullahi, H. Firouzjahi, and D. Wands, "Tunneling in Stochastic Inflation," arXiv:1806.09634 [hep-th].

[43] A. A. Starobinsky, "STOCHASTIC DE SITTER (INFLATIONARY) STAGE IN THE EARLY UNIVERSE," *Lect. Notes Phys.* **246** (1986) 107–126.

[44] C. P. Burgess, R. Holman, G. Tasinato, and M. Williams, "EFT Beyond the Horizon: Stochastic Inflation and How Primordial Quantum Fluctuations Go Classical," *JHEP* **03** (2015) 090, arXiv:1408.5002 [hep-th].

[45] L. Pinol, S. Renaux-Petel, and Y. Tada, "A critical look at stochastic inflation," arXiv:1806.10126 [gr-qc].

[46] A. Ijjas, P. J. Steinhardt, and A. Loeb, "Inflationary paradigm in trouble after Planck2013," *Phys. Lett.* **B723** (2013) 261–266, arXiv:1304.2785 [astro-ph.CO].

[47] J.-L. Lehners, "Cosmic Bounces and Cyclic Universes," *Class. Quant. Grav.* **28** (2011) 204004, arXiv:1106.0172 [hep-th].

[48] R. Brandenberger and P. Peter, "Bouncing Cosmologies: Progress and Problems," *Found. Phys.* **47** (2017) no. 6, 797–850, arXiv:1603.05834 [hep-th].

[49] G. F. R. Ellis and H. van Elst, "Cosmological models: Cargese lectures 1998," *NATO Sci. Ser. C* **541** (1999) 1–116, arXiv:gr-qc/9812046 [gr-qc].

[50] G. F. R. Ellis and M. A. H. MacCallum, "A Class of homogeneous cosmological models," *Commun. Math. Phys.* **12** (1969) 108–141.

[51] V. A. Belinsky, I. M. Khalatnikov, and E. M. Lifshitz, "Oscillatory approach to a singular point in the relativistic cosmology," *Adv. Phys.* **19** (1970) 525–573.

[52] C. W. Misner, "Mixmaster universe," *Phys. Rev. Lett.* **22** (1969) 1071–1074.

[53] T. Damour, M. Henneaux, and H. Nicolai, "Cosmological billiards," *Class. Quant. Grav.* **20** (2003) R145–R200, arXiv:hep-th/0212256 [hep-th].

[54] A. Kleinschmidt, M. Koehn, and H. Nicolai, "Supersymmetric quantum cosmological billiards," *Phys. Rev.* **D80** (2009) 061701, arXiv:0907.3048 [gr-qc].

[55] M. Koehn, "Relativistic Wavepackets in Classically Chaotic Quantum Cosmological Billiards," *Phys. Rev.* **D85** (2012) 063501, arXiv:1107.6023 [gr-qc].

[56] C. de Rham, "Massive Gravity," *Living Rev. Rel.* **17** (2014) 7, arXiv:1401.4173 [hep-th].

[57] A. A. Starobinsky, "A New Type of Isotropic Cosmological Models Without Singularity," *Phys. Lett.* **B91** (1980) 99–102. [,771(1980)].

[58] C. Brans and R. H. Dicke, "Mach's principle and a relativistic theory of gravitation," *Phys. Rev.* **124** (1961) 925–935. [,142(1961)].

[59] A. Wang, "Ho?ava gravity at a Lifshitz point: A progress report," *Int. J. Mod. Phys.* **D26** (2017) no. 07, 1730014, arXiv:1701.06087 [gr-qc].

[60] S. Hawking, "The occurrence of singularities in cosmology. III. Causality and singularities," *Proc. Roy. Soc. Lond.* **A300** (1967) 187–201.

[61] T. Qiu, J. Evslin, Y.-F. Cai, M. Li, and X. Zhang, "Bouncing Galileon Cosmologies," *JCAP* **1110** (2011) 036, arXiv:1108.0593 [hep-th].

[62] D. A. Easson, I. Sawicki, and A. Vikman, "G-Bounce," *JCAP* **1111** (2011) 021, arXiv:1109.1047 [hep-th].

[63] M. Koehn, J.-L. Lehners, and B. A. Ovrut, "Cosmological super-bounce," *Phys. Rev.* **D90** (2014) no. 2, 025005, arXiv:1310.7577 [hep-th].

[64] A. Ijjas and P. J. Steinhardt, "Classically stable nonsingular cosmological bounces," *Phys. Rev. Lett.* **117** (2016) no. 12, 121304, arXiv:1606.08880 [gr-qc].

[65] J. Magueijo, T. G. Zlosnik, and T. W. B. Kibble, "Cosmology with a spin," *Phys. Rev.* **D87** (2013) no. 6, 063504, arXiv:1212.0585 [astro-ph.CO].

[66] S. Farnsworth, J.-L. Lehners, and T. Qiu, "Spinor driven cosmic bounces and their cosmological perturbations," *Phys. Rev.* **D96** (2017) no. 8, 083530, arXiv:1709.03171 [gr-qc].

[67] D. M. Scolnic *et al.*, "The Complete Light-curve Sample of Spectroscopically Confirmed SNe Ia from Pan-STARRS1 and Cosmological Constraints from the Combined Pantheon Sample," *Astrophys. J.* **859** (2018) no. 2, 101, arXiv:1710.00845 [astro-ph.CO].

[68] R. H. Brandenberger and C. Vafa, "Superstrings in the Early Universe," *Nucl. Phys.* **B316** (1989) 391–410.

[69] J. B. Hartle and S. W. Hawking, "Wave Function of the Universe," *Phys. Rev.* **D28** (1983) 2960–2975. [Adv. Ser. Astrophys. Cosmol.3,174(1987)].

[70] A. Anabalon and J. Oliva, "Four-dimensional Traversable Wormholes and Bouncing Cosmologies in Vacuum," arXiv:1811.03497 [hep-th].

[71] K. Schwarzschild, "On the gravitational field of a mass point according to Einstein's theory," *Sitzungsber. Preuss. Akad. Wiss. Berlin (Math. Phys.)* **1916** (1916) 189–196, arXiv:physics/9905030 [physics].

[72] R. Kantowski and R. K. Sachs, "Some spatially homogeneous anisotropic relativistic cosmological models," *J. Math. Phys.* **7** (1966) 443.

[73] J. B. Griffiths and J. Podolsky, "A New look at the Plebanski-Demianski family of solutions," *Int. J. Mod. Phys.* **D15** (2006) 335–370, arXiv:gr-qc/0511091 [gr-qc].

[74] R. L. Arnowitt, S. Deser, and C. W. Misner, "The Dynamics of general relativity," *Gen. Rel. Grav.* **40** (2008) 1997–2027, arXiv:gr-qc/0405109 [gr-qc].

[75] P. Creminelli, L. Senatore, and A. Vasy, "Asymptotic Behavior of Cosmologies with $\Lambda > 0$ in 2+1 Dimensions," arXiv:1902.00519 [hep-th].

[76] W. E. East, M. Kleban, A. Linde, and L. Senatore, "Beginning inflation in an inhomogeneous universe," *JCAP* **1609** (2016) no. 09, 010, arXiv:1511.05143 [hep-th].

[77] K. Clough, E. A. Lim, B. S. DiNunno, W. Fischler, R. Flauger, and S. Paban, "Robustness of Inflation to Inhomogeneous Initial Conditions," *JCAP* **1709** (2017) no. 09, 025, arXiv:1608.04408 [hep-th].

[78] R. H. Dicke and P. J. E. Peebles, "The big bang cosmology: Enigmas and nostrums," in *General Relativity: An Einstein Centenary Survey*. 1979.

[79] A. Yu. Kamenshchik, I. M. Khalatnikov, and A. V. Toporensky, "Simplest cosmological model with the scalar field," *Int. J. Mod. Phys.* **D6** (1997) 673–692, arXiv:gr-qc/9801064 [gr-qc].

[80] A. Yu. Kamenshchik, I. M. Khalatnikov, and A. V. Toporensky, "Simplest cosmological model with the scalar field. 2. Influence of cosmological constant," *Int. J. Mod. Phys.* **D7** (1998) 129–138, arXiv:gr-qc/9801082 [gr-qc].

[81] A. Yu. Kamenshchik, I. M. Khalatnikov, S. V. Savchenko, and A. V. Toporensky, "Topological entropy for some isotropic cosmological models," *Phys. Rev.* **D59** (1999) 123516, arXiv:gr-qc/9809048 [gr-qc].

[82] L. Smolin, *The lifetime of the cosmos*. 1997.

[83] T. Buchert and J. Ehlers, "Averaging inhomogeneous Newtonian cosmologies," *Astron. Astrophys.* **320** (1997) 1–7, arXiv:astro-ph/9510056 [astro-ph].

[84] L. Battarra, M. Koehn, J.-L. Lehners, and B. A. Ovrut, "Cosmological Perturbations Through a Non-Singular Ghost-Condensate/Galileon Bounce," *JCAP* **1407** (2014) 007, arXiv:1404.5067 [hep-th].

[85] J. Khoury, B. A. Ovrut, and J. Stokes, "The Worldvolume Action of Kink Solitons in AdS Spacetime," *JHEP* **08** (2012) 015, arXiv:1203.4562 [hep-th].

[86] B. A. Ovrut and J. Stokes, "Heterotic Kink Solitons and their Worldvolume Action," *JHEP* **09** (2012) 065, arXiv:1205.4236 [hep-th].

[87] J. D. Barrow and R. A. Matzner, "Size of a bouncing mixmaster universe," *Phys. Rev.* **D21** (1980) 336–340.

[88] Y.-S. Piao, B. Feng, and X.-m. Zhang, "Suppressing CMB quadrupole with a bounce from contracting phase to inflation," *Phys. Rev.* **D69** (2004) 103520, arXiv:hep-th/0310206 [hep-th].

[89] T. Qiu and Y.-T. Wang, "G-Bounce Inflation: Towards Nonsingular Inflation Cosmology with Galileon Field," *JHEP* **04** (2015) 130, arXiv:1501.03568 [astro-ph.CO].

[90] J.-L. Lehners and P. J. Steinhardt, "Dark Energy and the Return of the Phoenix Universe," *Phys. Rev.* **D79** (2009) 063503, arXiv:0812.3388 [hep-th].

[91] J.-L. Lehners, P. J. Steinhardt, and N. Turok, "The Return of the Phoenix Universe," *Int. J. Mod. Phys.* **D18** (2009) 2231–2235, arXiv:0910.0834 [hep-th].

[92] J.-L. Lehners and P. J. Steinhardt, "Dynamical Selection of the Primordial Density Fluctuation Amplitude," *Phys. Rev. Lett.* **106** (2011) 081301, arXiv:1008.4567 [hep-th].

[93] G. Obied, H. Ooguri, L. Spodyneiko, and C. Vafa, "De Sitter Space and the Swampland," arXiv:1806.08362 [hep-th].

[94] U. H. Danielsson and T. Van Riet, "What if string theory has no de Sitter vacua?," *Int. J. Mod. Phys.* **D27** (2018) no. 12, 1830007, arXiv:1804.01120 [hep-th].

[95] D. Andriot, "On the de Sitter swampland criterion," *Phys. Lett.* **B785** (2018) 570–573, arXiv:1806.10999 [hep-th].

[96] P. Agrawal, G. Obied, P. J. Steinhardt, and C. Vafa, "On the Cosmological Implications of the String Swampland," *Phys. Lett.* **B784** (2018) 271–276, arXiv:1806.09718 [hep-th].

[97] S. K. Garg and C. Krishnan, "Bounds on Slow Roll and the de Sitter Swampland," arXiv:1807.05193 [hep-th].

[98] J.-L. Lehners, "Small-Field and Scale-Free: Inflation and Ekpyrosis at their Extremes," *JCAP* **1811** (2018) no. 11, 001, arXiv:1807.05240 [hep-th].

[99] S. R. Coleman, "The Uses of Instantons," *Subnucl. Ser.* **15** (1979) 805.

[100] S. R. Coleman, "The Fate of the False Vacuum. 1. Semiclassical Theory," *Phys. Rev.* **D15** (1977) 2929–2936. [Erratum: Phys. Rev.D16,1248(1977)].

[101] A. M. Polyakov, "Quark Confinement and Topology of Gauge Groups," *Nucl. Phys.* **B120** (1977) 429–458.

[102] C. M. Bender, D. C. Brody, and D. W. Hook, "Quantum effects in classical systems having complex energy," *J. Phys.* **A41** (2008) 352003, arXiv:0804.4169 [hep-th].

[103] C. M. Bender, "Classical Particles Having Complex Energy Exhibit Quantum-Like Behavior,". [eCONFC0906083,22(2009)].

[104] C. M. Bender, D. W. Hook, P. N. Meisinger, and Q.-h. Wang, "Complex Correspondence Principle," *Phys. Rev. Lett.* **104** (2010) 061601, arXiv:0912.2069 [hep-th].

[105] C. M. Bender and D. W. Hook, "Quantum tunneling as a classical anomaly," *J. Phys.* **A44** (2011) 372001, arXiv:1011.0121 [hep-th].

[106] C. K. Dumlu and G. V. Dunne, "Complex Worldline Instantons and Quantum Interference in Vacuum Pair Production," *Phys. Rev.* **D84** (2011) 125023, arXiv:1110.1657 [hep-th].

[107] A. Behtash, G. V. Dunne, T. Schafer, T. Sulejmanpasic, and M. Unsal, "Complexified path integrals, exact saddles and supersymmetry," *Phys. Rev. Lett.* **116** (2016) no. 1, 011601, arXiv:1510.00978 [hep-th].

[108] N. Turok, "On Quantum Tunneling in Real Time," *New J. Phys.* **16** (2014) 063006, arXiv:1312.1772 [quant-ph].

[109] A. Cherman and M. Unsal, "Real-Time Feynman Path Integral Realization of Instantons," arXiv:1408.0012 [hep-th].

[110] C. G. Callan, Jr. and S. R. Coleman, "The Fate of the False Vacuum. 2. First Quantum Corrections," *Phys. Rev.* **D16** (1977) 1762–1768.

[111] S. R. Coleman, "Quantum Tunneling and Negative Eigenvalues," *Nucl. Phys.* **B298** (1988) 178.

[112] H. Amann and P. Quittner, "A nodal theorem for coupled systems of Schrödinger equations and the number of bound states," *J. Math. Phys.* **36** (1995) 4553–4560.

[113] J. C. Hackworth and E. J. Weinberg, "Oscillating bounce solutions and vacuum tunneling in de Sitter spacetime," *Phys. Rev.* **D71** (2005) 044014, arXiv:hep-th/0410142 [hep-th].

[114] G. Lavrelashvili, "The Number of negative modes of the oscillating bounces," *Phys. Rev.* **D73** (2006) 083513, arXiv:gr-qc/0602039 [gr-qc].

[115] L. Battarra, G. Lavrelashvili, and J.-L. Lehners, "Negative Modes of Oscillating Instantons," *Phys. Rev.* **D86** (2012) 124001, arXiv:1208.2182 [hep-th].

[116] G. V. Lavrelashvili, V. A. Rubakov, and P. G. Tinyakov, "Tunneling transitions with gravitation: breaking of the quasiclassical approximation," *Phys. Lett.* **B161** (1985) 280–284.

[117] G. V. Lavrelashvili, "Negative mode problem in false vacuum decay with gravity," *Nucl. Phys. Proc. Suppl.* **88** (2000) 75–82, arXiv:gr-qc/0004025 [gr-qc].

[118] A. Khvedelidze, G. V. Lavrelashvili, and T. Tanaka, "On cosmological perturbations in closed FRW model with scalar field and false vacuum decay," *Phys. Rev.* **D62** (2000) 083501, arXiv:gr-qc/0001041 [gr-qc].

[119] S. Gratton and N. Turok, "Homogeneous modes of cosmological instantons," *Phys. Rev.* **D63** (2001) 123514, arXiv:hep-th/0008235 [hep-th].

[120] G. V. Dunne and Q.-h. Wang, "Fluctuations about Cosmological Instantons," *Phys. Rev.* **D74** (2006) 024018, arXiv:hep-th/0605176 [hep-th].

[121] L. Battarra, G. Lavrelashvili, and J.-L. Lehners, "Zoology of instanton solutions in flat potential barriers," *Phys. Rev.* **D88** (2013) 104012, arXiv:1307.7954.

[122] H. Lee and E. J. Weinberg, "Negative modes of Coleman-De Luccia bounces," *Phys. Rev.* **D90** (2014) no. 12, 124002, arXiv:1408.6547 [hep-th].

[123] M. Koehn, G. Lavrelashvili, and J.-L. Lehners, "Towards a Solution of the Negative Mode Problem in Quantum Tunnelling with Gravity," *Phys. Rev.* **D92** (2015) no. 2, 023506, arXiv:1504.04334 [hep-th].

[124] B.-H. Lee, C. H. Lee, W. Lee, and C. Oh, "Instanton solutions mediating tunneling between the degenerate vacua in curved space," *Phys. Rev.* **D82** (2010) 024019, arXiv:0910.1653 [hep-th].

[125] B.-H. Lee, C. H. Lee, W. Lee, and C. Oh, "Oscillating instanton solutions in curved space," *Phys. Rev.* **D85** (2012) 024022, arXiv:1106.5865 [hep-th].

[126] S. J. Parke, "Gravity, the Decay of the False Vacuum and the New Inflationary Universe Scenario," *Phys. Lett.* **121B** (1983) 313–315.

[127] L. G. Jensen and P. J. Steinhardt, "Bubble Nucleation and the Coleman-Weinberg Model," *Nucl. Phys.* **B237** (1984) 176–188.

[128] T. Markkanen, A. Rajantie, and S. Stopyra, "Cosmological Aspects of Higgs Vacuum Metastability," *Front. Astron. Space Sci.* **5** (2018) 40, arXiv:1809.06923 [astro-ph.CO].

[129] R. Gregory, K. M. Marshall, F. Michel, and I. G. Moss, "Negative modes of Coleman - De Luccia and black hole bubbles," *Phys. Rev.* **D98** (2018) no. 8, 085017, arXiv:1808.02305 [hep-th].

[130] V. A. Rubakov and O. Yu. Shvedov, "A Negative mode about Euclidean wormhole," *Phys. Lett.* **B383** (1996) 258–261, arXiv:gr-qc/9604038 [gr-qc].

[131] R. Alonso and A. Urbano, "Wormholes and masses for Goldstone bosons," *JHEP* **02** (2019) 136, arXiv:1706.07415 [hep-ph].

[132] G. V. Lavrelashvili, V. A. Rubakov, and P. G. Tinyakov, "Disruption of Quantum Coherence upon a Change in Spatial Topology in Quantum Gravity," *JETP Lett.* **46** (1987) 167–169. [Pisma Zh. Eksp. Teor. Fiz.46,134(1987)].

[133] S. B. Giddings and A. Strominger, "Axion Induced Topology Change in Quantum Gravity and String Theory," *Nucl. Phys.* **B306** (1988) 890–907.

[134] T. Hertog, B. Truijen, and T. Van Riet, "Euclidean axion wormholes have multiple negative modes," arXiv:1811.12690 [hep-th].

[135] C. Kiefer and B. Sandhoefer, "Quantum Cosmology," arXiv:0804.0672 [gr-qc].

[136] P. A. M. Dirac, "Generalized Hamiltonian dynamics," *Can. J. Math.* **2** (1950) 129–148.

[137] P. W. Higgs, "Integration of Secondary Constraints in Quantized General Relativity," *Phys. Rev. Lett.* **1** (1958) 373–374. [Erratum: Phys. Rev. Lett.3,66(1959)].

[138] S. W. Hawking, "The Boundary Conditions of the Universe," *Pontif. Acad. Sci. Scr. Varia* **48** (1982) 563–574.

[139] S. W. Hawking, "The Quantum State of the Universe," *Nucl. Phys.* **B239** (1984) 257.

[140] J. B. Hartle, S. W. Hawking, and T. Hertog, "The Classical Universes of the No-Boundary Quantum State," *Phys. Rev.* **D77** (2008) 123537, arXiv:0803.1663 [hep-th].

[141] A. Vilenkin, "Quantum Creation of Universes," *Phys. Rev.* **D30** (1984) 509–511.

[142] A. Vilenkin, "Boundary Conditions in Quantum Cosmology," *Phys. Rev.* **D33** (1986) 3560.

[143] L. Battarra and J.-L. Lehners, "On the No-Boundary Proposal for Ekpyrotic and Cyclic Cosmologies," *JCAP* **1412** (2014) no. 12, 023, arXiv:1407.4814 [hep-th].

[144] A. Vilenkin, "The Interpretation of the Wave Function of the Universe," *Phys. Rev.* **D39** (1989) 1116.

[145] J. Hartle and T. Hertog, "Quantum transitions between classical histories," *Phys. Rev.* **D92** (2015) no. 6, 063509, arXiv:1502.06770 [hep-th].

[146] S. W. Hawking and J. C. Luttrell, "The Isotropy of the Universe," *Phys. Lett.* **B143** (1984) 83.

[147] W. A. Wright and I. G. Moss, "The Anisotropy of the Universe," *Phys. Lett.* **B154** (1985) 115–119.

[148] S. del Campo and A. Vilenkin, "Tunneling Wave Function for Anisotropic Universe," *Phys. Lett.* **B224** (1989) 45–48.

[149] P. Amsterdamski, "Wave Function of an Anisotropic Universe," *Phys. Rev.* **D31** (1985) 3073–3078.

[150] M. J. Duncan and L. G. Jensen, "The Quantum Cosmology of an Anisotropic Universe," *Nucl. Phys.* **B312** (1989) 662–672.

[151] K. Fujio and T. Futamase, "Appearance of classical Mixmaster Universe from the No-Boundary Quantum State," *Phys. Rev.* **D80** (2009) 023504, arXiv:0906.2616 [gr-qc].

[152] L. Battarra and J.-L. Lehners, "On the Creation of the Universe via Ekpyrotic Instantons," *Phys. Lett.* **B742** (2015) 167–171, arXiv:1406.5896 [hep-th].

[153] J. J. Halliwell, "Derivation of the Wheeler-De Witt Equation from a Path Integral for Minisuperspace Models," *Phys. Rev.* **D38** (1988) 2468.

[154] G. W. Lyons, "Complex solutions for the scalar field model of the universe," *Phys. Rev.* **D46** (1992) 1546–1550.

[155] J.-L. Lehners, "Classical Inflationary and Ekpyrotic Universes in the No-Boundary Wavefunction," *Phys. Rev.* **D91** (2015) no. 8, 083525, arXiv:1502.00629 [hep-th].

[156] J. Hartle and T. Hertog, "Arrows of Time in the Bouncing Universes of the No-boundary Quantum State," *Phys. Rev.* **D85** (2012) 103524, arXiv:1104.1733 [hep-th].

[157] J. Khoury, B. A. Ovrut, N. Seiberg, P. J. Steinhardt, and N. Turok, "From big crunch to big bang," *Phys. Rev.* **D65** (2002) 086007, arXiv:hep-th/0108187 [hep-th].

[158] J.-L. Lehners, P. McFadden, and N. Turok, "Colliding Branes in Heterotic M-theory," *Phys. Rev.* **D75** (2007) 103510, arXiv:hep-th/0611259 [hep-th].

[159] C. Cartier, R. Durrer, and E. J. Copeland, "Cosmological perturbations and the transition from contraction to expansion," *Phys. Rev.* **D67** (2003) 103517, arXiv:hep-th/0301198 [hep-th].

[160] A. J. Tolley, N. Turok, and P. J. Steinhardt, "Cosmological perturbations in a big crunch / big bang space-time," *Phys. Rev.* **D69** (2004) 106005, arXiv:hep-th/0306109 [hep-th].

[161] E. I. Buchbinder, J. Khoury, and B. A. Ovrut, "New Ekpyrotic cosmology," *Phys. Rev.* **D76** (2007) 123503, arXiv:hep-th/0702154 [hep-th].

[162] P. Creminelli and L. Senatore, "A Smooth bouncing cosmology with scale invariant spectrum," *JCAP* **0711** (2007) 010, arXiv:hep-th/0702165 [hep-th].

[163] A. Ijjas and P. J. Steinhardt, "Fully stable cosmological solutions with a non-singular classical bounce," arXiv:1609.01253 [gr-qc].

[164] J.-L. Lehners, "New Ekpyrotic Quantum Cosmology," *Phys. Lett.* **B750** (2015) 242–246, arXiv:1504.02467 [hep-th].

[165] P. Creminelli, M. A. Luty, A. Nicolis, and L. Senatore, "Starting the Universe: Stable Violation of the Null Energy Condition and Non-standard Cosmologies," *JHEP* **12** (2006) 080, arXiv:hep-th/0606090 [hep-th].

[166] B. Craps, T. Hertog, and N. Turok, "On the Quantum Resolution of Cosmological Singularities using AdS/CFT," *Phys. Rev.* **D86** (2012) 043513, arXiv:0712.4180 [hep-th].

[167] T. Hertog and G. T. Horowitz, "Holographic description of AdS cosmologies," *JHEP* **04** (2005) 005, arXiv:hep-th/0503071 [hep-th].

[168] J. L. F. Barbon and E. Rabinovici, "AdS Crunches, CFT Falls And Cosmological Complementarity," *JHEP* **04** (2011) 044, arXiv:1102.3015 [hep-th].

[169] A. Awad, S. R. Das, A. Ghosh, J.-H. Oh, and S. P. Trivedi, "Slowly Varying Dilaton Cosmologies and their Field Theory Duals," *Phys. Rev.* **D80** (2009) 126011, arXiv:0906.3275 [hep-th].

[170] L. Battarra and T. Hertog, "Particle Production near an AdS Crunch," *JHEP* **12** (2010) 017, arXiv:1009.0992 [hep-th].

[171] G. W. Gibbons, "The Einstein Action of Riemannian Metrics and Its Relation to Quantum Gravity and Thermodynamics," *Phys. Lett.* **A61** (1977) 3–5.

[172] J. Feldbrugge, J.-L. Lehners, and N. Turok, "No rescue for the no boundary proposal: Pointers to the future of quantum cosmology," *Phys. Rev.* **D97** (2018) no. 2, 023509, arXiv:1708.05104 [hep-th].

[173] J. Feldbrugge, J.-L. Lehners, and N. Turok, "No smooth beginning for spacetime," *Phys. Rev. Lett.* **119** (2017) no. 17, 171301, arXiv:1705.00192 [hep-th].

[174] A. Di Tucci and J.-L. Lehners, "Unstable no-boundary fluctuations from sums over regular metrics," arXiv:1806.07134 [gr-qc].

[175] C. Teitelboim, "The Proper Time Gauge in Quantum Theory of Gravitation," *Phys. Rev.* **D28** (1983) 297.

[176] C. Teitelboim, "Causality Versus Gauge Invariance in Quantum Gravity and Supergravity," *Phys. Rev. Lett.* **50** (1983) 705.

[177] J. J. Halliwell and J. Louko, "Steepest Descent Contours in the Path Integral Approach to Quantum Cosmology. 1. The De Sitter Minisuperspace Model," *Phys. Rev.* **D39** (1989) 2206.

[178] A. Di Tucci and J.-L. Lehners, "The No-Boundary Proposal as a Path Integral with Robin Boundary Conditions," `arXiv:1903.06757 [hep-th]`.

[179] L. J. Garay, J. J. Halliwell, and G. A. Mena Marugan, "Path integral quantum cosmology: A Class of exactly soluble scalar field minisuperspace models with exponential potentials," *Phys. Rev.* **D43** (1991) 2572–2589.

[180] A. D. Sakharov, "Nachal'naia stadija rasshirenija Vselennoj i vozniknovenije neodnorodnosti raspredelenija veshchestva," *Zh. Eksp. Teor. Fiz.* **49** (1966) no. 1, 345–358. [Sov. Phys. JETP22,241(1966)].

[181] A. A. Starobinsky, "Spectrum of relict gravitational radiation and the early state of the universe," *JETP Lett.* **30** (1979) 682–685. [,767(1979)].

[182] F. Finelli and R. Brandenberger, "On the generation of a scale invariant spectrum of adiabatic fluctuations in cosmological models with a contracting phase," *Phys. Rev.* **D65** (2002) 103522, `arXiv:hep-th/0112249 [hep-th]`.

[183] F. Finelli, "Assisted contraction," *Phys. Lett.* **B545** (2002) 1–7, `arXiv:hep-th/0206112 [hep-th]`.

[184] J.-L. Lehners, P. McFadden, N. Turok, and P. J. Steinhardt, "Generating ekpyrotic curvature perturbations before the big bang," *Phys. Rev.* **D76** (2007) 103501, `arXiv:hep-th/0702153 [HEP-TH]`.

[185] T. Qiu, X. Gao, and E. N. Saridakis, "Towards anisotropy-free and nonsingular bounce cosmology with scale-invariant perturbations," *Phys. Rev.* **D88** (2013) no. 4, 043525, `arXiv:1303.2372 [astro-ph.CO]`.

[186] M. Li, "Note on the production of scale-invariant entropy perturbation in the Ekpyrotic universe," *Phys. Lett.* **B724** (2013) 192–197, `arXiv:1306.0191 [hep-th]`.

[187] A. Ijjas, J.-L. Lehners, and P. J. Steinhardt, "General mechanism for producing scale-invariant perturbations and small non-Gaussianity in ekpyrotic models," *Phys. Rev.* **D89** (2014) no. 12, 123520, `arXiv:1404.1265 [astro-ph.CO]`.

[188] C. Kiefer, D. Polarski, and A. A. Starobinsky, "Quantum to classical transition for fluctuations in the early universe," *Int. J. Mod. Phys.* **D7** (1998) 455–462, arXiv:gr-qc/9802003 [gr-qc].

[189] L. Battarra and J.-L. Lehners, "Quantum-to-classical transition for ekpyrotic perturbations," *Phys. Rev.* **D89** (2014) no. 6, 063516, arXiv:1309.2281 [hep-th].

[190] N. D. Birrell and P. C. W. Davies, *Quantum Fields in Curved Space*. Cambridge Monographs on Mathematical Physics. Cambridge Univ. Press, Cambridge, UK, 1984.

[191] P. J. Steinhardt, "NATURAL INFLATION," in *Nuffield Workshop on the Very Early Universe Cambridge, England, June 21-July 9, 1982*, pp. 251–266. 1982.

[192] A. Aguirre, "Eternal Inflation, past and future," arXiv:0712.0571 [hep-th].

[193] M. C. Johnson and J.-L. Lehners, "Cycles in the Multiverse," *Phys. Rev.* **D85** (2012) 103509, arXiv:1112.3360 [hep-th].

[194] A. Di Tucci, J. Feldbrugge, J.-L. Lehners, and N. Turok, "Quantum Incompleteness of Inflation," arXiv:1906.09007 [hep-th].

[195] J. J. Halliwell, J. B. Hartle, and T. Hertog, "What is the No-Boundary Wave Function of the Universe?," *Phys. Rev.* **D99** (2019) no. 4, 043526, arXiv:1812.01760 [hep-th].

[196] S. Gielen and N. Turok, "A Perfect Bounce," arXiv:1510.00699 [hep-th].

[197] S. M. Carroll, "Lecture notes on general relativity," arXiv:gr-qc/9712019 [gr-qc].

[198] M. Koehn, J.-L. Lehners, and B. Ovrut, "Nonsingular bouncing cosmology: Consistency of the effective description," *Phys. Rev.* **D93** (2016) no. 10, 103501, arXiv:1512.03807 [hep-th].

[199] A. Anabalon and A. Cisterna, "Asymptotically (anti) de Sitter Black Holes and Wormholes with a Self Interacting Scalar Field in Four Dimensions," *Phys. Rev.* **D85** (2012) 084035, arXiv:1201.2008 [hep-th].

[200] T. P. Sotiriou, M. Visser, and S. Weinfurtner, "Quantum gravity without Lorentz invariance," *JHEP* **10** (2009) 033, arXiv:0905.2798 [hep-th].

[201] A. O. Barvinsky, D. Blas, M. Herrero-Valea, S. M. Sibiryakov, and C. F. Steinwachs, "Renormalization of Ho?ava gravity," *Phys. Rev.* **D93** (2016) no. 6, 064022, arXiv:1512.02250 [hep-th].

[202] A. O. Barvinsky, D. Blas, M. Herrero-Valea, S. M. Sibiryakov, and C. F. Steinwachs, "Renormalization of gauge theories in the background-field approach," *JHEP* **07** (2018) 035, arXiv:1705.03480 [hep-th].

[203] S. Mukohyama, "Scale-invariant cosmological perturbations from Horava-Lifshitz gravity without inflation," *JCAP* **0906** (2009) 001, arXiv:0904.2190 [hep-th].

[204] S. Mukohyama, "Horava-Lifshitz Cosmology: A Review," *Class. Quant. Grav.* **27** (2010) 223101, arXiv:1007.5199 [hep-th].

[205] S. Mukohyama, "Dark matter as integration constant in Horava-Lifshitz gravity," *Phys. Rev.* **D80** (2009) 064005, arXiv:0905.3563 [hep-th].

[206] S. Mukohyama, "Caustic avoidance in Horava-Lifshitz gravity," *JCAP* **0909** (2009) 005, arXiv:0906.5069 [hep-th].

[207] A. O. Barvinsky, D. Blas, M. Herrero-Valea, S. M. Sibiryakov, and C. F. Steinwachs, "Ho?ava Gravity is Asymptotically Free in 2 + 1 Dimensions," *Phys. Rev. Lett.* **119** (2017) no. 21, 211301, arXiv:1706.06809 [hep-th].

[208] J. Magueijo, "New varying speed of light theories," *Rept. Prog. Phys.* **66** (2003) 2025, arXiv:astro-ph/0305457 [astro-ph].

[209] G. Amelino-Camelia, "Relativity in space-times with short distance structure governed by an observer independent (Planckian) length scale," *Int. J. Mod. Phys.* **D11** (2002) 35–60, arXiv:gr-qc/0012051 [gr-qc].

[210] G. Amelino-Camelia, M. Arzano, G. Gubitosi, and J. Magueijo, "Dimensional reduction in the sky," *Phys. Rev.* **D87** (2013) no. 12, 123532, arXiv:1305.3153 [gr-qc].

[211] A. Albrecht and J. Magueijo, "A Time varying speed of light as a solution to cosmological puzzles," *Phys. Rev.* **D59** (1999) 043516, arXiv:astro-ph/9811018 [astro-ph].

Acknowledgements

Throughout this thesis I have not used the pronoun *I* but *we*. This is because research is almost never performed alone but rests on the shoulders of a wide network of people. This is especially true in my case, and I wish to thank everyone who contributed.

Many people have impacted my development as a scientist since I have arrived in Berlin. I wish to express my sincere gratitude to my supervisor Jean-Luc Lehners for continuously offering his time, expertise and guidance, and for his sharing of ideas which had a crucial impact in shaping how I think about theoretical physics and cosmology today. The many opportunities to visit my collaborators, to participate in international conferences, schools, and workshops and to grow and prosper as an independent scientist were possible due to his support.

My academic progress has been aided significantly by the unwavering support of Robert Brandenberger, who provided me with many opportunities to present my work and whose advice I continue to regard highly into the next stages of my career.I further wish to thank my collaborators Andres Anabalon, Mariam Chitishvili, Andrew Coates, Alice Di Tucci, Shane Farnsworth, Thomas Hertog, George Lavrelashvili, Joo Magueijo, Shinji Mukohyama, Ryo Namba, Yannick Vreys, and Yota Watanabe for the pleasant and fruitful work together. These exchanges and to and fros of their ideas, points of view, and interpretations, has had a significant influence on me and this thesis.

For hosting me for extended periods of time at their institutions I wish to thank Alexander Vilenkin, Shinji Mukohyama, and Thomas Hertog. By doing so, I was exposed to different approaches and attitudes in cosmology and theoretical physics as a whole.

During my studies I benefited from discussions and correspondences with many, extraordinary people including Olof Ahlen, Stephon Alexander, Antonio De Felice, Angelika Fertig, Marco Finocchiaro, Jan Gerken, Anna Ijjas, Matt Johnson, Lars Kreuzer, Evan McDonough, Daniele Oriti, Misao Sasaki, Paul Steinhardt, Neil Turok, Masaki Yamada and the members of the Max Planck Institute for Gravitational Physics' theoretical cosmology group.

I am thankful to the Max Planck Institute for Gravitational Physics (Albert Einstein Institute) for their continued support, and in particular Hermann Nicolai's quantum gravity division, which creates a pleasant and stimulating environment for exciting research. Anika Rast was incredibly patient and quick to resolve any of my administrative needs. I found the AEI's IMPRS program an excellent way of structuring my PhD studies and thank Axel Kleinschmidt, Hadi Godazgar, and Oliver Schlotterer for its organization. The Studiens-

tiftung des Deutschen Volkes has not only provided financial support but also an exciting network of people and endless possibilities for self-improvement.
It has been a pleasure to share an office with Isha Kotecha and to begin our doctorate journey in tandem. Enno Mallwitz and Alice Di Tucci have been trusted friends and our discussions on research, life and beyond will stay with me as a fond memory of my time in Berlin.
I wish to thank my parents and sister for their unconditional and tremendous support. Finally, Dani, thank you for being a constant source of inspiration, a safe haven for troubled days, and a wonderfully exciting companion.

Declaration of Authorship

Ich erkläre, dass ich die Dissertation selbständig und nur unter Verwendung der von mir gemäss § 7 Abs. 3 der Promotionsordnung der Mathematisch-Naturwissenschaftlichen Fakultät, veröffentlicht im Amtlichen Mitteilungsblatt der Humboldt-Universität zu Berlin Nr. 42/2018 am 11.07.2018 angegebenen Hilfsmittel angefertigt habe.

Berlin, July 17, 2019

Sebastian F. Bramberger